

thrustMIT - Project Vayuvega
Team 207 Project Technical Report to the 2025 IREC

Satvik Agrawal [1], Madhav Sonkusare [2], Akash Siddarth [3], Ajinkya Sathe [4], Tejas Patil [5], Geethika Sree Ravu [6], Mohul Podder [7], Samarth Vinod [8], Ayyan Nikunj Bhartia, Adithi Shetty N, Jahnavi U, Aryan Gupta, Shreemad Burade
Manipal Institute of Technology, Manipal, Karnataka (576104), India

---

This report details the technical specifications of thrustMIT's latest rocket, Vayuvega, for the 2025 International Rocket Engineering Competition in the 30k COTS Category. Project Vayuvega aims to achieve an apogee of 30,000 feet carrying a non-deployable payload and recover through dual-bay separation. Powered by the AeroTech O5500X-PS solid propellant COTS motor, the rocket incorporates a combination of carbon fibre and glass fibre composite fuselage, reinforced by Aluminium components including bulkheads, centring rings, stringer-fins, and coupler to ensure structural integrity. The rocket avionics, supplemented by COTS electronics for redundancy, underpin dual-event recovery through efficient tracking of the mission life cycle. The CanSat payload features a cube mounted on a spring, tracked by a servo-actuated camera. The experiment aims to validate real-time visual tracking in extreme flight conditions through 3D object tracking, pose estimation, and the generation of point clouds for deriving detailed 3D spatial information.

---

[1]Project Manager; Team Leader
[2]Deputy Project Manager; Mechanical and Propulsion Head
[3]Safety Operations Lead; Structures Head
[4]Recovery Operations Lead; Aerodynamics Head
[5]Launch Operations Lead; Payload Computational Co-head
[6]Team Manager
[7]Payload Electronics Co-head
[8]Avionics Head

Nomenclature

ABS	Acrylonitrile Butadiene Styrene	
AGL	Above Ground Level	
ASL	Above Sea Level	
AWG	American Wire Gauge	
BEC	Battery Eliminator Circuit	
CAD	Computer-Aided Design	
CFD	Computational Fluid Dynamics	
$CFRP$	Carbon Fibre Reinforced Polymer	
CNC	Computer Numerical Control	
$COTS$	Commercial Off-The-Shelf	
DMP	Digital Motion Processor	
DMS	Disposable Motor System	
DoF	Degrees of Freedom	
$DTEG$	Design, Test, & Evaluation Guide	
FC	Flight Computer	
FOS	Factor of Safety	
FPS	Frames per Second	
FSI	Fluid Structure Interaction	
FSM	Finite State Machine	
$GFRP$	Glass Fibre Reinforced Polymer	
$GPIO$	General Purpose Input/Output	
GPS	Global Positioning System	
GSM	Grams per Square Metre	
$I2C$	Inter-Integrated Circuit	
IDE	Integrated Development Environment	
IMU	Inertial Measurement Unit	
$IREC$	International Rocket Engineering Competition	
LED	Light Emitting Diode	
$Li-ion$	Lithium-ion Battery	
$LiPo$	Lithium Polymer Battery	
MP	Mega Pixel	
NPU	Neural Processing Unit	
PCB	Printed Circuit Board	
PLA	Polylactic Acid	
PSD	Power Spectral Density	
SD	Secure Digital	
SPI	Serial Peripheral Interface	
$SRAD$	Student Researched and Developed	
$UART$	Universal Asynchronous Receive and Transmit	
a	Speed of Sound	$\mathrm{m\,s^{-1}}$
$MaxQ$	Maximum Dynamic Pressure	
G	Modulus of Rigidity	MPa
AR	Aspect Ratio of the Fin	
t	Thickness of the wing	mm
P	Ambient/Air Pressure at the Altitude where the Speed of Sound was determined	MPa
α	Half Wedge Angle	
λ	Taper Ratio of the Fin	
c	Chord Length of Fin	mm
C_f	Viscous Drag Coefficient	
C_g	Centre of Gravity	m
C_p	Centre of Pressure	m
V_f	Fin Flutter Velocity	$\mathrm{m\,s^{-1}}$

Contents

I Introduction **7**
- I.A Project Background & Scope . . . 7
- I.B Design Goals and Success Criteria . . . 7
- I.C Stakeholders . . . 8
- I.D Team Management Strategies . . . 8
- I.E Team Structure . . . 8

II System Architecture Overview **10**
- II.A Aerostructures . . . 11
  - II.A.1 Nosecone . . . 11
  - II.A.2 Body Tubes . . . 14
  - II.A.3 Couplers . . . 20
  - II.A.4 Fins . . . 21
  - II.A.5 Boattail . . . 33
  - II.A.6 Rail Buttons . . . 34
  - II.A.7 Flight Analysis . . . 35
- II.B Propulsion . . . 37
  - II.B.1 Motor Details . . . 38
  - II.B.2 Retainer . . . 38
- II.C Recovery . . . 39
  - II.C.1 Recovery Bulkheads . . . 39
  - II.C.2 Parachute and Shock Cords . . . 41
- II.D Payload . . . 44
  - II.D.1 Computation . . . 44
  - II.D.2 Electrical and Electronics . . . 49
  - II.D.3 Mechanical Design . . . 51
- II.E Avionics . . . 55
  - II.E.1 COTS Electronics . . . 55
  - II.E.2 SRAD Electronics . . . 56
  - II.E.3 Avionics Coupler . . . 60

III Mission Concept of Operations Overview **62**
- III.A Mission Structure & Defining Mission Events . . . 62

IV Conclusions & Lessons Learnt **64**
- IV.A Lessons Learnt . . . 64

Acknowledgements **65**

V Appendix **67**

A Appendix: System Weights, Measures, and Performance Data **67**
- A.A Rocket Information . . . 67
- A.B Propulsion Details . . . 68
- A.C Predicted Flight Data . . . 69
- A.D Recovery Information . . . 70
- A.E Software Used . . . 71

B Appendix: Project Test Reports **72**
B.A Recovery System Testing . . . 72
B.B SRAD Propulsion System Testing . . . 85
B.C SRAD Pressure Vessel Testing . . . 86
B.D SRAD GPS Testing & Avionics System Testing . . . 87
B.E Payload Recovery System Testing . . . 91
B.F Payload Testing . . . 92
B.G Surface Roughness Testing . . . 107
B.H Composite Tubes Compressive Testing . . . 114

C Appendix: Hazard Analysis **123**

D Appendix: Risk Assessment **127**

E Appendix: Assembly, Pre-Flight, Launch, Recovery, and Off-Nominal Checklists **133**
E.A Tools Checklist . . . 134
E.B Airframe Assembly Checklist . . . 135
E.C Avionics Assembly Checklist . . . 138
E.D Payload Assembly Checklist . . . 139
E.E Pre-Flight & Pre-Launch Checklist . . . 141
E.F Recovery Checklist . . . 142
E.G Off-Nominal Checklist . . . 143

F Appendix: Engineering Drawings **145**

G Appendix: Team Structure **163**
G.A Faculty Advisor . . . 163
G.B Team Mentors . . . 163
G.C Project Leads . . . 163
G.D Senior Members . . . 163
G.E Aerodynamics Team . . . 163
G.F Avionics Team . . . 163
G.G Structures Team . . . 163
G.H Propulsion Team . . . 163
G.I Payload Team . . . 164
G.J Management Team . . . 164

H Appendix: Wiring Diagrams **165**
H.A Avionics . . . 165
H.B Payload . . . 166

I Appendix: Aerodynamic Analysis and Stability Considerations **167**
I.A Nosecone . . . 167
I.B Fins . . . 167
I.B.1 Aerodynamic Analysis of Various Fin Cross Sections . . . 167
I.B.2 FSI & Modal Analysis . . . 169
I.C Boattail . . . 172
I.D Drag & Stability Analysis . . . 172

J Appendix: MATLAB Code for Fin Flutter **175**

K Appendix: Payload **176**
K.A Understanding Requirements . . . 176
K.B Hardware Compatibility and Performance . . . 176
K.C Computational Workflow . . . 178
K.D Spring Deflection Calculation & Optimisation Code . . . 179

L Appendix: Simulations and Calculations **182**
L.A Nosecone . . . 182
L.A.1 Computational Fluid Dynamics . . . 182
L.B Fins . . . 186
L.B.1 Computational Fluid Dynamics . . . 186
L.B.2 Fluid Structure Interaction . . . 216
L.B.3 Modal Analysis . . . 229
L.C Boattail . . . 237
L.C.1 Computational Fluid Dynamics . . . 237
L.D Payload . . . 241
L.D.1 CanSat Vibrational Analysis . . . 241
L.D.2 Spring Deflection Calculations . . . 247
L.E Retainer . . . 248
L.F Motor Bay Coupler . . . 249
L.G Rocket with Circular Bolts . . . 251
L.G.1 Computational Fluid Dynamics . . . 251
L.H Rocket with Hex Bolts . . . 255
L.H.1 Computational Fluid Dynamics . . . 255
L.I Deployment Forces and Shock Loading Calculations . . . 260
L.J Load Analysis on Vayuvega . . . 261

M Appendix: SRAD 6-DoF Simulator Code **266**

N Appendix: Apogee Detection **284**

O Previous Progress Reports **285**

List of Tables

1 Vayuvega's System Requirements . . . 7
2 Fasteners Used in Vayuvega . . . 11
3 Bay Dimensions . . . 15
4 Void and Fibre Volume Fraction Results . . . 18
5 Coupler Dimensions . . . 20
6 Fin Dimensions . . . 22
7 Excitation Frequencies with varying Root Chord . . . 31
8 Boattail Dimensions . . . 33
9 Performance Characteristics of AeroTech O5500X-PS motor . . . 38
10 COTS Components . . . 55
11 Batteries for COTS Systems . . . 55
12 SRAD System Objectives . . . 56
13 SRAD Components . . . 57
14 SRAD Components Specifications . . . 58
15 Batteries for SRAD Systems . . . 59
16 Rocket Information . . . 67
17 Propulsion Details . . . 68
18 Predicted Flight Data . . . 69
19 Recovery Information . . . 70
20 Hazard Analysis Matrix . . . 123
21 Hazard Analysis Matrix . . . 123
22 Severity Scale . . . 127
23 Occurrence Scale . . . 127
24 Detection Scale . . . 128
25 Failure Modes Effect Analysis . . . 129
26 Nosecone Drag Data . . . 167
27 Aerodynamic Forces on Hexagonal Fin Cross Section at Varying Angles of Attack . . . 167
28 Aerodynamic Forces on Bi-Convex Cross Section at Varying Angles of Attack . . . 168
29 Aerodynamic Forces on Double Wedge Cross Section at Varying Angles of Attack . . . 168
30 Aerodynamic Forces on Single Wedge Cross Section at Varying Angles of Attack . . . 168
31 Aerodynamic Forces on Hexagonal Blunt-Based Cross Section at Varying Angles of Attack . . . 168
32 Aerodynamic Forces on Airfoil Cross Sections at Varying Angles of Attack . . . 169
33 Structural Response of Double Wedge Fin Cross Section Under Varying Angles of Attack . . . 169
34 Structural Response of Bi-Convex Fin Cross Section Under Varying Angles of Attack . . . 169
35 Structural Response of Hexagonal Fin Cross Section Under Varying Angles of Attack . . . 169
36 Vibration Modes and Deformation for Double Wedge Cross Section . . . 170
37 Vibration Modes and Deformation for Bi-Convex Cross Section . . . 170
38 Vibration Modes and Deformation for Hexagonal Cross Section . . . 170
39 Effect of Root Chord and Fin Height on Rocket Stability and Fin Flutter . . . 171
40 Effect of Boattail Length on Rocket Stability and Drag . . . 172
41 Rocket Flight Stability Comparison: OpenRocket vs CFD Data . . . 172
42 Drag Analysis of Vayuvega across Varying Mach Numbers . . . 173
43 Comparison of Aerodynamic Drag Forces on Hexagonal vs Circular Bolts Across Varying Mach Numbers 173
44 Drag Analysis of Components on Vayuvega across Varying Mach Numbers . . . 174
45 Springs Tested . . . 181

I. Introduction

A. Project Background & Scope

thrustMIT was formed in February 2016 to nurture amateur rocketry in India. The team started their competitive rocketry journey by entering the Spaceport America Cup in 2018, and has maintained consistent participation since. This international platform gives the team a chance to share its knowledge and learn from fellow amateur rocketeers all around the world. Project Vayuvega is thrustMIT's 7th manufactured rocket and serves as the team's official entry into the International Rocket Engineering Competition 2025.

After the team's maiden attempt in the 30K COTS category in the Spaceport America Cup 2024 with AgniAstra, which attained an apogee of 17 010 ft, Vayuvega aims to address previous shortcomings and complete a non-hazardous descent and successful recovery. The secondary mission goal is to test the functioning of the scientific payload, which aims to demonstrate real-time 3D tracking, pose estimation, and point cloud generation under high vibrations and G-forces. The overall objective of the team is to provide the team members an opportunity to engage in hands-on experience and scientific and technological challenges. This immersive experience will encourage more students to get involved in research and practice in the aerospace industry.

To meet the outlined objectives, the team has researched, designed, manufactured and tested each component of Vayuvega separately, making it one of the most intricate and advanced challenges the team has ever worked on. Despite substantial financial constraints and the absence of domestic flight test authorisation, we have been able to successfully manufacture Vayuvega ready for flight in the competition.

B. Design Goals and Success Criteria

Table 1 Vayuvega's System Requirements

1.0	**Vehicle Requirements**
1.1	The rocket shall reach an altitude of 30 093 ft (9172 m).
1.2	The rocket shall deploy parachutes and land safely.
1.3	The rocket shall maintain static stability margin between 1.65 and 5.8 throughout its ascent.
2.0	**Propulsion Requirements**
2.1	The total impulse of the motor shall remain within the limits of O-class.
3.0	**Recovery Requirements**
3.1	The recovery system shall deploy the drogue parachute when the rocket reaches apogee.
3.2	The recovery system shall deploy the main parachute when the rocket descends to an altitude of 457 m (1500 ft) above ground level (AGL).
3.3	The recovery system shall be armed manually through a pull-pin switch.
4.0	**Avionics Requirements**
4.1	The onboard avionics shall gather and log all sensor data during flight for post-flight analysis.
4.2	The acquired flight data shall be transmitted via telemetry throughout the flight, from ignition until recovery.
4.3	All flight electronics shall comply with Appendix B of the IREC DTEG, Safety Critical Wiring Guidelines.
5.0	**Aerostructures Requirements**
5.1	The airframe and the internal components shall withstand all operating stresses and retain structural integrity during flight.
5.2	The rocket fin flutter velocity must remain at least 50% higher than the maximum expected rocket velocity.
6.0	**Payload Requirements**
6.1	The payload shall conform to a CanSat form factor.
6.2	The payload shall be non-influential to nominal rocket performance, with all objectives met when replaced by an equivalent dead weight.

C. Stakeholders

The development of thrustMIT's Project Vayuvega has been made possible through extensive support from academic departments and industry partners, significantly contributing to the technical maturity of the project. Institutional backing from the Department of Aeronautical and Automobile Engineering, the Research Department, and various management divisions at Manipal Institute of Technology enabled access to critical infrastructure, research facilities, and administrative resources, thereby facilitating systematic testing and development. The encouragement of the university leadership throughout the research and validation phases further motivated the team to refine their technical expertise and push the boundaries of innovation.

Additionally, external organisations provided essential financial and in-kind support. At the same time, leading vendors supplied high-performance materials — including avionics systems, structural composites, research instrumentation, and aerodynamic components — ensuring the use of state-of-the-art technologies in the rocket's development. This integrated support network has been pivotal in enabling thrustMIT to realise a high-performance launch vehicle for the 30K COTS category at the IREC 2025.

D. Team Management Strategies

Team thrustMIT is organised into six subsystems, each specialising in a particular area of expertise critical to the successful completion of our projects and the smooth functioning of the team. At the top of the hierarchy are the Team Leader and Team Manager. The Team Leader represents thrustMIT externally, maintaining communication with the university and external organisations regarding all technical and project-related matters. The Team Manager oversees fund management, sponsorships, marketing, and outreach activities, ensuring smooth coordination and support for the team's operations. Together, they facilitate all external communication and provide the facilities necessary for the completion of the projects and team harmony. The second level of leadership consists of the subsystem heads, who are responsible for the execution of technical aspects within their respective domains. Their coordinated efforts are essential to the success of achieving the set project goals.

The remaining team members are distributed among the six subsystems, contributing to specific technical and operational tasks critical to the success of the project. Each subsystem typically consists of three to eight members. All thrustMIT members are full-time students at Manipal Institute of Technology, coming from various academic backgrounds ranging from Mechanical Engineering to Computer Science Engineering. Every member is a highly motivated individual, committed to balancing academics alongside their responsibilities and contributions to the team.

E. Team Structure

thrustMIT comprises 35 full-time undergraduate students studying in various fields of engineering at Manipal Institute of Technology, Manipal, Karnataka, India. While the project is managed by the active team members, the team also consults the alumni for their constructive input and occasional assistance. The Team Leader and Team Manager oversee the overall functioning of the team and the management of projects. They advise regarding technical activities and ensure the completion of administrative and operational activities necessary to achieve the main objectives and goals. Subsystem Leads are accountable for managing and leading operations within different subsystems that focus on specific sections of the rocket, such as avionics, aerostructures, recovery, propulsion, and payload. They are responsible for ensuring the completion of tasks and the project development under their domain is accomplished in a timely manner.

Project Leads are appointed based on their expertise, experience, and areas of interest. They oversee all the technical aspects of the projects. Their responsibilities begin from the start of the project, from design, manufacturing, testing, and ensuring the successful integration of the vehicle and ground systems. Though team members choose projects that align with their interests and areas of expertise, frequent collaboration across subsystems is essential.

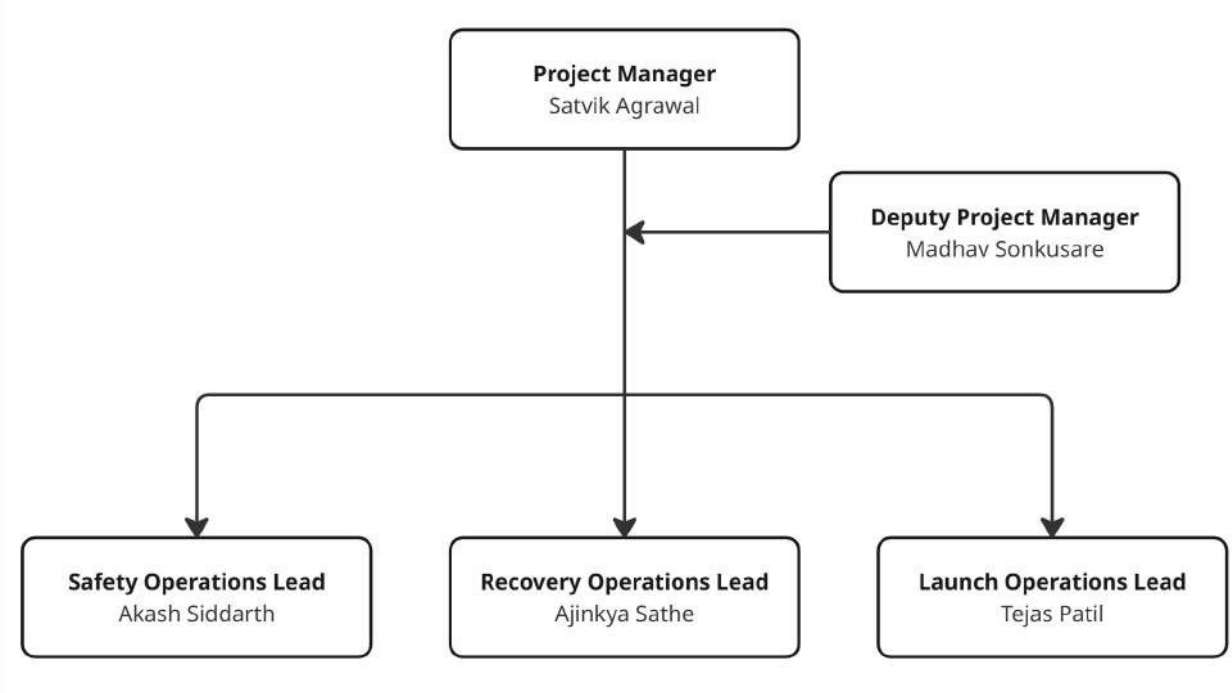


Figure 1 Team Leadership

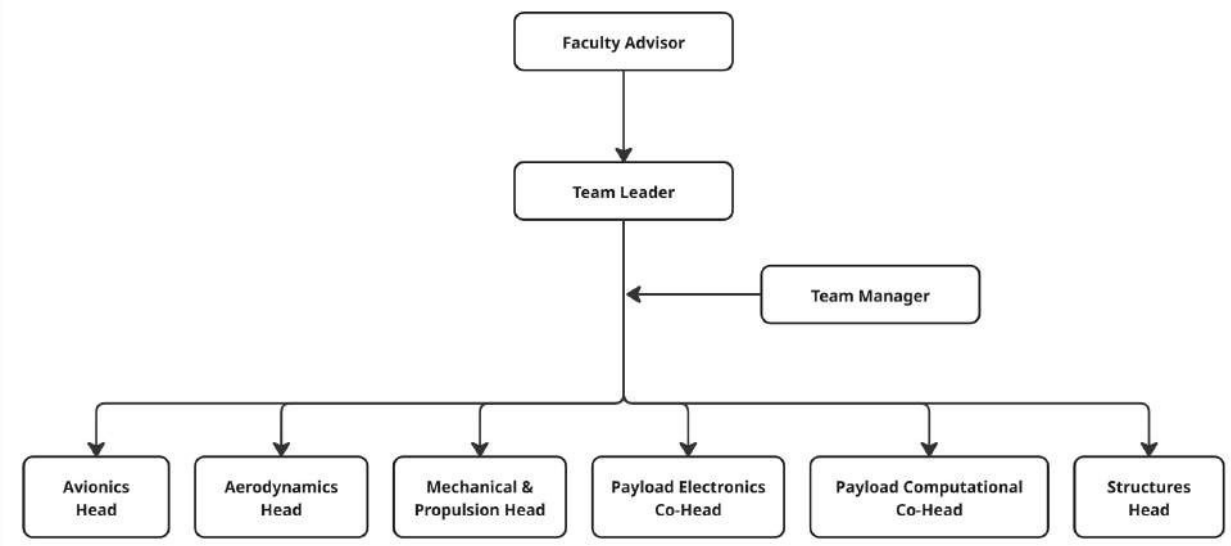


Figure 2 Team Structure

II. System Architecture Overview

Vayuvega is a 3.5 m tall rocket consisting of three composite body tubes. The tubes have an outer diameter of 126 mm and a thickness of 2.5 mm. The recovery bays housing the parachutes are manufactured from GFRP. These tubes are joined with a GFRP coupler enclosing the avionics system. The CFRP motor bay will be coupled to the fuselage with an Aluminium 6061-T6 coupler. The rocket features a set of 4 hexagonal fins designed to fly in the supersonic regime. The aft end of the rocket concludes with a boattail. The Aerotech 05500X-PS motor powers the rocket.



Figure 3 The Vayuvega rocket

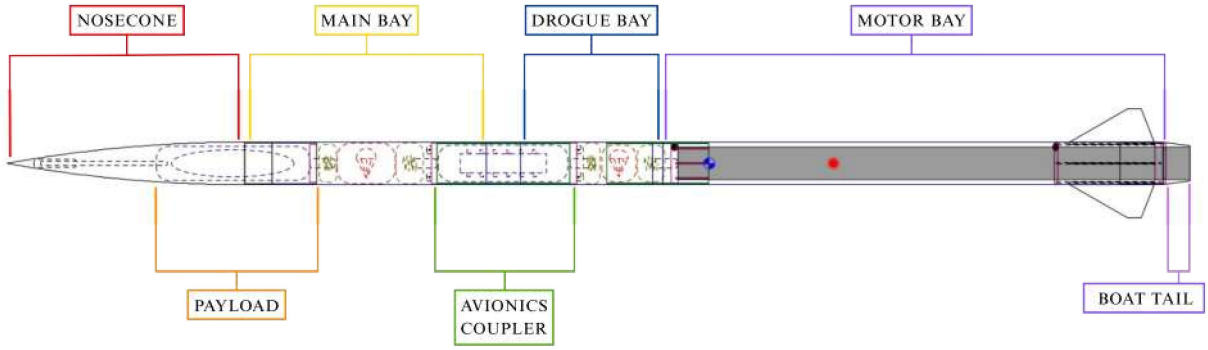


Figure 4 Schematic of Vayuvega as viewed on OpenRocket



Figure 5 Inner structure of Vayuvega

A. Aerostructures

The aerodynamics and structures team adopted an integrated design approach for Project Vayuvega. This approach focused on achieving the target apogee of 30 000 ft while ensuring the structural integrity of the vehicle throughout the flight. The design process prioritised flight safety and vehicle stability across the entire flight regime.

Table 2 Fasteners Used in Vayuvega

Thread Designation	Type	Reference Standard	Material / Grade	Comments
M1.6 × 0.35	Phillips drive with countersunk head	ISO 7046	SS-304	Payload Mount
M1.6 × 0.35	Hex Nuts	ISO 4032	SS-304	Payload Mount
M2 × 0.4	Phillips drive with pan head	ISO 7045	SS-304	Payload Mount
M2 × 0.4	Hex Nuts	ISO 4032	SS-304	Payload Mount
M2.5 × 0.45	Phillips drive with pan head	ISO 7045	SS-304	Payload Mount
M3 × 0.5	Hex socket drive with button head	ISO 7380-1	SS-304	Avionics Mount
M3 × 0.5	Hex Nuts	ISO 4032	SS-304	Avionics Mount
M3 × 0.5	Phillips drive with pan head	ISO 7045	SS-304	Avionics Mount
#6-32	Shear Pins	-	Nylon	Recovery
M4 × 0.7	Phillips drive with pan head	ISO 7045	SS-304	Avionics Mount
M4 × 0.7	Hex socket drive with countersunk head	ISO 10642	Grade 10.9	CanSat
M4 × 0.7	Hex socket drive with button head	ISO 7380-1	Grade 10.9	Retainer
M5 × 0.8	Hex socket drive with button head	ISO 7380-1	Grade 10.9	Bulkheads
M6 × 1	Hex socket drive with countersunk head	ISO 10642	Grade 10.9	Rail Button Attachment
M6 × 1	Hex Nuts	ISO 4032	Grade 8	Avionics Mount
M6 × 1	Wing Nuts	DIN 315 A	SS-304	Avionics Mount
M10 × 1.5	Eye Bolts	ISO 3266	SS-316	Recovery
M10 × 1.5	Hex Nuts	ISO 4032	Grade 8	Recovery
M10 × 1.5	Half Nuts	ISO 4035	SS-316	Recovery
3/8"-16 UNC	Eye Bolt	ANSI/ASME B1.1	SS-316	Recovery
M12 × 1.75	Threaded Rod	DIN 975	SS-304	NoseTip Attachment

1. Nosecone

The rocket features a nosecone with a 5.6 fineness ratio, designed as a tangent ogive and constructed from carbon fibre reinforced polymer (CFRP) using polyurethane female moulds. The maximum stagnation temperature at the nose tip is 461.18 K during the MaxQ phase. The nosecone is designed using Aluminium 6061-T6 as its melting point ranges from approximately 855 K to 925 K, providing a comfortable thermal margin.

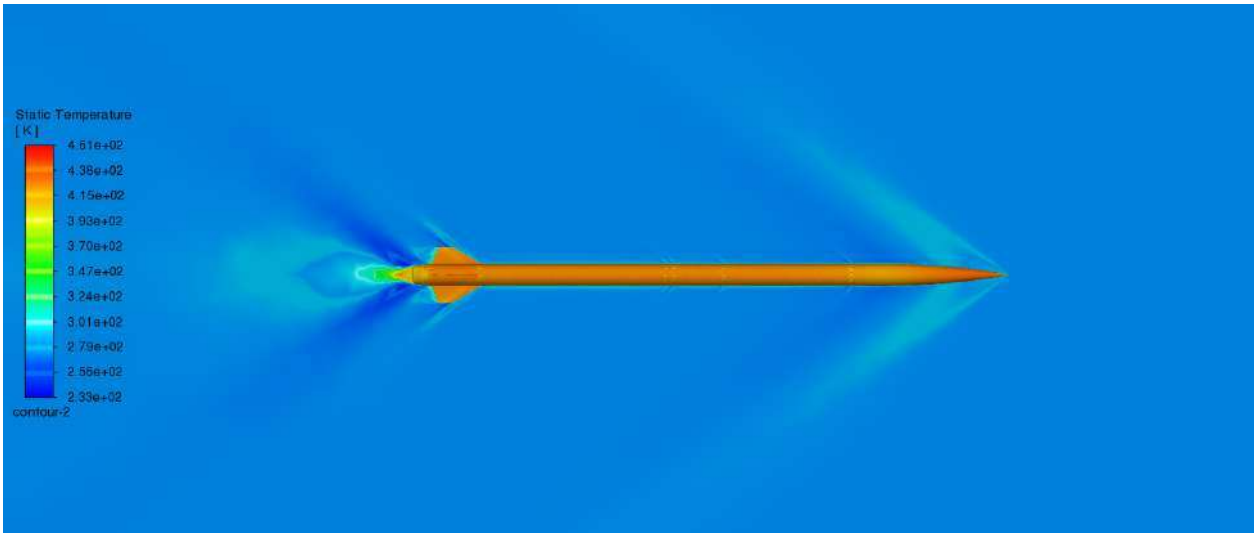


Figure 6 Static Temperature Contour around Vayuvega (at MaxQ)

The team executed a hand layup, incorporating carbon fibre fabric and resin into each polyurethane mould. Once the layup was completed, the two moulds were aligned and secured with threaded rods to maintain pressure and ensure proper curing. The nose cone profile extends slightly into the cylindrical section beyond the shoulder, ensuring true tangency between the ogive and the fuselage transition, thus avoiding discontinuities. The shoulder is seamlessly integrated into the layup, with fibre layers continuing into the extended cylindrical region, resulting in a single bonded structure that eliminates the need for post-moulding attachment.

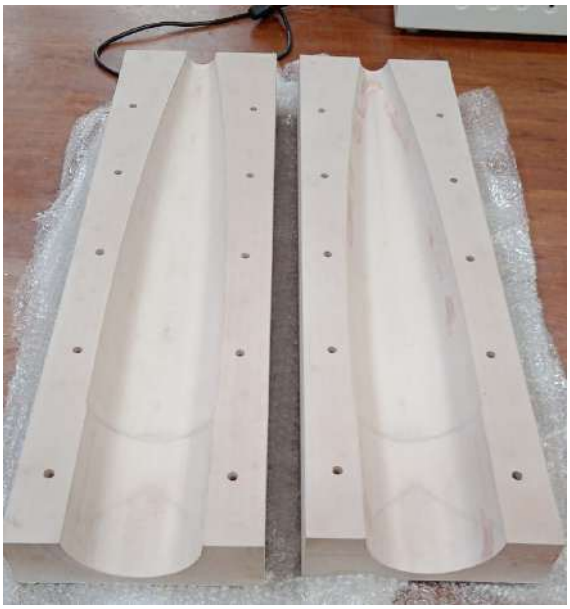


Figure 7 Polyurethane Mould

A bulkhead sits at the end of the shoulder, forming a foundation for the CanSat. The bulkhead supports the eyebolt that threads into the payload bottom plate. With a shock load shear failure of bolts in the shoulder last year, two layers of bolt planes were added to the bulkhead to bolster the structural integrity under sudden shock loads. A step is added to the bulkhead to ensure it sits on the shoulder axially. For radial alignment, the bulkhead features an extrusion at its end that sits in the slot cut in the shoulder. Figure 8 underlines the assembly of the nosecone and its child components.

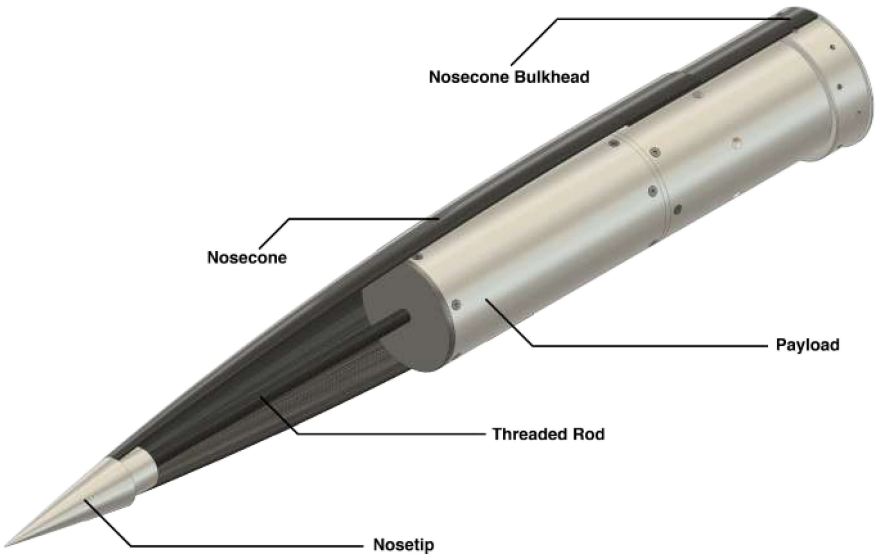


Figure 8 Nosecone Assembly

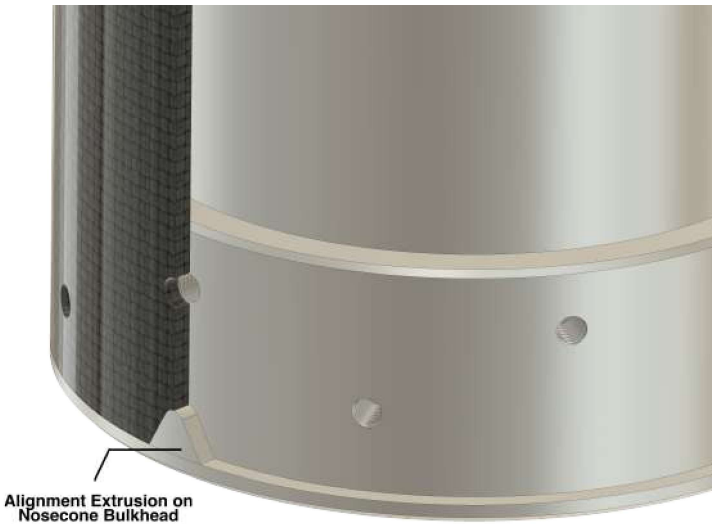


Figure 9 Self-Alignment of Bulkhead

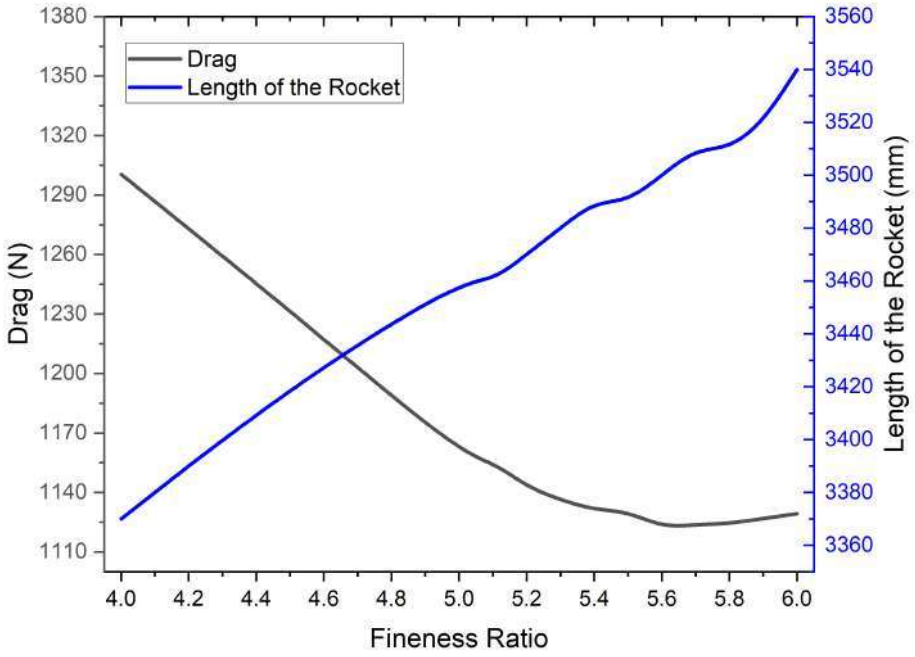


Figure 10 Fineness Ratio vs. Drag and Rocket Length

The design of Vayuvega's nosecone followed a dual parameter methodology, aimed at optimising aerodynamic performance while ensuring seamless payload integration, reliable recovery and ease of assembly. The payload is housed in a 450 mm tall CanSat, which sits within the nose cone and interfaces directly with the nose cone shoulder, simplifying payload integration during assembly.

To evaluate the aerodynamic characteristics of the nosecone, the team conducted CFD simulations at MaxQ conditions. According to RASAero II, the rocket reaches MaxQ at an altitude of 6816 ft ASL, with a Mach number of 1.71, static pressure and temperature of 78 781 Pa and 274.18 K, respectively. These simulations captured the rocket's behaviour during the supersonic regime, where it spends a total of 13.72 seconds. In this regime, pressure drag is the dominant component of total drag due to the formation of shock waves and the associated pressure drop behind them. The simulation scheme commenced from a fineness ratio of 4:1, with increments of 0.5. A significant reduction of drag was achieved until the fineness ratio of 5:1. Post 5:1, the decrements in drag were observed to be considerably lower. Owing to this observation, a finer simulation scheme was derived, starting from 5:1 to 6:1, with increments of 0.1. It was observed that as the fineness ratio increased, the aerodynamic drag decreased consistently to a ratio of 5.6. This was primarily because increasing the fineness ratio allowed the payload to shift further inside the nose cone, which in turn reduced the fuselage length and made the rocket more streamlined overall. This streamlining effect led to improved aerodynamic efficiency by lowering total drag. However, beyond a fineness ratio of 5.6, the payload could no longer move further inside the nose cone due to its interface with the shoulder. As a result, any further increase in fineness ratio contributed only to an increase in viscous drag, which led to a rise in overall drag.

Therefore, the fineness ratio of 5.6 was selected as the optimal design configuration. It provided the lowest drag in supersonic conditions while accommodating the payload in a structurally favourable position that interfaces cleanly with the nose cone shoulder.

2. Body Tubes

Vayuvega houses all its components in three body tube sections. The tubes feature an outer diameter of 126 mm and an inner diameter of 121 mm. The team constructed the main and drogue bays using GFRP to allow radio transparency. The motor bay is manufactured using CFRP due to its higher specific strength[1]. The team disregarded GFRP for the motor bay because it added unnecessary weight to the aft end of the rocket. With prior experience, the epoxy pair chosen was the Araldite LY 5052 and Aradur 5052 for the layups. 200 GSM Bidirectional Plain-Woven fabric was chosen for

carbon fibre, and 450 GSM Plain Woven S fabric for glass fibre. Table 3 details the dimensions of the body tubes.

Table 3 Bay Dimensions

Bay Name	Length	Material
Main Bay	630 mm	GFRP
Drogue Bay	390 mm	GFRP
Motor Bay	1490 mm	CFRP

Load Analysis

The team commenced the fuselage design by investigating the structural failure of Agniastra at the Spaceport America Cup 2024. The failure was identified in the motor bay coupler, which was located approximately 1773.5 mm from the nosecone. In response, the team performed a redesign of Vayuvega, opting to increase the thickness of the fuselage wall to 2.5 mm rather than enlarging the diameter, thus being efficient in terms of base drag. This approach is taken with the worst-case scenario loadings of drag forces, maximum thrust and the maximum inertial load. As a result of this modification, we realized a 36% increase in the section modulus compared to the prior design.

We computed the bending moments, bending stresses, and shear loads along the lengths of both rockets, considering aerodynamic force distributions and inertial effects[2] by applying standard beam theory and established loading profiles during flight. This produced Fig. 11 and 12 to contrast the structural loads experienced by Agniastra and Vayuvega.

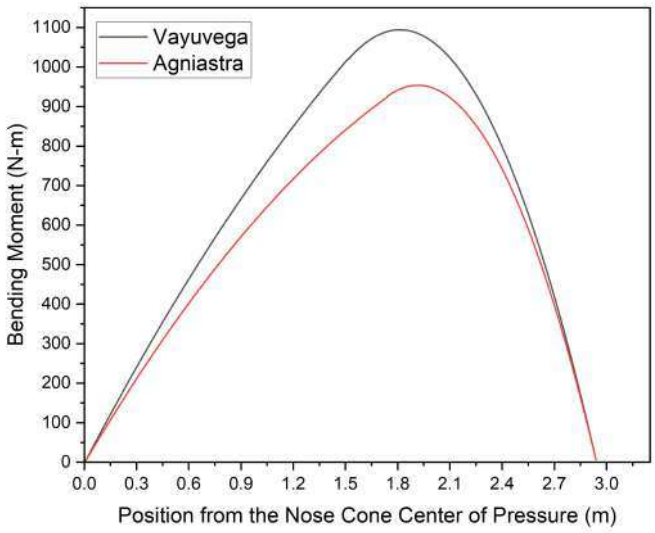


Figure 11 Position vs. Bending Moment

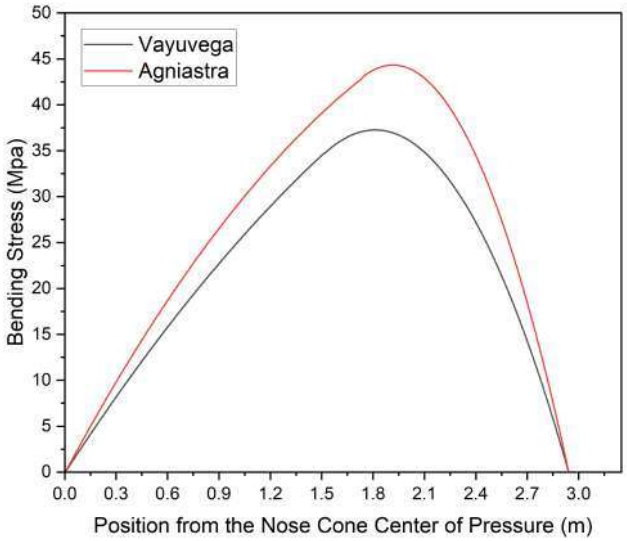


Figure 12 Position vs. Bending Stress

The bending moment plot indicates that Vayuvega encounters marginally higher peak bending moments; however, the bending stress plot reveals that Vayuvega sustains lower maximum bending stresses despite the higher moments, a result that directly correlates with the increased section modulus.

The shear load distribution between both rockets remains consistent, affirming that the overall aerodynamic loading profile is similar. It is observed that the shear load distribution is zero at the position of the maximum bending moment, verifying the study[2].

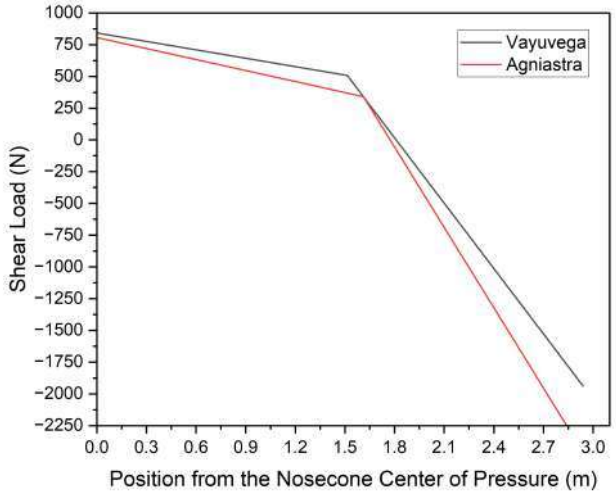


Figure 13 Position vs. Shear Load

Based on the calculated outcomes and plotted comparisons, the team deduced that Vayuvega achieves a FOS of 1.51, representing an advancement over Agniastra's FOS of 0.84. These enhancements substantiate our design choices and confirm that Vayuvega is capable of enduring greater structural loads during flight without the risk of failure. Refer to Appendix L for calculations of the load analysis on Vayuvega.

Surface Roughness

Minimising viscous drag was a primary goal during the rocket development phase. A study was undertaken to assess the influence of surface treatments, particularly painting, on the roughness of the body tube and its subsequent effect on viscous drag during ascent. The test setup involved surface roughness measurements conducted with ST400, a 3D Non-Contact Confocal Profilometer, suitable for surface topographical analysis. Two body tube samples were prepared for evaluation. The first sample was an unpainted composite body tube, representing the raw material immediately after manufacturing. The second sample, while identical in material, was treated with a primer and paint coating to replicate the final flight configuration. Each sample underwent surface levelling to address microscopic form deviations. Measurements were performed in accordance with ISO 25178 surface texture standards[3]. No S-filter was applied, and a Gaussian L-filter with a cut-off of 0.8 mm was employed to isolate the relevant texture wavelengths.

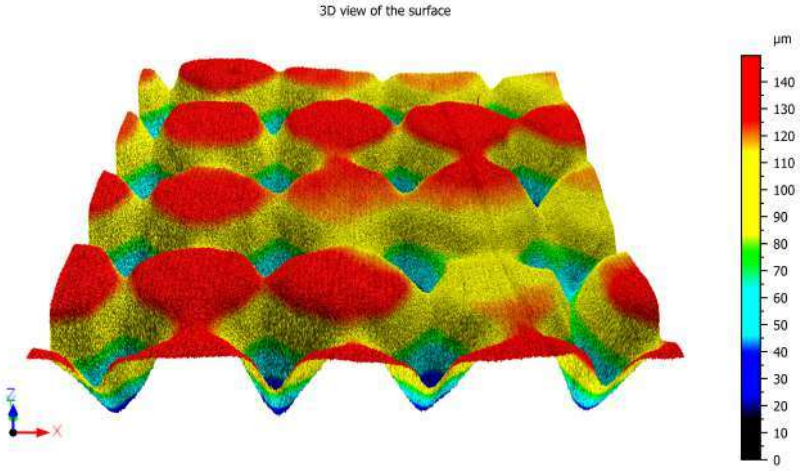


Figure 14 Surface Topology of Unpainted Body Tube

The unpainted composite body tube displayed an average surface roughness height (S_a) of 4.007 µm and a maximum surface roughness height (S_z) of 45.69 µm. Additional parameters, including skewness (S_{sk}) of -0.60 and kurtosis (S_{ku}) of 3.745, suggested a surface characterised by valley features.

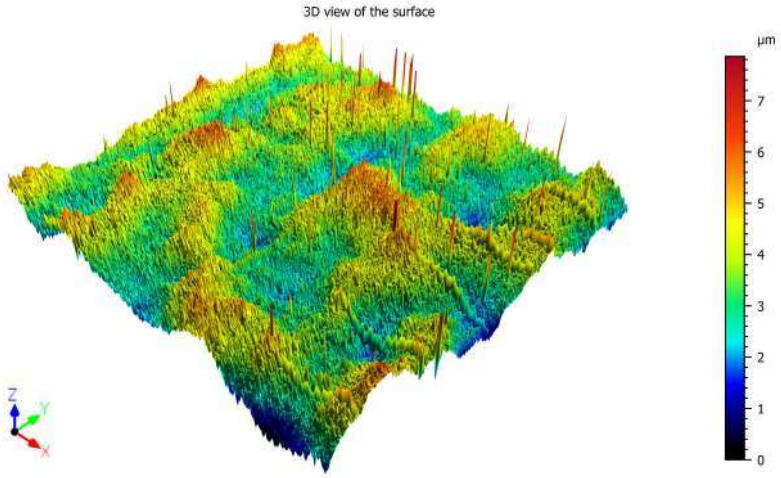


Figure 15 Surface Topology of a Painted Body Tube

In contrast, the painted composite body tube exhibited a markedly smoother surface, with an average surface roughness height (S_a) of 0.3408 µm and a maximum surface roughness height (S_z) of 8.262 µm. The positive skewness

(S_{sk}) of 0.3764 and the higher kurtosis (S_{ku}) of 5.814 indicated a more favourable surface texture. For further details, refer to Appendix B.G.

The experimental results confirmed that the application of a paint layer significantly diminishes surface roughness in composite body tubes. The painting process effectively smooths the micro-roughness present in raw composites, leading to a smoother surface. To further assess the aerodynamic advantages, we determined the viscous drag coefficient (C_f) for both samples. The unpainted body tube recorded a viscous drag coefficient of 0.401, whereas the painted body tube showed a lower coefficient of 0.285. The reduction in C_f was strongly correlated with the observed decrease in surface roughness. The notable reduction in both surface roughness and viscous drag coefficient underscores the efficacy of applying a painted finish.

Manufacturing

This year, the team manufactured the body tubes on 3D-printed mandrels made from PLA+ filament. The tolerances for the mandrels were determined by analysing multiple test prints on a single printer. The team designed the mandrels in separate parts to facilitate long layups.



Figure 16 Mandrel Assembled during Layups

The printed mandrels are prepared by smoothing the surfaces and ensuring tangency between each part. Next, a dual-layer coating of PVA to the mandrel is applied to prevent the composite layup from sticking. Then, the mandrel is covered with a plastic sheet, ensuring no surface remains exposed to the environment.

For this project, the team adopted the heat shrink tape method to ensure uniform pressure throughout the part. The shrink tape evens out resin-rich areas and minimises air voids. These improvements allowed the team to add more layers than possible with conventional hand layup methods. The team quantified the comparison between the shrink tape method and conventional hand layup by calculating the void fraction and fibre volume fraction using ASTM D2734-164[4] and ASTM D3171 Method II[5]. The properties of the constituent components of the layup are taken from datasheets and calculated accordingly. For uniform comparison, a single dimension was followed for all layups.

Table 4 Void and Fibre Volume Fraction Results

Composite	Method	Void Fraction (%)	Fibre Volume Fraction (%)
GFRP	Conventional	1.56	47.2
	Heat Shrink Tape	0.55	56.3
CFRP	Conventional	2.03	48.6
	Heat Shrink Tape	0.94	54.3

From the results shown in Table 4, we see lower void fractions and higher fibre volume fractions achieved through the shrink tape method, validating the layup process.



Figure 17 Composite Tubes Manufactured using Shrink Tape



Figure 18 Body Tubes Pre-Painting

3. Couplers

Two couplers support the body tubes with an inner diameter of 116 mm, each serving different purposes. Both couplers have a thickness of 2.5 mm with the same backing derived earlier. The coupler adjoining the main and drogue bay is made of GFRP to ensure RF transparency. The team securely fastened the avionics setup inside the GFRP coupler, bordered by the recovery bulkheads. A switch band is affixed at the centre with epoxy, supporting the camera mount and the pull pin slots while simplifying the bay assembly. The team manufactured this coupler using the methods described in Section II.A.2.

Table 5 Coupler Dimensions

Coupler Name	Length	Material
Avionics Coupler	390 mm	GFRP
Motor Bay Coupler	300 mm	Aluminium



Figure 19 GFRP Avionics Coupler

The team manufactured the motor bay coupler using Aluminium 6061-T6, shifting from its CFRP predecessor. Post-flight analysis of the AgniAstra rocket revealed a structural failure originating at the motor bay coupler. The team corroborated this failure with a subsequent study of the stress and bending moment on the rocket. Since this coupler experiences the highest axial stress, the team opted for aluminium as its isotropic behaviour ensures uniform strength in all directions, offering consistent multidirectional load resistance[6].



Figure 20 Motor Bay Coupler (a) Isometric View, (b) Section View

The team also optimised the coupler assembly by utilising aluminium's machinability. The design integrated a thrust plate and centring extrusions into the coupler, thereby reducing assembly complexity with the fuselage. The team machined an outer ring of 126 mm on the coupler to facilitate smoother airframe integration. The team performed specific design iterations to distribute local stress concentrations by improving load paths. Offsetting bolts across different stress planes and filleting sharp regions enhanced the coupler's ability to handle loads safely, achieving a safety factor of 9.45.

4. Fins

The team fabricated the set of four trapezoidal fins using Aluminium 6061-T6. Vayuvega follows a fin attachment style similar to the prior fin-stringer system rockets with some changes. This year, the stringers and fins are integrated and machined from a 5-axis CNC milling machine. This removes the complex welding setup followed by prior rockets, which has risks of microcracks or thermal distortion. The single-machined part also provides better stress distribution while streamlining the assembly. This fin-stringer part fastens at the proper aerodynamic alignment with the two centring rings on either side. The bolts chosen for this year are M5, shifted from M3 from last year, to provide better thread engagement and a larger shear cross-section.

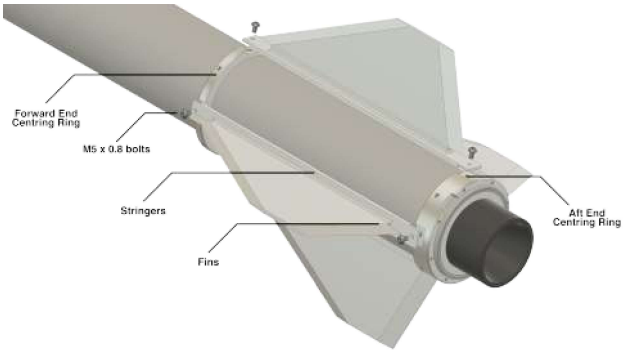


Figure 21 Exploded View of Fin-Stringer Attachment

The trapezoidal shape is chosen due to its capability to provide increased surface area away from the root chord, thereby generating more counter-rotating moment essential for stabilising the rocket. This shape offers improved resistance to deformation resulting from impact damage. Specific fin parameters were filtered to optimise performance after extensive analysis using computational tools such as ORK, RASAero II and AeroFinSim.

Table 6 Fin Dimensions

Shape	Trapezoidal with hexagonal cross section
Number of Fins	4
Material	Aluminium 6061
Root Chord	250 mm
Tip Chord	40 mm
Semi Span	98.50 mm
Thickness	4.50 mm
Sweep Length	171.16 mm
Half Wedge Angle	5°



Figure 22 Fin Isometric View and Profile

The fin design optimisation was conducted through a parametric iteration process using OpenRocket and AeroFinSim software. OpenRocket was employed to construct the baseline rocket model and simulate a range of fin geometries by systematically varying the root chord length from 240 mm to 300 mm and the semi-span from 95.5 mm to 98.5 mm. For each configuration, we evaluated key performance parameters such as stability margin at the launch rod, in-flight dynamic behaviour, and the ability to achieve the target apogee of 30 000 ft.

Each fin design was then analysed using AeroFinSim to determine key aeroelastic and structural dynamic parameters, including flutter velocity, divergence speed, bending frequency and torsional frequency. These metrics were essential in assessing the fin's ability to withstand high dynamic pressure conditions and resist structural instabilities throughout the transonic and supersonic regimes.

The final configuration was selected using a multi-objective optimisation framework, ensuring sufficient static margin on the launch rail, maintaining a flutter velocity safely above 1.5 times the rocket's maximum velocity and achieving favourable dynamic stability with adequate separation between excitation frequencies and structural natural modes. This comprehensive methodology ensured a fin design with optimal aerodynamic performance, structural integrity and stability throughout the entire flight. Refer to Appendix I for a summary of fin design iterations and associated performance parameters.

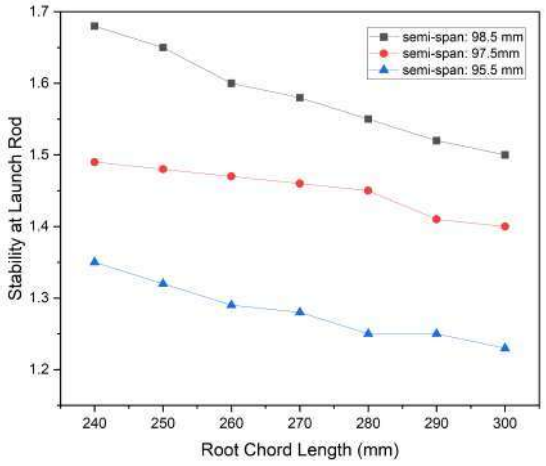


Figure 23 Root Chord vs Launch Rod Stability

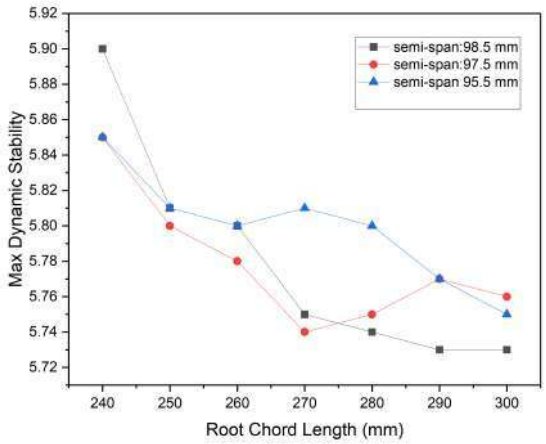


Figure 24 Root Chord vs Max Dynamic Stability

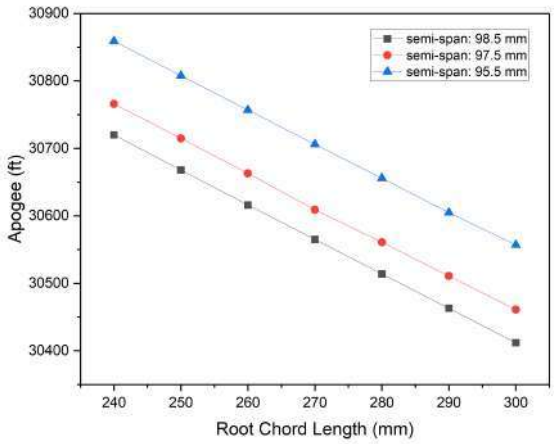


Figure 25 Root Chord vs Apogee

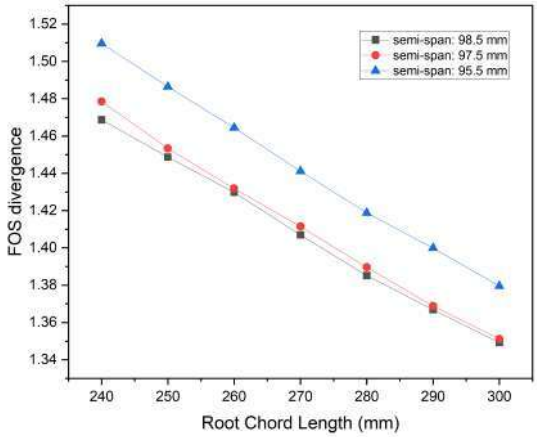


Figure 26 Root Chord vs FOS Divergence

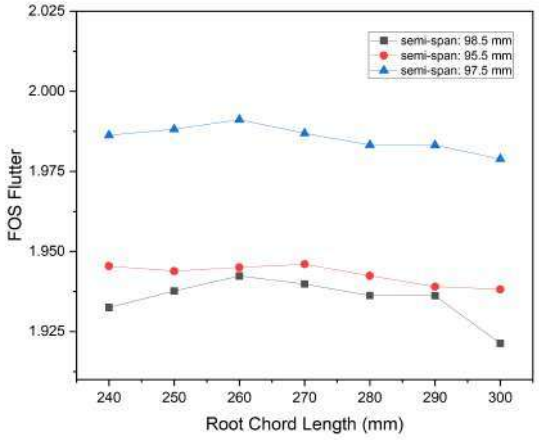


Figure 27 Root Chord vs FOS Flutter

A significant factor during the design process is fin flutter, an aeroelastic phenomenon that occurs at high speeds. This instability arises from the physical characteristics of the fins, triggering an amplification feedback loop, which leads to increased oscillation and eventual failure. The flutter velocity of the fins is determined by Eq. (1).

$$v_f = a \times \sqrt{\frac{2 \times G \times (AR + 2) \times t^3}{1.337 \times P \times (\lambda + 1)(c \times AR)^3}} \tag{1}$$

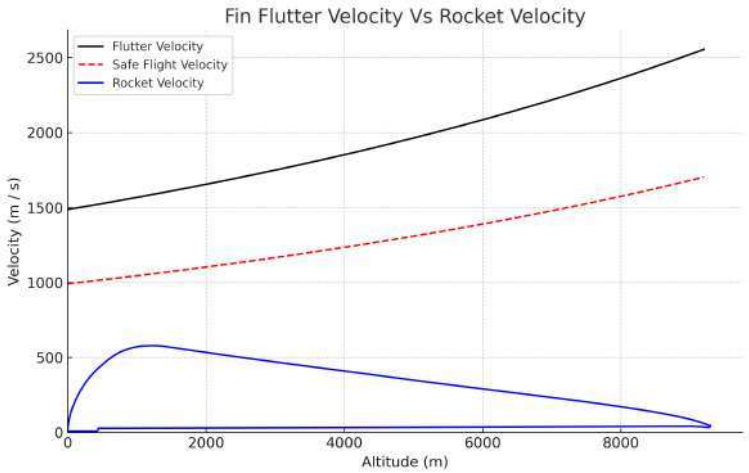


Figure 28 Fin Flutter Velocity and Rocket Velocity vs. Altitude

A MATLAB code is developed to visualise the difference between the fin flutter velocity and the rocket's speed throughout the entire ascent phase. Flutter velocity is also assessed using the FinSim software. The calculated flutter velocities from Equation 1 and FinSim are 1267.69 m s^{-1} and 1119.96 m s^{-1} respectively, surpassing both the maximum rocket velocity and the safe flight velocity (as shown in Fig. 28). Furthermore, fin divergence is also considered, with the divergence velocity coming out to be 837.33 m s^{-1}. Refer to Appendix J for the MATLAB code for Fin Flutter.

The simulation results revealed critical insights:

1) Decreasing sweep angle led to an increase in drag, consequently reducing the apogee.
2) Increasing the root chord resulted in decreased stability caliber and fin flutter velocity.
3) Conversely, decreasing the tip chord led to higher apogee and fin flutter velocity.
4) Increasing the semi-span increases the stability caliber but significantly reduces the fin flutter velocity. Increasing the thickness of the fin reduces the apogee while increasing the fin flutter velocity.

Aerodynamic Analysis of Various Fin Cross Sections

To determine the most aerodynamically efficient cross-sectional geometry for Vayuvega's fins, several fin cross sections were analysed based on their relevance to supersonic and transonic fin designs in aerospace applications such as: hexagonal, bi-convex, double wedge, single wedge, hexagonal blunt-based, NACA 2411 and NACA 0011 airfoils. Each profile was first modelled with uniform reference dimensions to ensure consistent comparative analysis. To simulate aerodynamic performance parameters, the simulations were run at MaxQ conditions. The simulations were conducted across multiple angles of attack varying from 0° to 12°, to evaluate performance under varying flight conditions.

The k-ω SST turbulence model was employed due to its superior capability in resolving near-wall flows and boundary layer behaviour through its blending function approach. Boundary conditions included Pressure Inlet, Pressure Farfield, and No-Slip Wall applied to the fin surfaces. Steady-state simulations were performed at Mach numbers and Reynolds numbers representative of the rocket's actual flight environment.

For each configuration and angle of attack, both drag force and lift force were extracted. Additionally, pressure and velocity contours were analysed to visualise flow separation, stagnation, and wake regions. The fin geometry exhibiting the lowest drag across angles of attack was identified as the most suitable for enhancing Vayuvega's flight performance and stability.

a) Hexagonal Cross-Section

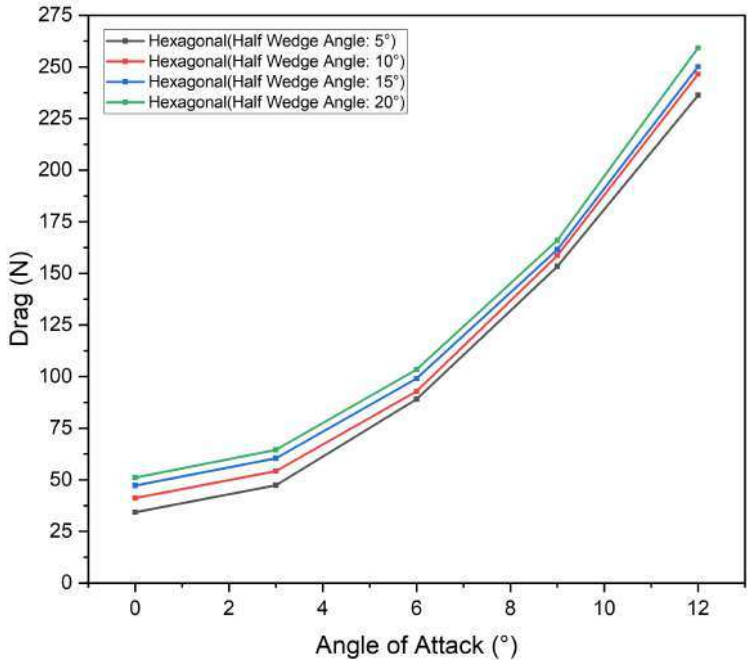


Figure 29 Angle of Attack vs Drag for Hexagonal Cross Section across varying Wedge Angles

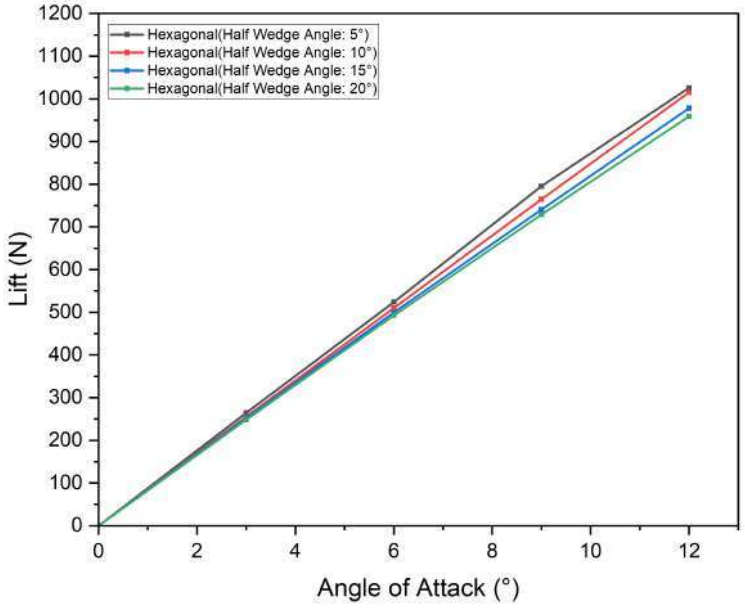


Figure 30 Angle of Attack vs Lift for Hexagonal Cross Section across varying Wedge Angles

b) Bi-Convex Cross Section

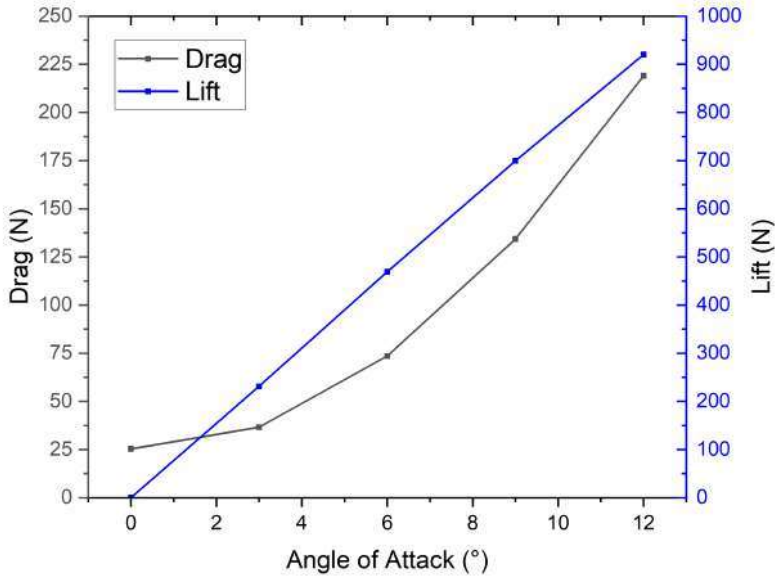


Figure 31 Angle of Attack vs. Drag and Lift for Bi-Convex Cross Section

c) Double Wedge Cross Section

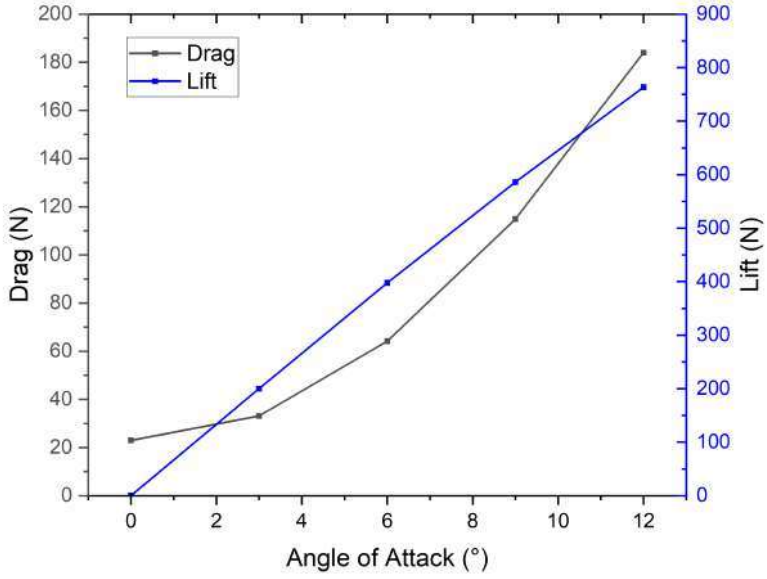


Figure 32 Angle of Attack vs Drag and Lift for Double wedge Cross Section

d) Single Wedge Cross Section

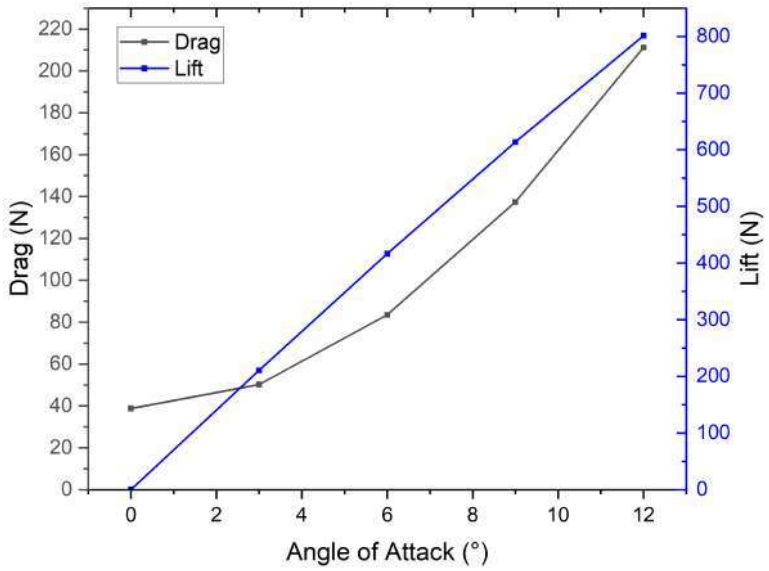


Figure 33 Angle of Attack vs Drag and Lift for Single wedge Cross Section

e) Hexagonal Blunt-Based Cross Section

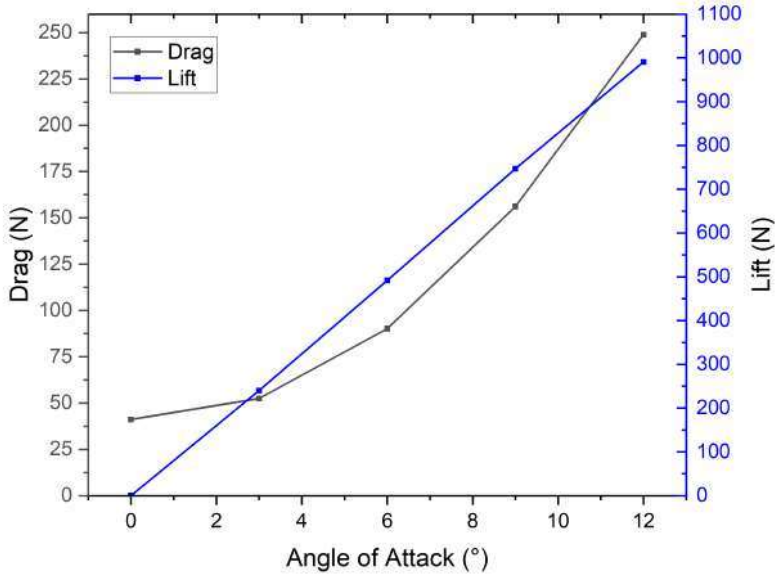


Figure 34 Angle of Attack vs Drag and Lift for Hexagonal Blunt Based Cross Section

f) NACA Airfoil Cross Sections

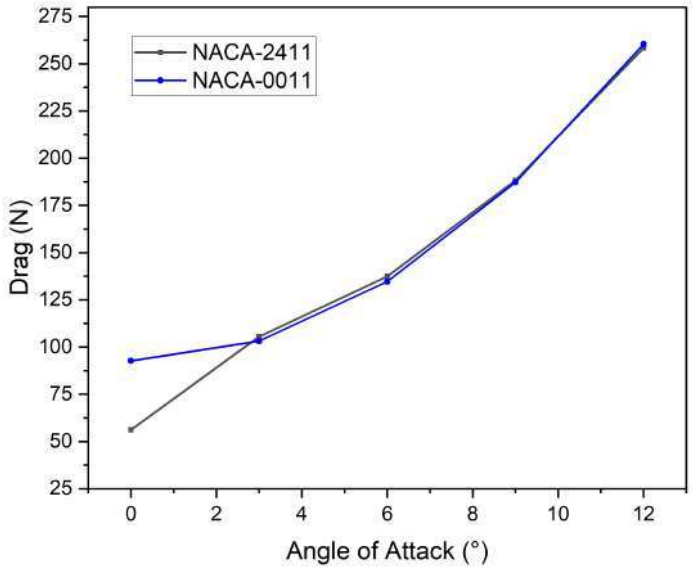


Figure 35 Angle of Attack vs Drag for NACA Airfoils 2411 and 0011

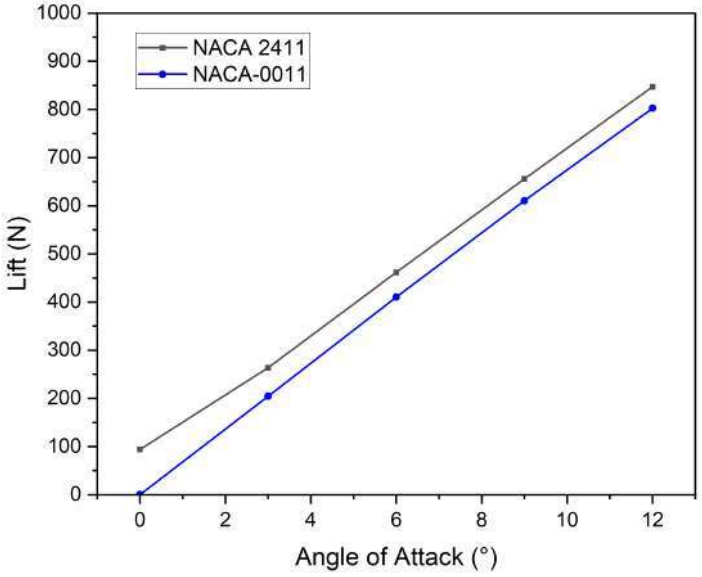


Figure 36 Angle of Attack vs Lift for NACA Airfoils 2411 and 0011

Based on CFD simulations across angles of attack ranging from 0° to 12° at Mach 1.71, three fin cross-sectional geometries were chosen: (a) double wedge; (b) bi-convex; and (c) hexagonal. These were chosen due to their superior aerodynamic performance, specifically for the lower drag values under MaxQ conditions. The double wedge profile

exhibited the least drag overall, making it ideal for supersonic regimes where sharp leading edges help maintain attached flow. The bi-convex section followed closely, offering a balance between low drag and moderate lift, optimal for stability. The hexagonal cross section, while slightly higher in drag, was selected for its structural simplicity in manufacturing.

FSI and Modal Analysis

Following the aerodynamic analysis, FSI was conducted to evaluate the structural response of the three selected fin cross sections: double wedge, bi-convex, and hexagonal under MaxQ conditions. The primary objective was to assess the deformation and stress distribution on each fin at various angles of attack - 0°, 3°, 6°, 9°, and 12°. A two-way coupled FSI setup was used, where pressure loads were mapped from Fluent onto the structural solver to account for realistic aeroelastic behaviour.

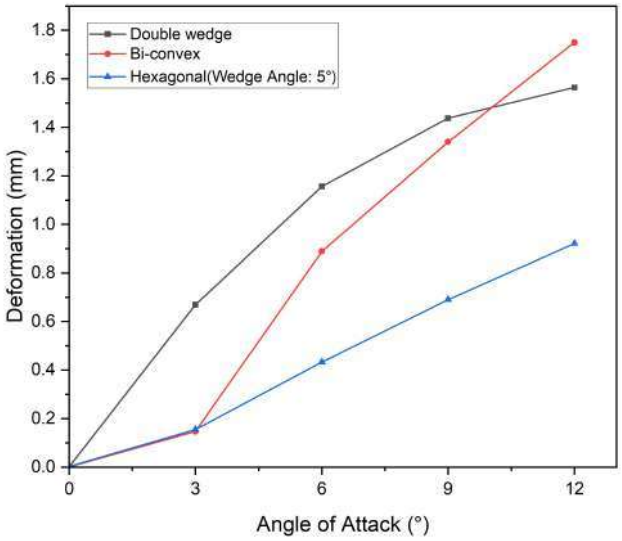


Figure 37 Angle of Attack vs Total Deformation

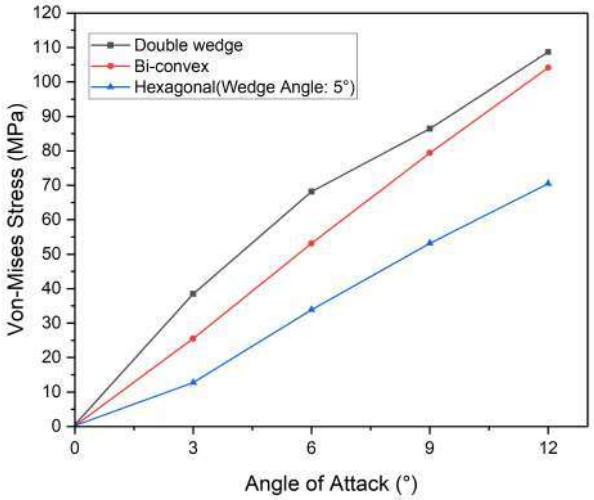


Figure 38 Angle of Attack vs Von-Mises Stress

Following the CFD and FSI studies, a modal analysis was performed to determine the natural vibration characteristics of the fins. This was essential to ensure that the structural frequencies of the fins did not coincide with the aerodynamic excitation frequencies, which could lead to resonance and potential structural failure.

Table 7 Excitation Frequencies with varying Root Chord

Root chord (mm)	Height (mm)	Thickness (mm)	F_bending (Hz)	F_Torsional (Hz)
240	98.5	4.5	377.798	498.688
250	98.5	4.5	377.798	481.668
260	98.5	4.5	377.798	465.81
270	98.5	4.5	377.798	450.926
280	98.5	4.5	377.798	436.963
290	98.5	4.5	377.798	423.87
300	98.5	4.5	377.798	411.509

The analysis was conducted using AeroFinSim, where the geometric parameters of the fin, such as semi-span (98.5 mm), and thickness (4.5 mm), were kept constant, except for root chord, which was varied to study its effect on modal characteristics. The natural frequencies for bending and torsional modes were extracted for each configuration.

Results showed that while the bending frequency remained constant at 377.798 Hz due to unchanged semi-span and thickness, the torsional frequency decreased progressively with increasing root chord. This indicates increased flexibility in torsion as the chord lengthens, which must be considered in dynamic stability assessments. The modal analysis ensured that the final fin design optimised aerodynamic performance and maintained structural integrity under vibrational loads.

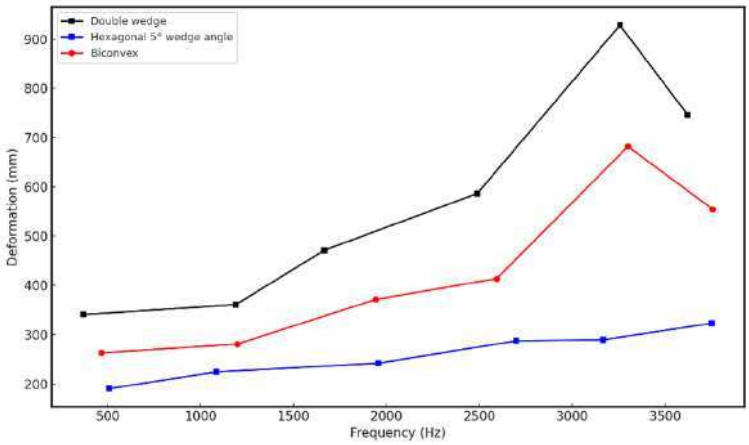


Figure 39 Natural Frequency vs Total Deformation

Among the three shortlisted geometries: double wedge, bi-convex, and 5° hexagonal, the double wedge fin exhibited a first bending frequency lower than the excitation range, making it highly vulnerable to resonance. This could result in large amplitude oscillations and potential structural failure under flight loads.

The bi-convex fin's bending frequency was just below that of the hexagonal fin. Although this design offered a moderate safety margin, it posed some risk, especially under fluctuating dynamic pressures during supersonic flight.

The 5° hexagonal fin demonstrated both bending and torsional natural frequencies safely above the excitation range, confirming its resonant stability. Additionally, the simplicity of its geometry made it easier to manufacture and more structurally robust, providing an ideal balance between aerodynamic performance and structural integrity. Considering the combined results from aerodynamic drag, total deformation, stress and modal frequency separation from excitation, the 5° hexagonal fin was ultimately chosen as the optimal configuration for Vayuvega.

Decision Tree for Fin Parameters

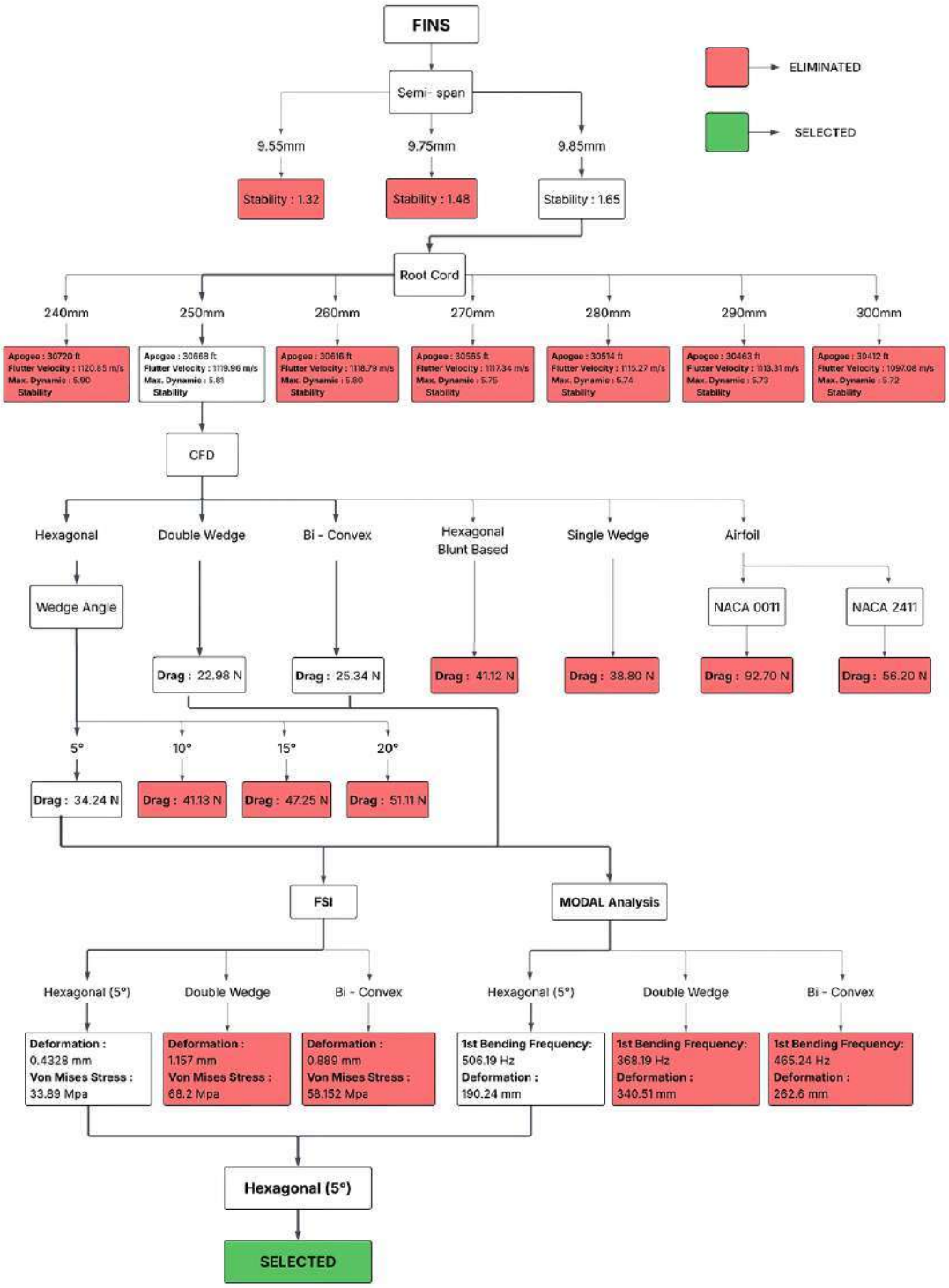


Figure 40 Decision Tree for Fin Parameters

5. Boattail

Vayuvega features a significant design enhancement with the introduction of a boattail. This addition marks a key improvement over previous iterations by addressing base drag, one of the major contributors to aerodynamic resistance in reaching the desired apogee. The boattail tapers the rear end of the rocket, allowing smoother airflow separation and reducing the low-pressure wake region behind the rocket. By incorporating this, we aim to optimise flight dynamics and achieve better performance in our launch objectives. The team decided to manufacture the boattail with Aluminium 6061 T6. This choice is owed to the machinability of the part to accommodate slots for the fins and holes for the centring ring. This eases assembly at the aft end of the fuselage.



Figure 41 Boattail Isometric View

Table 8 Boattail Dimensions

Parameter	**Value**
Shape	Conical
Material	Aluminium 6061
Total Length	80 mm
Fore Diameter	126 mm
Aft Diameter	106 mm
Wall Thickness	2.5 mm

CFD analysis was conducted to determine the optimal length that minimises drag while maintaining flight stability. The aft diameter was fixed at 106 mm to ensure adequate clearance between the motor and the boattail. Simulations were run for boattail lengths ranging from 60 mm to 110 mm. Results showed a steady decrease in drag from 1045.7 N at 60 mm to 952.56 N at 110 mm. However, increasing length also lowered the static stability margin, which dropped from 1.67 to 1.39. Since stability below 1.5 is undesirable, lengths beyond 90 mm were ruled out. An 80 mm boattail was chosen as the optimal configuration, offering a low drag of 985.63 N while maintaining a safe stability margin of 1.65. This selection provides a balanced trade-off between aerodynamic efficiency and flight stability.

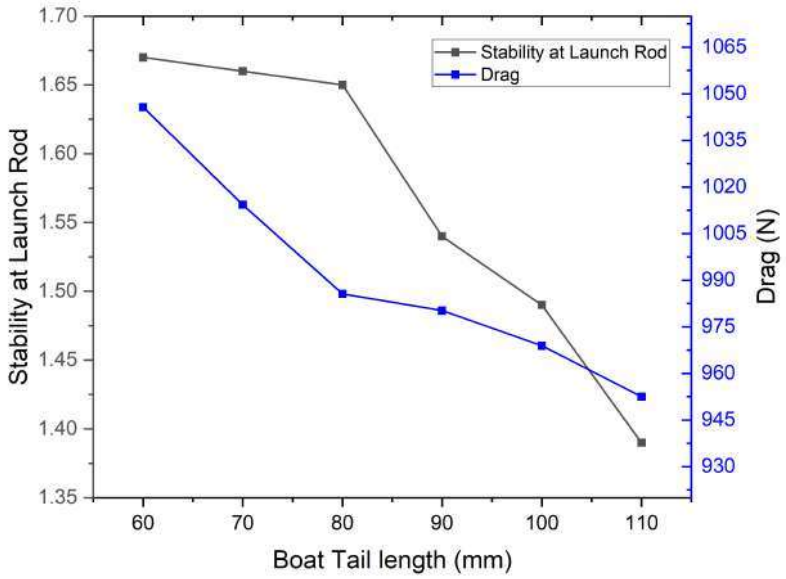


Figure 42 Boattail Length vs Stability at Launch Rod and Drag

6. Rail Buttons

This year's rocket design incorporates two large airfoiled 1515 rail buttons, replacing the standard Delrin COTS buttons used in prior iterations. These components are positioned to provide optimal guidance along the launch rail, ensuring a straight and stable ascent. One rail button is mounted to a centring ring in the motor bay, while the other is affixed directly to the thrust plate, offering support under the full load of the rocket's weight on the launch rail secured using M6 $\times$ 1.0 bolts with countersunk head. The switch to airfoiled rail buttons was driven by the goal of minimising aerodynamic drag[7].



Figure 43 Rail Buttons

7. Flight Analysis

Flight simulations are conducted using OpenRocket, RASAero II, and the in-house 6-DoF simulator code. The simulation environment is configured to reflect the geographic and meteorological conditions prevalent in Texas during summer. Specifically, the simulations are set at an elevation of 2683 ft ASL, with average wind speeds of 5 m s^{-1}, a temperature of 35 °C, and a pressure equivalent to 0.903 atm. The launch angle is set at 6°, and the effective launch rail length is determined to be 4.84 m. OpenRocket was primarily utilised for rocket design, providing an apogee estimate of 30 632 ft, while RASAero II yielded an apogee estimate of 30 967 ft for the same conditions. The 6-DoF simulator code was employed to ascertain an apogee approximation of 30 093 ft. The stability calibre is calculated using Eq. (2), and the stability at the launch rod is calculated to be 1.65, with a maximum value of 5.80, as shown in Fig. 44.

$$\text{Stability Margin} = \frac{(C_p - C_g)}{D} \tag{2}$$

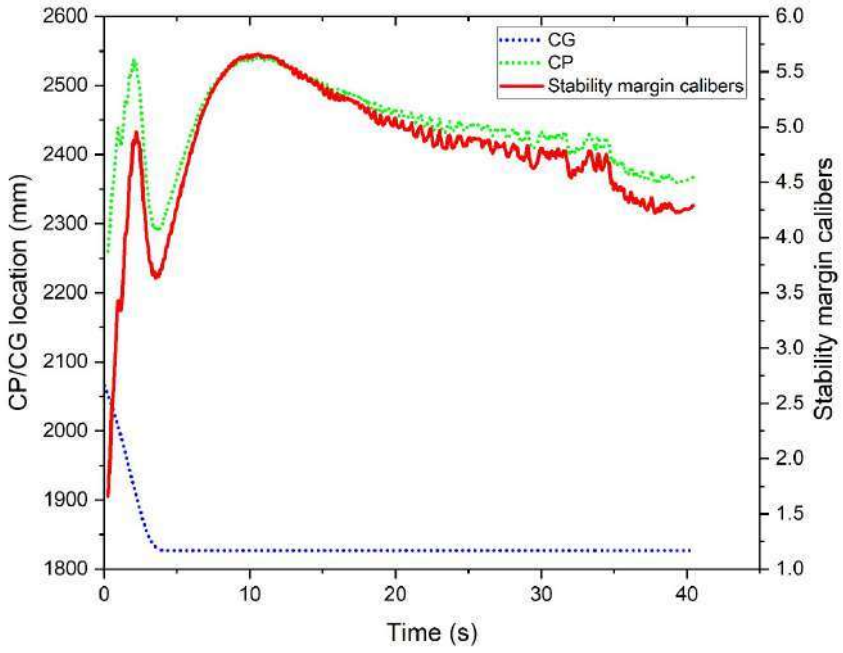


Figure 44 Stability Margin Graph

Aerodynamic stability of the rocket is evaluated through a combination of simulation-based and analytical methods to ensure a comprehensive and cross-validated assessment. One of the primary tools used for this purpose is OpenRocket, which provides detailed flight simulations and stability analyses. To supplement this, CFD simulations are performed across a range of Mach numbers from 0.3 to 1.71, encompassing the subsonic, transonic, and supersonic regimes. This Mach range is selected to capture the full aerodynamic behaviour during the powered ascent phase up to motor burnout.

For each Mach number within this range, the simulations yield precise flow field data from which the CP is extracted. These values are then combined with the corresponding CG, derived from OpenRocket, to analytically compute the static stability margin. The stability values from OpenRocket are plotted alongside those obtained from CFD analysis. This combined approach has validated that the rocket maintains aerodynamic stability throughout its flight envelope. Consistent results from both OpenRocket simulations and CFD analysis confirm the reliability of the design, affirming the robustness of the rocket's stability characteristics.

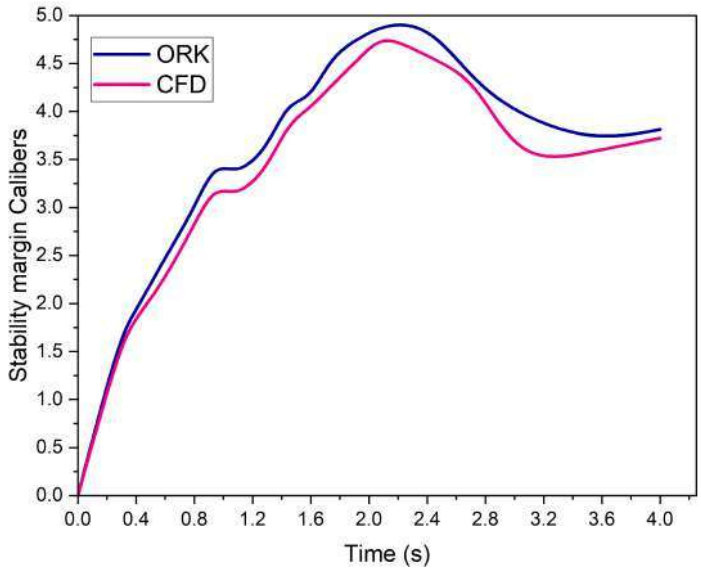


Figure 45 Stability Analysis during the Boost Phase

Drag Analysis

To analyse and enhance the aerodynamic performance of Vayuvega, the team performed an extensive set of CFD simulations using the full rocket geometry. Simulations were conducted at Mach numbers ranging from 0.3 to 1.7, in increments of 0.1. Each simulation was run at the corresponding altitude and atmospheric conditions to reflect realistic flight scenarios. In the subsonic regime, drag was mainly due to viscous effects with the flow remaining mostly attached. Surface geometry had a direct impact on this drag. As the rocket entered the transonic regime, shock bubbles formed near the surface, sharply increasing drag due to emerging compressibility effects. In the supersonic regime, pressure drag became dominant, driven by strong shock waves at the nosecone and other discontinuities. Viscous drag remained but was much less significant compared to wave and compressibility-induced drag. This methodology supported a data-driven design process that enhanced aerodynamic performance across the full flight profile. Refer to Appendix L for a detailed analysis of the drag contributed by various components of the rocket.

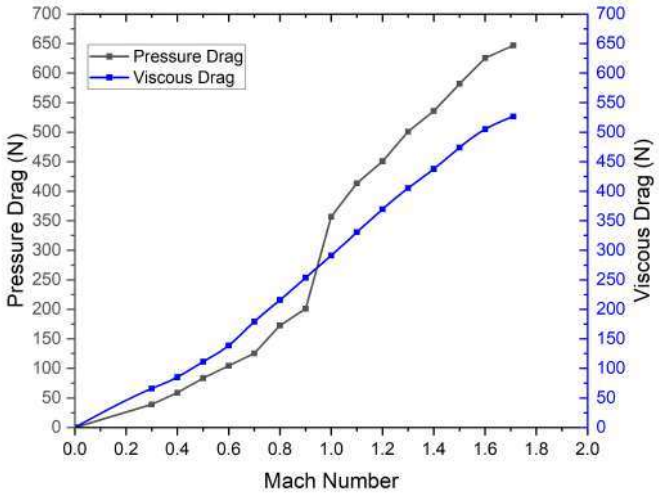


Figure 46 Pressure and Viscous Drag vs Mach Number

Additionally, CFD simulations were performed on two configurations: one with hexagonal bolts and another with circular bolts. This was done to assess the bolts' contribution to overall drag. Across all Mach regimes, the configuration with circular bolts consistently showed lower drag compared to hexagonal bolts. The smoother profile of the circular bolts resulted in reduced flow separation and minimised localised pressure build-up, leading to better aerodynamic performance. These findings guided the selection of bolt geometry for final design optimisation.

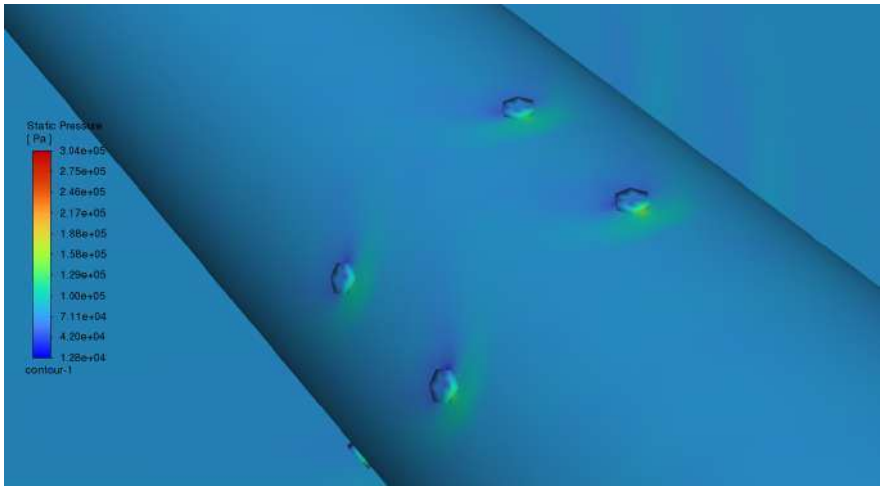


Figure 47 Static Pressure Contour on Hexagonal Bolts

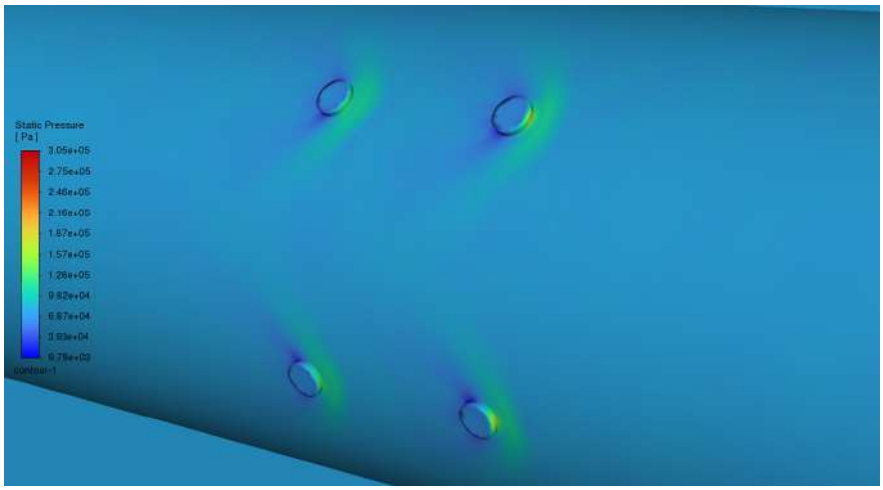


Figure 48 Static Pressure Contour around Circular Bolts

B. Propulsion

Vayuvega employs the COTS AeroTech O5500X-PS solid rocket motor for its propulsion system. The motor is housed in the CFRP motor bay and is attached to the integrated thrust plate and motor bay coupler using a 3/8"-16 UNC eyebolt that bears the motor's thrust. Twelve M5×0.8 bolts evenly distribute this thrust load. To ensure proper alignment, the team set two centring rings at the aft end and integrated extrusions on the motor bay coupler at the forward end.

The team selected this motor for its total impulse of 21 348.0 N s, which enables the rocket to achieve its target apogee. Its high thrust-to-weight ratio of 15.32:1 ensures compliance with rail departure velocity and stability requirements as per DTEG guidelines. The team also considered the motor's availability, which helped minimise potential logistical challenges during competition preparation.

1. Motor Details

The AeroTech O5500X-PS motor was certified by TRA in January 2023, making it eligible for use as a COTS motor in the 2025 IREC. The motor measures 98 mm in diameter and 1491.2 mm in length, with a wet mass of 16.78 kg, including 9.78 kg of propellant. The motor uses Propellant X™—a high-Isp formulation known for its bright white flame and moderate smoke. The O5500X-PS is built with a thick filament-wound integrated fibreglass liner and casing and a glass-reinforced phenolic nozzle. The motor is a DMS, indicating it is designed for single-use operation, where 7 grains are permanently bonded inside the integrated liner and casing. The forward bulkhead of the motor is bonded to the casing with manufacturer-supplied epoxy. Table 9 outlines the motor's performance characteristics, and Fig. 49 depicts the thrust-time curve.



Figure 49 Thrust-Time Curve

Table 9 Performance Characteristics of AeroTech O5500X-PS motor

Letter Classification	O
Total Impulse	21 384.0 N s (4807.31 lb s)
Average Thrust	5514.6 N (1239.73 lb)
Initial Thrust	6046.9 N (1359.39 lb)
Maximum Thrust	7551.5 N (1697.64 lb)
Burn Time	4.0 s
Propellant	Propellant X

Ignition is performed using the proprietary pyrogen igniter supplied with the motor. Two igniters will be installed to enhance reliability and minimise the risk of a hangfire. Ignition will be initiated through the ESRA-provided ignition system.

2. Retainer

An aluminium 6061-T6 aft retainer, 10 mm thick, is positioned at the bottom of the motor as a secondary retention mechanism to support its weight after burnout in the event of thrust plate bolt failure. Maintaining the axial position of the motor casing within the airframe ensures proper alignment and preserves the integrity of the propulsion system throughout the flight sequence. The retainer is attached to the aft centring ring via eight M4 bolts; for ease of assembly and precise alignment, the retainer features machined extrusions that fit into corresponding slots in the aft centring ring. This design simplifies installation and ensures accurate positioning of the bolt holes, reducing the chance of misalignment during assembly.

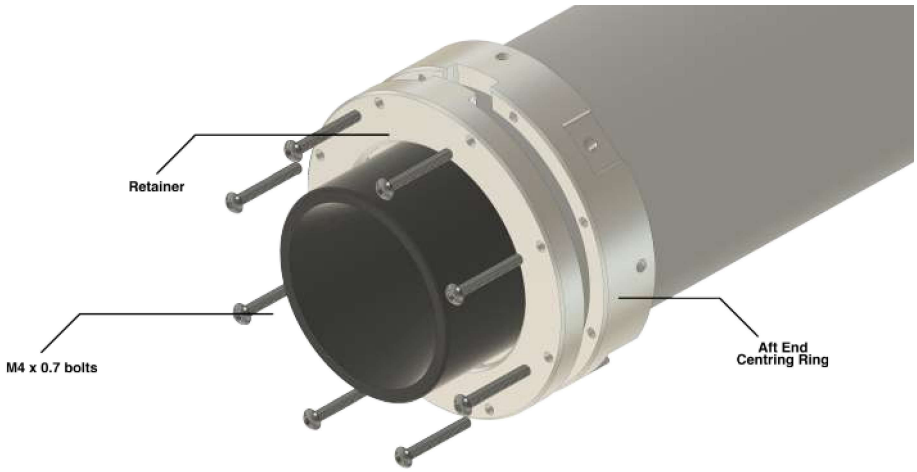


Figure 50 Retainer - Exploded View of Assembly

C. Recovery

The rocket is recovered as a whole using a dual-event parachute recovery system. This system consists of a drogue and a main bay, attached to the avionics coupler using four #6-32 shear pins. The drogue parachute is deployed at apogee, and the main parachute is deployed at 1500 ft AGL using 4F black powder. The recovery bulkheads consist of two charge wells each, containing the primary and redundant charges. The primary charge is activated first using the SRAD altimeter, and then the redundant charge is activated using the COTS altimeter.

1. Recovery Bulkheads

Two recovery bulkheads facilitate the recovery of Vayuvega. They are positioned to border the avionics coupler on both sides. Each recovery bulkhead has two charge wells integrated with the bulkhead. The dual charge well configuration was chosen for redundancy, further cementing the surety of the recovery events. The bulkheads are also designed with a step in their outer diameter. Along with that, a similar self-alignment extrusion is machined and sits on the triangular slot on the coupler, making assembly and positioning in the coupler easier. Four M6 shafts with threaded ends fasten the bulkheads while securing the avionics setup. One bulkhead bolts to the drogue bay to aid recovery. M10 eye bolts also fit the bulkheads for shock cord attachment.



Figure 51 Recovery Bulkheads

In this year's rocket, the team designed the bulkheads to reduce weight compared to its predecessor. The initial version of the bulkheads was analysed with structural simulations, giving us design space to work with[8]. The design space refers to the areas with the lowest stress concentration from the simulation. The main objective of the final version

was to maximise the performance of the bulkhead in terms of the stiffness-to-weight parameter with a safety factor[9]. Through an iterative design process, the team optimised the bulkhead topologically so that the shaved material geometry could provide the most efficient load path and a smoother stress gradient throughout the component[10].

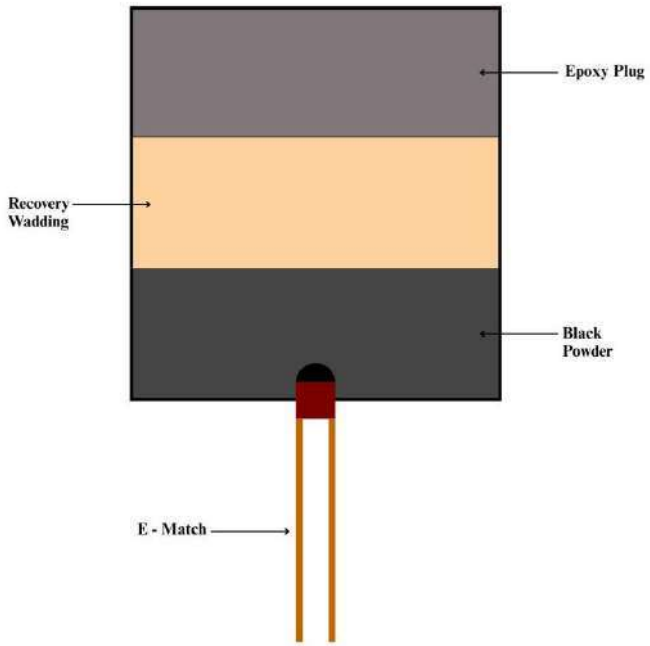


Figure 52 Charge Well Setup

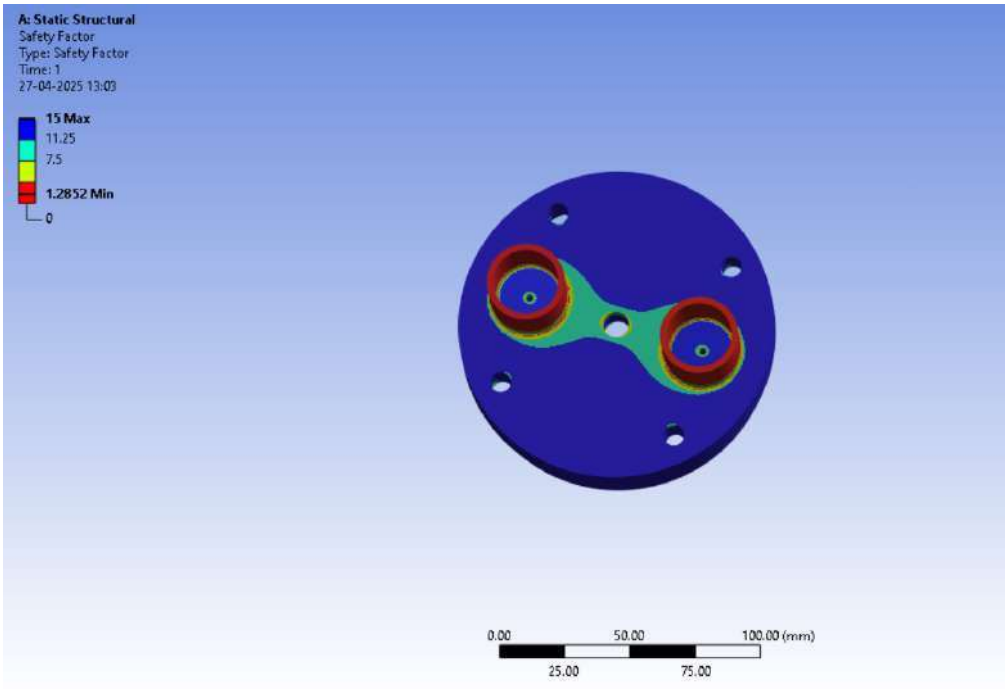


Figure 53 Safety Factor Obtained in the Basic Bulkhead

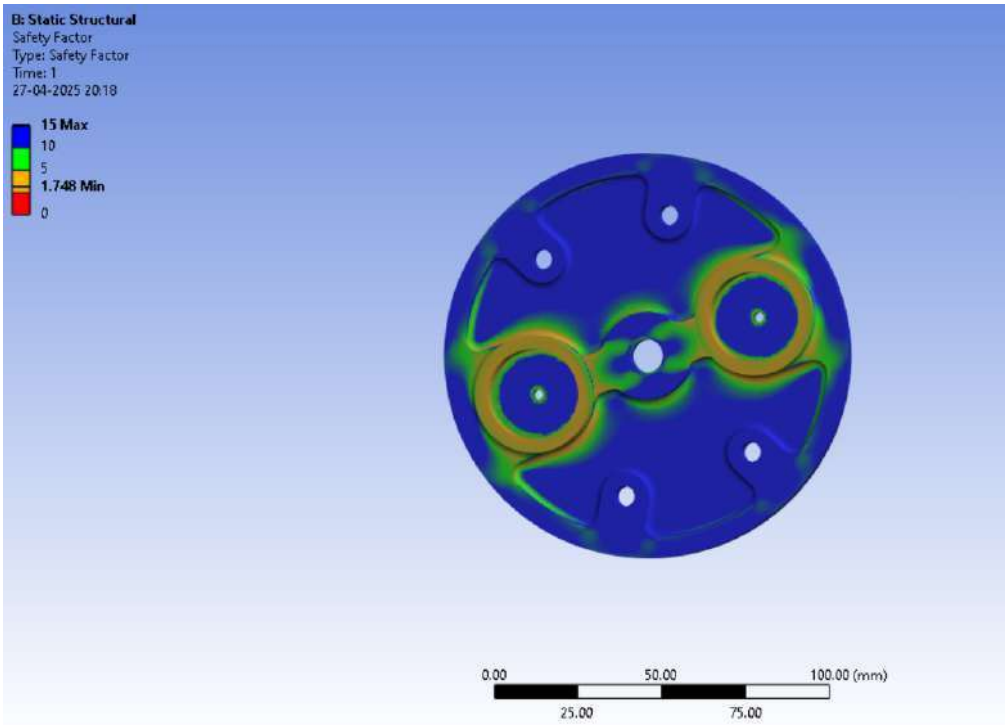


Figure 54 Safety Factor Obtained in the Topology Optimised Bulkhead

The minimum safety factor for the non-optimised version is 1.285, which is below the acceptable threshold of 1.4[9]. The simulation shows the minimum safety factors around the connection zones, indicating poor stress distribution. The minimum safety factor for the optimised version is 1.748, showing a uniform stress flow and no overtly stressed regions.

2. Parachute and Shock Cords

The drogue parachute is a 30" elliptical parachute, and the main is a 72" Iris compact parachute, from Fruity Chutes. The drogue and main parachutes are selected to achieve descent speeds of 27.89 m s^{-1} and 8.93 m s^{-1}, respectively. In the drogue bay, a 7 m long shock chord is connected to the parachute from the thrust plate. It attaches to the motor head using an eyebolt and links to the parachute with a quick link. Another 4 m long shock cord attaches from the parachute to the lower recovery bulkhead. It is secured to the bulkhead with an eyebolt, which connects the parachute using a quick link. Additionally, a swivel is attached to prevent entanglement of the suspension lines. The length of the shock chords is decided to ensure that the upper airframe does not collide with the lower airframe after drogue deployment.

In the main bay, a 7 m long shock chord is linked from the parachute to the upper recovery bulkhead. It is fastened to the bulkhead through an eyebolt and connected to the parachute using a quick link. Another 4 m long shock chord is attached from the parachute to the nosecone bulkhead. This is secured to the bulkhead via an eyebolt and connected to the parachute using a quick link. A swivel is attached to the main chute as well. The shock chords used are Kevlar, 1/2 in, 6000 lb as given by the manufacturer. Nomex blankets are used to protect the drogue and main parachutes.



Figure 55 Drogue Parachute setup



Figure 56 Main Parachute setup

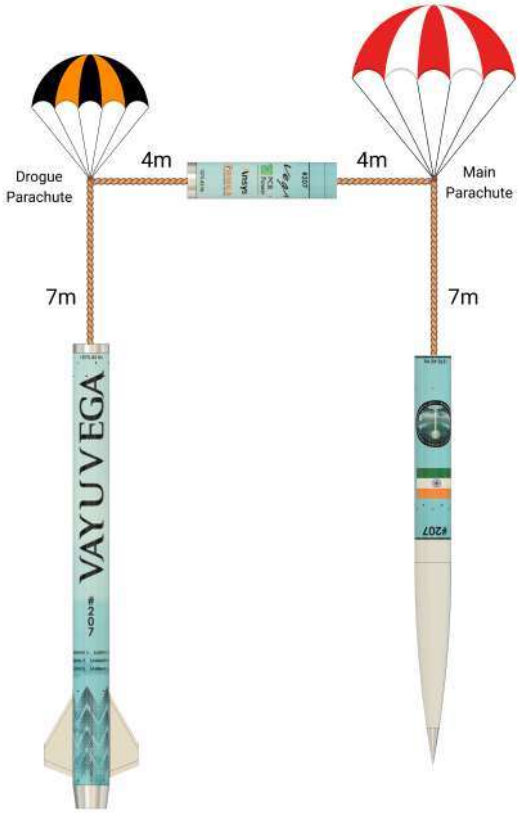


Figure 57 Shock Cord Lengths

Deployment Forces and Shock Loading

Deployment forces are calculated using the drag equation as shown in Eq.(3).

$$FD = C_D A \frac{\rho V^2}{2} \tag{3}$$

The deployment forces calculated for the drogue and main deployment, considering a safety factor, are found to be approximately 0.6 kN and 5.3 kN respectively. The maximum load ratings of the parachutes are more than what is calculated. The shock loading force for the shock chords is calculated to be approximately 1.4 kN and 5.2 kN for drogue and main ejection, respectively. The rating of the shock chord utilised is 26.7 kN (6000 lb), which is sufficiently higher than the calculations. Refer to Appendix L.I for the corresponding hand calculations.

Black Powder Mass

Determining the required charge for ejection involves calculating the shear strength of the shear pins and determining the necessary pressure buildup in the bay for their shearing. The shear strength of the #6 – 32 shear pin is 114 lb. The ideal gas equation, as shown in Eq. (4), is then used to calculate the amount of charge required.

$$pV = nRT \tag{4}$$

The calculated charge comes out to be 0.09 g, but considering inefficient burning of the charge at higher altitudes and a factor of safety, the decided amount of charge is 5 g and 5.5 g for drogue and main deployment, respectively.

D. Payload

Vrishabha, developed under the Vayuvega mission, is a compact 4.55 kg (10.03 lb) non-deployable payload following the CanSat configuration, designed to validate real-time visual perception in extreme flight conditions. It performs 3D object tracking and pose estimation in real time. It allows for 3D point cloud generation from saved camera frames even under the effect of high vibrations, G-forces, and rapid motion typical of sounding rocket flights.

At the core of the experiment is a cube mounted on a spring, simulating a target undergoing unpredictable movement. A camera, mounted on a dual-shaft 35 kg − cm torque servo motor, tracks the cube using colour-based detection within a limited and dynamically shifting field of view. The servo tilts the camera to follow the cube's movement, enabling near real-time tracking despite motion blur, frame drops and rotational skew. A pose estimation model based on YOLOv8 and trained on a custom dataset predicts the positions of the cube's vertices and thereby determines its orientation. The camera's raw frames are processed using the Depth-Anything-V2 architecture to generate point clouds, providing detailed 3D spatial information of the object. All computation processes run on a Raspberry Pi 5 coupled with the Raspberry Pi AI HAT+, acting as an AI accelerator.

The mission aims to prove the reliability of AI-based visual inference in fast-changing, resource-constrained environments. Its success supports future developments in space robotics, autonomous spacecraft operations and defence, where intelligent systems must perform under minimal sensor feedback and high uncertainty.



Figure 58 Payload Render

1. Computation

Custom Dataset

The dataset captures the chaotic motion of a spring-mounted cube within a CanSat module under simulated high-vibration flight conditions.

1) **Simulated Flight Dynamics**: The CanSat was manually shaken and rotated to simulate high vibration and high-G conditions, causing the cube to oscillate unpredictably—mimicking in-flight disturbances. Images of the cube captured in the process were used to train our model.
2) **Dynamic Target Behaviour**: The movement of the cube under varying intensities and directions of shaking introduced frame distortion, motion blur, and rapid positional changes, contributing to a robust and diverse

dataset for training.

3) **Payload Relevance**: This dataset tries to reflect the physical constraints and visual challenges of the real mission, enabling the model to learn and generalise effectively for real-time object tracking and pose estimation in the actual flight environment.
4) **Data Augmentation**: We applied extensive augmentations including 30% brightness/darkness adjustments, 4.5px Gaussian blur, 15% exposure changes, and 40% saturation enhancement, expanding the dataset from 1200 to 4500 images to boost model generalisation capabilities and make it robust to motion blur, lighting variations and a wide range of other visual distortions.



Figure 59 Manually Annotated Cube with 8 Vertices

Computation Pipelines

We use two distinct pipelines to achieve our objectives (refer to Appendix K.C for the computational workflow). The tracking pipeline detects and tracks the cube using colour detection. It updates the servo's angle based on the cube's vertical position. If the cube is not detected for four frames, scanning mode activates, sweeping the servo back and forth to reacquire the target. The inference pipeline is built around YOLOv8, leveraging its ultra-light, anchor-free architecture, meaning it directly predicts object centre points and box dimensions (width and height) instead of using predefined boxes, making the pipeline simpler, faster and more flexible (see Appendix K for detailed information on the architecture). Raw frames from the servo-mounted camera are preprocessed—resized, normalised and then fed into the YOLOv8 model, which outputs 2D bounding boxes, pose details of each keypoint and confidence scores for the oscillating cube on top of the frame in real time.

a) Tracking Pipeline

The following stages are implemented to track the cube and move the servo accordingly:

1) **Image Pre-processing**: Each frame is first converted from RGB(Red-Green-Blue) to HSV (Hue-Saturation-Value) format to improve detection in varying lighting. A binary mask is then created by filtering for pixels with high saturation and brightness values, isolating the red cube's hue.

2) **Cube Identification**: Next, contours are extracted from the binary mask. Small contours with a size under 90 pixels are removed to eliminate noise. Among the valid contours, the largest one is selected as the target.

3) **Position Calculation**: A bounding rectangle is computed around the selected contour, from which the centre point is calculated. Since processing occurs on a scaled-down 320×240 image, a scaling factor adjusts the

coordinates to match the full camera resolution.

4) **Target Calculation**: The servo control algorithm uses a proportional control approach to determine how much the servo should move based on the cube's position. The target angle is calculated using Eq.(5):

$$\text{target\_angle} = \text{current\_angle} + (\text{center\_y} - \text{CENTER\_Y}) * \text{tilt\_gain} \tag{5}$$

where, current_angle is the servo's current position in degrees, center_y is the vertical coordinate of the detected cube's center, CENTER_Y is the vertical centre of the camera frame (reference point), and tilt_gain (set to a value of 0.01) determines how aggressively the servo responds to position errors.

5) **Motion Rate Limiting**: To prevent jerky or damaging servo movements, the system implements motion rate limiting with a maximum speed constraint of 450 degrees per second. For each cycle, the maximum allowable movement is calculated as per Eq. (6):

$$\text{max\_movement} = \text{max\_speed} * dt \tag{6}$$

where dt is the time elapsed since the last update, and max_speed is the maximum rotation speed (450 degrees/second).

6) **Scanning Behaviour**: If the cube is not detected for four consecutive frames, the scanning mode is triggered. The servo begins sweeping to and fro at 450 degrees per second, reversing direction at 80° and 130° angles, increasing the chance of reacquiring the target.

b) Inference Pipeline

The system uses a Hailo-optimised neural network (loaded from a $.hef$ (hailo executable file)), which is an optimised YOLOv8 model specialised to run on Hailo NPUs (Neural Processing Input) to run edge AI tasks.. This model:

1) Detects the cube as an object.
2) Identifies 8 keypoints representing the cube's vertices, labelled from 0-7.
3) Provides confidence scores for each keypoint.

The model produces three types of outputs:

1) Box coordinates (for the cube's bounding box) in the format [x_min, y_min, x_max, y_max], where, x_min is the leftmost coordinate of the bounding box, y_min is the topmost coordinate of the bounding box, x_max is the rightmost coordinate of the bounding box,

Visualisation

The cube is shown with coloured faces in the original image (using different colours for each face). The heatmap helps visualise the probability distribution of the cube's corners. In YOLOv8s, during training, ground truth heatmaps are generated by placing Gaussian blobs at true keypoint positions, representing each corner as a smooth probability distribution. During inference, the model predicts these heatmaps to localise the vertices. A heatmap for bounding box movement over time is also created, tracking the last 30 detections with decreasing opacity for older positions, normalised and converted to a colour map for display. This ultimately helps identify the most probable region where the target object is expected to appear, enabling more accurate and consistent tracking.

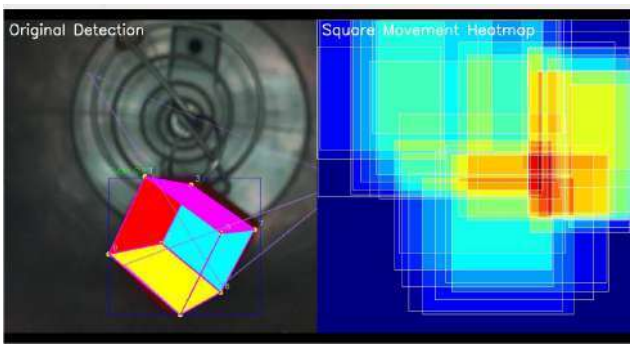


Figure 60 Cube vertices detected by the model, Cube's heatmap

Perimeter and Area Calculations

The perimeter is computed as $2 * (\text{width} + \text{height})$, where width and height are derived from the bounding box coordinates ($\text{width} = \text{xmax} - \text{xmin}$, $\text{height} = \text{ymax} - \text{ymin}$). The area is calculated as $\text{width} \times \text{height}$.

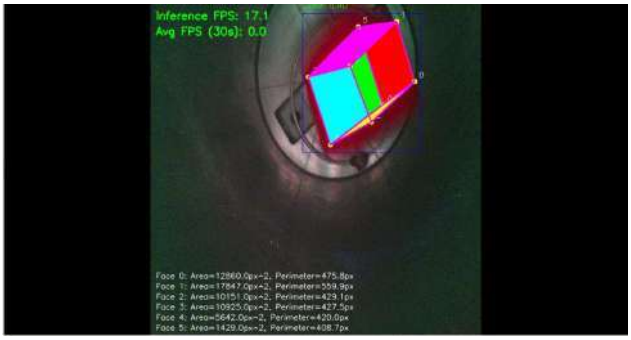


Figure 61 Calculating Area and Perimeter using Bounding Box Coordinates of 6 Faces of the Cube

Depth & Point Cloud Generation

For depth estimation, we conducted a comprehensive evaluation of leading algorithms, including Depth Pro by Apple, Depth-Anything V2, Lotus, MiDaS and ZoeDepth. After benchmarking these models using our dataset, we selected Depth-Anything V2 due to its superior performance and reliability in generating dense monocular depth maps.

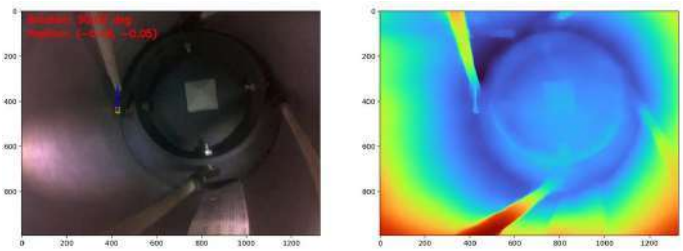


Figure 62 Depth Estimation using depth-pro



Figure 63 Depth Estimation using Lotus

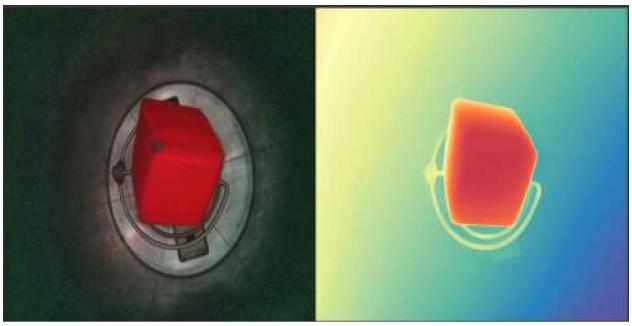


Figure 64 Depth Estimation using depth-anything-V2

The system leverages the "Depth Anything V2" model to estimate depth information from standard RGB images captured by the camera. Depth Anything V2 is a deep learning model developed by Meta AI that predicts dense depth maps from a single RGB image using a self-supervised technique called data distillation, eliminating the need for ground-truth depth during training. The resulting depth map, where each pixel represents the estimated distance from the camera, is then combined with colour data to generate detailed 3D point cloud representations of scenes. To focus on the object of interest—the cube—the system uses bounding box information provided by the YOLOv8 algorithm during pose estimation to segment the relevant regions from these point clouds. **Key Processing Pipeline**:

1) **Depth Estimation**: The system uses a pre-trained publicly available Depth Anything V2 model to predict depth values for each pixel in an image.
2) **Point Cloud Generation**: Depth data is converted into 3D spatial coordinates, creating a point cloud where each point has both position and color information.
3) **Object Segmentation**: Using predefined bounding box coordinates, the system isolates the cube from the overall scene.
4) **Motion Analysis**: For video sequences, the system performs a comprehensive motion analysis of the cube using multiple techniques. First, it tracks the cube's centroid over time by detecting its position frame-by-frame using YOLOv8-based bounding boxes and computing the center of each box. Second, it estimates the cube's orientation in 3D space using Principal Component Analysis (PCA) on the segmented 3D point cloud; PCA identifies the major axes of the cube's geometry, allowing for accurate estimation of its rotation. Third, the system fits physical motion models, such as constant velocity or acceleration models, to the observed centroid trajectory using least squares regression, enabling a quantitative understanding of the cube's dynamics. Finally, the system records all motion trajectory data and generates an MP4 video overlaying the cube's path and orientation over time for clear and intuitive visualisation.

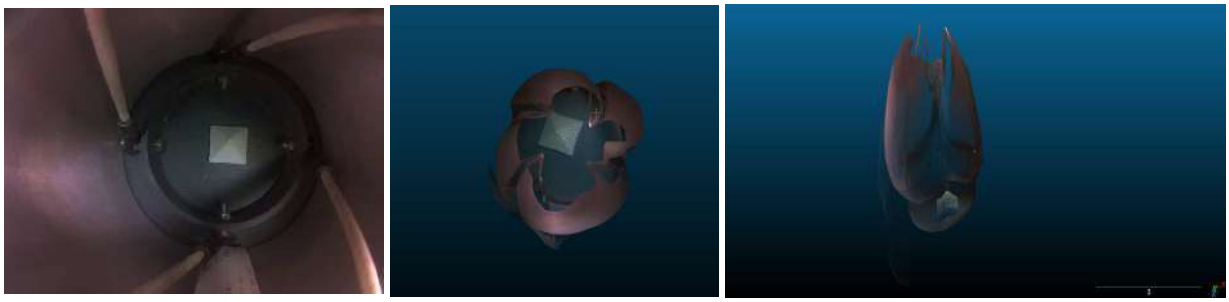


Figure 65 (from left to right) Input Frame, Top View of Generated Point Cloud during Testing, Side View of Generated Point Cloud during Testing

MPU9250 Trigger System

The MPU9250 trigger system uses I2C communication on the Raspberry Pi, beginning by waking the sensor with a write command to its power management register. The system monitors motion at a sampling rate of 100 Hz. Before active detection begins, it establishes a baseline reference by averaging 100 acceleration samples collected at 10 ms intervals, accounting for the sensor's resting state, including gravitational acceleration (approximately 1 g) along the vertical axis. This calibration enables the system to detect relative motion. The trigger activates when the acceleration magnitude (calculated as the square root of the sum of squared differences in acceleration, $\sqrt{^2 + ^2 + ^2}$), between consecutive 10 ms readings along all three axes) exceeds a threshold of 6 g or more for 20 consecutive readings, relative to the established baseline.

Camera

The Arducam 12MP IMX708 wide-angle camera was selected for the payload due to its high-resolution Sony sensor, 120° field of view, and robust HDR(High Dynamic Range) capabilities, enabling it to capture detailed, low-distortion images even under challenging lighting and motion conditions. Its compatibility with the Raspberry Pi 5 and native support for real-time video processing made it ideal for the mission's requirements of rapid 3D object tracking, pose estimation, and point cloud generation during high-vibration rocket flights. In the payload, the camera serves as the primary visual sensor, continuously supplying raw frames to the onboard AI system for real-time perception and tracking of the oscillating target cube.



Figure 66 Arducam 12MP IMX708 Wide-Angle Camera Module

2. Electrical and Electronics

Power Management System

The power system begins with a Pro Range 7.4 V 6000 mAh Lithium-Ion battery serving as the primary power source. A pull-pin switch is incorporated as a safety mechanism to control the power supply, allowing for activation only when the experiment is ready to begin. This design prevents premature battery drain and accidental activation.

The Battery Eliminator Circuit (BEC) 5 V-5 A module serves as the critical voltage regulator, converting the 7.4 V battery input to a stable 5 V output required by most electronics in the system. This module can handle input voltages

from 7.4 V to 55 V and provide a consistent 5 V output with up to 5 A current capacity, ensuring reliable power to all components even under variable load conditions.

Computing Hardware

At the core of the system is the Raspberry Pi 5 AI Kit, which integrates:

1) **Raspberry Pi 5 (8GB RAM)**
   The Raspberry Pi 5 provides robust processing power with 8GB of RAM and a quad-core ARM Cortex-A76 processor, enabling efficient handling of complex tasks. Its GPIO pins and I2C connections offer versatile peripheral integration, making it ideal for real-time AI and sensor-based applications.
2) **Hailo 8 AI accelerator (AI HAT+)**
   The Hailo 8 AI Accelerator adds a 26 TOPS Neural Processing Unit (NPU) to the system, significantly boosting AI inference performance. It accelerates models like YOLOv8 and Depth-Anything V2, offering real-time capabilities with low power consumption. Compared to GPU-based solutions like the NVIDIA Jetson Nano (which has a 128-core Maxwell GPU and delivers only 0.5 TOPS), the Hailo 8 provides up to 52x better performance while consuming far less power. Additionally, it is more cost-effective, offering a high-performance solution at a lower price point than comparable GPUs, making it an ideal choice for embedded AI systems. The AI HAT+ integrates seamlessly with the Raspberry Pi for an optimised edge-computing setup. (refer to Appendix H.B for the complete wiring diagram).

Powered by the Raspberry Pi 5 (8 GB RAM) paired with a *26 TOPS (Tera Operations Per Second) Hailo Neural Processing Unit (NPU), this powerful computing platform was selected for its superior energy efficiency, lower cost, and better real-time performance compared to traditional GPU-based alternatives. The AI kit draws power from the main system and interfaces with various peripherals via GPIO pins, I^2C connections, and dedicated camera inputs. It leverages advanced models like YOLOv8 and Depth-Anything V2 to perform real-time object detection, tracking, and 3D point cloud generation (refer to Appendix H.B for the complete wiring diagram).

Sensor Systems

The camera connects to the Raspberry Pi via a CSI Adapter through a 22/22 pin CSI interface. It provides the raw visual data needed for the tracking and pose estimation algorithms. The MPU9250 integrates a 3-axis accelerometer, gyroscope, and compass to detect motion and orientation. It connects to the Raspberry Pi via I2C communication protocol using:

1) SDA (data line) - connected to GPIO pin.
2) SCL (clock line) - connected to GPIO pin.
3) VCC - connected to 5 V power.
4) GND - connected to ground.

The MPU9250 is configured for a ± 8 g accelerometer range to enable detection of events exceeding 6 g compared to the calibrated baseline. It serves as a trigger system that initiates tracking and inference pipelines when the acceleration magnitude surpasses this threshold.

Actuation System

The PCA9685 serves as a 16-channel Servo Driver, communicating with the Raspberry Pi via an I2C bus. This controller receives commands from the Raspberry Pi and translates them into precise PWM (Pulse Width Modulation) signals to control the servo motor's position. High torque dual shaft servo motors require precise PWM signals (50 Hz with a pulse width of 1-2 milliseconds) for accurate positioning. The PCA9685 offers 12-bit resolution PWM, providing 4096 possible duty cycle steps, which is significantly more precise than the Raspberry Pi's native PWM capabilities. It also reduces the computational load on the Raspberry Pi and ensures stable power delivery.

The dual shaft 35 kg $-$ cm torque servo motor is mounted to the middle bulkhead and connects to the PCA9685 through three wires:

1) SIGNAL (PWM) - for control signals.
2) VCC - for power.
3) GND - for ground reference.

Illumination and Indicator Systems

The system incorporates components for audible indication and visual enhancement. A $5 - 24$ V buzzer provides

audible indications of system status during various operational phases, facilitating debugging and operation verification. Additionally, an LED controller manages a WS2812 Ring LED, connected via a JST connector. This LED illuminates the cube to ensure its visibility for the camera.

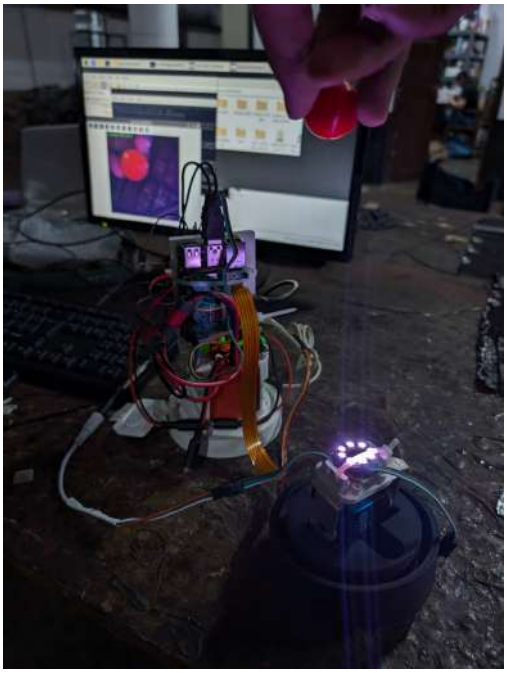


Figure 67 Electrical Setup Testing

Signal and Data Flow

The electrical system employs the following arrangement:

1) The Raspberry Pi 5 serves as the main controller, processing camera inputs through AI models.
2) The MPU9250 detects motion events exceeding threshold values.
3) The PCA9685 receives clean hardware-level I2C commands from the Raspberry Pi to position the servo.
4) The servo adjusts the camera position to track the oscillating cube.

3. Mechanical Design

Vrishabha is housed within the rocket's nosecone and follows a modular payload design based on a CanSat form factor. The primary structure consists of a cylindrical body manufactured from Aluminium 6061, featuring an outer diameter of 100 mm and a wall thickness of 6 mm. The cylinder is enclosed by two bulkheads: the top bulkhead is fabricated from Stainless Steel 316, while the bottom bulkhead is made from Aluminium 6061, with each bulkhead measuring 21 mm in thickness.

The overall length of the CanSat is 450 mm, and it is internally divided into two sections by a middle bulkhead, also made of Aluminium 6061, with a thickness of 37 mm. This internal division facilitates ease of assembly and modularity. The top and bottom bulkheads are secured to the cylindrical structure using six M4 countersunk bolts each, positioned at 60° intervals around the circumference. Similarly, the middle bulkhead is attached using six M4 countersunk bolts each, also equally spaced at 60° intervals.

The bottom bulkhead serves as a robust mounting interface, anchoring the payload securely within the rocket and providing a stable base for the integration of electrical components. These components are mounted onto a 3D-printed fixture manufactured from ABS, which is affixed to the bottom bulkhead. All critical electronics, including the Li-ion battery, PCA board, BEC board, MPU, Airtag, pull-pin switch and Raspberry Pi 5 board are secured to the fixture using threaded inserts.

The use of a 3D-printed ABS mount was chosen due to its high melting point compared to its counterparts and the design flexibility it offers, allowing for efficient integration. To ensure the structural integrity and vibrational resilience of the payload, extensive vibrational simulations were conducted before manufacturing (refer to Appendix L.D.1).

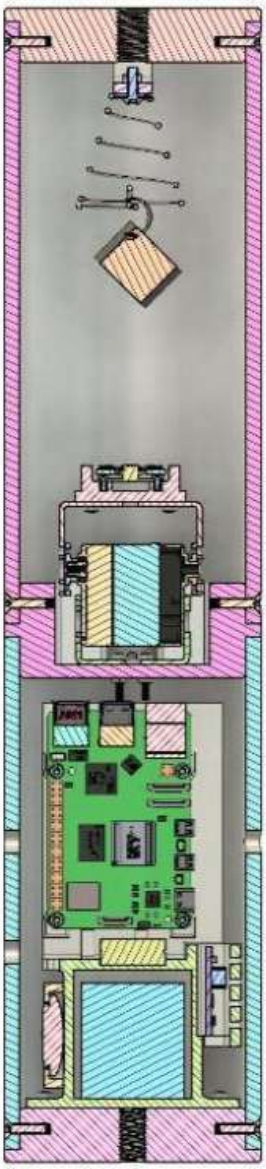


Figure 68 Sectional View of the Payload

Spring Design

A conical spring was selected due to its superior space efficiency and mechanical properties. Its geometry provides enhanced freedom of both lateral and longitudinal movement, making it an ideal choice for supporting the object. This design enables maximum translation of random vibrations experienced during rocket flight, allowing the object to move as freely and responsively as possible within the constraints of the payload structure (refer to Appendix L.D.2 for the corresponding calculations).

From the test outputs (as shown in Table 45), Spring No. 6 was chosen as it offered the maximum deflection.



Figure 69 Spring attached to the U-Bracket with the Cube Mounted on it

Spring Force Analysis in an Accelerating Non-Inertial Frame of Reference

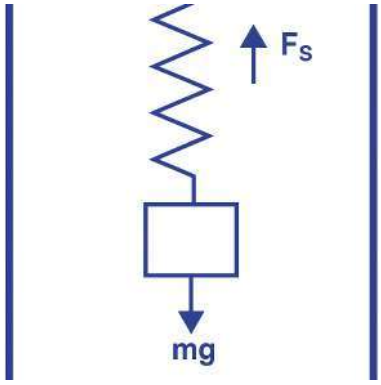


Figure 70 Spring-mass system in a non-inertial reference frame experiencing 22 g **upward acceleration. The spring force (**F_s**) must counterbalance both the mass's weight** (mg) **and the effective inertial force (**$m * 22\,\mathrm{g}$**), resulting in a total spring force of** $F_s = m * 22\,\mathrm{g}$

The forces acting on the spring system are the spring force upwards: $F_S = k * x$, the weight downwards: $m * \mathrm{g}$, and the acceleration of the system: 22g upwards. If the upwards direction is considered negative:

$$-k * x + m * \mathrm{g} + m * (22 * \mathrm{g}) = 0$$

$$k * x = m * (g + 22 * \mathrm{g})$$

$$Fs = m * 23 * \mathrm{g}$$

Where k is the spring constant, x is the spring elongation, and g is the acceleration due to gravity ($9.81\,\mathrm{m/s^2}$). The rocket experiences a maximum upward acceleration of 22 g.

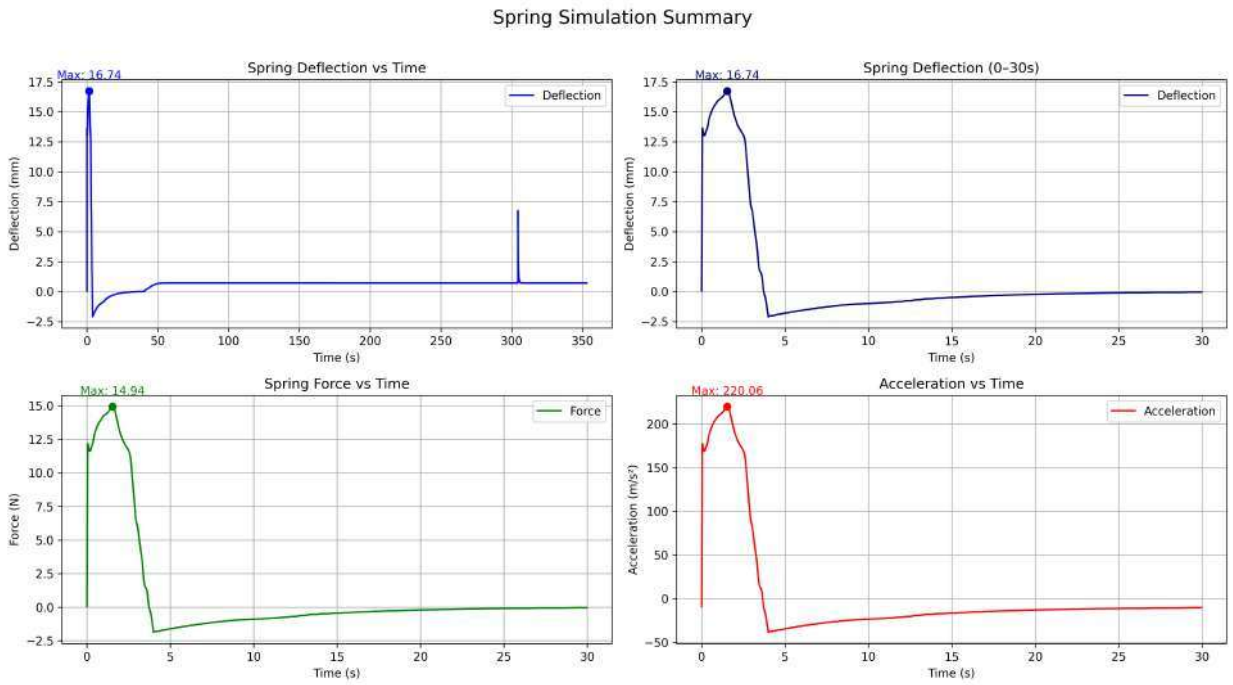


Figure 71 Dynamic Response of a Conical Spring System showing Deflection, Force, Acceleration, Velocity, and Position over time

Object

The object chosen for detection is a custom-manufactured cube, weighing 42.875 g. It has a surface area of 1837.5 mm^2 and a perimeter of 210 mm. The cube is manufactured using Stainless Steel 316.

Experiment

In the upper section of the payload, a 3D-printed U-bracket fabricated from PLA+ is mounted using M3 bolts. This bracket houses both the conical spring and the object of interest, a cube. Positioned directly beneath the object is the camera, mounted on a small 3D-printed PLA+ plate. This plate is securely attached to a dual-shaft servo motor, which is itself fixed to the middle bulkhead using M3 nuts and bolts. The object, secured to the conical spring, is free to move laterally and longitudinally in response to the random vibrations induced during rocket flight. Meanwhile, the camera, actuated by the servo motor, continuously moves to track the movement of the object.



Figure 72 Middle plate of CanSat with the Camera Mounted on Servo along with LEDs

E. Avionics

The avionics system for Vayuvega is called LTS-Iris. It consists of two independent sets of electronics: a primary SRAD system and a redundant COTS system. Both systems perform recovery tasks, deploying the parachute and tracking the rocket's location.

The SRAD system has various sensors and a microcontroller to interface with sensors and handle recovery events. The microcontroller processes the acquired data and transmits it to the ground station via the telemetry link. The SRAD system runs on an FSM-based architecture, which is used to determine the rocket's current state. It also comprises a horizon-facing flight camera, which records and stores a horizon view of the flight. The COTS system comprises a GPS and an Altimeter for safe recovery and official altitude logging.

1. COTS Electronics

The COTS electronics for Vayuvega consist of an altimeter and a GPS to ensure safe recovery and to officially log the altitude of the rocket. AltusMetrum EasyMini was chosen to be the COTS altimeter, which acts as the redundant altimeter. Likewise, the COTS Featherweight GPS was chosen as the redundant GPS module. Details and features of the two modules are discussed in the following section.

Table 10 COTS Components

S/N	Name of Component	Functionality	**Features** [11, 12]
1	AltusMetrum EasyMini	Altimeter	1) Dual-Deployment Altimeter 2) Small form factor 3) Operates up to 100 000 ft
2	Featherweight GPS	GPS	1) Long battery life 2) Long Range communication with Ground Station, up to 300 000 ft 3) Easy to use mobile app

Batteries for COTS Systems

The batteries used for the COTS components are described in this section. The batteries were selected following the guidelines provided in Section 6.18 of the DTEG, while also ensuring the components could operate for long hours. The batteries used are provided in Table 11.

Table 11 Batteries for COTS Systems

S/N	Component	Form Factor	Battery Specifications	Battery Runtime (hours)
1	AltusMetrum EasyMini	2 × Li-ion 18650 cells	3.6 V 2800 mAh 13C	13 (Drain Test Performed)
2	Featherweight GPS	LiPo 1S1P (Recommended and provided by manufacturer)	3.7 V 400 mAh	4.5 (Featherweight GPS Manual)

The manufacturer of EasyMini recommends a battery with a voltage between 4 V and 12 V and advises performing ground tests for e-match firing. DTEG guidelines specify the usage of cylindrical metal-cased Lithium-ion batteries, validating the selection of $Li-ion$ 18650 cells. Each cell is rated at 3.7 V, 2800 mAh, with a 13C charge/discharge rate. Two cells are configured in a 2S1P arrangement with a commercial battery holder to yield 7.4 V. This battery is placed in the battery compartment in the avionics bay and is described in detail in the avionics setup section. The EasyMini was tested for a battery life of over 13 hours using the above-specified battery. After conducting the test, the EasyMini was used to fire two e-matches via the AltosUI software. Further information on this test can be found in Appendix B.D.

The manufacturer of Featherweight GPS recommends using a 1S1P Lithium Polymer battery with a capacity of 400 mAh. The voltage range specified is 3.4 V to 4.5 V.

COTS Electronics Switches and Arming

Two mechanical pull-pin switches are used for the COTS components to arm them independently. These are placed in the bottom part of the avionics bay near the static band for ease of access. Once the pins are removed, they will power "on" or "ARM" the COTS electronics. Once ARMED, the EasyMini turns on and periodically beeps, which will be used to confirm that the EasyMini is armed, whereas the Featherweight GPS will be detected and confirmed on the designated mobile app. This ensures that the COTS electronics are properly initialised.

2. SRAD Electronics

The SRAD System is designed to perform the objectives listed in Table 12.

Table 12 SRAD System Objectives

S/N	Objective
1	To deploy parachutes for the recovery of the rocket
2	To track the rocket in real time to recover post-landing
3	To acquire, process and log data from all the sensors
4	To transmit the data via the telemetry link

The SRAD system consists of a PCB designed to fulfil the above objectives and is powered using 2 batteries, which are selected per Section 6.18 of the DTEG. The batteries are discussed below in Section II.E.2 in detail. The PCB also houses two additional sensors to obtain the acceleration and velocity of the rocket. This is done using a 3-axis accelerometer and also a 9DoF IMU. It houses a barometric pressure sensor for altitude, a GPS module for coordinates and a transceiver module for telemetry. It also consists of 2 MOSFETs to fire the parachutes. Linear voltage regulators with capacitors are used in the PCB to ensure the components get the required, stable and filtered power supply. An additional battery, called the Pyro Battery, is used to fire the parachute.. Additionally, another battery to power the flight camera is present.

There are two antennas present in the SRAD system: one dipole antenna used for the GPS module and the other a helical antenna for the transceiver module. Figures 73 & 74 show the designed PCB along with the components. The components are discussed in detail in the following section.

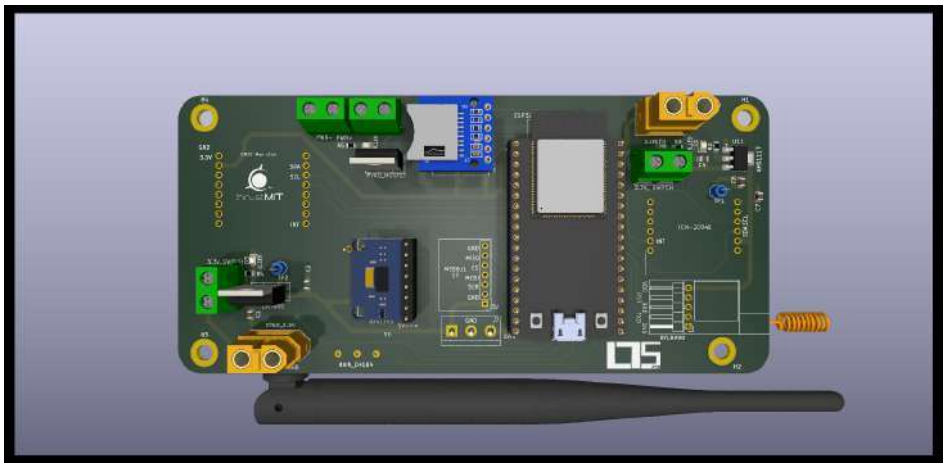


Figure 73 SRAD PCB - Front View

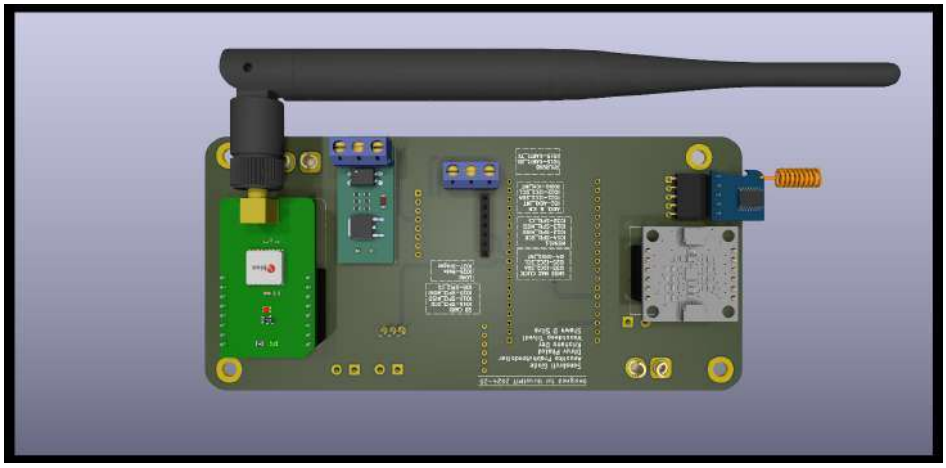


Figure 74 SRAD PCB - Back View

SRAD Components

Table 13 SRAD Components

S/N	Component Name	Description	Manufacturer
1	ESP32-WROOM-32E	Microcontroller	Espressif Systems[13]
2	ADXL345	3-Axis Accelerometer	Analog Devices[14]
3	ICM20948	High-Accuracy 9-DoF IMU	TDK Invensense[15]
4	MS5611	Barometric Pressure Sensor	TE Connectivity[16]
5	RYLR998	Telemetry Module (915 MHz)	Reyax Technologies[17]
6	u-Blox MAX M10S	GNSS/GPS module (1575.42 MHz)	MIKROE Electronics[18]
7	SD Card Adapter	Module to interface with the SD Card	Commercially available[19]
8	D4184	MOSFET for Drogue Parachute Deployment	ONSEMI[20]
9	IRLB8748	MOSFET for Main Parachute Deployment	Infineon Technologies[21]

There are two power lines present on the PCB, namely a 5 V line and a 3.3 V line. Both these lines are powered independently with separate batteries. Table 14 describes each component, the power line they are present on, their main features and the reason for choosing the same.

Table 14 SRAD Components Specifications

Component	Power Line	Features	Reason of Choice
ESP32-WROOM-32E	5 V	1) Dual-Core. 2) Rich Peripheral set. 3) High Clock Speed, up to 240 MHz. 4) GPIO Matrix; ease of pin assignment.	Many pins along with GPIO matrix. Dual core technology allows for dividing tasks and enables parallel processing.
ADXL345	5 V	1) Low Power Consumption (140 µA). 2) 3-Axis Accelerometer.	Used to identify flight stages through filtered data.
ICM20948	3.3 V	1) 9-Axis IMU. 2) In-built DMP for improved battery power utilisation.	Cross-verification of identified flight stages through high-accuracy 9-DoF IMU data.
MS5611	5 V	1) Low Power consumption, peak of 1.4 mA. 2) Wide range of pressure (10 – 1200 mbar). 3) Altitude resolution of 10 cm.	Measures a wide range of altitudes from 5000 ft to 100 000 ft at US Standard Atmosphere; used for detecting rocket lift-off and apogee.
RYLR998	3.3 V	1) Range upto 10 km. 2) 915 MHz LoRa module.	Long range and easy to interface using UART and AT commands with a compact form factor.
u-Blox MAX M10S	3.3 V	1) Low power consumption. 2) Position Accuracy of 1.5 m. 3) Cold start of 29 s and Hot start of 1 s.	High Location Accuracy, quick cold start and hot starts (29 s and 1 s). Tests gave accurate tracking. Low power consumption allows it to be powered using the microcontroller. Typical tracking consumption is about 9.5 mA.
SD Card Adapter	3.3 V	1) Adapter for SPI Interfacing with SD Card. 2) Houses a 32 GB microSD Card with 120 MB/s Read/Write speed.	To log flight data onto an onboard SD Card.

The ESP32-WROOM-32E has a GPIO matrix feature, which allows us to flexibly configure I2C and UART pins in the software to any GPIO pins. This way, the placement of components and routing on the PCB was made easier. The remaining components on the PCB are connectors, regulators and passive elements. It was ensured that the connectors are placed towards the edges of the board for ease of wiring and access, especially the ones for connecting the recovery wires. The GPS and RYLR998, which have antennas, were placed such that they are not obstructed by other components or wiring. An image showing the same can be found in the Avionics Setup section. The components requiring 5 V are powered using a 7.4 V 2S1P 21700 battery, which is regulated using the popular LM7805 linear regulator. Filter capacitors are placed to ensure the power supply remains stable. The 3.3 V components are powered using a 7.4 V 2S1P 18650 battery, regulated using the AMS1117 LDO, and a stable power supply is ensured using capacitors. LEDs are present to indicate that the power supply is on. Screw terminals and XT60s are used to ensure that wires are firmly connected to the board and will remain so during the flight.

Batteries for SRAD Systems

SRAD electronics contains 4 batteries in total. The batteries used are Lithium-ion metal cased cylindrical cells, as per requirements mentioned in section 6.18 of the DTEG. 3 batteries are 2S1P configuration 18650 cells, whereas the last battery is a 2S1P configuration 21700 cells. Table 15 provides clear information regarding the batteries present for the SRAD system.

Table 15 Batteries for SRAD Systems

S/N	Battery Name	Description	Function	Tested/Estimated Runtime
1	Li-ion 18650 – 3.3 V battery	Two 3.6 V 5C 3000 mAh configured in 2S1P using commercial battery holders	Powers 3.3 V line	5+ hours
2	Li-ion 18650 – Pyro battery	Two 3.6 V 10C 2800 mAh configured in 2S1P using commercial battery holders	Provides power to Pyro MOSFETs	e-match firing was tested using both MOSFETs, runtime is 13+ hours on standby
3	Li-ion 21700 – 5 V Battery	7.4 V 5000 mAh 3C 2S1P commercially available battery pack	Powers 5 V line	5+ hours
4	Li-ion 18650 – Camera Battery	7.4 V 3500 mAh 3C 2S1P commercially available battery pack	Power Flight Camera	4 hours

Before selecting the batteries, power consumption calculations were performed for the components during the design phase, from which the battery capacity was determined. The pyro battery has a higher C rating, which specifies how quickly a battery can discharge current safely. A higher C rating implies a battery can discharge more current, faster, which is needed to fire the pyrotechnic charges.

The commercial battery holders for the 18650 cells had thin leads; hence they were replaced by 22 AWG wires to ensure Wiring Guidelines of the DTEG were met. All wires coming out of the battery holders will be colour coded in red (for positive) and black (for negative) and will be labelled for identification. The batteries used for powering the PCB and to fire the electronics are present in the battery mount (Batteries 1, 2, and 3 in Table 15), whereas the flight camera battery is placed on the other side of the PCB along with the flight camera.

SRAD Electronics Switches and Arming

The SRAD batteries are connected via mechanical pull-pin switches. The 5 V and 3.3 V power batteries use two switches which can be activated using a single pin. This way, the PCB gets completely powered by pulling out one pin. This helps us reduce the number of holes to drill on the rocket body and to reduce the number of components in the avionics bay. Another pull-pin switch is used to control the pyro batteries. The pull-pin switches will also be labelled according to the set of electronics they will control. Once the 3 pins (of the pull-pin switches) are pulled, the system will be completely ARMED. The ARM state is verified via the telemetry link. A message is sent on startup, and periodic messages are sent with information about the current state of the rocket. The state of the rocket includes the coordinates obtained from the GPS, which can be used to confirm the working of the primary recovery and tracking system.

SRAD Software

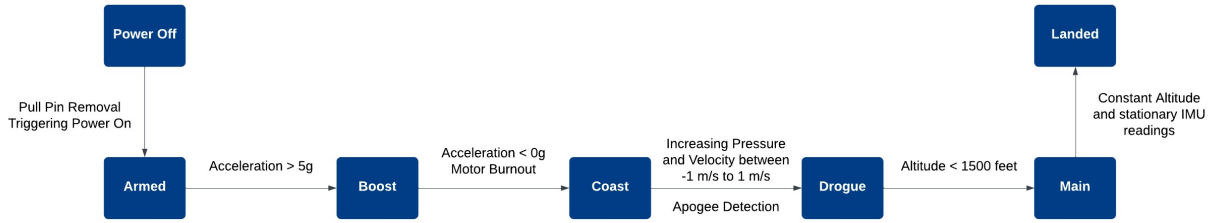


Figure 75 State Transition Diagram

At the launchpad, the rocket enters the ARMED state once the pull pin is removed, and the FC is powered on. Launch is detected when the onboard accelerometer measures acceleration greater than 5 g for three consecutive readings, signalling a transition to the BOOST phase. Once the motor burns out, it is identified by acceleration readings dropping below 0 g for three consecutive measurements, triggering the rocket to transition into the COAST phase. During the COAST phase, the apogee detection algorithm begins running to monitor the rocket's peak altitude.

As the rocket nears its peak altitude, apogee detection is based on a combination of velocity and pressure data. Specifically, when the vertical velocity approaches zero and pressure readings consistently increase over five samples, apogee is confirmed the system transitions to the DROGUE state, deploying the drogue parachute by firing the drogue charge. As the descent continues and the altitude becomes lower than 1500 ft, transition to MAIN state occurs, deploying the main parachute, ensuring a slower, controlled descent. Finally, once the altitude readings stabilise and the IMU detects no significant motion, the rocket transitions to the LANDED state, concluding the mission. In the LANDED state, the system periodically pings the coordinates and the apogee to the ground station via telemetry. Throughout all phases, flight data from the sensors is continuously logged and transmitted for monitoring and post-flight analysis.

Apogee detection uses a sensor fusion approach, combining inputs from three distinct sensors: one barometric sensor, one IMU, and one accelerometer. The IMU and accelerometer are used to find the vertical velocity, and atmospheric pressure is obtained from the barometric pressure sensor. The system ensures a robust and reliable apogee detection mechanism by relying on vertical velocity and atmospheric pressure readings. This strategy helps improve accuracy and mitigates the risk of false detections due to isolated sensor anomalies, thereby enhancing the safety and performance of the overall recovery sequence.

Camera

The avionics mount of Vayuvega incorporates a horizon-facing RunCam Thumb Pro camera to record the flight trajectory. It provides a 150° field of view and captures footage at a resolution of 1080p at 60 frames per second. The camera is powered by a 2S1P Li-ion 18650 battery pack, providing 7.4 V and a capacity of 3500 mAh. This power is routed through a distribution board that ensures a stable 5 V regulated output for the camera. Video footage is stored on a 256 GB microSD card, providing ample storage for high-definition recording throughout the flight.

3. Avionics Coupler

The avionics coupler is a modular, space-optimised assembly designed to house all critical flight electronics, including the SRAD flight computer, Featherweight GPS, EasyMini altimeter, RunCam Thumb Pro camera, and a battery system. The coupler is structurally supported by two recovery bulkheads located at each end, with four M6 threaded shafts running the full length to provide mounting points for all internal sub-assemblies. The battery mounting system is constructed from ABS and consists of a two-part configuration: a fixed battery mount and a sliding battery holder. This arrangement enables quick and efficient installation or removal of batteries during pre-flight preparation. The batteries are secured within the holder using mechanical fastening, supplemented by Velcro straps and zip ties to ensure robust retention under high-vibration and high-acceleration conditions. Following the battery system is the avionics mount, also manufactured from ABS, which integrates all electronic boards and the camera setup. Each component is strategically placed to maximize internal volume efficiency, achieved through iterative design and prototyping. All boards are mounted using machine screws threaded into heat-set brass inserts, with additional zip tie reinforcement to

guard against in-flight vibrations. A key design consideration is the alignment of the main avionics mount with the switch band on the coupler's exterior. This placement facilitates straightforward access to the horizon-facing camera and pull-pin arming switches after full vehicle integration, enhancing operational convenience and safety.



Figure 76 Avionics Coupler Assembly

III. Mission Concept of Operations Overview

Vayuvega's primary objective is to attain an altitude of 30 000 ft in line with the IREC guidelines, while ensuring a safe and successful recovery. The successful accomplishment of these objectives is crucial for achieving the project's goals of competitiveness and operational safety. The secondary objective of Vayuvega's mission is to test the functioning of the scientific payload Vrishabha, which aims to demonstrate real-time 3D tracking, pose estimation, and point cloud generation under high vibrations and G-forces. A camera module mounted on a servo tracks a cube attached to a spring within the CanSat. The system operates within the limited field of view, validating the performance of AI-driven perception in extreme dynamic conditions.

A. Mission Structure & Defining Mission Events

Vayuvega's mission structure consists of nine successive stages: Assembly, Launch Pad Integration, Arming, Ignition and Lift-off, Powered Ascent, Coasting, Apogee and Drogue Parachute Deployment, Main Parachute Deployment, and Landing and Ground Recovery.

1) **ASSEMBLY**
The rocket is completely assembled with energetics and pull-pin switches. The rocket is then ready to be sent to the launch pad.

2) **LAUNCH PAD INTEGRATION**
During this phase, Vayuvega is carefully placed on the launch rail and secured in place. The payload electronics are then turned on, and the rail is raised vertically and locked.

3) **ARMING**
The flight computers are powered on, and all E-matches are checked for continuity. Telemetry and GPS lock are confirmed, and the rocket is ready for ignition. This phase also involves clearing unnecessary personnel from the launch area and installing the motor igniter.

4) **IGNITION & LIFT-OFF (T = 0.00 - 0.27 s)**
The ignition phase marks the start of Vayuvega's rocket flight. The motor is lit by sending a current through the igniter, and smoke is visible coming out of the aft end of the motor. As the motor produces thrust, the rocket lifts off the rail in just 0.27 seconds, reaching a velocity of 41.85 $\mathrm{m\,s^{-1}}$.

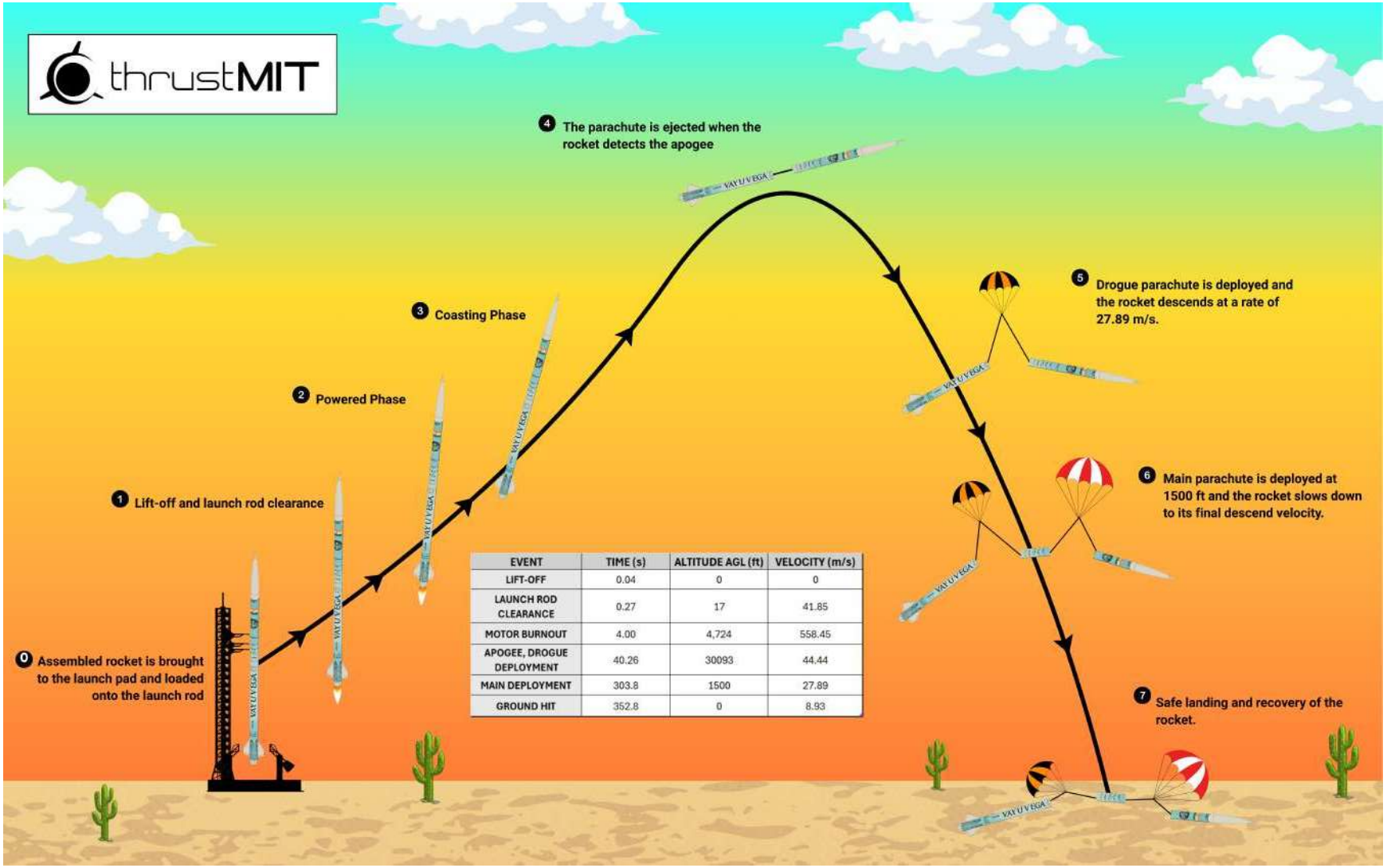
5) **POWERED ASCENT (T = 0.27 - 4.00 s)**
During the powered ascent phase (from the time of launch rod clearance), the rocket accelerates upward under motor power for 4 seconds, reaching an altitude of 4724 ft AGL.

6) **COASTING (T = 4.00 - 40.26 s)**
After 4 seconds of powered ascent, the motor burns out and the rocket coasts to apogee, which occurs 40 seconds into flight.

7) **APOGEE & DROGUE DEPLOYMENT (T = 40.26 - 303.8 s)**
The rocket fires its ejection charges at apogee, separating the drogue bay from the nosecone. The parachute inflates, and the rocket falls at a rate of 27.89 $\mathrm{m\,s^{-1}}$.

8) **MAIN DEPLOYMENT (T = 303.8 - 352.8 s)**
The recovery electronics track the altitude, and upon reaching an altitude of 1500 ft AGL, they fire the main charge. This enables the opening of the parachute and leads to a smooth descent velocity of approximately 8.93 $\mathrm{m\,s^{-1}}$.

9) **GROUND HIT & RECOVERY (T = 352.8 s -)**
After the successful completion of the flight, the rocket is located using GPS data received from the Featherweight GPS Tracker and onboard SRAD GPS. Once found, the rocket's electronics are powered off, and it is taken back to the judges for post-flight evaluation, including data analysis of flight and payload data.



EVENT	TIME (s)	ALTITUDE AGL (ft)	VELOCITY (m/s)
LIFT-OFF	0.04	0	0
LAUNCH ROD CLEARANCE	0.27	17	41.85
MOTOR BURNOUT	4.00	4,724	558.45
APOGEE, DROGUE DEPLOYMENT	40.26	30093	44.44
MAIN DEPLOYMENT	303.8	1500	27.89
GROUND HIT	352.8	0	8.93

Figure 77 Mission Concept of Operations

IV. Conclusions & Lessons Learnt

The development and design cycle of Vayuvega was built upon insights gained from previous projects, addressing past shortcomings and prioritising iterative development. The project aimed to introduce significant engineering improvements while maintaining consistency with established design practices. Aligning with thrustMIT's core philosophy to innovate, our team innovates and advances the design of Vayuvega. This approach enhances our technical capabilities and reinforces our resilience and ability to navigate the complex challenges faced in high-powered rocketry.

A. Lessons Learnt

1) **Application of DFMA Principles**

The design of Vayuvega incorporated core principles of Design for Manufacturing and Assembly (DFMA) to streamline production and reduce assembly complexity. Conscious decisions were made during the early stages of the design process to ensure manufacturability without compromising performance or structural integrity. One of the notable implementations was the stepped interface on the bulkheads and the integration of radial alignment extrusions, which improved positional accuracy during assembly. Regular communication with manufacturers was maintained throughout the development process to assess the feasibility of complex geometries and to implement design changes that facilitated faster and more cost-effective machining. This proactive collaboration enabled the team to avoid design bottlenecks, maintain progress, and minimise potential delays in fabrication and integration.

2) **Advancements in Composite Layups**

To improve structural consistency and reduce manufacturing defects, the team transitioned from traditional hand lay-up techniques to the roll-wrapping method with heat-shrink tape consolidation for all body tubes. This change was based on a detailed analysis of previous years' manufacturing challenges and material performance outcomes. The use of heat shrink tape during curing provided uniform pressure over the composite surface, minimising resin-rich zones and entrapped air voids. As a result, the fabricated tubes exhibited improved fibre volume fractions and reduced void fraction, contributing to enhanced mechanical performance and lower surface roughness. This not only improved the structural quality but also contributed to drag reduction during flight.

3) **Testing and Experimental Framework**

A test-driven development approach was central to the design evolution of Vayuvega. Each subsystem underwent rigorous experimentation, and the data collected informed iterative improvements across structural, aerodynamic, and integration aspects of the rocket. Detailed reports were compiled for each test, documenting procedures, results, and actionable insights. These test logs formed a comprehensive knowledge base that guided informed decision-making throughout the project and established a reproducible standard for future development cycles.

4) **Conservative Timeline**

Maintaining a precautionary timeline is crucial, considering the lead times for manufacturing and shipping. With unexpected delays faced in acquiring various components, a conservative timeline reduces the risk of disruption during integration and testing. This practice ensures the smooth flow of the project development cycle, providing a sufficient buffer to accommodate contingencies without compromising project milestones.

5) **Documentation and Knowledge Transfer**

Thorough documentation and transfer of knowledge about legacy designs from previous projects are essential in conserving the integrity and continuity of proven practices across future development cycles. The team incorporated a strategy to maintain design documents and conduct post-test evaluations, emphasising compliance with standard operating procedures.

Acknowledgements

We extend our heartfelt gratitude to Dr. Srinivas G, the faculty advisor of thrustMIT and Associate Professor at Manipal Institute of Technology, for his unwavering support and invaluable guidance throughout our journey. Our sincere appreciation goes to our college, Manipal Institute of Technology (MIT), and by extension, to our university, Manipal Academy of Higher Education (MAHE) for generously providing us with their support and facilities. The team would like to acknowledge the valuable inputs and recommendations of our various mentors and advisors at Manipal Institute of Technology; Prof. Nagaraj, and Mr. Ganesha Nayak. Special thanks to our mentor, Mr. Bob Schoner, for his role as our Flyer of Record and his invaluable guidance in optimising the design for a safe and reliable flight. We are immensely thankful to ESRA, Space Dynamics Laboratory (SDL), and all other organisations and individuals involved in organising this competition, providing us with a remarkable platform for learning and growth. We express our deepest gratitude to our sponsors and their representatives, including Shapefy, Vega, Babaji Shivram, OpenMV, PCB Power, Ansys, and Robu, whose support made this project possible. Finally, we express our deepest gratitude to our families and friends, whose unwavering support has been a constant source of encouragement throughout every stage of this journey.

References

[1] Mallick, P. K., *Fiber-reinforced composites: materials, manufacturing, and design*, CRC press, 2007.

[2] Newlands, R., Heywood, M., and Lee, A., "Rocket vehicle loads and airframe design," *Aspire Space*, 2011.

[3] Bulaha, N., "Analysis of service properties of cylindrically ground surfaces, using standard ISO 25178-2: 2012 surface texture parameters," *Environment. Technologies. Resources. Proceedings of the international scientific and practical conference*, Vol. 1, 2015, pp. 16–21.

[4] Standard, A., "D2734-16: Standard Test Methods for Void Content of Reinforced Plastics," *ASTM International, West Conshohocken: West Conshohocken, PA, USA*, 2016.

[5] ASTM International, "ASTM D3171-22: Standard Test Methods for Constituent Content of Composite Materials," https://www.astm.org/d3171-22.html, 2022. ASTM International, West Conshohocken, PA.

[6] Kutz, M., *Mechanical engineers' handbook, volume 1: Materials and engineering mechanics*, Vol. 1, John Wiley & Sons, 2015.

[7] Milligan, T. V., "Drag of Launch Lugs, Rail Buttons, and Launch Guides," *NARCON 2017*, National Association of Rocketry, 2017. Presented at NARCON 2017, Feb. 24, 2017.

[8] Mackerle, J., "Finite elements in the analysis of pressure vessels and piping, an addendum: a bibliography (1998–2001)," *International Journal of Pressure Vessels and Piping*, Vol. 79, No. 1, 2002, pp. 1–26.

[9] Mulville, D. R., "Structural design and test factors of safety for spaceflight hardware," *Technical Standard NASA-STD-5001B w*, 1996.

[10] Bendsoe, M. P., and Sigmund, O., *Topology optimization: theory, methods, and applications*, Springer Science & Business Media, 2013.

[11] Altus Metrum, "EasyMini Altimeter Documentation - Batteries," https://altusmetrum.org/AltOS/doc/easymini.html#_batteries, 2025. Documentation page.

[12] Featherweight Altimeters, "Featherweight GPS Tracker Manual," https://www.featherweightaltimeters.com/uploads/1/0/9/5/109510427/gps_tracker_manual_2025feb20b.pdf, 2025. User manual, February 2025.

[13] Espressif Systems, "ESP32-WROOM-32E/32UE Datasheet," https://www.espressif.com/sites/default/files/documentation/esp32-wroom-32e_esp32-wroom-32ue_datasheet_en.pdf, 2025. Technical datasheet.

[14] Analog Devices, "ADXL345: 3-Axis, ±2g/±4g/±8g/±16g Digital Accelerometer," https://www.analog.com/en/products/adxl345.html, 2025. Product page and datasheet.

[15] TDK InvenSense, "ICM-20948 Datasheet," , 2025. InvenSense 9-axis MotionTracking Sensor.

[16] TE Connectivity, "MS5611-01BA03 Barometric Pressure Sensor with Stainless Steel Cap," , June 2017. URL https://www.te.com/commerce/DocumentDelivery/DDEController?Action=showdoc&DocId=Data+Sheet%7FMS5611-01BA03%7FB3%7Fpdf%7FEnglish%7FENG_DS_MS5611-01BA03_B3.pdf%7FCAT-BLPS0036, datasheet, Revision B3.

[17] Reyax Technology, "RYLR998 LoRa Transceiver Module," https://reyax.com/products/rylr998/, 2025. Product page.

[18] u-blox, "MAX-M10 Series GNSS Modules," https://www.u-blox.com/en/product/max-m10-series, 2025. Product page.

[19] Robu.in, "Mini Micro SD Card Reader Module," https://robu.in/product/mini-micro-sd-card-reader-module/, 2025. Product listing.

[20] onsemi, "NTMD4184PF Datasheet," https://www.onsemi.com/pdf/datasheet/ntmd4184pf-d.pdf, 2025. MOSFET datasheet.

[21] Infineon Technologies, "IRLB8748 Datasheet," https://www.infineon.com/cms/en/product/power/mosfet/n-channel/irlb8748/, 2025. N-channel MOSFET datasheet.

[22] Featherweight Altimeters, "Featherweight GPS Tracker," https://www.featherweightaltimeters.com/featherweight-gps-tracker.html, 2025. Product page.

[23] SensorsONE, "Altitude Pressure Units Conversion," https://www.sensorsone.com/altitude-pressure-units-conversion/, 2025. Conversion tool.

V. Appendix

A. Appendix: System Weights, Measures, and Performance Data

A. Rocket Information

Table 16 Rocket Information

Parameter	Value
Number of stages	1
Vehicle Length	3500 mm
Airframe Outer Diameter	126 mm
Airframe Inner Diameter	121 mm
Nosecone Length	700 mm
Propellant Mass	9.78 kg
Motor Wet Mass	16.78 kg
Wet Mass	36.8 kg
Number of Fins	4
Fin Semi-Span	98.5 mm
Fin Thickness	4.5 mm
Fin Tip Chord	40 mm
Fin Root Chord	250 mm
CP at Launch-Rod Clearance	2270 mm
CG at Launch-Rod Clearance	2062 mm

B. Propulsion Details

Table 17 Propulsion Details

Parameter	Specification/Value
Cluster	No
Number of Motors	1
Type	Solid, Single-Use
COTS / SRAD	COTS
Manufacturer	AeroTech
Manufacturer Designation	O5500X-PS
Motor Length	1491.2 mm
Casing Diameter	98 mm
Propellant Mass	9.78 kg
Motor Wet Mass	16.78 kg
Motor Dry Mass	7 kg
Letter Classification	O
Total Impulse	21 384.0 N s
Average Thrust	5514.6 N
Initial Thrust	6046.9 N
Maximum Thrust	7551.5 N
Burn Time	4.0 s
Propellant	Propellant X

C. Predicted Flight Data

Table 18 Predicted Flight Data

Parameter	Value	Source
Launch Rail	ESRA-Provided	
Launch Rail Length	5816 mm	ESRA
Liftoff Thrust-to-Weight Ratio	15.32:1	Calculated
Launch Rail Departure Velocity	41.85 m s^{-1}	ORK
Minimum Static Margin	1.65	ORK
Maximum Acceleration	22.75 g	ORK
Maximum Velocity	568.43 m s^{-1}	Calculated
Fin Flutter Velocity	1119.96 m s^{-1}	AeroFinSim
Target Apogee	30 000 ft	-
Predicted Apogee	30 093 ft	6-DoF

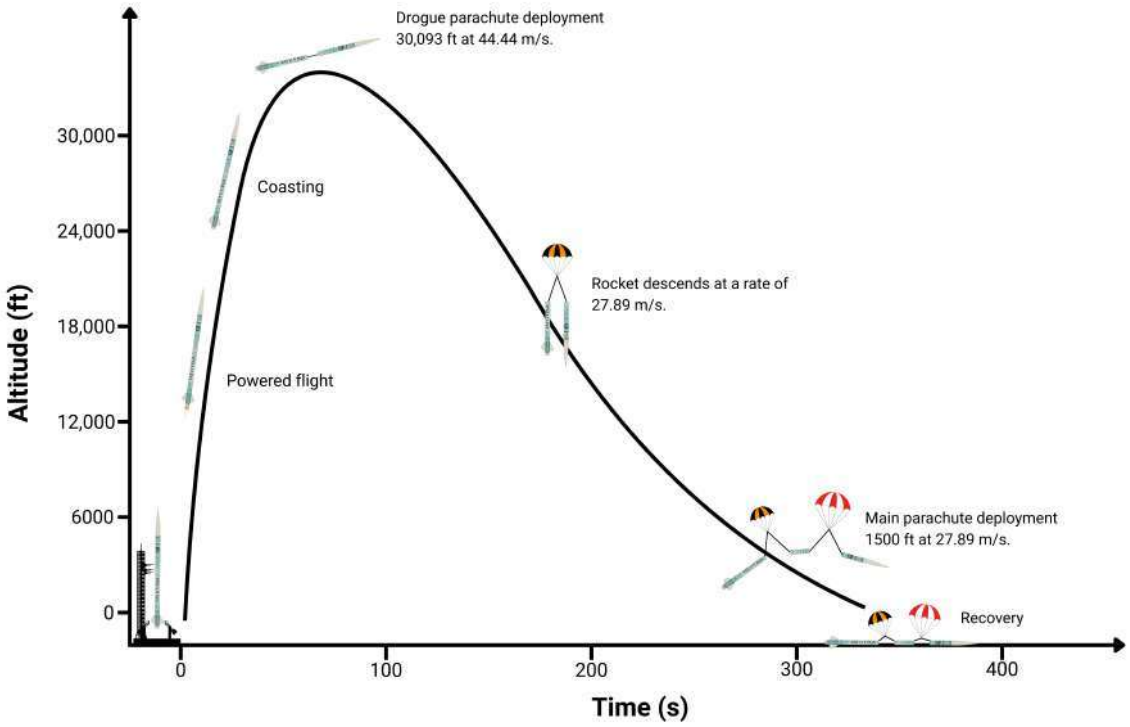


Figure 78 Flight Profile Graph

D. Recovery Information

Table 19 Recovery Information

Parameter	Value	Comments
COTS Altimeter	Altus Metrum EasyMini	-
Redundant Altimeter	SRAD	-
Drogue Deployment Charge (Primary)	5 g	4F black powder
Drogue Deployment Charge (Backup)	5.5 g	4F black powder
Main Deployment Charge (Primary)	5 g	4F black powder
Main Deployment Charge (Backup)	5.5 g	4F black powder
Drogue Deployment Altitude	30 093 ft	-
Drogue Descent Velocity	27.89 m s^{-1}	-
Main Deployment Altitude	1500 ft	-
Main Descent Velocity	8.93 m s^{-1}	-
Shock Chords and Mechanical Links	-	Kevlar, 1/2 in, 6000 lb, Drogue - Eyebolt (Lower Avionics Bulkhead) and Quick link (Parachute), Swivel link, Quick link and Eyebolt (Thrust Plate). Main - Eyebolt (Upper Avionics Bulkhead) and Quick link (Parachute), Swivel link, Quick link and Eyebolt (Nosecone Bulkhead).

E. Software Used

The following software is used for the design and simulation of the rocket:

1) **OpenRocket v23.09** - Open-source software for the 2D design plan of the rocket. This software is also used to get flight simulation results and obtain a geometrical understanding of the design.
2) **Fusion360 v.2.0.18961** - 3D CAD modelling software used to model the entire rocket.
3) **ANSYS 2024 R1** - The Static Structural module is used to obtain the stress analysis results using the finite element method for various components of the rocket. The FLUENT module is used to simulate the flow around the rocket and to calculate the aerodynamic forces on it during flight using the finite-volume method. The Explicit Dynamics module is used to obtain impact-loading results for the boattail. The Modal Analysis module is used to obtain the natural frequencies and vibrational characteristics of the fins. The Coupled Field Transient module is used for the FSI simulation of the fins.
4) **RASAero II v1.0.2.0** - This software is used for obtaining accurate flight simulation data in the supersonic regime.
5) **MATLAB R2024a** - The team's 6-DoF Simulator code and the fin flutter code are written using MATLAB.
6) **FinSim v5.7** - To calculate fin flutter velocity and deflection.

B. Appendix: Project Test Reports

A. Recovery System Testing

THIS PAGE INTENTIONALLY LEFT BLANK.
APPENDIX B.A BEGINS ON THE FOLLOWING PAGE.

thrustMIT Test Report

2024 - 25

Test: Single Deployment		
Date:14/04/2024	**Test no.: 1**	**Result: Partial Success**

Objective:
To test the Deployment system of the Parachute.

Modifications/changes from last test:
-

Setup & procedure:

- Choose a safe, open test area away from flammable materials and mark a 10-meter safety zone.
- Mount the rocket or test section securely on a stable stand to prevent movement.
- Connect firing electronics and check continuity, then disconnect to prepare charges safely.
- Measure and install charges last, insert igniters and secure all connections properly.
- Reconnect the firing system but keep it disarmed while the team clears to a safe distance.
- Arm the system, give a loud countdown, and fire remotely while observing from cover.
- Wait a few seconds, disarm the system, inspect components, and record test results.



Safety:

- Wear safety glasses, gloves, and hearing protection at all times.
- Keep a clear area of at least 10 meters around the test site.
- Load ejection charges last and ensure only trained team members handle them.
- Secure the rocket firmly and check continuity before arming the system.
- Fire the system remotely with a clear countdown and stay behind cover.

Success criteria:			
No.:	**Criteria description:**	**Method of validation:**	**Comments:**
1	Charge Ignition	Visual	The charge was successfully ignited.
2	Body Tube separation	Visual	The body tubes separated successfully

Results:

Charge leak through one of the charge-wells, reasons may include excessive amount of M-seal used or cyclic loading as the charge-well was used multiple times.
Charge-well wire holes expanded, thus rendering both charge-wells unusable for further use.



The parachute burned due to improper wrapping in the fire blanket.
Conclusion:
The test was partly successful, with the charge-wells damaged



Video Link:
https://drive.google.com/drive/folders/1M31JRMyIuHuZ8azYT8gsIq4VriU4Wu73?usp=drive_link

Tested and Recorded By:
Madhav Sonkusare
Approved By:
Ayyan Nikunj Bhartia

thrustMIT Test Report

2024 - 25

Test: Dual Deployment		
Date:20/04/2024	**Test no.: 2**	**Result: Failure**

Objective:
To test the Dual Deployment system of the Parachute.

Modifications/changes from last test:
Dual deployment of parachutes was tested.

Setup & procedure:

- Choose a safe, open test area away from flammable materials and mark a 10-meter safety zone.
- Mount the rocket or test section securely on a stable stand to prevent movement.
- Connect firing electronics and check continuity, then disconnect to prepare charges safely.
- Measure and install charges last, insert igniters and secure all connections properly.
- Reconnect the firing system but keep it disarmed while the team clears to a safe distance.
- Arm the system, give a loud countdown, and fire remotely while observing from cover.
- Wait a few seconds, disarm the system, inspect components, and record test results.



Safety:

- Wear safety glasses, gloves, and hearing protection at all times.
- Keep a clear area of at least 10 meters around the test site.
- Load ejection charges last and ensure only trained team members handle them.
- Secure the rocket firmly and check continuity before arming the system.
- Fire the system remotely with a clear countdown and stay behind cover.

Success criteria:			
No.:	**Criteria description:**	**Method of validation:**	**Comments:**
1	Charge Ignition	Visual	The charge was successfully ignited.
2			
3			

Results:

Nose Cone ejected because of the improper alignment of the bolts.



No charge-well wire holes expansion was observed.
No charge leak was observed.

Conclusion:
The Test was a failure due to the complete separation of the nose cone from the setup due to the misalignment of bolts.

Video Link:
https://drive.google.com/drive/folders/1Q1K1RnHcJOfAfwaLlGWRHZ4bP_Qf9sAL?usp=drive_link

Tested and Recorded By:
Shreemad Burade
Approved By:
Ayyan Nikunj Bhartia

thrustMIT Test Report

2024 - 25

Test: Dual Deployment		
Date:21/04/2024	**Test no.: 3**	**Result: Success**

Objective:
To test the Dual Deployment system of the Parachute.

Modifications/changes from last test:
Dual deployment of parachutes was tested with all the bolts aligned properly.

Setup & procedure:

- Choose a safe, open test area away from flammable materials and mark a 10-meter safety zone.
- Mount the rocket or test section securely on a stable stand to prevent movement.
- Connect firing electronics and check continuity, then disconnect to prepare charges safely.
- Measure and install charges last, insert igniters and secure all connections properly.
- Reconnect the firing system but keep it disarmed while the team clears to a safe distance.
- Arm the system, give a loud countdown, and fire remotely while observing from cover.
- Wait a few seconds, disarm the system, inspect components, and record test results.



Safety:

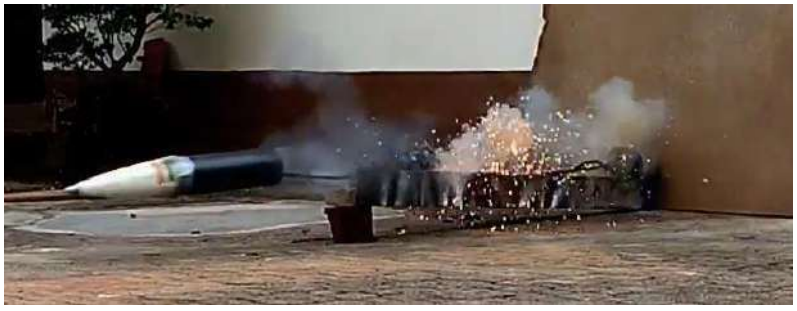
- Wear safety glasses, gloves, and hearing protection at all times.
- Keep a clear area of at least 10 meters around the test site.
- Load ejection charges last and ensure only trained team members handle them.
- Secure the rocket firmly and check continuity before arming the system.
- Fire the system remotely with a clear countdown and stay behind cover.

Success criteria:

No.:	Criteria description:	Method of validation:	Comments:
1	Charge Ignition	Visual	The charge was successfully ignited.
2	Body Tube separation	Visual	The body tubes separated successfully
3	Parachute Safety	Visual	No damage to the parachute fabric was observed.

Results:

Mass of the charge was reduced but still observed a successful ejection.
No expansion of charge-well holes.
No damage to any other components.



Conclusion:
First successful dual deployment test by the team.

Video Link:
https://drive.google.com/drive/folders/1J5xLXIbSNniWGYhNVJ2Mf91cwQLPQDPP?usp=drive_link

Tested and Recorded By:
Shreemad Burade
Approved By:
Ayyan Nikunj Bhartia

thrustMIT Test Report

2024 - 25

Test: Single Deployment		
Date:01/05/2024	**Test no.: 4**	**Result: Success**

Objective:
To test the Dual Deployment system of Parachute with a different charge-well setup.

Modifications/changes from last test:
Deployment of parachute was tested with Epoxy plug.

Setup & procedure:

- Choose a safe, open test area away from flammable materials and mark a 10-meter safety zone.
- Mount the rocket or test section securely on a stable stand to prevent movement.
- Connect firing electronics and check continuity, then disconnect to prepare charges safely.
- Measure and install charges last, insert igniters and secure all connections properly.
- Reconnect the firing system but keep it disarmed while the team clears to a safe distance.
- Arm the system, give a loud countdown, and fire remotely while observing from cover.
- Wait a few seconds, disarm the system, inspect components, and record test results.



Safety:

- Wear safety glasses, gloves, and hearing protection at all times.
- Keep a clear area of at least 10 meters around the test site.
- Load ejection charges last and ensure only trained team members handle them.
- Secure the rocket firmly and check continuity before arming the system.
- Fire the system remotely with a clear countdown and stay behind cover.

Success criteria:			
No.:	**Criteria description:**	**Method of validation:**	**Comments:**
1	Charge Ignition	Visual	The charge was successfully ignited.
2	Body Tube separation	Visual	The body tubes separated successfully
3	Parachute Safety	Visual	No damage to the parachute fabric was observed.

Results:

Successful ejection of the charge placed in the charge-well.
No expansion of charge-well holes.
No damage to any other components.



Conclusion:
Successful deployment test by the team.

Video Link:
https://drive.google.com/drive/folders/1Dg26pgf_tkIlS54rulZafB0O9ED3riPV?usp=drive_link

Tested and Recorded By:
Ajinkya Sathe
Approved By:
Ayyan Nikunj Bhartia

thrustMIT Test Report

2024 - 25

Test: Dual Deployment		
Date:11/11/2024	**Test no.: 5**	**Result: Success**

Objective:
To test the Dual Deployment system of Parachute with a different setup.

Modifications/changes from last test:
Deployment of parachute was tested with a setup mimicking the competition setup.

Setup & procedure:

- Choose a safe, open test area away from flammable materials and mark a 10-meter safety zone.
- Mount the rocket or test section securely on a stable stand to prevent movement.
- Connect firing electronics and check continuity, then disconnect to prepare charges safely.
- Measure and install charges last, insert igniters and secure all connections properly.
- Reconnect the firing system but keep it disarmed while the team clears to a safe distance.
- Arm the system, give a loud countdown, and fire remotely while observing from cover.
- Wait a few seconds, disarm the system, inspect components, and record test results.



Safety:

- Wear safety glasses, gloves, and hearing protection at all times.
- Keep a clear area of at least 10 meters around the test site.
- Load ejection charges last and ensure only trained team members handle them.
- Secure the rocket firmly and check continuity before arming the system.
- Fire the system remotely with a clear countdown and stay behind cover.

Success criteria:			
No.:	**Criteria description:**	**Method of validation:**	**Comments:**
1	Charge Ignition	Visual	The charge was successfully ignited.
2	Body Tube separation	Visual	The body tubes separated successfully
3	Parachute Safety	Visual	No damage to the parachute fabric was observed.

Results:

Successful ejection of the charge placed in the charge-well.
No expansion of charge-well holes.
No damage to any other components.



Conclusion:
Successful deployment test by the team.

Video Link:

https://drive.google.com/drive/folders/1CGGMgkPflFVOkKaWdovNgb629tjQx0A2?usp=drive_link

Tested and Recorded By:
Akash Siddharth
Approved By:
Ayyan Nikunj Bhartia

thrustMIT Test Report

2024 - 25

Test: Parachute Inflation		
Date:26/04/2025	**Test no.: 6**	**Result: Success**

Objective:
To ensure the parachutes inflate properly and without damage, ensuring reliable deployment during flight.

Modifications/changes from last test:
-

Setup & procedure:

- Inspect the parachute carefully and confirm there is no damage.
- Attach the parachute securely to the test rig or setup.
- Move to an open, clear area away from obstacles and crowds.
- Deploy the parachute smoothly and observe how it inflates.
- Check the parachute after the test for any tears, tangles or issues.

Safety:

- Stay completely away from the parachute's path during deployment.
- Wear gloves and safety glasses to protect yourself.
- Block off the area and keep all non-test people at least 30 meters away.
- Check the weather and cancel the test if winds are too strong.
- Assign a spotter to watch for danger and call an emergency stop if needed.

Success criteria:

No.:	Criteria description:	Method of validation:	Comments:
1	Parachute Inflation	Visual	Parachute inflated to its full size.

Results:

- No tears, line tangles or canopy damage were found after testing.
- The parachute maintained full shape and stability during inflation.
- Deployment was reliable across multiple tests under light wind conditions.



Conclusion:
The test was Successful.

Tested and Recorded By:
Ajinkya Sathe
Approved By:
Ayyan Nikunj Bhartia

B. SRAD Propulsion System Testing

THIS PAGE INTENTIONALLY LEFT BLANK.

C. SRAD Pressure Vessel Testing

THIS PAGE INTENTIONALLY LEFT BLANK.

D. SRAD GPS Testing & Avionics System Testing

THIS PAGE INTENTIONALLY LEFT BLANK.
APPENDIX B.D BEGINS ON THE FOLLOWING PAGE.

thrustMIT Test Report

2024 - 25

SRAD GPS & Avionics System Testing

Result	Colour
SUCCESS	
PARTIAL SUCCESS	
FAIL	

Date of Test	Name of Test	Objective	Results	Comments
15 October 2024	ESP32 – Sensors Test	Testing of ESP32 (microcontroller) along with barometric pressure sensor and the GPS for validation.	SUCCESS	The test was conducted to ensure that the microcontroller and the basic recovery components, the pressure sensor, and the GPS worked.
21 October 2024	MOSFET Ignition test	To test the ignition capability of the IRLB8748 MOSFET, which will be used on the SRAD Flight Computer.	SUCCESS	The MOSFET could burn Nichrome Wire with the help of 7.4V Lithium Ion 18650 13C cells in 2S1P fashion.
12 January 2025	Range Test	To verify the range capability of the telemetry link.	PARTIAL SUCCESS	The range obtained was 4.5 km, modules did not perform as expected, and the test was conducted in extremely humid and hot conditions.
2 February 2025	GPS Location Accuracy Test	To test the accuracy of GPS coordinates in a static condition.	PARTIAL SUCCESS	GPS accuracy was close to 30-40 cm; the test was performed in humid conditions, post sunset.
14 February 2025	IMU Test	To gauge the performance capability and accuracy of the 3-DoF IMU.	FAIL	Due to loose jumper cables, Data connections between microcontroller and peripheral were poor, leading to inconsistent data reception; Testing through SRAD PCB with secure connections recommended.
16 February 2025	IMU Test	To gauge the performance capability and accuracy of the 3-DoF IMU.	SUCCESS	Obtained consistent readings for 3-Axis Acceleration.

12 March 2025	SRAD Barometric Pressure Sensor Test	To test the values obtained by the barometric pressure sensor and its reliability.	SUCCESS	Average readings given by the sensor were accurate with low to no noise in the data, altitude conversion tables yielded altitude accurate up to about 10 m or approximately 30 feet. Must be followed by a vacuum test to confirm the working of the barometric pressure sensor at higher altitudes.
31 March 2025	Range Test	To validate the theoretical maximum range of the telemetry link as required between the rocket and the ground station.	PARTIAL SUCCESS	A stable data link of 6.25 km was obtained. Post 6.25 km, the data link became unstable; stability here refers to the accuracy and the rate at which the data was transmitted.
1 April 2025	SRAD GPS and Telemetry Test	To test the SRAD GPS location accuracy, along with transmission of the coordinates to the ground station via telemetry link in moving conditions.	SUCCESS	A range of about 1.5 – 2 km with accurate coordinates were obtained, the coordinates were plotted and compared with GPS plot obtained from a mobile phone using the Strava Application.
3 April 2025	COTS EasyMini Battery Drain Test	To test the battery runtime for the standby condition of the EasyMini Altimeter.	SUCCESS	EasyMini had a battery runtime of 13+ hours. The test was concluded with 7.09V in the battery, starting voltage was 7.09V. Lithium-ion 18650 cells in a 2S1P configuration (as is on the rocket) were used.
3 April 2025	SRAD Barometric Pressure Sensor Vacuum Test	To test the pressure sensor under low-pressure/vacuum conditions to simulate altitude and check flagging of DROGUE and MAIN.	FAIL	The microcontroller used was found to be faulty; another vacuum test with a working microcontroller will be conducted.
4 April 2025	SRAD Barometric Pressure Sensor Vacuum Test	To test the pressure sensor under low-pressure/vacuum conditions to simulate altitude and check flagging of DROGUE and MAIN.	SUCCESS	Pressure readings dropped as a vacuum was created. When the chamber was repressurised, the microcontroller flagged apogee and main correctly.
6 April 2025	COTS EasyMini Vacuum Test	To test the deployment of the COTS EasyMini Altimeter by simulating altitude using a vacuum pump.	SUCCESS	The EasyMini Altimeter identified and fired drogue and main signals correctly.

11 April 2025	SRAD Integrated System Test	To test and verify the functionality of SRAD Electronics entirely.	PARTIAL SUCCESS	The test was conducted indoors; hence, the GPS could not acquire a fix.
12 April 2025	SRAD Integrated System Test	To test and verify the functionality of SRAD Electronics entirely.	SUCCESS	The system worked as desired, and the GPS acquired a fix in a few minutes; in hot and dry conditions during the test.
24 April 2025	SRAD Runtime Test	To test and verify the battery runtime for the SRAD system as it undergoes integrated system testing.	SUCCESS	SRAD electronics system ran for 3 hours without the batteries being recharged.
26 April 2025	SRAD Pyro Test	To reverify the Pyro triggers of the SRAD Electronics.	SUCCESS	The SRAD system, along with the 2S1P configured Li-ion 18650 cells (7.4V), could ignite an e-match connected with wires with a practical wire length.

Tested & Recorded By:

Anushka Prabhutendolkar, Dhruv Phalod, Krishanu Dey, Shawn Chris, Sanskruti Gitan Ginde, Vanshdeep Trivedi, Adithi Shetty, Uppaluri Jahnavi

Approved By:

Samarth Vinod, Satvik Agrawal

E. Payload Recovery System Testing

THIS PAGE INTENTIONALLY LEFT BLANK.

F. Payload Testing

THIS PAGE INTENTIONALLY LEFT BLANK.
APPENDIX B.F BEGINS ON THE FOLLOWING PAGE.

thrustMIT Test Report

2024 - 25

Test: Pose Estimation Pipeline on Custom Trained Dataset		
Date: 12/11/24	**Test no.: 1**	**Result: Success**

Objective:
To test the accuracy and reliability of Yolov8 Pose Estimation on a custom trained dataset on our target object.

Modifications/changes from last test:
First Test

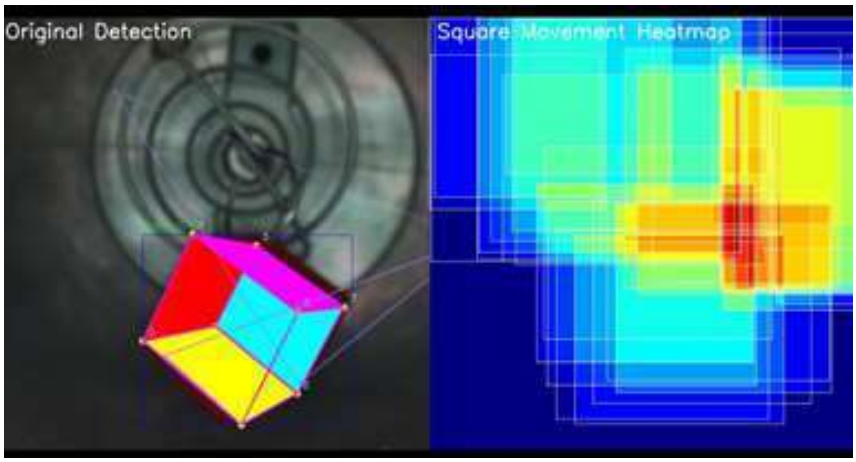
Setup & procedure:
- Install YOLOv8:
  pip install ultralytics
- Prepare dataset in COCO keypoint format
- Create pose.yaml with:
  path: /path/to/dataset
  train: images/train
  val: images/val
  kpt_shape: [num_keypoints, 8]
  names:
    0: class_name
- Train:
  yolo pose train model=yolov8s-pose.pt data=pose.yam
- Validate:
  yolo pose val model=best.pt data=pose.yaml
- Predict:
  yolo pose predict model=best.pt source=/path/to/images

Safety:
N/A (Software Test)

Success criteria:			
No.:	**Criteria description:**	**Method of validation:**	**Comments:**
1	Pose Estimation Accuracy & Confidence	Visual	Success
2	NA	NA	NA
3	NA	NA	NA

Results:

We got an accuracy of 98% on our custom trained yolov8s_pose model. Average confidence over a duration of 10 mins of test remained above 95%.



Tested & Recorded By:

Adi Narayan R S

Approved By:

Tejas Patil

thrustMIT Test Report

2024 - 25

Test: Object Tracking through Servo Actuation		
Date: 14/12/24	**Test no.: 2**	**Result: Success**

Objective:
To test if our dual shaft servo motor can actuate itself using a proportional loop to keep the target object in our region of interest from the feedback received from the camera.

Modifications/changes from last test:
First Test

Setup & procedure:
1. Connect all the components together. (Servo to PCA9685 and RPi 5).
2. Power on the system.
3. Execute the code which includes the proportional loop from the camera feedback.

Safety:
N/A (Software Test)

Success criteria:			
No.:	**Criteria description:**	**Method of validation:**	**Comments:**
1	The servo actuated accurately and always kept the target object in ROI	Visual	Success
2	NA	NA	NA
3	NA	NA	NA

Results:

During the entire test of 10 minutes, the servo accurately turned in the direction of the target object, keeping it in the ROI (region of interest) at any given point. This completed our tracking pipeline for computation.

Drive Video Link for the 1st Tracking Pipeline Test:
https://drive.google.com/file/d/1GeAUWZYEmMlaZjEvKvkyxAEWLnKqQrp_/view?usp=sharing

Tested & Recorded By:
Tejas Patil
Approved By:
Aryan Gupta

thrustMIT Test Report

2024 - 25

Test: Depth Estimation on Target Object		
Date: 27/12/2024	**Test no.: 3**	**Result: Failure**

Objective:
To estimate depth on sample dataset using DepthCrafter, Midas, Zoe Depth and other depth estimation models to verify if it can be used in the payload.

Modifications/changes from last test:
First Test

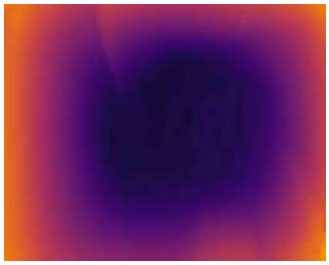
Setup & procedure:
1. Clone the model GitHub repository onto your machine.
2. Install all required Python libraries by following the requirements.txt file.
3. Download the model from Hugging Face to use for inference.
4. Run the run.py script, providing the video path and desired image resolution as arguments, adjusting the resolution based on your GPU's available VRAM for optimal inference performance.

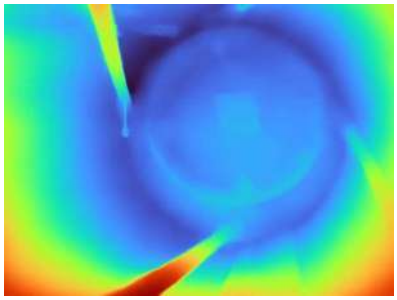
Safety:
N/A(Software Test)

Success criteria:			
No.:	**Criteria description:**	**Method of validation:**	**Comments:**
1	Accuracy of Depth Estimation	Visual	Inaccurate Estimation
2	NA	NA	NA
3	NA	NA	NA

Results:

The depth of the sample object was not estimated correctly as displayed in the second image.



Tested & Recorded By:

Aryan Gupta

Approved By:

Tejas Patil

thrustMIT Test Report

2024 - 25

Test: Depth Estimation on Target Object		
Date: 3/01/2024	**Test no.: 4**	**Result: Success**

Objective:
To estimate depth on our target object using DepthAnything v2 model to verify if it can be used in the payload.

Modifications/changes from last test:
Changed the Model to DepthAnything v2.

Setup & procedure:

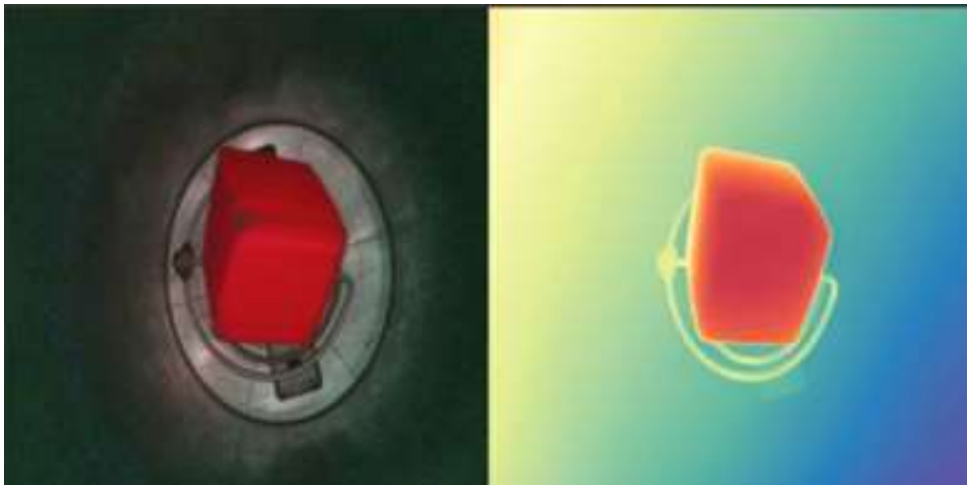
1. Install the required packages including transformers, torch, and pillow using pip.
2. Load the pre-trained Depth Anything V2 model, specifying which size variant you want (Small, Base, Large, or Giant).
3. Process your sample image by loading it with PIL or OpenCV and passing it through the model.
4. Save the resulting depth map as an image file after normalizing the values for better visualization.

Safety:
NA(Software Test)

Success criteria:			
No.:	**Criteria description:**	**Method of validation:**	**Comments:**
1	Accuracy of Depth Estimation	Visual	Accurate Estimation
2	NA	NA	NA
3	NA	NA	NA

Results:

The depth of the sample object was estimated correctly as displayed in the second image.



Tested & Recorded By:

Adi Narayan R S

Approved By:

Tejas Patil

thrustMIT Test Report

2024 - 25

Test: Conical Spring Analysis and Optimization		
Date: 25/12/25	**Test no.:** 5	**Result:** Success

Objective:
To find the right spring for our use case that provides us with max deflection at the peak g-force our rocket will undergo.

Modifications/changes from last test:
N/A (First Test)

Setup & procedure:

1. Run computer simulations to shortlist a few parameters that closely match the required spring characteristics based on real-life performance criteria such as load, displacement, and stiffness.
2. Select the wire type, diameter, and material.
3. Mount a mandrel (rod) that defines the spring's inner diameter.
4. Feed and wrap the wire tightly around the rotating mandrel.
5. Control the coil spacing (pitch) during winding.
6. Shape the spring ends as needed (loops, hooks, flat, etc.).
7. Heat-treat the spring to relieve stress and harden it.
8. Cut to final length and apply any finishing or coating.

Safety:
Wear gloves and eye protection to prevent injuries from sharp wire or spring recoil.
Use guarded machinery and controlled speeds to avoid accidents during coiling.

Success criteria:			
No.:	**Criteria description:**	**Method of validation:**	**Comments:**
1	The final spring was decided based on deflection created.	Visual	Success
2	NA	NA	NA
3	NA	NA	NA

Results:

Out of the multiple springs manufactured and tested under load, the final spring we chose was of the following parameters:

ID (smaller side) : 9 mm
ID (larger side) : 39 mm
Wire Diameter : 1.5 mm
No of coils : 5
Length : 42 mm
Material : Stainless Steel (SS)







Tested & Recorded By:
Mutra Sai Tharun
Approved By:
Tejas Patil

thrustMIT Test Report

2024 - 25

Test: Battery Drain Test for Payload		
Date: 15/03/2024	**Test no.: 5**	**Result: Failure**

Objective:
To Drain the entire battery while powering up the Payload and testing and recording peak performance and how long it takes for the entire battery to run out.

Modifications/changes from last test:
N/A

Setup & procedure:
1. Setup the entire payload and make connections as per the battery diagram.
2. Run the script that switches the inference on so as to allow the payload to run at peak capacity.
3. Before making all the connections check the voltage level of the battery.
4. Check the voltage routinely every 30 minutes.

Safety:
Lithium-ion batteries were placed in fireproof battery safes during charging and testing to prevent any short circuits or thermal runaway events that could lead to a catastrophe.

Success criteria:			
No.:	**Criteria description:**	**Method of validation:**	**Comments:**
1	Charge gets depleted.	Measurement using Multimeter	Failure
2	Inference	Visual	Success
3	NA	NA	NA

Results:

The battery test was a failure as the battery was disconnected before depletion. The entire capacity was not fully utilized. The PDB (Power Distribution Board) is not able to provide standard 5V-5A to power the Raspberry Pi. The dual shaft servo motor was also drawing overcurrent when pushed to its limits causing the voltage to sag.

Link to Drive Video:

https://drive.google.com/file/d/1Dx41XqYd-pJMj7e71WwnNybpMcPN91_W/view?usp=sharing

Tested & Recorded By:

Tejas Patil

Approved By:

Aryan Gupta

thrustMIT Test Report

2024 - 25

Test: Battery Drain Test for Payload		
Date: 21/03/2024	**Test no.: 6**	**Result: Success**

Objective:
To Drain the entire battery while powering up the Payload and testing and recording peak performance and how long it takes for the entire battery to run out.

Modifications/changes from last test:
We swapped the usage of PDB(Power Distribution Board) to a BEC (Battery Eliminator Circuit) which was able to provide us with steady 5V-5A supply for the Raspberry Pi 5. The servo movement was restricted to 60 degrees to avoid overcurrent and voltage sag.
The battery was allowed to run until depletion.

Setup & procedure:
1. Setup the entire payload and make connections as per the battery diagram.
2. Run the script that switches the inference on so as to allow the payload to run at peak capacity.
3. Before making all the connections check the voltage level of the battery.
4. Check the voltage routinely every 30 minutes.

Safety:

Lithium-ion batteries were placed in fireproof battery safes during charging and testing to prevent any short circuits or thermal runaway events that could lead to a catastrophe.

Success criteria:			
No.:	**Criteria description:**	**Method of validation:**	**Comments:**
1	Charge gets depleted.	Measurement using Multimeter	Success
2	Inference	Visual	Success
3	NA	NA	NA

Results:
The battery test was successful. The battery was depleted at 3 hours and 7 minutes which fulfills our requirements as per competition standards.

Drive Link to test:
https://drive.google.com/file/d/16jviYXdcU9tzGH5KnALWDqpaH_laeQuW/view?pli=1

Tested & Recorded By:
Tejas Patil
Approved By:
Aryan Gupta

G. Surface Roughness Testing

THIS PAGE INTENTIONALLY LEFT BLANK.
APPENDIX B.G BEGINS ON THE FOLLOWING PAGE.

thrustMIT Test Report

2024 - 25

Test: Surface Roughness Measurement of Unpainted Rough Body Tube		
Date:10/09/2024	**Test no.: 1**	**Result: Success**

Objective:
The objective of this test is to characterize the roughness of an unpainted, rough body tube.

Modifications/changes from last test:
-

Setup & procedure:

- The unpainted rough body tube was subjected to an initial visual inspection to confirm the absence of loose particles, surface contaminants, or visible damage, ensuring the specimen's readiness for non-destructive surface analysis.

- The Contact Confocal Profilometer was calibrated immediately prior to testing using a traceable surface roughness calibration artifact certified to international standards with verification of both lateral and vertical measurement axes

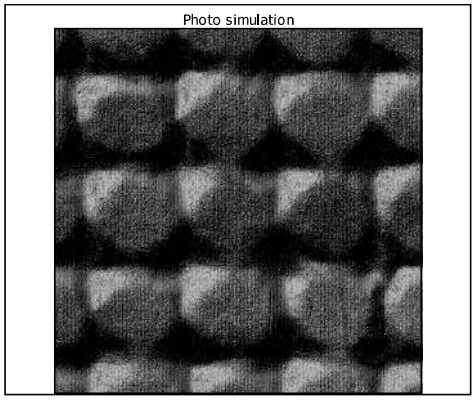
- The specimen was securely mounted on a vibration-isolated, precision-leveled stage using a non-deforming clamping system designed to prevent mechanical stresses of the test surface during measurement.



- Environmental conditions within the measurement laboratory were maintained within tightly controlled parameters, with temperature held at 22 ± 2 °C and relative humidity at 45% to 55%, to eliminate thermally induced dimensional changes and maintain equipment accuracy.

- The surface was scanned using a sub-micron vertical resolution setup, without application of an S-filter, while a Gaussian L-filter with a cutoff wavelength (λc) of 0.8 mm was applied according to ISO 25178 to remove surface form deviations.

- The LS-plane leveling function was employed to eliminate tilt across the surface, following which a full three-dimensional topographical scan was conducted across a 10 mm × 10 mm measurement area with high point-density acquisition.



- Surface texture parameters, including Sa, Sq, Ssk, Sku, Sp, Sv, and Sz, were calculated through standardized analysis software, with statistical outlier removal performed according to best practices to ensure data reliability and traceability.

Safety:

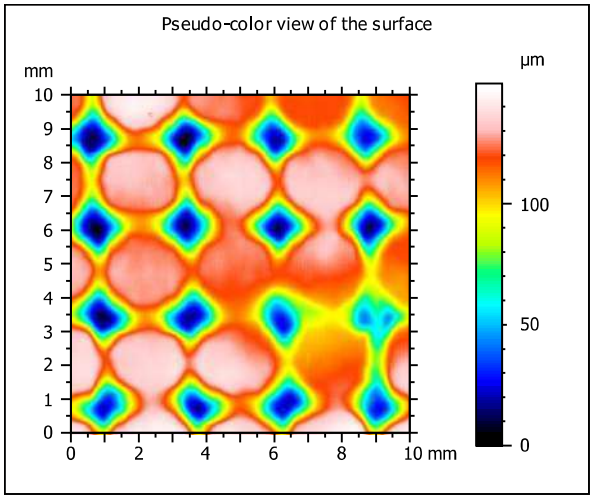
- The surface roughness testing was conducted under standard laboratory safety protocols to ensure the protection of personnel and equipment.
- All operators involved in the measurement were required to wear appropriate personal protective equipment (PPE), including laboratory coats, gloves, and anti-static wrist straps where applicable.
- The profilometer equipment was operated exclusively by trained and certified personnel to prevent handling errors and to maintain the integrity of the sensitive optical system.
- The specimen mounting and handling processes were carried out carefully to avoid mechanical damage to both the test sample and the profilometer stage.

- The testing environment was maintained at controlled temperature and humidity levels to prevent environmental factors from affecting the measurement accuracy and to ensure safe equipment operation.
- As the surface roughness testing process did not involve the use of hazardous chemicals, open flames, or high-voltage systems, the overall risk associated with the procedure was assessed as low.

Success criteria:

No.	Criteria description	Method of validation	Comments
1.	The arithmetic mean surface roughness shall be less than 5 µm.	Verified through profilometer data output.	Pass
2.	No individual valley depth shall exceed 50 µm.	Confirmed through surface profile visualization and analysis.	Pass
3.	Surface skewness > -1, surface dominated by valleys.	Validated through statistical analysis of surface height distribution.	Pass

Results:



ISO 25178 - Roughness (S-L)		
F: [Workflow] Leveled (LS-plane)		
S-filter (λs): None		
L-filter (λc): Gaussian, 0.8 mm		
Height parameters		
Sq	4.007	µm
Ssk	-0.60	
Sku	3.745	
Sp	24.12	µm
Sv	21.57	µm
Sz	45.69	µm
Sa	2.948	µm

The surface roughness of the unpainted rough body tube falls within acceptable limits for aerodynamic surfaces. No anomalies or excessive defects were detected. Surface treatment before painting or coating should consider the existing peak-valley profile.

Tested and Recorded By:
Ajinkya Sathe
Approved By:
Ayyan Nikunj Bhartia

thrustMIT Test Report

2024 - 25

Test: Surface Roughness Measurement of Painted Body tube		
Date:10/09/2024	**Test no.: 2**	**Result: Success**

Objective:
The objective of this test is to characterize the roughness of a painted body tube.

Modifications/changes from last test:
-

Setup & procedure:

- The unpainted rough body tube was subjected to an initial visual inspection to confirm the absence of loose particles, surface contaminants, or visible damage, ensuring the specimen's readiness for non-destructive surface analysis.

- The Contact Confocal Profilometer was calibrated immediately prior to testing using a traceable surface roughness calibration artifact certified to international standards with verification of both lateral and vertical measurement axes

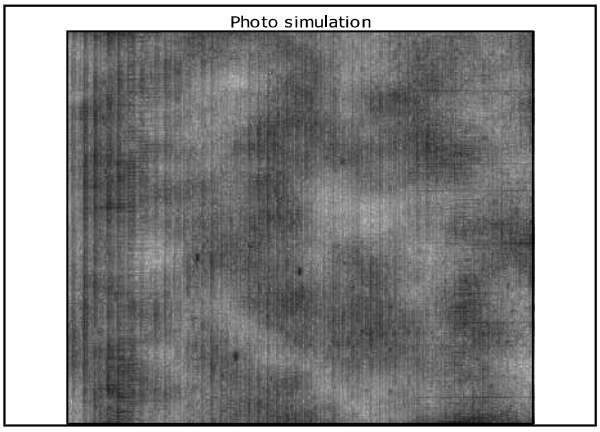
- The specimen was securely mounted on a vibration-isolated, precision-leveled stage using a non-deforming clamping system designed to prevent mechanical stresses of the test surface during measurement.



- Environmental conditions within the measurement laboratory were maintained within tightly controlled parameters, with temperature held at 22 ± 2 °C and relative humidity at 45% to 55%, to eliminate thermally induced dimensional changes and maintain equipment accuracy.

- The surface was scanned using a sub-micron vertical resolution setup, without application of an S-filter, while a Gaussian L-filter with a cutoff wavelength (λc) of 0.8 mm was applied according to ISO 25178 to remove surface form deviations.

- The LS-plane leveling function was employed to eliminate tilt across the surface, following which a full three-dimensional topographical scan was conducted across a 10 mm × 10 mm measurement area with high point-density acquisition.



- Surface texture parameters, including Sa, Sq, Ssk, Sku, Sp, Sv, and Sz, were calculated through standardized analysis software, with statistical outlier removal performed according to best practices to ensure data reliability and traceability.

Safety:

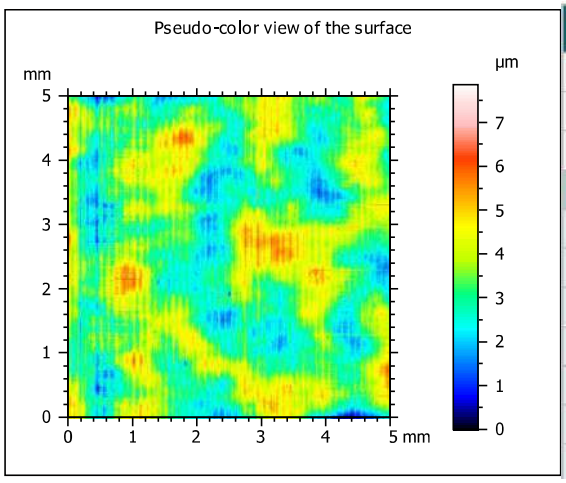
- The surface roughness testing was conducted under standard laboratory safety protocols to ensure the protection of personnel and equipment.
- All operators involved in the measurement were required to wear appropriate personal protective equipment (PPE), including laboratory coats, gloves, and anti-static wrist straps where applicable.
- The profilometer equipment was operated exclusively by trained and certified personnel to prevent handling errors and to maintain the integrity of the sensitive optical system.

- The specimen mounting and handling processes were carried out carefully to avoid mechanical damage to both the test sample and the profilometer stage.
- The testing environment was maintained at controlled temperature and humidity levels to prevent environmental factors from affecting the measurement accuracy and to ensure safe equipment operation.
- As the surface roughness testing process did not involve the use of hazardous chemicals, open flames, or high-voltage systems, the overall risk associated with the procedure was assessed as low.

Success criteria:

No.	Criteria description	Method of validation	Comments
1.	The arithmetic mean surface roughness shall be less than 5 µm.	Verified through profilometer data output.	Pass
2.	No individual valley depth shall exceed 10 µm.	Confirmed through surface profile visualization and analysis.	Pass
3.	Surface skewness > -1, surface dominated by valleys.	Validated through statistical analysis of surface height distribution.	Pass

Results:



ISO 25178 - Roughness (S-L)

F: [Workflow] Form removed (LS-poly 5)

S-filter (λs): None

L-filter (λc): Gaussian, 0.8 mm

Height parameters

Sq	0.4396	µm
Ssk	0.3764	
Sku	5.814	
Sp	5.680	µm
Sv	2.582	µm
Sz	8.262	µm
Sa	0.3408	µm

The painted smooth body tube exhibited an excellent surface finish. All success criteria were satisfied without any anomalies detected. The surface condition is deemed fully compliant for operational use.

Tested and Recorded By:
Ajinkya Sathe
Approved By:
Ayyan Nikunj Bhartia

H. Composite Tubes Compressive Testing

THIS PAGE INTENTIONALLY LEFT BLANK.
APPENDIX B.H BEGINS ON THE FOLLOWING PAGE.

thrustMIT Test Report

2024 - 25

Test: Glass Fibre Tube Compression Test (Destructive)		
Date: 22/08/2024	**Test No:** S1	**Result:** Maximum Load (Fmax) = 27.504 kN

Objective:

To obtain a Load vs Displacement plot for the GFRP specimen using a UTM (UTES-40).

Setup & procedure:

- Tested specimen is taken from the 2024 set of layups



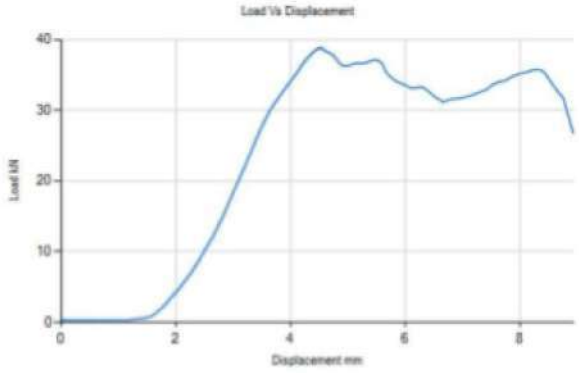
- The specimen is placed in between the two parallel platens of the UTM. For better distribution of load, cast iron plates are placed between the specimen and the platen.
- The platens are then tightened to the maximum extent such that there is no unnecessary movement of the specimen or the plates.
- Once they are tightened, the inbuilt software is fed the data required and the cycle is then initiated.
- Record the values and the plot obtained.

Safety:

- Faces of the specimen must be flat, parallel, and clean to ensure uniform contact with compression platens.
- Ensure the specimen is perfectly aligned along the loading axis to avoid eccentric loading and buckling.
- Verify that the compression fixture is properly assembled and calibrated before testing.
- Apply load at a controlled rate as specified by the standard to prevent dynamic effects or premature failure.
- Maintain a safe distance during testing; composite specimens may shatter or eject debris upon failure—use protective barriers and wear safety goggles at all times.

Success criteria:			
No.:	**Criteria description:**	**Method of validation:**	**Comments:**
1	No premature failure.	References.	The plots do not comply. Crack initiation at the bolt hole. No standards followed.
2			
3			

Results:



- Fmax = 38.832 kN.
- Displacement at Fmax = 4.53 mm

Tested and Recorded By:
Akash Siddarth
Approved By:
Madhav Sonkusare

thrustMIT Test Report
2024 - 25

Test: Carbon Fibre Tube Compression Test (Destructive)		
Date: 22/08/2024	**Test No:** S0	**Result:** Maximum Load (Fmax) = 27.504 kN

Objective:

To obtain a stress vs strain plot for the CFRP specimen using a UTM (UTES-40).

To obtain the compressive strength of the composite tube.

Setup & procedure:

- Tested specimen is taken from the 2024 set of layups.
- The specimen is placed in between the two parallel platens of the UTM. For better distribution of load, cast iron plates are placed between the specimen and the platen.
- The platens are then tightened to the maximum extent such that there is no unnecessary movement of the specimen or the plates.



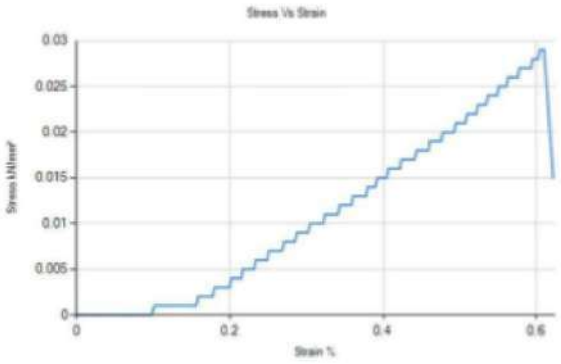
- Once they are tightened, the inbuilt software is fed the data required and the cycle is then initiated.
- Record the values and the plot obtained.

Safety:

- Faces of the specimen must be flat, parallel, and clean to ensure uniform contact with compression platens.
- Ensure the specimen is perfectly aligned along the loading axis to avoid eccentric loading and buckling.
- Verify that the compression fixture is properly assembled and calibrated before testing.
- Apply load at a controlled rate as specified by the standard to prevent dynamic effects or premature failure.
- Maintain a safe distance during testing; composite specimens may shatter or eject debris upon failure—use protective barriers and wear safety goggles at all times.

Success criteria:			
No.:	**Criteria description:**	**Method of validation:**	**Comments:**
1	No premature failure.	References.	The plots do not comply. The bored hole must be a factor. No standards followed.
2			
3			

Results:



- Fmax = 27.504 kN.
- Displacement at Fmax = 2.55 mm

Tested and Recorded By:
Akash Siddarth
Approved By:
Madhav Sonkusare

thrustMIT Test Report
2024 - 25

Test: Carbon Fibre Hand Layup Body Tube Compression Test (Destructive)		
Date: 02/04/2025	**Test No:** S2	**Result:** Compressive Strength = 0.08 kN/mm²

Objective:
To obtain a load vs displacement plot for the CFRP specimen using a UTM (UTES-40).

Modifications/changes from last test:
The cylindrical specimens were manufactured with the ASTM D695 standard procedure. The specimen maintains a L/D ratio of 2:1. The specimen also does not have any notches or holes.

Setup & procedure:

- Specimen is laid up according to the dimensions from the ASTM D695 (L/D ratio) and also conforming to the rocket dimensions.
- The specimen is placed in between the two parallel platens of the UTM. For better distribution of load, cast iron plates are placed between the specimen and the platen.
- The platens are then tightened to the maximum extent such that there is no unnecessary movement of the specimen or the plates.



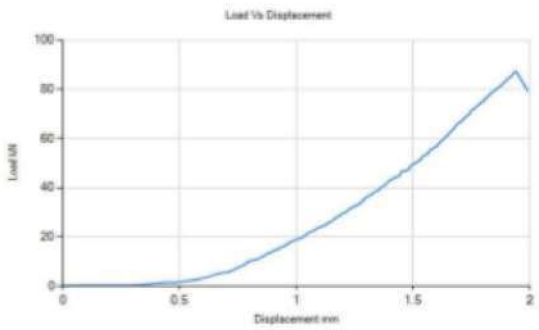
- Once they are tightened, the inbuilt software is fed the data required and the cycle is then initiated.
- Record the values and the plot obtained.

Safety:

- Faces of the specimen must be flat, parallel, and clean to ensure uniform contact with compression platens.
- Ensure the specimen is perfectly aligned along the loading axis to avoid eccentric loading and buckling.
- Verify that the compression fixture is properly assembled and calibrated before testing.
- Apply load at a controlled rate as specified by the standard to prevent dynamic effects or premature failure.
- Maintain a safe distance during testing; composite specimens may shatter or eject debris upon failure—use protective barriers and wear safety goggles at all times.

Success criteria:			
No.:	**Criteria description:**	**Method of validation:**	**Comments:**
1	No premature failure.	References.	The plots comply with earlier references.
2	No structural failure (displacement only in the ends).	Machine program.	
3			

Results:



- Fmax = 87.936 kN.
- Displacement at Fmax = 1.99 mm

Tested and Recorded By:
Tushit Chatterjee
Approved By:
Akash Siddarth

thrustMIT Test Report

2024 - 25

Test: Glass Fibre Hand Layup Body Tube Compression Test (Destructive)		
Date: 02/04/2025	**Test No:** S3	**Result:** Compressive Strength = 0.06kN/mm²

Objective:

To obtain a load vs displacement plot for the GFRP specimen using a UTM (UTES-40).

Modifications/changes from last test:

The cylindrical specimens were manufactured with the ASTM D695 standard procedure. The specimen maintains a L/D ratio of 2:1. The specimen also does not have any notches or holes.

Setup & procedure:

- Specimen is laid up according to the dimensions from the ASTM D695 (L/D ratio) and also conforming to the rocket dimensions.
- The specimen is placed in between the two parallel platens of the UTM. For better distribution of load, cast iron plates are placed between the specimen and the platen.
- The platens are then tightened to the maximum extent such that there is no unnecessary movement of the specimen or the plates.



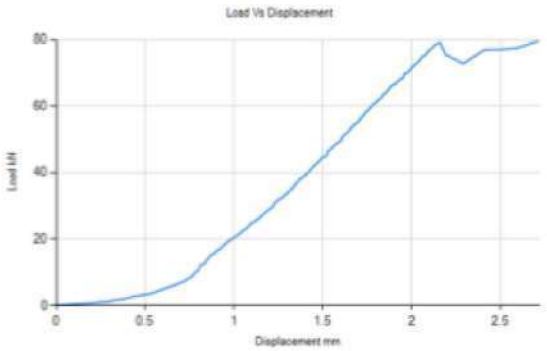
- Once they are tightened, the inbuilt software is fed the data required and the cycle is then initiated.
- Record the values and the plot obtained.

Safety:

- Faces of the specimen must be flat, parallel, and clean to ensure uniform contact with compression platens.
- Ensure the specimen is perfectly aligned along the loading axis to avoid eccentric loading and buckling.
- Verify that the compression fixture is properly assembled and calibrated before testing.
- Apply load at a controlled rate as specified by the standard to prevent dynamic effects or premature failure.
- Maintain a safe distance during testing; composite specimens may shatter or eject debris upon failure—use protective barriers and wear safety goggles at all times.

Success criteria:			
No.:	**Criteria description:**	**Method of validation:**	**Comments:**
1	No premature failure.	References.	The plots comply with earlier references.
2	No structural failure (displacement at only the end).	Machine program.	
3			

Results:



- Fmax = 79.488 kN.
- Displacement at Fmax = 2.71 mm

Tested By:

Tushit Chatterjee

Approved By:

Akash Siddarth

C. Appendix: Hazard Analysis

Table 20 Hazard Analysis Matrix

		Severity			
		1: Negligible	4: Marginal	9: Critical	16: Severe
Probability	1: Extremely Unlikely	1	4	9	16
	2: Unlikely	2	8	18	32
	3: Likely	3	12	27	48
	4: Very Likely	4	16	36	64

Table 21 Hazard Analysis Matrix

Category	Hazard	Severity	Likelihood	Hazard Rating	Mitigation Approach	Hazard Rating Post Mitigation
PRE-FLIGHT	Skin, eye, and respiratory hazards associated with composite airframe manufacturing.	9	3	27	Use of Respirators and gloves while handling composite. Ensure proper ventilation to control dust and fumes. Training members on safe handling practices and maintaining clean work areas.	8
	Improper handling of tools during rocket assembly.	4	3	12	To prevent improper tool handling during assembly, personnel must be trained, use approved tools, and follow a check-in system. Organised workspaces and peer checks help ensure safety.	4
	Misalignment of components in rocket assembly.	9	2	18	To mitigate misalignment during rocket assembly, use 3D-printed custom jigs and fixtures to ensure precise positioning of components. Perform step-by-step alignment. Tight tolerance machining, mock assemblies, and independent inspections further reduce the risk of errors.	9
	Missing rocket parts during assembly	9	2	18	To prevent missing parts during rocket assembly, maintain a detailed checklist verified at each step, and use a well-organised parts tray with labelled sections. Pre-assembly dry runs and independent inspections help catch missing components early.	9
	Improper handling of machined metal components during rocket assembly.	4	2	8	Wear gloves to prevent contamination, and store parts in padded, labelled trays. Training assembly teams on careful handling further minimises risks.	4

PRE-FLIGHT	Inadvertent ignition of solid rocket motor during storage.	16	1	16	Maintain strict control over environmental conditions such as temperature, humidity, and static electricity. Store motors in approved, grounded containers, away from heat sources, and ensure clear labelling, restricted access, and regular safety inspections.	9
	Inadvertent ignition of solid rocket motor during handling/assembly.	16	1	16	Ground motor to prevent static, use non-sparking tools, and handle components carefully. Follow strict procedures and ensure personnel are trained.	9
	Inadvertent ignition of black powder during assembly/handling.	16	1	16	Control static electricity through grounding, use non-sparking tools, avoid friction and heat, and handle the powder in a cool, dry environment following strict safety procedures.	9
	Thermal Runaway of Lithium Battery.	16	1	16	Proper Storage and Handling of the battery to be ensured. The battery should not be left exposed and unattended at anytime, especially during charging and use.	2
	Inadvertent Short Circuit in Recovery Electronics.	16	2	32	Proper Handling, wiring and insulation to ensure no shorting occurs.	8
	Electronic Component damage.	9	2	18	Handling Components with Care and ensuring proper storage and transportation.	4
	Damaged composite components during handling/-transport.	9	2	18	Use protective packaging, such as foam or padded enclosures, to prevent impact. Ensure that components are handled with care, using gloves to avoid contamination. Securely fasten components during transport to avoid shifting, and train personnel on proper handling techniques.	4
LAUNCH-PAD	Loosened metal components at launch-pad.	9	3	27	Ensure all fasteners are tightened and secured. Perform regular inspections and maintenance checks.	9
	Rocket is stuck on the launch rail due to misalignment of rail buttons.	16	1	16	Ensure proper alignment during pre-launch setup using precise alignment tools. Regularly inspect and maintain the rail system and buttons, and verify correct positioning before launch.	9

LAUNCH-PAD	Parachutes deploy with shear pins ejecting at the launchpad.	16	1	16	Use correctly rated shear pins, ensure proper installation, and confirm that black powder charges are secured and cannot inadvertently ignite. Thorough pre-launch inspections are required.	9
	Delayed ignition of solid rocket motor occurs during troubleshooting after failed initial command.	9	2	18	Always treat the motor as live until fully disarmed. Maintain a safe distance, follow strict misfire procedures, and allow sufficient wait time before approaching. Troubleshooting should only begin once the motor is confirmed safe.	9
	Electromagnetic Interference.	16	2	32	Proper Design to ensure EMI does not affect sensor readings and data, additionally use of Carbon fibre and metal components to be avoided in the electronics bay to facilitate telemetry.	8
	Thermal Runaway of Lithium Battery.	16	1	16	Batteries are to be DTEG compliant, with insulation and metallic casing. Batteries must be handled carefully, and the terminals must not be shorted.	9
	Voltage Fluctuations and Inadequate Power.	9	2	18	Proper Board design and extensive testing to ensure that power does not fluctuate and remains constant, to ensure the system remains powered.	2
	Complete Discharge of Battery.	16	1	16	Power Calculations, Battery Drain tests performed to validate system runs for long hours as desired.	1
FLIGHT	Rocket faces structural failure during flight, debris falls to ground.	16	1	16	Conduct thorough design validation, material testing, and pre-flight inspections to ensure structural integrity. Establish a safe flight zone with a clear debris recovery plan.	9
	Rocket trajectory deviates to turn ballistic.	16	1	16	To prevent inadvertent ignition of black powder during assembly or handling, ground components to avoid static discharge, use non-sparking tools, and handle with care. Store black powder securely, away from heat sources, and ensure proper safety procedures are followed at all times.	9
	Recovery mechanism fails to ignite the charge; the rocket falls to the ground.	16	1	16	Use redundant ignition systems and thoroughly test before flight. Verify correct installation and secure connections during pre-launch checks.	9

FLIGHT	Shock cords rip during ejection.	16	1	16	Use licensed equipment appropriately for the rocket's mass and deployment forces. Pre-flight inspections and proper attachment techniques.	9
	Parachutes deploy at unwanted altitudes.	9	2	18	To prevent parachutes from deploying at unwanted altitudes, ensure accurate calibration and programming of altimeters or timers, use redundant deployment systems, and perform thorough ground tests to verify correct functioning before flight.	9
	Thermal Runaway of Lithium Battery.	1	1	16	Proper Pre-Flight checks for the safety of the battery.	4
	High Acceleration forces damage electronics.	1	1	16	Proper mounting and fastening of electronics onto the designed mount, which is held by metallic rods.	4
	Freezing of components at high altitudes.	9	1	9	Ensure the components selected can withstand extreme temperatures.	1
POST-FLIGHT	Landing forces damage the electronics.	9	2	18	Ensure the components are mounted properly and the mount is able to withstand the landing forces.	2
	Injuries when handling rocket components post ground hit.	9	2	18	To prevent injuries when handling rocket components after a ground hit, treat all components as potentially hazardous, wear appropriate PPE, and approach cautiously. Inspect for sharp edges, residual pressure, or unexploded charges before any recovery or handling.	9

D. Appendix: Risk Assessment

Table 22 Severity Scale

Effect	Criteria: Severity of Effect	Ranking
Catastrophic - Without Warning	Total mission failure or system destruction occurring without any prior indication or warning	10
Catastrophic - With Warning	Total mission failure or system destruction occurring with prior warning, allowing limited response	9
Very High	Severe impact on mission success, significant system malfunction or degradation	8
High	Major impact on mission performance, requiring mission abort or significant corrective action	7
Moderate	Noticeable impact on mission objectives, manageable without mission abort	6
Low	Minor impact on mission performance, minor deviations from planned operation	5
Very Low	Very slight impact on performance, correctable or negligible	4
Minor	Minimal effect on system operation, lesser action required	3
Very Minor	No meaningful effect on system or mission performance	2
None	No effect on system or mission performance	1

Table 23 Occurrence Scale

Probability of Failure	Time Period	Ranking
Very High: Failure is almost inevitable	Every test	10
	Every 2–3 tests	9
High: Generally associated with processes similar to previous processes that have often failed	Every 5–7 tests	8
	Every 10 tests	7
Moderate: Generally associated with processes similar to previous processes which have experienced occasional failures, but not in major proportions	Once in 20 tests	6
	Once in 30+ tests	5
	Once during an entire test campaign	4
Low: Isolated failures associated with similar processes	Once across multiple test campaigns	3
Very Low: Only isolated failures associated with almost identical processes	Once in the lifetime of the project	2
Remote: Failure is unlikely. No failures associated with almost identical processes	Never Observed	1

Table 24 Detection Scale

Detection	Criteria: Likelihood the existence of a defect will be detected by process controls before next or subsequent process.	Ranking
Almost Impossible	No known controls available to detect failure mode	10
Very Remote	Very remote likelihood current controls will detect failure mode	9
Remote	Remote likelihood current controls will detect failure mode	8
Very Low	Very low likelihood current controls will detect failure mode	7
Low	Low likelihood current controls will detect failure mode	6
Moderate	Moderate likelihood current controls will detect failure mode	5
Moderately High	Moderately high likelihood current controls will detect failure mode	4
High	High likelihood current controls will detect failure mode	3
Very High	Very high likelihood current controls will detect failure mode	2
Almost Certain	Current controls almost certain to detect the failure mode. Reliable detection controls are known with similar processes.	1

Table 25 Failure Modes Effect Analysis

Process Step/Input	**Potential Failure Mode**	**Potential Failure Effects**	**Potential Causes**	SEVERITY (1-10)	DETECTION (1-10)	OCCURENCE (1-10)	RPN (RiskProfile Number)	**Action Recommended**	SEVERITY (1-10)	OCCURENCE (1-10)	DETECTION (1-10)	New RPN
What is the process step, change or feature under investigation?	In what ways could the step, change or feature go wrong?	What is the impact on the project if this failure is not prevented or corrected?	What causes the step, change or feature to go wrong? (How could it occur?)					What are the recommended actions for reducing the occurrence of the cause or improving detection?				
Recovery/ Black Powder	No detonation on command.	Parachutes stay undeployed.	Loose connection with E-match. E-match is not connected properly.	9	4	5	180	Using certified products. Multiple rounds of verification post assembly.	6	2	5	60
Recovery/ Black Powder	No detonation on command.	Parachutes stay undeployed.	Contamination of charge.	9	5	4	180	Proper packaging of charge under storage. Training of Personnel.	4	1	5	20
Moulds for composite manufacturing	Incorrect dimensions of airframe.	Computed design parameters pose no meaning.	Printing tolerances are taken wrong.	6	2	7	84	Single printer with enough practice to be used. Verifications pre layup to be rigorous.	3	2	2	12
Nose tip	Structural failure to internal components and airframe.	The rocket experiences a CATO	Nose tip is not clamping the nosecone with tangency.	10	1	6	60	Additional usage of adhesives.	4	2	1	8
Composite body tubes	Non-uniform diameter across airframe.	The rocket experiences a CATO	Manufacturing defects of composite parts	9	1	7	63	Sanding of all bodytubes to ensure no changes in diameter.	4	2	1	8
Parachutes	No proper inflation of parachutes	Rocket falls to ground with no restrictions.	Improper packing of parachutes with other recovery hardware.	7	2	6	84	Verification of full recovery setup.	3	2	2	12

Recovery/ Shear pins	Inadvertent seperation of body tubes.	Parachutes deploy earlier.	Shear pins are damaged.	8	2	5	80	Same grade new shear pins to be used. Unwanted actions to impact the pins prior to launch to be avoided.	4	1	2	8
Recovery/ Avionics	Inadvertent seperation of body tubes.	Parachutes deploy earlier.	Misfiring of electronics.	9	6	4	216	Add redundancy in deployment logic and ensure shielding of electronics from premature signal triggers	9	2	2	36
Airframe	Rough surface of airframe	Increased drag exeperienced by the rocket	Uneven finish of paint.	5	1	5	25	Sanding and polishing of the surfaces, to ensure even finish. Application of decal.	2	1	1	2
Airframe	Seperation at rigid points.	The rocket experiences a CATO	Higher than expected bending moment.	10	3	6	180	Compressive testing of components.	6	2	3	36
Fin attachment	A fin attachment with an unintended cant angle.	trajectory deviation, increased drag thus reducing predicted apogee.	Manufacturing defects.	7	3	4	84	Inspection of assembly after manufacturing to meet tolerance specifications.	5	1	3	15
Boattail	Thermal damage.	Reduction in apogee. Other structural integrity issues to child components.	Motor with reference to boattail is incorrectly mounted. Exhaust fumes are directed at the boattail.	6	1	5	30	Boattail's end to be aligned with the nozzle.	3	3	1	9
Motor	Combustion gases escape through an improperly sealed forward closure	The rocket experiences a CATO	Improper assembly of motor	10	4	4	160	Having assembly checklist, and verify each step	7	2	4	56

Motor	Changes in flight parameters due to changes in motor burn	Deviation of motor performance from it's specifications	Improper assembly of motor grains	7	2	3	42	Having assembly checklist, and verify each step	3	1	2	6
Fins	Fins shear during flight	The rocket experiences a failure	Failure of the fin attachment to the centring rings	10	3	5	150	Fin geometry designed such that it has high factor of safety, preventing failure	7	2	3	42
Fins	Fins break on touchdown of rocket	Loss of recovery points	Rocket lands with higher tochdown velocity.	6	2	5	60	Explicit dynamic simulations confirm that the part is safe, with an adequate safety factor.	2	1	2	4
Boattail	Boattail breaks on tochdown of rocket	Loss of recovery points	Rocket lands with higher tochdown velocity.	6	2	5	60	Explicit dynamic simulations confirm that the part is safe, with an adequate safety factor.	2	1	2	4
Payload	Vibrational loads.	Child components inside metal CanSat will be damaged.	Poor design.	7	2	6	84	Testing with right parameters in a vibrations lab.	3	2	2	12
Nosecone	Tangency is not maintained with the airframe.	Rocket veers off course; results in CATO	Errors in manufacturing.	9	5	6	270	Extension to the cylindrical end of the nosecone to conform to tangency.	4	2	5	40
Electronics/ Avionics	Damage to electronics before, during and after flight	Recovery electronics fail	Improper Mounting and Fastening	8	6	5	240	Ensure electronics are mounted using industry-standard fasteners, test circuits on vibration test beds.	8	3	3	72

Batteries	Risk of batteries catching fire	Leads to fire hazard	Haphazard storing and usage of batteries, exposure of batteries to extreme heat from the sun.	10	7	4	280	Store batteries in insulated containers, ensure proper handling protocols	10	2	3	60
Batteries for recovery electronics	Risk of Batteries running out of charge	Electronics would not get powered, no recovery systems	Inadequate charge or launch gets delayed for very long hours	9	4	5	180	Ensure full charge before launch and keep backup batteries	9	2	2	36
GPS	No/Wrong fix coordinates obtained	Unable to recover rocket	EMI interference, improper power, battery running out	9	5	4	180	Shield GPS from EMI, use voltage regulators, test GPS lock before launch	9	2	2	36

E. Appendix: Assembly, Pre-Flight, Launch, Recovery, and Off-Nominal Checklists

THIS PAGE INTENTIONALLY LEFT BLANK.
APPENDIX E BEGINS ON THE FOLLOWING PAGE.

thrustMIT Assembly Checklist

2024 – 25

Tools Checklist

Document version	V3.0

S.No	Tools	Qty	Check-off
1	Mechanical Gloves	15 Pairs	☐
2	Latex Gloves	15 Pairs	☐
3	Safety Goggles	10	☐
4	N95 Masks	25	☐
5	Rocket Stand	2	☐
6	Allen Key	3 Sets	☐
7	Pliers	2	☐
8	Hand-Held Drill	1	☐
9	Dremel	1	☐
10	Measuring Tape	2	☐
11	Orbital Sander	1	☐
12	Electric Screwdriver	2	☐
13	Flat Head Screwdriver	2	☐
14	JB weld	5	☐
15	M-seal	10	☐
16	Mallet	1	☐
17	WD-40	2	☐
18	Duct Tape	3	☐
19	Spanners	2 Sets	☐

thrustMIT Assembly Checklist

2024 – 25

Airframe Assembly Checklist

Document version	V3.0
Lead Engineer	Madhav Sonkusare
Team members present	Akash Siddarth, Ajinkya Sathe, Dhruv Jadhav
Approved By	Akash Siddarth

A. Nosecone Assembly

Step	Action	Check-off
1	Fasten the M12 x 1.75 threaded rod to the payload top plate.	☐
2	Attach the assembled payload to the nosecone bulkhead by fastening it through the M10 x 1.5 eye bolt.	☐
3	Insert the assembly into the nosecone and radially align the bulkhead to the nosecone shoulder using the triangular extrusion feature, ensuring that the nosecone bulkhead holes align with the shoulder bolt holes.	☐
4	Attach the nosetip by fastening it to the threaded rod extending outside the top of the nosecone.	☐

B. Main Bay Assembly

Step	Action	Check-off
1	Attach shock chords, quick link, and swivel link to the Main parachute (72” Iris Ultra).	☐
2	Attach the shock cord connected to the Main Parachute to the eye bolt on the nosecone bulkhead.	☐
3	Slide in the main bay body tube over the nosecone shoulder.	☐
4	Align main bay body tube holes with shoulder bolt holes.	☐
5	Fasten the main bay body tube, nosecone shoulder and nosecone bulkhead with twelve M5 x 0.8 bolts.	☐
6	Insert the main parachute along with the shock chords.	☐

C. Avionics Coupler Assembly

Step	Action	Check-off
1	Attach M10 x 1.5 eyebolt to main recovery bulkhead using hex nuts.	☐
2	Attach the other end of the shock cord of the Main Parachute to the eyebolt on the main recovery bulkhead through a Nomex blanket in between the charge wells for thermal insulation.	☐
3	Slide four M6 shafts with threaded ends through respective holes on the drogue recovery bulkhead.	☐
4	Fasten each shaft using hex nuts and then use wing nuts over each hex nut.	☐
5	Slide the assembled battery and avionics mount through the shafts.	☐
8	Slide the avionics coupler and ensure the camera hole on the static band is aligned with the lens of the RunCam Thumb Pro camera.	☐
9	Place the main recovery bulkhead and secure it with hex nuts and wing nuts similar to the setup at the bottom.	☐
10	Slide in the avionics coupler into the main body tube.	☐
11	Align the shear pin holes on the coupler and the main body and fasten it with #6-32 shear pins.	☐

D. Drogue Bay Assembly

Step	Action	Check-off
1	Attach shock chords, quick link, and swivel link to the Drogue Parachute (30” Elliptical Parachute).	☐
2	Attach M10 x 1.5 eyebolt to drogue recovery bulkhead using hex nuts.	
3	Attach one end of the shock cord to the eyebolt on the drogue recovery bulkhead.	☐
4	Slide the drogue bay over the avionics coupler and fasten it with 6 M5 x 0.8 bolts.	☐
5	Insert the drogue parachute along with the shock chords.	☐
6	Slide the motor bay coupler into the drogue bay and align the shear pin holes.	☐
7	Fasten the shear pin holes with #6-32 shear pins.	☐

E. Motor Bay Assembly

Step	Action	Check-off
1	Assemble the motor	☐
2	Slide the motor bay coupler to the motor bay and secure it with twelve M5 x 0.8 bolts	☐
3	Attach the fins to the forward and aft centring rings with two M5 x 0.8 bolts for each fin.	☐
4	Slide in the fin assembly into the motor bay such that the fins are between the slots.	☐
5	Slide in the AeroTech O5500X-PS motor into the motor bay and attach the eyebolt to the 3/8"-16 UNC threaded hole on the motor forward closure.	☐
6	Tie the other end of the shock chord connecting the drogue parachute to the eyebolt connected to the report.	☐
7	Secure the retainer to the aft centering ring while aligning the extrusions, ensuring the bolt holes line up, and fasten using eight M4 x 0.7 bolts.	☐
8	Slide in the boattail while aligning the slots and secure with four M5 x 0.8 bolts.	☐

thrustMIT Assembly Checklist

2024 – 25

Avionics Assembly Checklist

Document version	V1.0
Lead Engineer	Satvik Agrawal
Team members present	Dhruv Phalod, Ajinkya Sathe, Madhav Sonkusare
Approved By	Akash Siddarth.

Step	Action	Check-off
1	Connect all SRAD electronic components to the PCB.	☐
2	Ensure they are firmly placed and oriented correctly, fasten the PCB onto the mount with M4 x 0.7 pan head bolts.	☐
3	Fasten the COTS components on the mount using M3 x 0.5 pan head bolts.	☐
4	Insert battery holders and battery packs into the battery mount and ensure they are fastened with M3 x 0.5 bolts.	☐
5	Place the camera setup on the mount and fasten it using M4 x 0.7 pan head bolts.	☐
6	Ensure all components and antennas are firmly connected.	☐
7	Connect and fasten pull-pin switches in the designated spots and ensure the pins are put (circuit is open).	☐
8	Connect the batteries as required using the pre-marked labels, ensure polarity is correct	☐
9	Connect “Drogue” and “Main” wires safely to SRAD recovery components, D4184 and MOSFET and check continuity of load.	☐
10	Connect “Drogue” and “Main” wires safely to COTS EasyMini and check continuity of load.	☐
11	Run zip ties through dedicated slots to ensure snug fit of all components.	☐

thrustMIT Assembly Checklist

2024 – 25

Payload Assembly Checklist

Document version	V2.0
Lead Engineer	Tejas Patil
Team members present	Tejas Patil, Aryan Gupta, Adi Narayan R S
Approved By	Aryan Gupta

Before starting this checklist, it is essential to ensure that all the components and parts necessary for the payload assembly are ready. This includes:

1. All electrical components such as: RPI Board, PCA Board, BEC Board, MPU, Airtag, Camera, Servo Motor.
2. Nuts, Bolts, and Washers, along with the required tools.
3. 3D printed PLA+ Payload Mount
4. 3D printed PLA+ Camera Plate
5. 3D printed PLA+ U-Bracket
6. Conical Spring and an SS 316 cube and their backups.
7. Backup 3D printed parts and electrical components.

Step	Action	Check-off
1	Attach the object to the main spring using the loop provided on the spring.	☐
2	By having an M4 bolt and its required spacer, place it inside the conical spring towards the smaller end.	☐
3	Using a lock nut, secure the spring to the 3D printed PLA+ U-bracket.	☐
4	Using M3 x 12 bolts, secure the U-bracket to the top bulkhead.	☐
5	Place the top bulkhead on top of the top CANSAT (longer CANSAT) and align the top CANSAT and the top bulkhead using the given markings and secure it using six M4 x 12 countersunk bolts (grade 10.9).	☐
6	Using M3 x 16 hex bolts, secure the 3D printed PLA+ payload mount to the bottom bulkhead.	☐
7	Using the same bolts, place them in the respective holes of the bottom axle of the servo, and then attach the bottom axle to the servo motor.	☐
8	Using M3 x 5 bolts, secure the camera plate to the top axle of the servo and then attach the top axle to the servo motor.	☐
9	Fasten the entire servo mechanism to the middle bulkhead using M3 nuts and washers (make sure it is fastened tightly).	☐
10	Using M3 x 6 bolts, secure the MPU first and then the AirTag in its case at the back and the side of the payload mount, respectively.	☐
11	Place the BEC board in its slot at the other side of the payload mount with its wires already soldered in.	☐
12	Using M2.5 x 6 bolts, secure the PCA board and the CSI adapter at the back of the payload mount.	☐

13	Using M2 x 20 bolts and M2 nuts, secure the pull pin switch with the head of the bolt facing downwards.	☐
14	Using M2.5 x 25 bolts, secure the RPI board in front of the payload mount.	☐
15	Using the M1.6 nuts and bolts, secure the buzzer placed just in front of the RPI.	☐
16	Place the battery in the slot provided in the payload mount and use zip ties to secure it.	☐
17	Make the required electrical connections as mentioned in the payload wiring diagram.	☐
18	Once all the electrical connections are done, slide the bottom CANSAT (smaller CANSAT) over the bottom bulkhead while holding the camera, servo, and LED wires outside from the top of the CANSAT.	☐
19	Align the bottom CANSAT holes using the given marking and ensure the pin goes into the pull-pin switch through the hole present. Then, using M4 x 12 countersunk bolts (grade 10.9), secure the bottom CANSAT to the bottom plate.	☐
20	Pass the three wires left outside the CANSAT through the given slots on the middle bulkhead and make the required electrical connections to the servo motor, camera, and LED.	☐
21	Then, align the middle bulkhead on top of the bottom CANSAT with the given marking and secure it using the same M4 x 12 countersunk bolts (grade 10.9).	☐
22	Secure the camera on top of the camera plate using M2 x 5 bolts.	☐
23	Place the top CANSAT over the middle bulkhead and align it with the given marking and secure it using the same M4 x 12 countersunk bolts (grade 10.9).	☐

thrustMIT Checklist

2024 – 25

Pre-Flight & Pre-Launch Checklist

Document version	V2.0
Lead Engineer	Akash Siddarth
Team members present	Ajinkya Sathe, Madhav Sonkusare, Tejas Patil, Satvik Agrawal.
Approved By	Tejas Patil

Step	Action	Check-off
1	Check and ensure that all avionics switches are in the dis-armed position.	☐
2	Perform a visual check to ensure the integrity of the rocket body and have the flight safety review.	☐
3	Fill in and submit the flight card to the Launch Control Officer.	☐
4	At the appointed time, transport the rocket to the launch pad accompanied by the required personnel only.	☐
5	Ensure launch pad and surrounding area are clear of all combustible material.	☐
6	Slide the rocket onto the launch rail.	☐
7	Perform a final visual inspection of the rocket to check for any damage during transportation.	☐
8	Raise the rocket and the rail to launch orientation.	☐
9	After obtaining all necessary clearances, enable the Altimeter and Flight Computer's power supplies and payload's power supply.	☐
10	Listen for an audible beep to confirm a successful power up and arming	☐
11	Power on the camera.	☐
12	Communicate with ground station to verify successful telemetry link.	☐
13	Acquire permission from the Range Manager to insert the igniter.	☐
14	Check for continuity and then proceed to insert the igniter into the motor, leaving the leads unconnected.	☐
15	Cross check if the firing line is not "hot".	☐
16	Confirm non-essential personnel have evacuated the launch pad area	☐
17	Authorised personnel shall connect the igniter to the firing line.	☐

thrustMIT Checklist

2024 – 25

Recovery Checklist

Document version	V2.0
Lead Engineer	Ajinkya Sathe
Team members present	Akash Siddarth, Tejas Patil, Satvik Agrawal
Approved By	Madhav Sonkusare

Step	Action	Check-off
1	Avionics team confirms apogee with telemetric data and reports GPS location using primary and redundant tracking system.	☐
2	MCC authorises the recovery team's departure to the identified location.	☐
3	In case of loss of GPS data, contact MCC with the backpack radio and provide the Team Identification Number. The Recovery Team then departs with coordinates provided by the MCC.	☐
4	Upon arrival at the location, capture photographs of all components.	☐
5	Verify that all energetics are spent.	☐
6	Listen to the beeps on the EasyMini for apogee and verify the apogee value sent to the ground station via telemetry by the SRAD system.	☐
7	Insert SRAD system pull-pin switches to power the SRAD system, but keep the EasyMini powered on to maintain beeps of apogee	☐
8	Recover the SD card on the SRAD system and in the flight camera	☐
9	Inspect all components for damage.	☐
9	Secure payload.	☐
10	Ensure parachutes are not tangled or damaged and pack them.	☐
11	Disassemble the rocket and place the parts on the loading bay of the truck.	☐
12	Report back to the MCC and provide necessary data.	☐
13	Return to the designated space for the team and debrief.	☐
14	Inspect all internal components.	☐
15	Remove and clean the motor casing.	☐
16	Pack all components safely.	☐

thrustMIT Checklist

2024 – 25

Off-Nominal Checklist

Document version	V2.0
Lead Engineer	Akash Siddarth
Team members present	Ajinkya Sathe, Tejas Patil, Satvik Agrawal
Approved By	Madhav Sonkusare

A. Critical System Malfunction

Step	Action	Check-off
1	Evaluate the seriousness of the malfunction and its effect on the launch.	☐
2	If conditions allow, attempt to isolate and resolve the malfunction.	☐
3	If resolution cannot be achieved within the allowable time frame, initiate launch scrub procedures.	☐
4	Disarm affected systems to prevent unintended activation or cascading failures.	☐

B. Environmental Hazards

Step	Action	Check-off
1	Evaluate the severity and potential impact on rocket stability, trajectory, and safety.	☐
2	Consult meteorological experts or relevant authorities for a situational assessment.	☐
3	If safety thresholds are exceeded, initiate launch scrub procedures.	☐
4	Neutralize systems susceptible to unfavorable environmental factors.	☐

C. Safety Violations

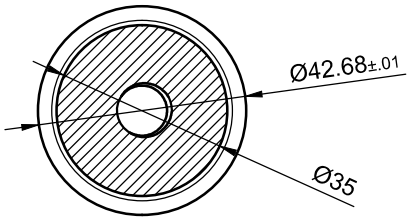
Step	Action	Check-off
1	Identify and address violations according to safety protocols and competition rules.	☐
2	If violations cannot be resolved in time or pose a risk to personnel or equipment, initiate a launch scrub.	☐
3	Safely disarm the rocket and correct all violations before resuming launch procedures.	☐

D. Launch Scrub

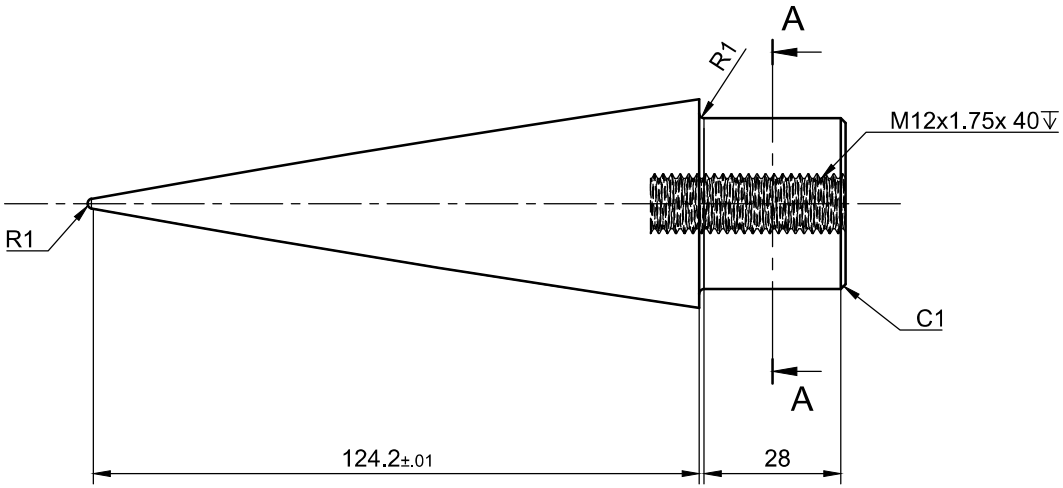
Step	Action	Check-off
1	Confirm scrub decision with the Mission Control Center (MCC) and any concerned authorities.	☐
2	Announce the launch scrub to the team and personnel via radio and ground communication systems.	☐
3	Immediately freeze all launch operations.	☐
4	Disarm the ignitor once scrub is confirmed.	☐
5	Remove the ignitor in the launch pad when deemed safe by the avionics team.	☐
6	Disable the flight computer and onboard power systems safely.	☐
7	Conduct a safety sweep of the launch pad to confirm all systems are powered down and safe.	☐
8	Secure the launch vehicle and ground support equipment for inspection or troubleshooting.	☐
9	Record the cause of the scrub and all related telemetry or sensor data.	☐
10	Secure the launch vehicle and ground support equipment for inspection or troubleshooting.	☐
11	Debrief the team and log all actions taken in the Launch Operations Log.	☐
12	Reassess environmental and system conditions before rescheduling or reattempting the launch.	☐

F. Appendix: Engineering Drawings

THIS PAGE INTENTIONALLY LEFT BLANK.
APPENDIX F BEGINS ON THE FOLLOWING PAGE.

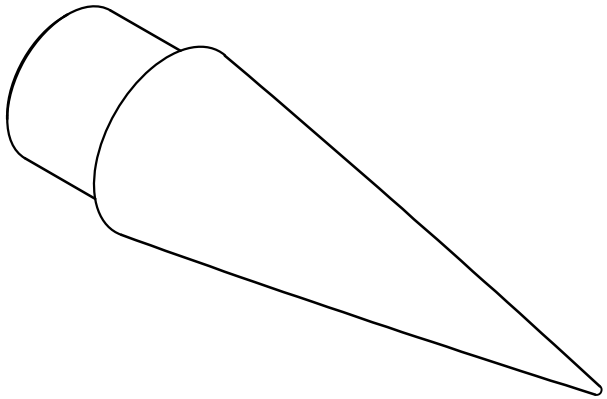


A-A (1:1)



FRONT VIEW (1:1)

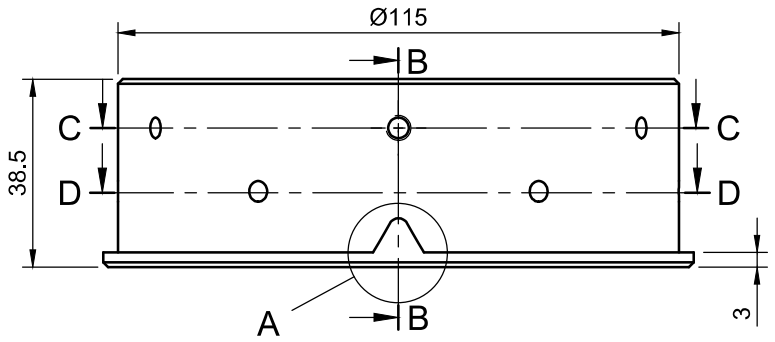
Parameter	Symbol	Value
Base Radius	R	6.3
Length	L	125.38
Radius (Tangent)	rho	1250.78



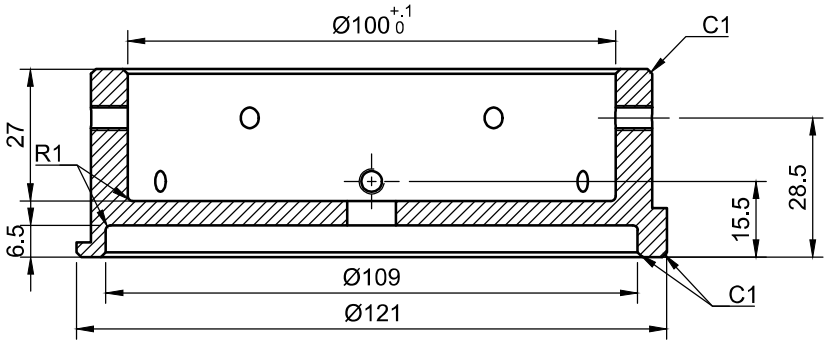
ISOMETRIC VIEW (1:1)

All Linear Dimensions are in mm.
Linear Tolerances are ±0.1 mm unless specified.
Angular Tolerances are ±1° unless specified.

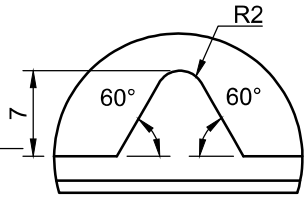
Dept.	Technical reference	Created by	Approved by
Structures	N/A	Akash Siddarth 01-04-2025	Madhav Sonkusare 03-04-2025
thrustMIT		Document type: Part Drawing	Document status: Released
		Title: Nose Cone Tip	DWG No.: VV_NC_TIP
			Rev.: 3 / Date of issue: / Sheet: 1/1



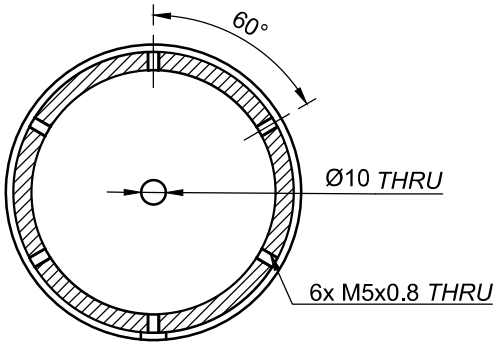
FRONT VIEW (1:1)



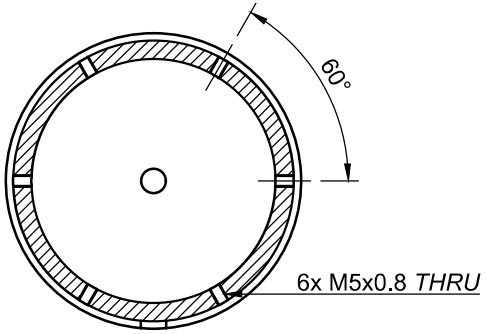
B-B (1:1)



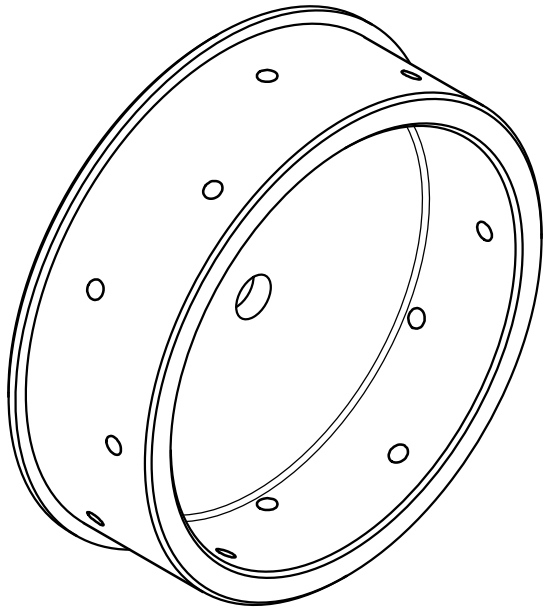
A (2.5:1)



C-C (1:2)



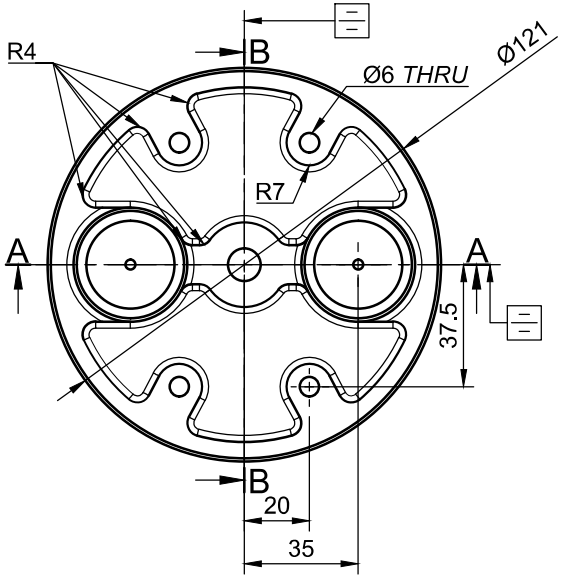
D-D (1:2)



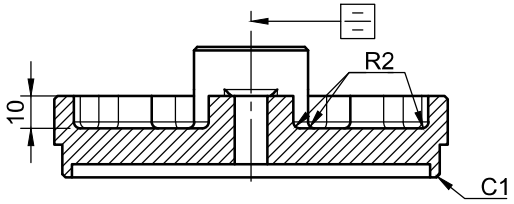
ISOMETRIC VIEW (1:1)

All Linear Dimensions are in mm.
Linear Tolerances are ±0.1 mm unless specified.
Angular Tolerances are ±1° unless specified.

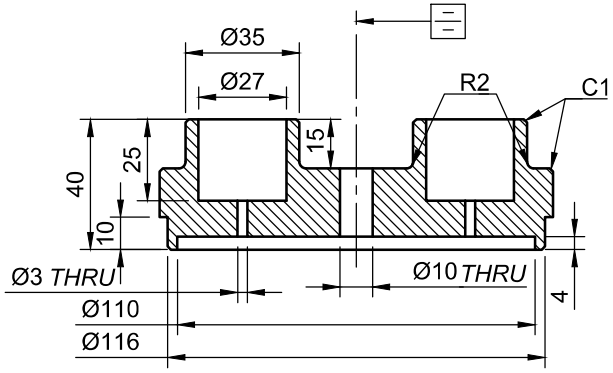
Dept.	Technical reference	Created by	Approved by
Structures	N/A	Madhav Sonkusare 13-03-2025	Akash Siddarth 15-03-2025
		Document type: Part Drawing	Document status: Released
thrustMIT		Title: Nosecone Bulkhead	DWG No.: VV_NC_BLK
		Rev.: 3	Date of issue:	Sheet: 1/1



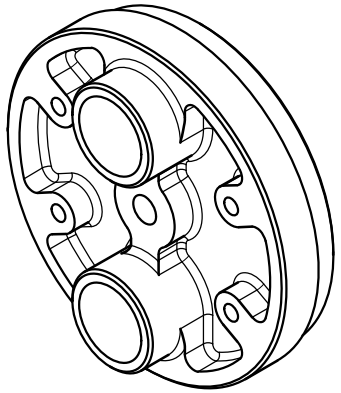
FRONT VIEW (1:1.5)



B-B (1:1.5)



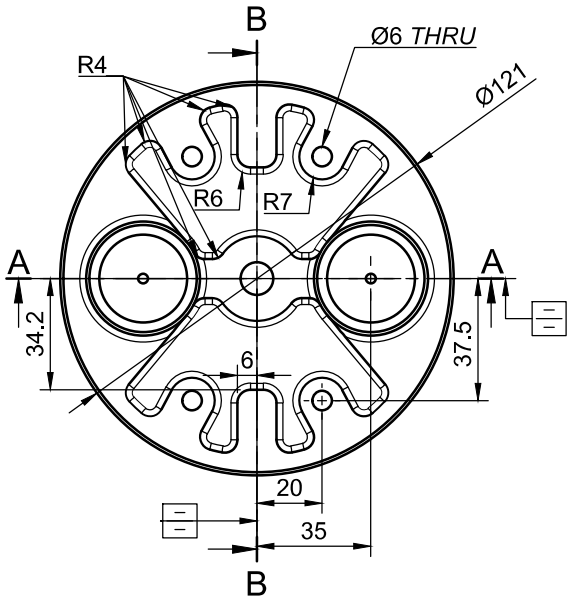
A-A (1:1.5)



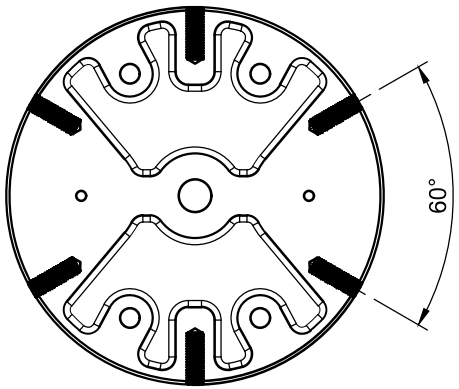
ISOMETRIC VIEW (1:1.5)

All Linear Dimensions are in mm.
Linear Tolerances are ±0.1 mm unless specified.
Angular Tolerances are ±1° unless specified.

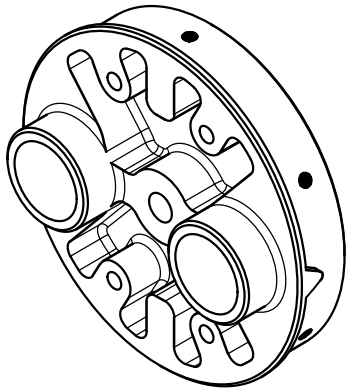
Dept.	Technical reference	Created by	Approved by
Structures	N/A	Madhav Sonkusare 14-03-2025	Akash Siddarth 16-03-2025
		Document type: Part Drawing	Document status: Released
thrustMIT		Title: Main Recovery Bulkhead	DWG No.: VV_MB_BLK
			Rev.: 3 / Date of issue: / Sheet: 1/1



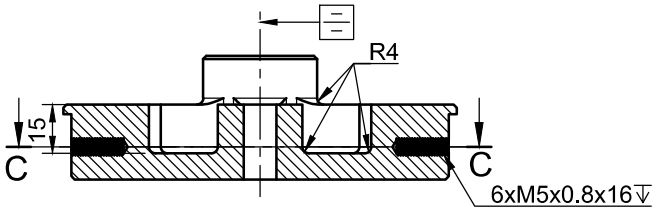
FRONT VIEW (1:1.5)



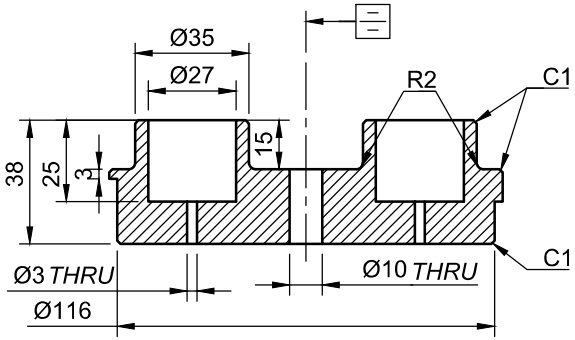
C-C (1:1.5)



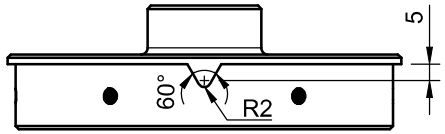
ISOMETRIC VIEW (1:1.5)



B-B (1:1.5)



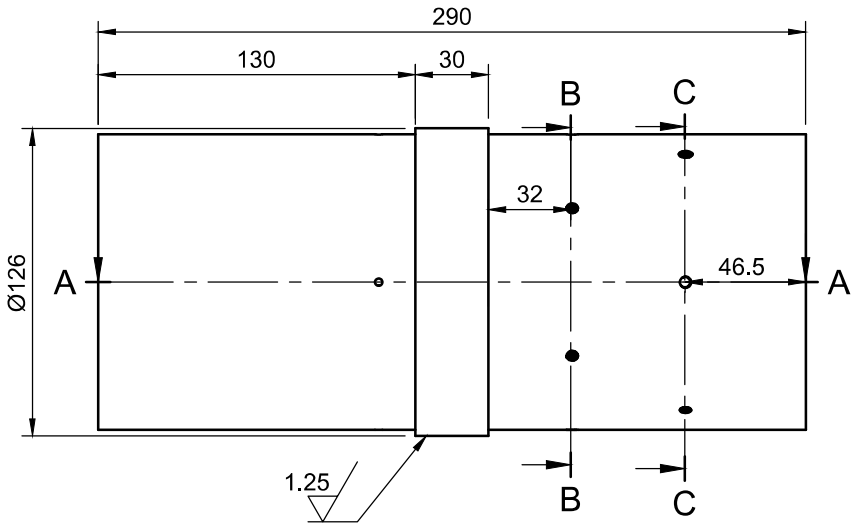
A-A (1:1.5)



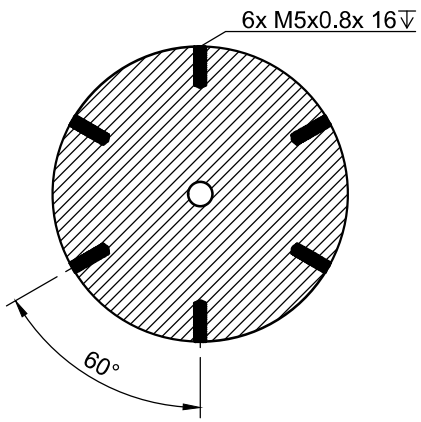
RIGHT VIEW (1:1.5)

All Linear Dimensions are in mm.
Linear Tolerances are ±0.1 mm unless specified.
Angular Tolerances are ±1° unless specified.

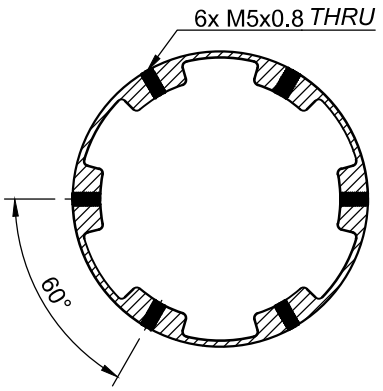
Dept.	Technical reference	Created by	Approved by
Structures	N/A	Madhav Sonkusare 14-03-2025	Akash Siddarth 16-03-2025
		Document type: Part Drawing	Document status: Released
thrustMIT		Title: Drogue Recovery Bulkhead	DWG No.: VV_DB_BLK
			Rev.: 2 | Date of issue: | Sheet: 1/1



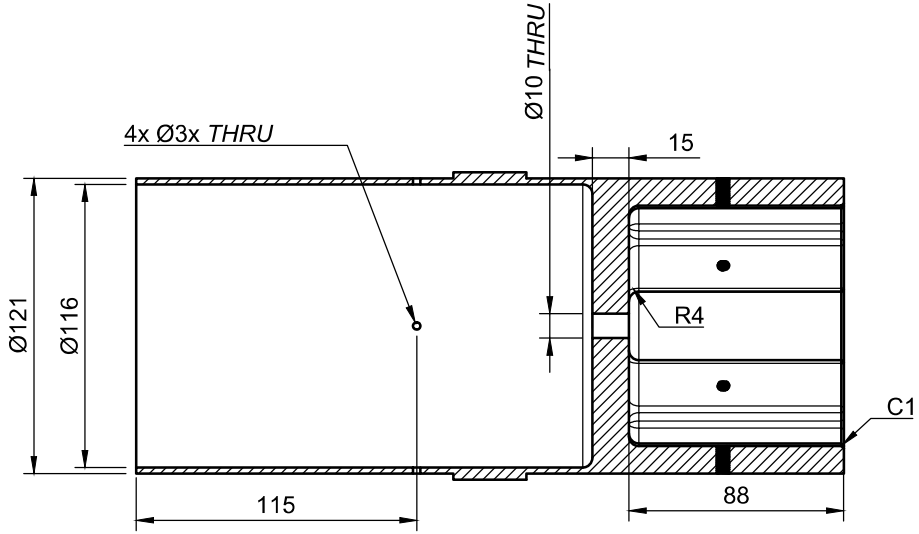
TOP VIEW (1:2)



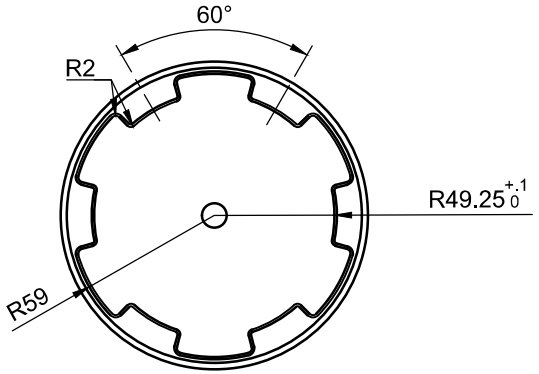
B-B (1:2)



C-C (1:2)



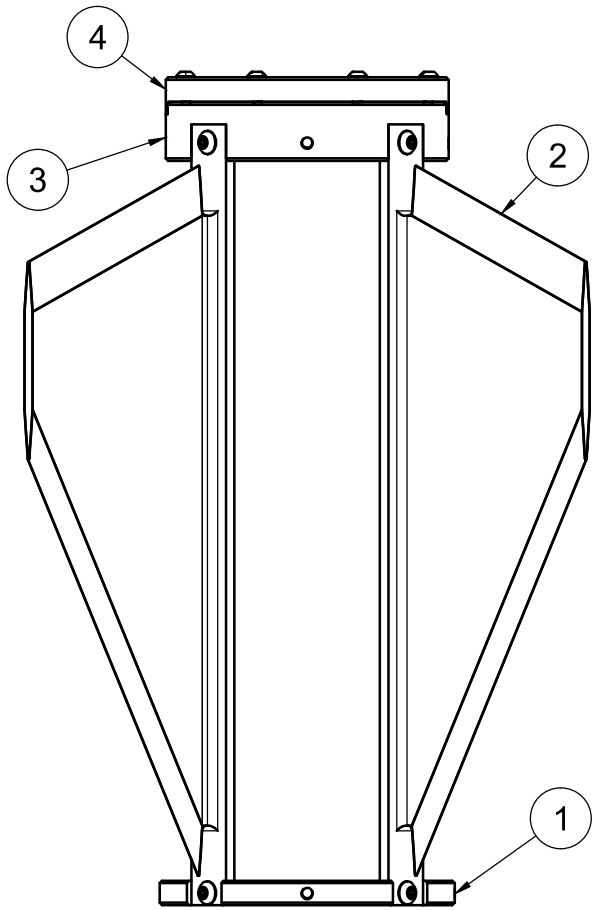
A-A (1:2)



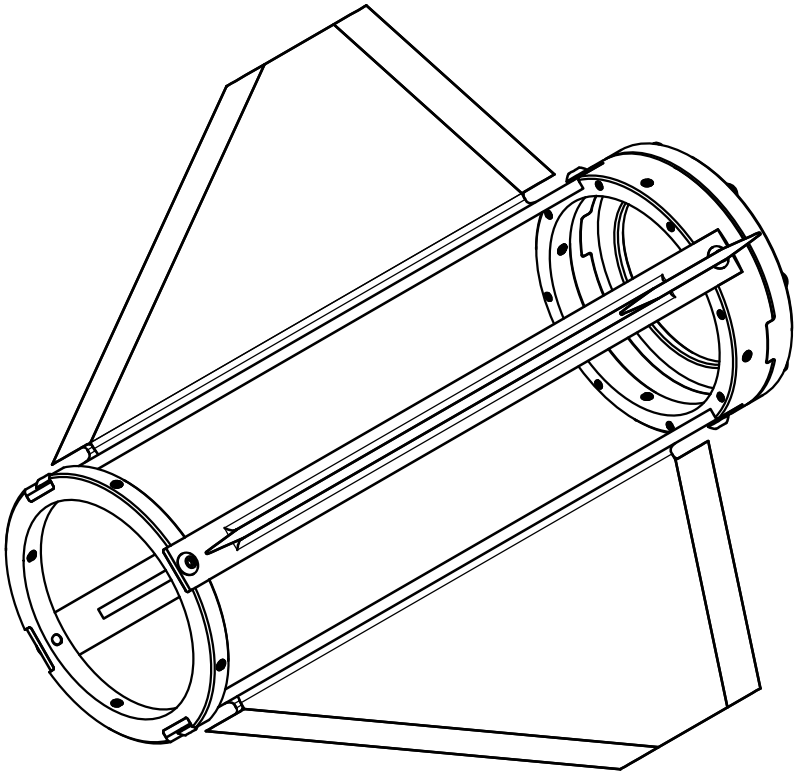
FRONT VIEW (1:2)

All Linear Dimensions are in mm.
Linear Tolerances are ±0.1 mm unless specified.
Angular Tolerances are ±0.1° unless specified.

Dept.	Technical reference	Created by	Approved by
Structures	N/A	Akash Siddarth 30-03-2025	Madhav Sonkusare 01-04-2025
		Document type: Part Drawing	Document status: Released
thrustMIT		Title: Motor Bay Coupler	DWG No.: VV_MB_CLR
			Rev.: 4 | Date of issue: | Sheet: 1/1



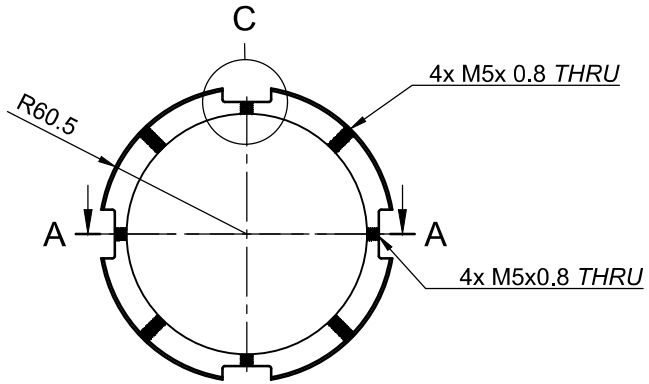
FRONT VIEW (1:2)



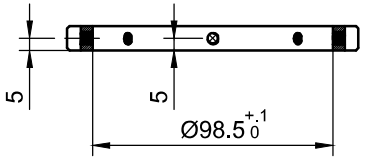
ISOMETRIC VIEW (1:2)

Parts List			
Item	Part Number	Qty	Material
1	VV_MB_FCR	1	Al 6061 T6
2	VV_MB_FIN	4	Al 6061 T6
3	VV_MB_ACR	1	Al 6061 T6
4	VV_MB_RTR	1	Al 6061 T6

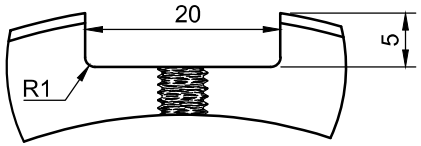
Dept. Structures	Technical reference N/A	Created by Akash Siddarth 30-03-2025	Approved by Madhav Sonkusare 02-04-2025
thrustMIT		Document type Assembly Drawing	Document status Released
		Title Fin Assembly	DWG No. VV_FIN_ASLY
			Rev. 2 / Date of issue / Sheet 1/1



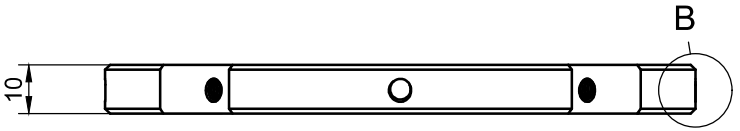
TOP VIEW (1:2)



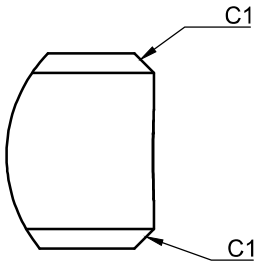
A-A (1:2)



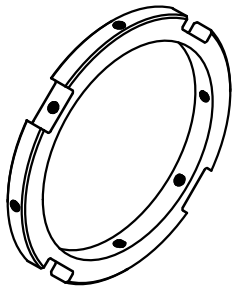
C (2:1)



FRONT VIEW (1:1)



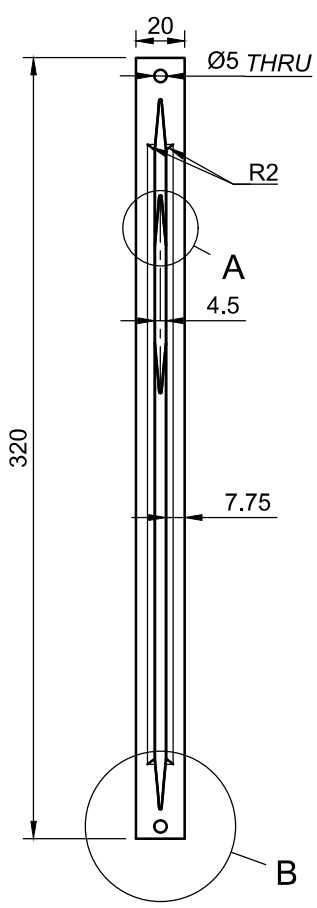
B (4:1)



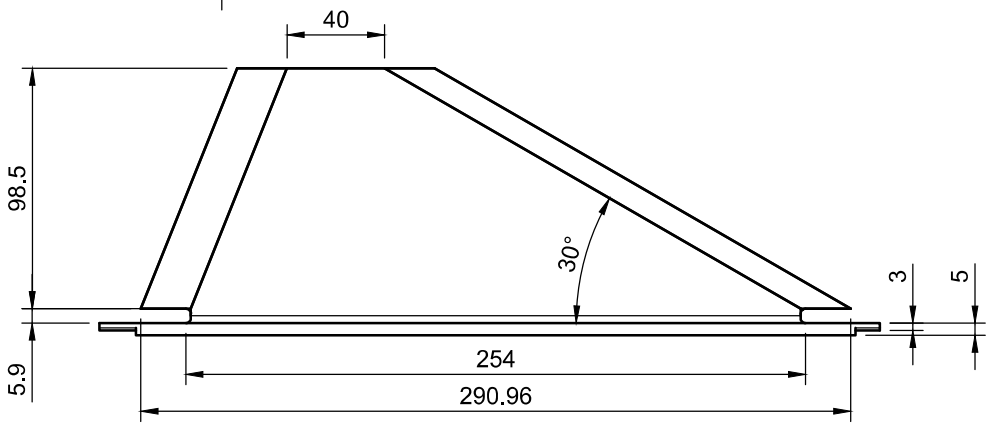
ISOMETRIC VIEW (1:2)

All Linear Dimensions are in mm.
Linear Tolerances are ±0.1 mm unless specified.
Angular Tolerances are ±0.1° unless specified.

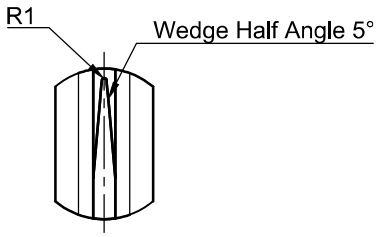
Dept.	Technical reference	Created by	Approved by
Structures	N/A	Akash Siddarth 29-03-2025	Madhav Sonkusare 01-04-2025
		Document type: Part Drawing	Document status: Released
thrustMIT		Title: Forward Centering Ring	DWG No.: VV_MB_FCR
			Rev.: 3 / Date of issue: / Sheet: 1/1



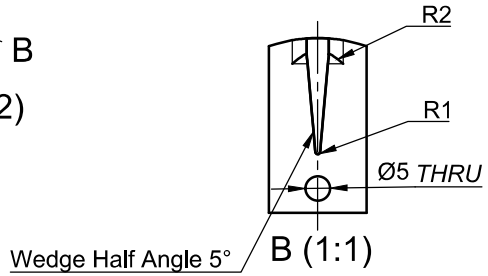
TOP VIEW (1:2)



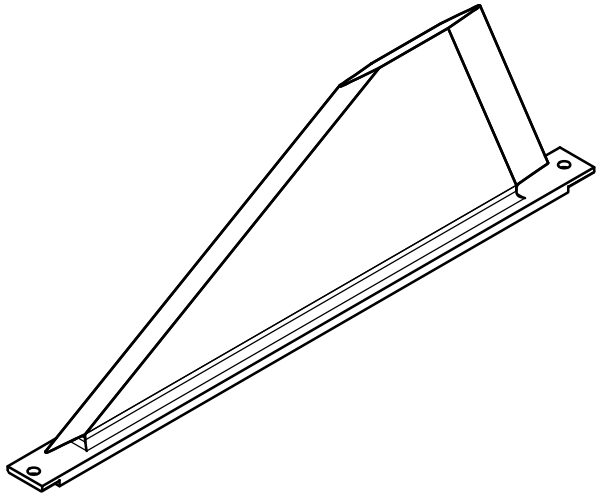
FRONT VIEW (1:2)



A (1:1)



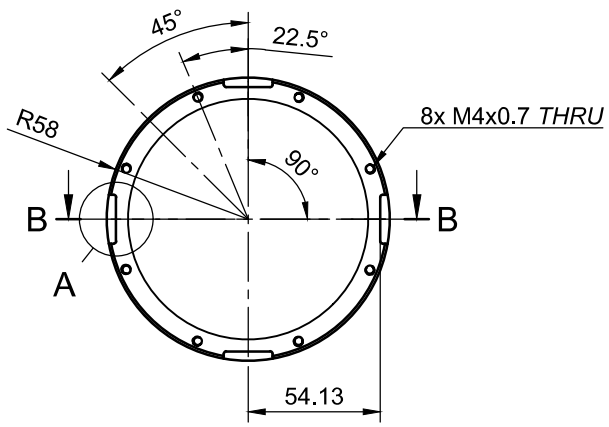
B (1:1)



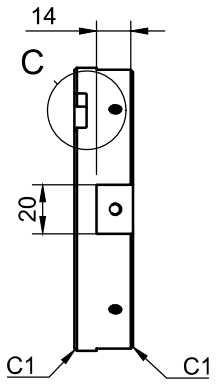
ISOMETRIC VIEW (1:2)

All Linear Dimensions are in mm.
Linear Tolerances are ±0.1 mm unless specified.
Angular Tolerances are ±0.1° unless specified.

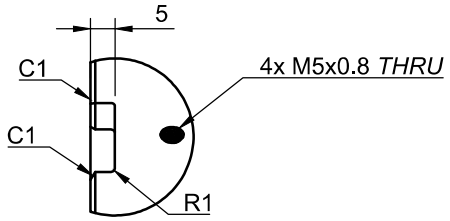
Dept.	Technical reference	Created by	Approved by
Structures	N/A	Akash Siddarth 01-04-2025	Ajinkya Sathe 02-04-2025
		Document type: Part Drawing	Document status: Released
thrustMIT		Title: Fin with Stringer	DWG No.: VV_MB_FIN
			Rev.: 5 / Date of issue: / Sheet: 1/1



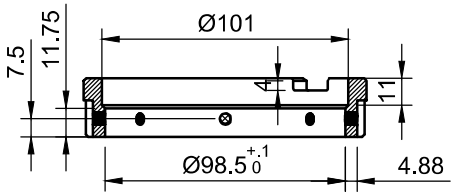
TOP VIEW (1:2)



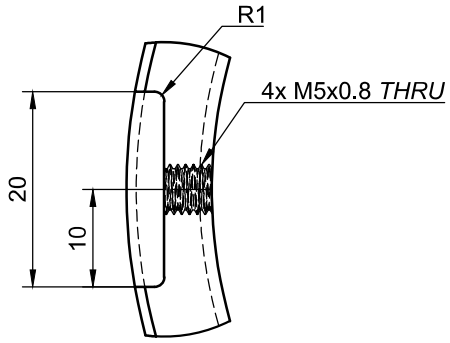
RIGHT VIEW (1:2)



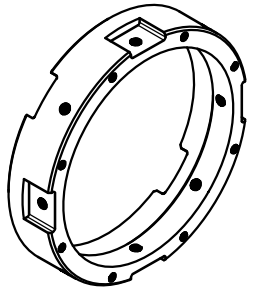
C (1:1)



B-B (1:2)



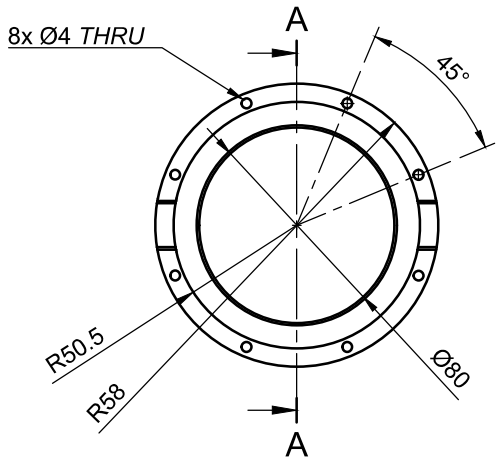
A (2:1)



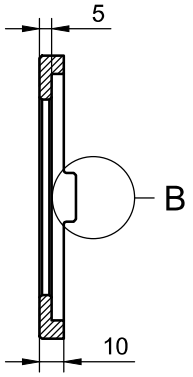
ISOMETRIC VIEW (1:2)

All Linear Dimensions are in mm.
Linear Tolerances are ±0.1 mm unless specified.
Angular Tolerances are ±1° unless specified.

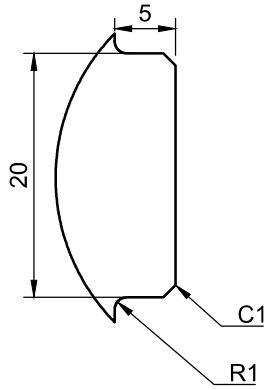
Dept.	Technical reference	Created by	Approved by
Structures	N/A	Akash Siddarth 28-03-2025	Madhav Sonkusare 01-04-2025
		Document type: Part Drawing	Document status: Released
thrustMIT		Title: Aft Centering Ring	DWG No.: VV_MB_ACR
			Rev.: 3 / Date of issue: / Sheet: 1/1



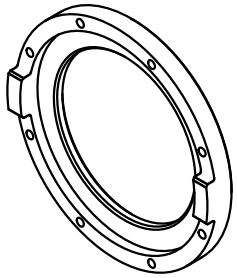
TOP VIEW (1:2)



A-A (1:2)



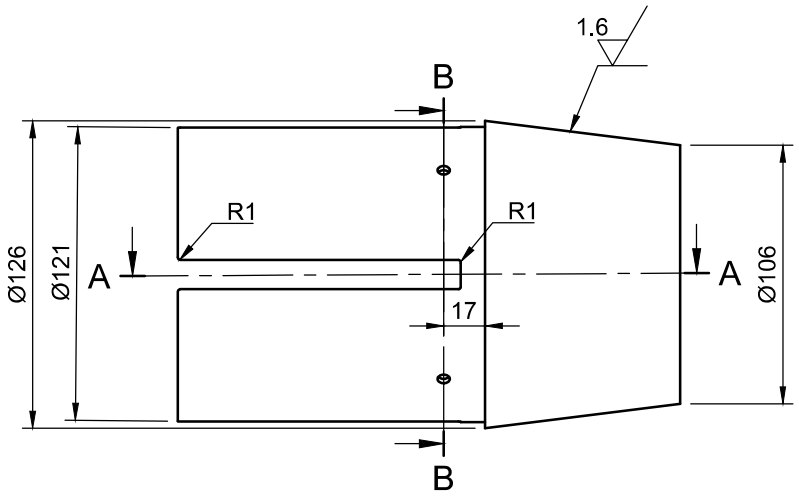
B
(2.5:1)



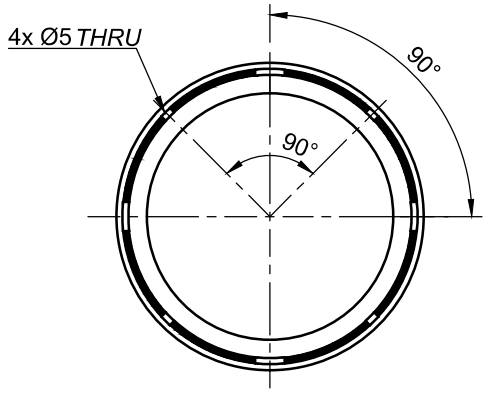
ISOMETRIC VIEW (1:2)

All Linear Dimensions are in mm.
Linear Tolerances are ±0.1 mm unless specified.
Angular Tolerances are ±0.1° unless specified.

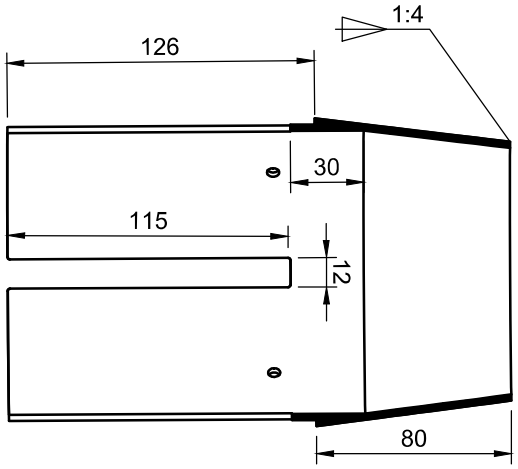
Dept.	Technical reference	Created by	Approved by
Structures	N/A	Akash Siddarth 29-04-2025	Madhav Sonkusare 01-04-2025
		Document type: Part Drawing	Document status: Released
thrustMIT		Title: Retainer	DWG No.: VV_MB_RTR
			Rev.: 2 | Date of issue: | Sheet: 1/1



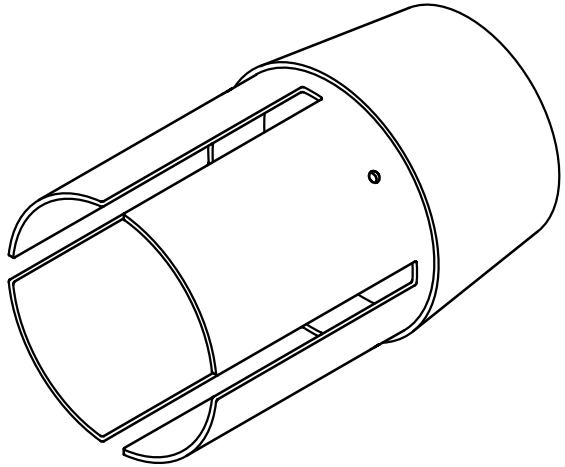
TOP VIEW (1:2)



B-B (1:2)



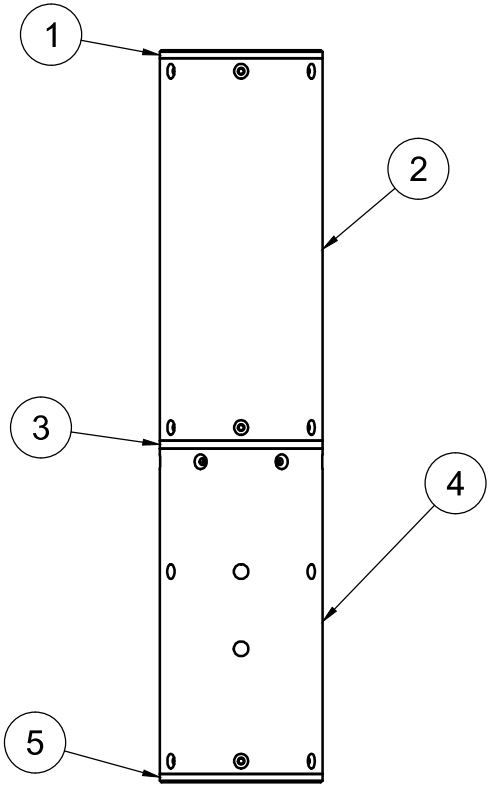
A-A (1:2)



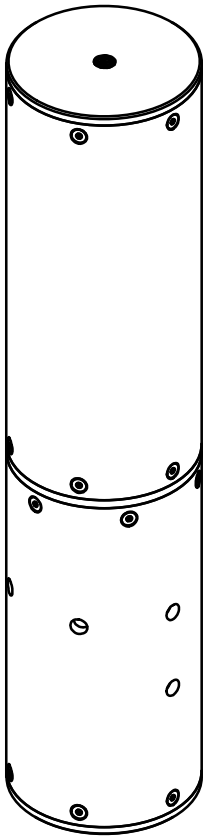
ISOMETRIC VIEW (1:2)

All Linear Dimensions are in mm.
Linear Tolerances are ±0.1 mm unless specified.
Angular Tolerances are ±0.1° unless specified.

Dept.	Technical reference	Created by	Approved by
Structures	N/A	Akash Siddarth 28-04-2025	Madhav Sonkusare 29-04-2025
		Document type: Part Drawing	Document status: Released
thrustMIT		Title: Boattail	DWG No.: VV_MB_BTL
			Rev.: 3 | Date of issue: | Sheet: 1/1



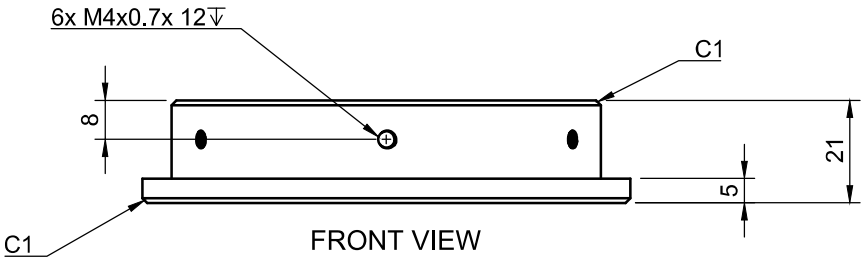
FRONT VIEW (1:3)



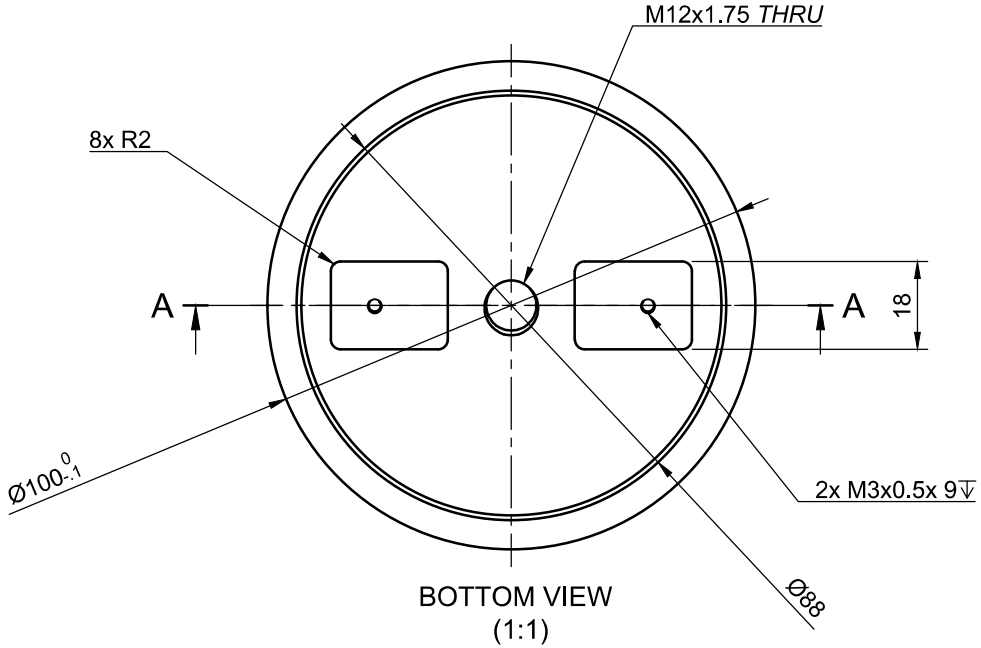
ISOMETRIC VIEW (1:2.5)

Parts List			
Item	Part Number	Qty	Material
1	VV_PLD_TOP	1	Stainless Steel 316
2	VV_PLD_TCS	1	Al 6061 T6
3	VV_PLD_MID	1	Al 6061 T6
4	VV_PLD_BCS	1	Al 6061 T6
5	VV_PLD_BOT	1	Al 6061 T6

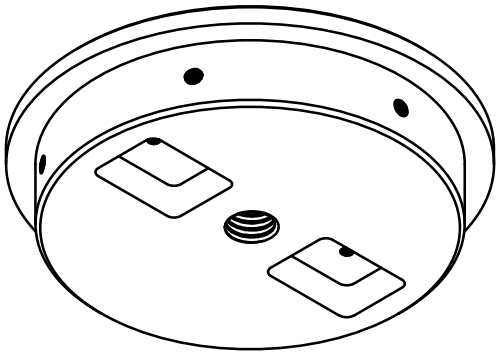
Dept.	Technical reference	Created by	Approved by
Payload	N/A	Madhav Sonkusare 13-03-2025	Akash Siddarth 15-03-2025
		Document type: Assembly Drawing	Document status: Released
thrustMIT		Title: Payload Assembly	DWG No.: VV_PLD_ASLY
			Rev.: 2 | Date of issue: | Sheet: 1/1



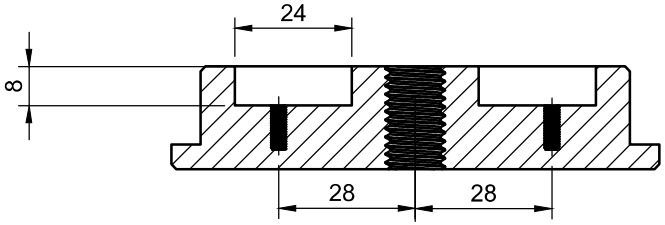
FRONT VIEW
(1:1)



BOTTOM VIEW
(1:1)



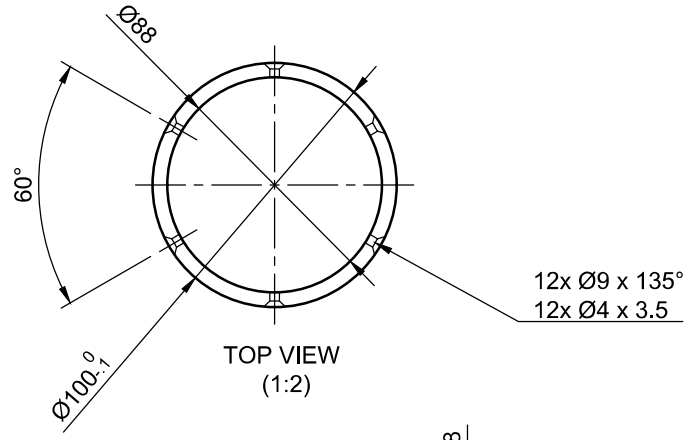
ISOMETRIC VIEW
(1:1)



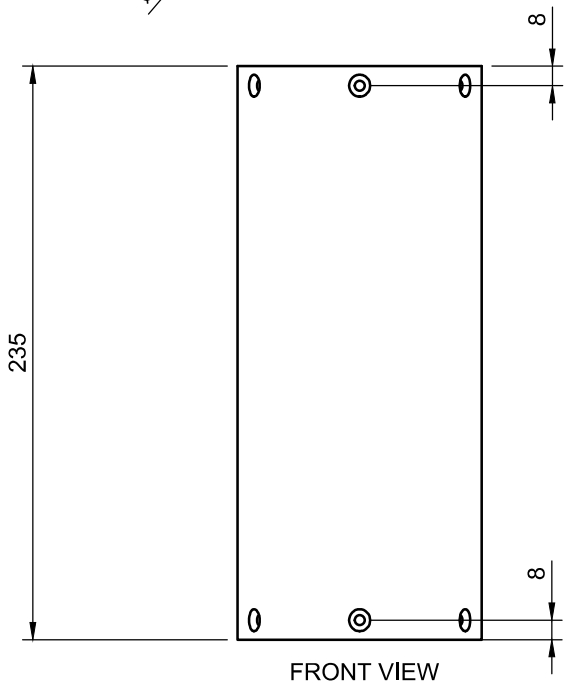
A-A (1:1)

All Linear Dimensions are in mm.
Linear Tolerances are ±0.1 mm unless specified.
Angular Tolerances are ±1° unless specified.

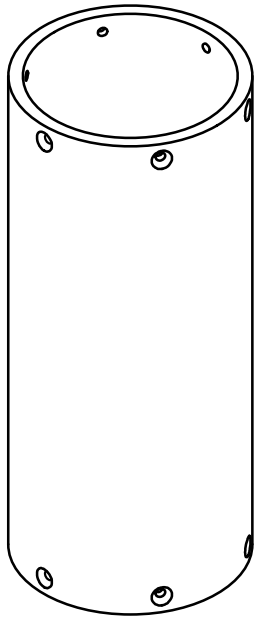
Dept.	Technical reference	Created by	Approved by
Payload	N/A	Sai Tharun Mutra 09-03-2025	Akash Siddarth 12-03-2025
		Document type: Part Drawing	Document status: Released
thrustMIT		Title: Payload Top Plate	DWG No.: VV_PLD_TOP
			Rev.: 2 | Date of issue: | Sheet: 1/1



TOP VIEW
(1:2)



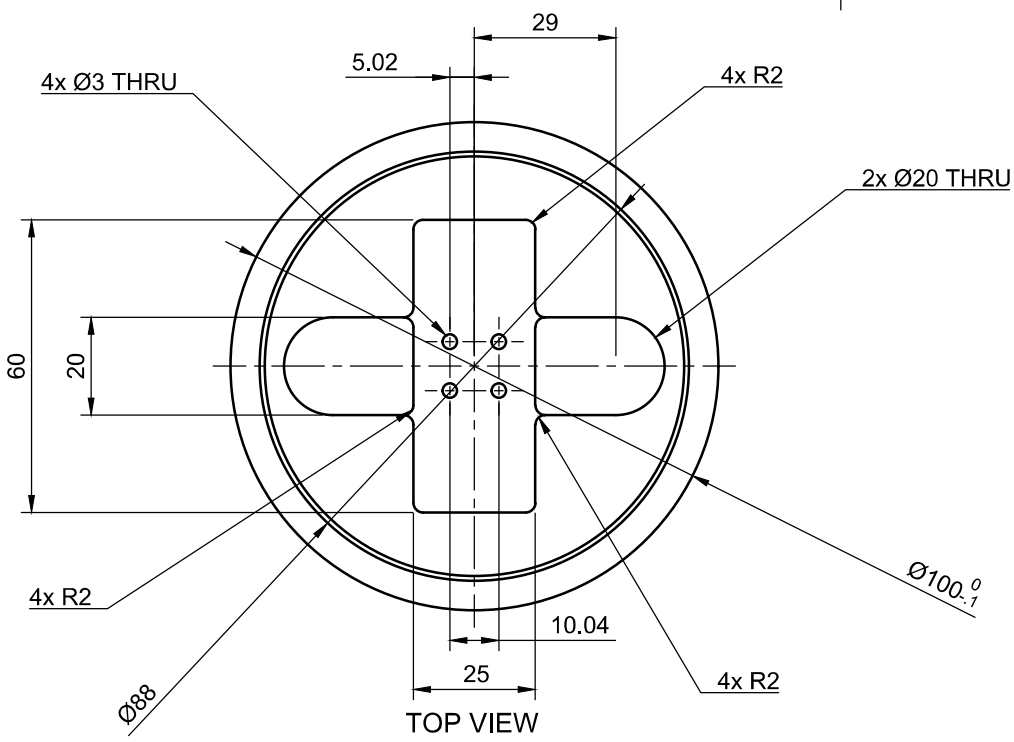
FRONT VIEW
(1:2)



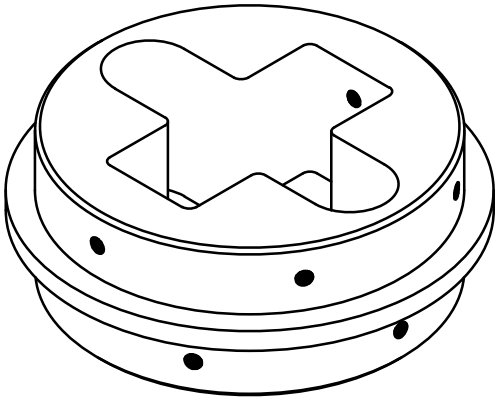
ISOMETRIC VIEW
(1:2)

All Linear Dimensions are in mm.
Linear Tolerances are ±0.1 mm unless specified.
Angular Tolerances are ±1° unless specified.

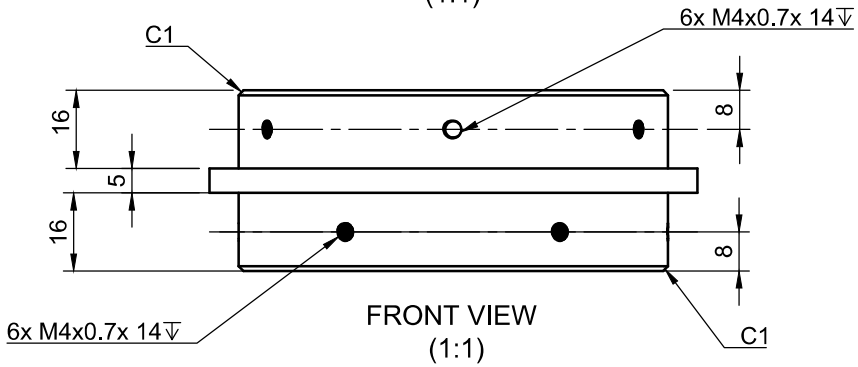
Dept. Payload	Technical reference N/A	Created by Sai Tharun Mutra 10-03-2025	Approved by Akash Siddarth 12-03-2025
thrustMIT		Document type Part Drawing	Document status Released
		Title Payload Top Cansat	DWG No. VV_PLD_TCS
			Rev. 2 / Date of issue / Sheet 1/1



TOP VIEW
(1:1)



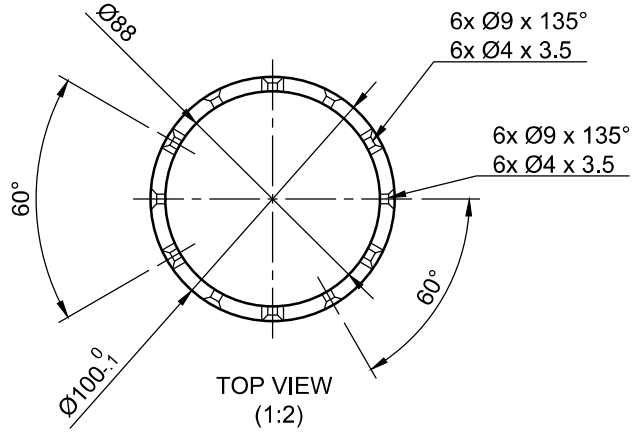
ISOMETRIC VIEW
(1:1)



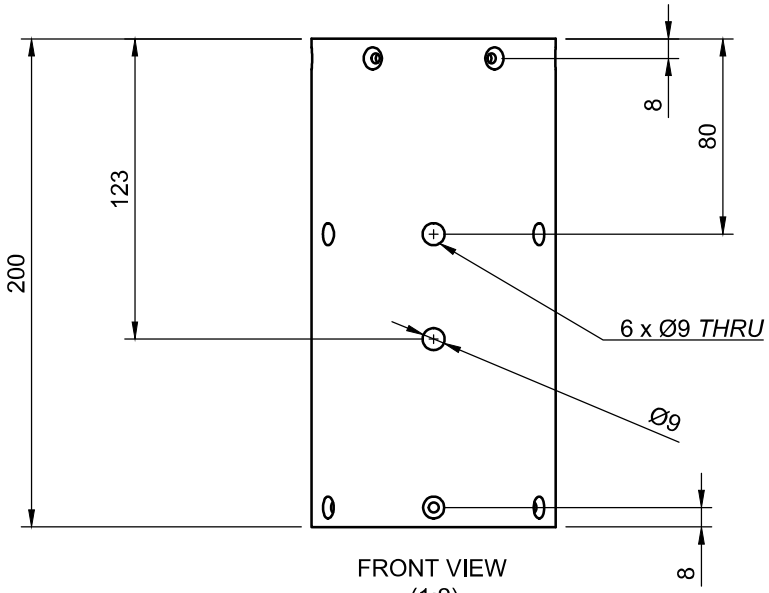
FRONT VIEW
(1:1)

All Linear Dimensions are in mm.
Linear Tolerances are ±0.1 mm unless specified.
Angular Tolerances are ±1° unless specified.

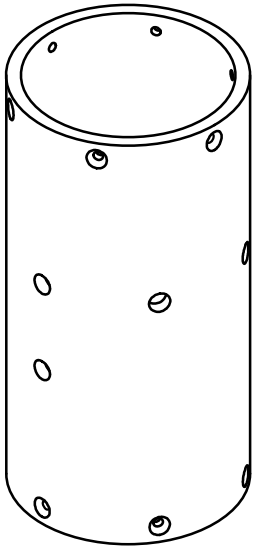
Dept. Payload	Technical reference N/A	Created by Sai Tharun Mutra 11-03-2025	Approved by Akash Siddarth 12-03-2025
thrustMIT		Document type Part Drawing	Document status Released
		Title Payload Middle Plate	DWG No. VV_PLD_MID
			Rev. 4 / Date of issue / Sheet 1/1



TOP VIEW
(1:2)



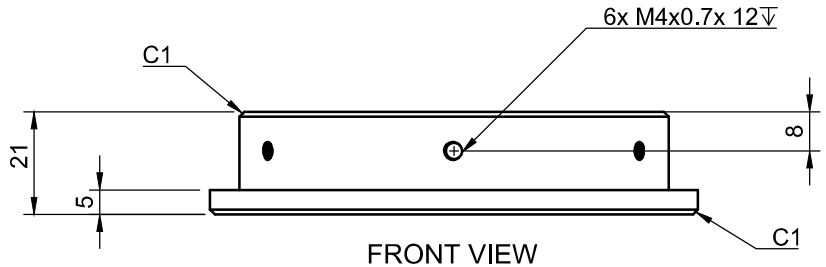
FRONT VIEW
(1:2)



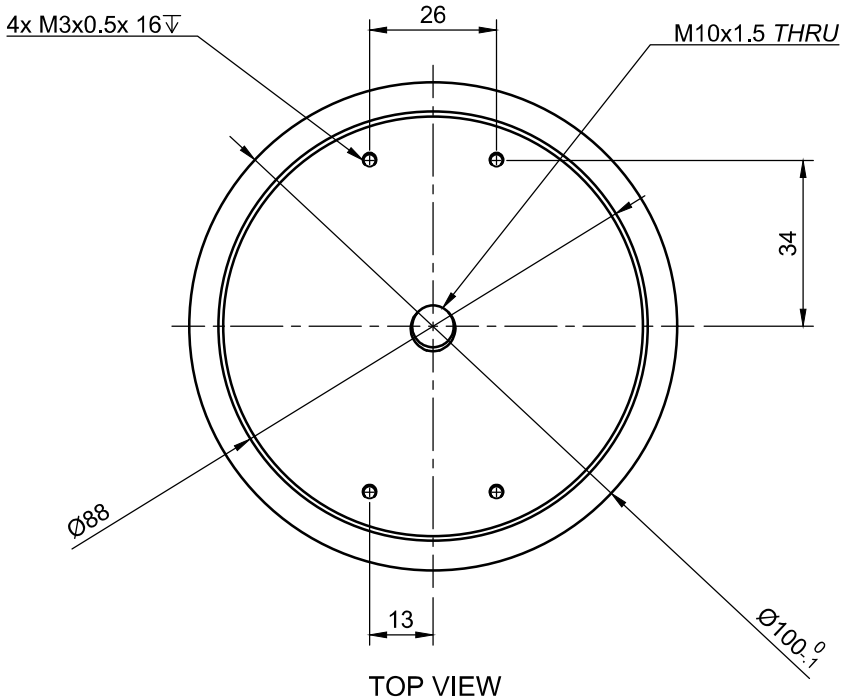
ISOMETRIC VIEW
(1:2)

All Linear Dimensions are in mm.
Linear Tolerances are ±0.1 mm unless specified.
Angular Tolerances are ±1° unless specified.

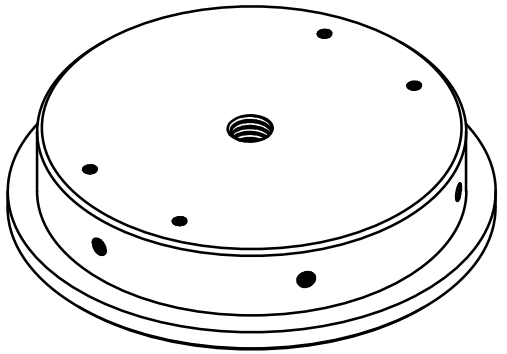
Dept. Payload	Technical reference N/A	Created by Sai Tharun Mutra 10-03-2025	Approved by Akash Siddarth 12-03-2025
thrustMIT		Document type Part Drawing	Document status Released
		Title Payload Bottom Cansat	DWG No. VV_PLD_BCS
			Rev. 2 / Date of issue / Sheet 1/1



FRONT VIEW
(1:1)



TOP VIEW
(1:1)



ISOMETRIC VIEW
(1:1)

All Linear Dimensions are in mm.
Linear Tolerances are ±0.1 mm unless specified.
Angular Tolerances are ±1° unless specified.

Dept. Payload	Technical reference N/A	Created by Sai Tharun Mutra 09-03-2025	Approved by Akash Siddarth 12-03-2025
thrustMIT		Document type Part Drawing	Document status Released
		Title Payload Bottom Plate	DWG No. VV_PLD_BOT
			Rev. 1 / Date of issue / Sheet 1/1

G. Appendix: Team Structure

A. Faculty Advisor

Dr. Srinivas G.	Associate Professor, Department of Aeronautical & Automobile Engineering, Manipal Institute of Technology, Manipal Academy of Higher Education

B. Team Mentors

Bob Schoner	TRA L3, Flyer of Record; Manager - Aerospace Engineering Design Lab (AEDL), Virginia Tech

C. Project Leads

Satvik Agrawal	Team Leader; B.Tech Computer & Communication Engineering, Batch of 2026
Geethika Sree Ravu	Team Manager; B.Tech Computer Science Engineering, Batch of 2026
Ajinkya Sathe	Aerodynamics Head; B.Tech Mechanical Engineering, Batch of 2026
Samarth Vinod	Avionics Head; B.Tech Aeronautical Engineering, Batch of 2026
Madhav Sonkusare	Mechanical & Propulsion Head; B.Tech Mechanical Engineering, Batch of 2026
Akash Siddarth	Structures Head; B.Tech Mechanical Engineering, Batch of 2026
Tejas Patil	Payload Computational Head; B.Tech Computer Science Engineering (AI & ML), Batch of 2026
Mohul Podder	Payload Electronics Head; B.Tech Electrical & Electronics Engineering, Batch of 2026

D. Senior Members

Ayyan Bhartia	B.Tech Aeronautical Engineering, Batch of 2026
Adithi Shetty N	B.Tech Electrical & Electronics Engineering, Batch of 2026
Jahnavi U	B.Tech Computer & Communication Engineering, Batch of 2026
Shreemad Burade	B.Tech Aeronautical Engineering, Batch of 2026
Aryan Gupta	B.Tech Computer Science Engineering (AI & ML), Batch of 2026

E. Aerodynamics Team

Samrudh Subhramanya Raja	B.Tech Mechanical Engineering, Batch of 2027
Shaurya Mittal	B.Tech Computer Science Engineering, Batch of 2027

F. Avionics Team

Anushka Prabhutendolkar	B.Tech Computer Science Engineering, Batch of 2027
Dhruv Phalod	B.Tech Computer Science Engineering, Batch of 2027
Krishanu Dey	B.Tech Very Large Scale Integration, Batch of 2027
Sanskruti Gitan Ginde	B.Tech Electronics & Communication Engineering, Batch of 2027
Shawn Chris	B.Tech Electrical & Electronics Engineering, Batch of 2027
Vanshdeep Trivedi	B.Tech Electronics & Communication Engineering, Batch of 2027

G. Structures Team

Avnish Kaur	B.Tech Aeronautical Engineering, Batch of 2027
Tushit Chatterjee	B.Tech Mechanical Engineering, Batch of 2027

H. Propulsion Team

Dhruv Jadhav	B.Tech Mechanical Engineering, Batch of 2027
Shaunak Purkayastha	B.Tech Mechanical Engineering, Batch of 2027
Varun Pillarisetty Venkata	B.Tech Mechanical Engineering, Batch of 2027

I. Payload Team

Adi Narayan R S	B.Tech Computer Science Engineering, Batch of 2027
Mutra Sai Tharun	B.Tech Aeronautical Engineering, Batch of 2027
Rudra Rajpurohit	B.Tech Information Technology, Batch of 2027

J. Management Team

Aayush Sinha	B.Tech Mechanical Engineering, Batch of 2027
Adithya M Adiga	B.Tech Computer Science Engineering, Batch of 2027
Prasanna Bhat	B.Tech Computer Science Engineering, Batch of 2027
Shubhendu Arya	B.Tech Computer Science Engineering, Batch of 2027
Swaraa Sule	B.Tech Aeronautical Engineering, Batch of 2027
Vedant Totla	B.Tech Information Technology, Batch of 2027

H. Appendix: Wiring Diagrams

A. Avionics

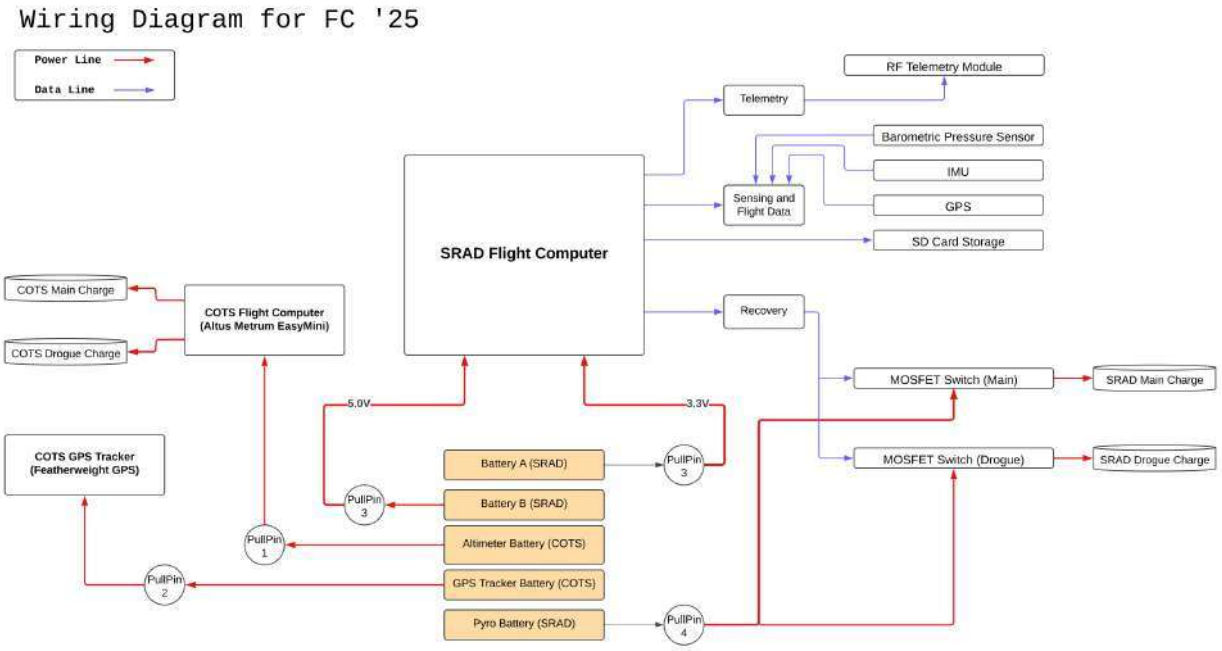


Figure 79 Avionics COTS and SRAD Wiring Diagram



Figure 80 Avionics Camera Wiring Diagram

B. Payload

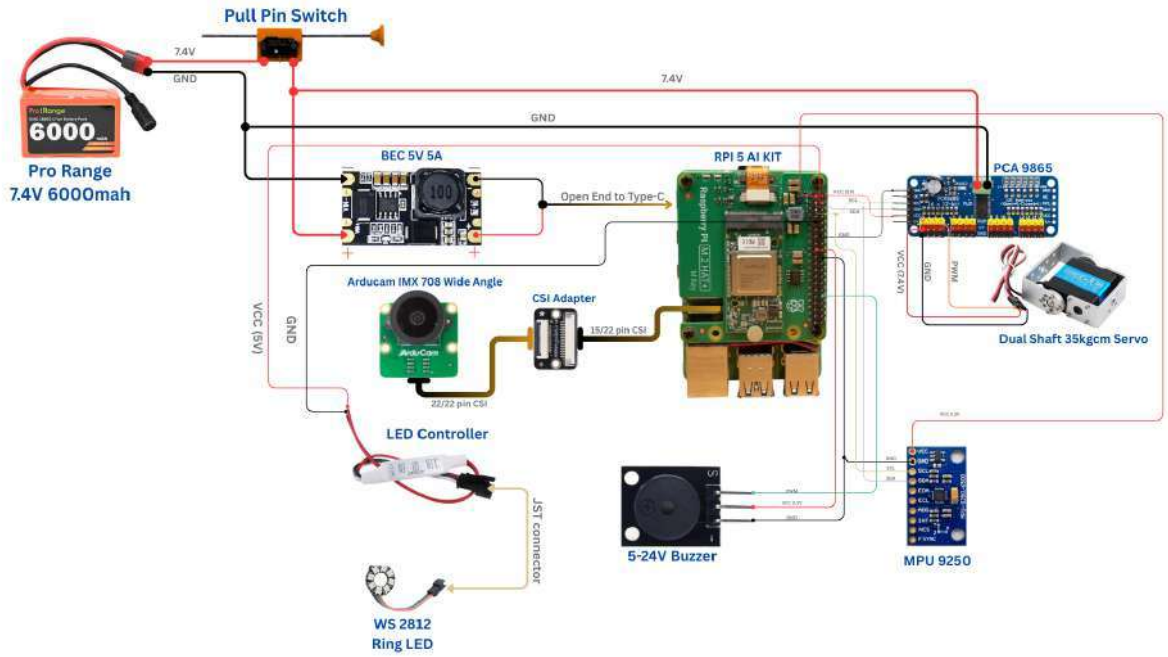


Figure 81 Payload Wiring Diagram

I. Appendix: Aerodynamic Analysis and Stability Considerations

A. Nosecone

Table 26 Nosecone Drag Data

Base Diameter (mm)	Length (mm)	Fineness Ratio	Length of the Rocket (mm)	Drag (N)
12.6	500	4	3370	1300.487
12.6	570	4.5	3420	1231.897
12.6	630	5	3460	1159.765
12.6	640	5.1	3460	1155.453
12.6	660	5.2	3470	1142.871
12.6	670	5.3	3480	1136.215
12.6	680	5.4	3490	1131.223
12.6	690	5.5	3490	1130.444
12.6	700	5.6	3500	1122.392
12.6	720	5.7	3510	1123.678
12.6	730	5.8	3510	1124.278
12.6	740	5.9	3520	1126.781
12.6	760	6	3540	1129.345

B. Fins

1. Aerodynamic Analysis of Various Fin Cross Sections

Table 27 Aerodynamic Forces on Hexagonal Fin Cross Section at Varying Angles of Attack

Angle of Attack (°)	Half Wedge Angle (°)							
	5		10		15		20	
	Lift (N)	Drag (N)	Lift (N)	Drag (N)	Lift (N)	Drag (N)	Lift (N)	Drag (N)
0	0	34.24	0	41.13	0	47.25	0	51.11
3	264.4	47.4	255.2	54.22	251.76	60.47	248.15	64.55
6	524	89.1	509.9	92.88	499.62	99.1	492.62	103.42
9	795.12	153.44	764.93	158.65	740.67	161.6	729.24	166
12	1025.76	236.34	1014.83	246.55	978.29	250.1	958.56	259.2

Table 28 Aerodynamic Forces on Bi-Convex Cross Section at Varying Angles of Attack

Angle of Attack (°)	**Lift** (N)	**Drag** (N)
0	0	25.34
3	231.23	36.6
6	469.15	73.51
9	699.44	134.26
12	920.08	219

Table 29 Aerodynamic Forces on Double Wedge Cross Section at Varying Angles of Attack

Angle of Attack (°)	**Lift** (N)	**Drag** (N)
0	0	22.98
3	199.82	33.127
6	397.67	64.18
9	586.03	114.87
12	763.5	184

Table 30 Aerodynamic Forces on Single Wedge Cross Section at Varying Angles of Attack

Angle of Attack (°)	**Lift** (N)	**Drag** (N)
0	0	38.8
3	210.55	50.24
6	416.5	83.5
9	613.5	137.42
12	801.4	211.2

Table 31 Aerodynamic Forces on Hexagonal Blunt-Based Cross Section at Varying Angles of Attack

Half Wedge Angle (N)	**5**	
Angle of Attack (°)	**Lift** (N)	**Drag** (N)
0	0	41.12
3	240.01	52.49
6	491.92	90.2
9	746.66	156.12
12	990.69	248.92

Table 32 Aerodynamic Forces on Airfoil Cross Sections at Varying Angles of Attack

NACA-2411			NACA-0011		
Angle of Attack (°)	**Lift** (N)	**Drag** (N)	**Angle of Attack** (°)	**Lift** (N)	**Drag** (N)
0	93.7	56.2	0	0	92.71
3	263.42	105.54	3	204.36	103.17
6	461.56	137.42	6	410.41	134.58
9	655.94	188.23	9	610.29	187.19
12	846.88	258.38	12	802.42	260.38

2. FSI & Modal Analysis

Table 33 Structural Response of Double Wedge Fin Cross Section Under Varying Angles of Attack

Angle of Attack (°)	**Deformation** (mm)	**Stress** (MPa)
0	0.0021	0.5371
3	0.669	38.5
6	1.157	68.2
9	1.438	86.44
12	1.564	108.69

Table 34 Structural Response of Bi-Convex Fin Cross Section Under Varying Angles of Attack

Angle of Attack (°)	**Deformation** (mm)	**Stress** (MPa)
0	0.00056	0.2043
3	0.147	25.486
6	0.889	53.152
9	1.34	79.394
12	1.75	104.13

Table 35 Structural Response of Hexagonal Fin Cross Section Under Varying Angles of Attack

Angle of Attack (°)	**Deformation** (mm)	**Stress** (MPa)
0	0.003	0.233
3	0.1553	12.74
6	0.4328	33.89
9	0.69	53.19
12	0.9211	70.489

Table 36 Vibration Modes and Deformation for Double Wedge Cross Section

Mode	Frequency(Hz)	Deformation(mm)
First Bending Mode	368.19	340.51
First Torsional Mode	1189.6	360.87
Second Torsional Mode	1665.5	471.2
Torsion And Bending Mode	2489.3	586.49
Two Point Bending	3257	928.24
Third Torsional Mode	3621.4	746.17

Table 37 Vibration Modes and Deformation for Bi-Convex Cross Section

Mode	Frequency(Hz)	Deformation(mm)
First Bending Mode	465.92	262.6
First Torsional Mode	1196.7	280.73
Second Torsional Mode	1942.8	371.35
Torsion And Bending Mode	2593.3	413.6
Two Point Bending	3300.3	681.93
Third Torsional Mode	3756.3	554.55

Table 38 Vibration Modes and Deformation for Hexagonal Cross Section

Mode	Frequency(Hz)	Deformation(mm)
First Bending Mode	506.14	190.24
First Torsional Mode	1085.3	224.25
Torsion And Bending Mode	1955.2	241.92
Two Point Bending	2699.1	287.22
Second Torsional Mode	3166.5	289.51
Third Torsional Mode	3751.9	323.1

Table 39 Effect of Root Chord and Fin Height on Rocket Stability and Fin Flutter

Root Chord (mm)	Height (mm)	Thickness (mm)	Stability at Launch Rod	Max Dynamic Stability	Apogee (ft)	Rocket Velocity (m/s)	FOS Divergence	FOS Flutter
240	98.5	0.45	1.68	5.85	30720	580	1.4687	1.9322
250	98.5	0.45	1.65	5.81	30668	578	1.4487	1.8977
260	98.5	0.45	1.6	5.8	30616	576	1.4289	1.8425
270	98.5	0.45	1.58	5.8	30561	576	1.4098	1.7989
280	98.5	0.45	1.55	5.74	30514	576	1.3852	1.7396
290	98.5	0.45	1.52	5.73	30451	574	1.3625	1.6959
300	98.5	0.45	1.5	5.73	30412	574	1.3492	1.6819
240	97.5	0.45	1.49	5.85	30716	582	1.4785	1.9415
250	97.5	0.45	1.48	5.8	30715	582	1.4533	1.9433
260	97.5	0.45	1.46	5.8	30683	581	1.4319	1.9141
270	97.5	0.45	1.45	5.74	30691	581	1.4114	1.8883
280	97.5	0.45	1.41	5.73	30659	581	1.3916	1.8663
290	97.5	0.45	1.4	5.75	30511	580	1.3512	1.8338
300	97.5	0.45	1.4	5.76	30461	579	1.3512	1.8338
240	95.5	0.45	1.35	5.83	30859	582	1.5096	1.9696
250	95.5	0.45	1.3	5.8	30808	581	1.4684	1.9322
260	95.5	0.45	1.28	5.8	30753	580	1.4459	1.9052
270	95.5	0.45	1.26	5.8	30696	580	1.4261	1.8805
280	95.5	0.45	1.25	5.77	30656	579	1.4411	1.8838
290	95.5	0.45	1.23	5.77	30656	579	1.4	1.8383
300	95.5	0.45	1.23	5.76	30657	579	1.3796	1.7983

C. Boattail

Table 40 Effect of Boattail Length on Rocket Stability and Drag

Aft diameter (mm)	**Length** (mm)	**Stability at launch rod**	**Drag** (N)
106	60	1.67	1045.7
106	70	1.66	1014.3
106	80	1.65	985.63
106	90	1.54	980.21
106	100	1.49	968.89
106	110	1.39	952.56

D. Drag & Stability Analysis

Table 41 Rocket Flight Stability Comparison: OpenRocket vs CFD Data

	OpenRocket Data			**CFD Data**		
Time from Lift-off	**CP** (mm)	**CG** (mm)	**Stability Caliber**	**CP** (mm)	**CG** (mm)	**Stability Caliber**
0.29	2270.47	2062.57	1.65	2256.69	2062.57	1.54
0.39	2296.65	2056.27	1.91	2281.45	2056.27	1.79
0.59	2352.86	2043.37	2.46	2331.67	2043.37	2.29
0.79	2402.87	2029.49	2.96	2381.65	2029.49	2.79
0.94	2456.93	2018.6	3.48	2426.69	2018.6	3.24
1.09	2427.92	2007.26	3.34	2398.55	2007.26	3.11
1.29	2443.68	1991.5	3.59	2417.98	1991.5	3.38
1.44	2496.45	1979.13	4.11	2467.12	1979.13	3.87
1.59	2484.7	1966.33	4.11	2473.8	1966.33	4.03
1.74	2530.19	1953.45	4.58	2491.23	1953.45	4.27
1.94	2538.26	1936.63	4.78	2511.76	1936.63	4.56
2.09	2540.66	1924.48	4.89	2528.33	1924.48	4.79
2.29	2528.59	1908.59	4.92	2496.22	1908.59	4.66
2.49	2491.92	1892.4	4.76	2461.33	1892.4	4.52
2.74	2415.36	1874.65	4.29	2416.67	1874.65	4.3
3.04	2354.82	1856.79	3.95	2289.82	1856.79	3.44
3.54	2304.13	1840	3.68	2291.66	1840	3.58
4	2315.46	1835.16	3.81	2304.21	1835.16	3.72

Table 42 Drag Analysis of Vayuvega across Varying Mach Numbers

Mach Number	Total Pressure drag (N)	Total Viscous Drag (N)	Total Drag (N)
0.3	39.02	65.93	104.95
0.4	58.87	85.21	144.08
0.5	81.94	111.27	193.2
0.6	103.14	138.8	241.94
0.7	123.29	179.01	302.4
0.8	170.45	215.9	386.36
0.9	200.97	253.49	454.46
1	356.81	291.38	648.19
1.1	413.33	330.55	743.88
1.2	450.78	369.44	820.22
1.3	500.99	405.35	906.34
1.4	535.99	437.84	973.83
1.5	581.94	473.99	1055.93
1.6	625.62	505.01	1130.63
1.71	647	526.76	1173.76

Table 43 Comparison of Aerodynamic Drag Forces on Hexagonal vs Circular Bolts Across Varying Mach Numbers

Mach Number	Hexagonal Bolts		Circular Bolts	
	Pressure Drag (N)	Viscous Drag (N)	Pressure Drag (N)	Viscous Drag (N)
0.3	2.26	0.03	1.59	0.03
0.4	4.41	0.04	3.9	0.04
0.5	6.43	0.05	5.47	0.06
0.6	10.33	0.08	9.23	0.08
0.7	12.67	0.1	11.55	0.08
0.8	16.6	0.15	14.39	0.11
0.9	21.17	0.21	20.53	0.16
1	28.98	0.32	25.97	0.42
1.1	32.31	0.4	29.58	0.58
1.2	36.68	0.51	32.47	0.77
1.3	40.58	0.63	37.63	0.94
1.4	44.29	0.75	40.25	1.09
1.5	47.41	0.87	43.81	1.22
1.6	50.62	0.98	46.83	1.35
1.71	51.82	1.08	48.03	1.45

Table 44 Drag Analysis of Components on Vayuvega across Varying Mach Numbers

Mach Number	Bolts		Boattail		Fins		Nosecone		Fuselage & Base Drag		Total Drag (N)
	Pressure Drag (N)	Viscous Drag (N)	Pressure Drag (N)	Viscous Drag (N)	Pressure Drag (N)	Viscous Drag (N)	Pressure Drag (N)	Viscous Drag (N)	Pressure Drag (N)	Viscous Drag (N)	
0.3	1.59	0.03	7.23	0.621	6.21	2.429	4.78	10.87	19.21	51.98	104.95
0.4	3.9	0.04	13.78	1.11	7.56	4.42	6.23	14.67	27.1	64.97	144.08
0.5	5.47	0.06	20.69	1.51	11.89	7.026	8.78	16.26	35.11	86.41	193.2
0.6	9.23	0.08	24.32	1.9	14.35	14.388	12.18	22.65	43.06	99.78	241.34
0.7	11.55	0.08	24.77	2.82	17.81	16.988	15.21	29.77	54.05	129.35	302.4
0.8	14.98	0.11	30.23	3.396	28.88	21.604	24.77	34.79	72.18	150.63	381.36
0.9	20.53	0.16	36.1	4.34	31.89	22.401	28.32	38.41	84.13	185.18	454.46
1.0	25.97	0.42	61.48	5.14	46.69	30.158	46.43	42.37	176.24	213.29	648.19
1.1	29.58	0.58	65.63	5.9	50.64	34.994	50.47	48.63	217.01	239.68	736.04
1.2	32.47	0.77	58.48	6.61	53.49	39.35	54.79	53.73	241.55	268.98	820.22
1.3	37.63	0.93	72.56	7.87	61.87	47.5	61.87	59.36	272.49	298.11	926.48
1.4	40.25	1.09	78.74	7.82	59.33	47.5	65.46	60.33	292.21	321.1	973.83
1.5	43.81	1.22	83.26	8.34	62.54	51.3	70.35	63.34	321.98	344.8	1045.8
1.6	46.83	1.35	86.9	8.8	66.75	54.96	77.34	72.65	347.8	367.25	1130.63
1.71	48.03	1.45	87.31	8.99	70.47	57.33	82.63	78.44	358.56	380.55	1173.76

J. Appendix: MATLAB Code for Fin Flutter

```
%% CODE FOR CALCULATING FIN FLUTTER VELOCITY %%
close all;
clc;
clear all;

%% CONSTANTS %%
H = 0:10:9200;          % m (HEIGHT [AGL])
H1 = 1190:10:10390;     % m (ACTUAL HEIGHT)
T0 = 306;               % K (SEA LEVEL TEMPERATURE)
P0 = 101325;            % Pa (SEA LEVEL PRESSURE)
a0 = 353;               % m/s (SEA LEVEL SPEED OF SOUND)
G = 24e9;               % Pa (SHEAR MODULUS OF TORSION)

%% VARIATION WITH HEIGHT (ISA-like approximation) %%
T = T0 - 0.0065 .* H1;                                  % K
P = P0 .* (1 - 0.0065 .* (H1 ./ T0)) .^ 5.2561;         % Pa
a = a0 + 0.606 * ((5 / 9) .* (T - 32));                 % m/s

%% FIN DIMENSIONS %%
b = 0.0985;                     % m (FIN SEMISPAN)
cr = 0.25;                      % m (ROOT CHORD)
ct = 0.04;                      % m (TIP CHORD)
tmax = 0.0045;                  % m (THICKNESS OF FIN)
S = 0.5 * b * (cr + ct);        % m^2 (FIN AREA)
AR = b^2 / S;                   % (FIN ASPECT RATIO)
TR = cr / ct;                   % (FIN TAPER RATIO)

%% FLUTTER VELOCITY FORMULA %%
Vf = a .* sqrt((G .* 2 .* (AR + 2) .* (tmax ./ cr).^3) ./ ...
     (1.3 .* AR.^3 .* P .* (TR + 1)));   % m/s

SVf = (1/1.5) .* Vf;            % Safe Flight Velocity

%% IMPORTING DATA %%
A = xlsread('VayuvegaData.xlsx', 'A1:A1553');    % Rocket Velocity
B = xlsread('VayuvegaData.xlsx', 'B1:B1553');    % Height

%% GRAPH %%
plot(H1, Vf, 'k', 'LineWidth', 1.5)
hold on
plot(H1, SVf, '--r', 'LineWidth', 1.5)
plot(B, A, 'b', 'LineWidth', 1.2)
legend('Flutter Velocity', 'Safe Flight Velocity', 'Rocket Velocity', 'Location', 'best'
    );
grid on
xlabel('Altitude (m)');
ylabel('Velocity (m/s)');
title('Fin Flutter Velocity Vs Rocket Velocity');
```

K. Appendix: Payload

A. Understanding Requirements

The task of performing pose estimation on a cube using a Raspberry Pi 5 equipped with an AI kit (Hailo NPU), 8 GB RAM, and a 7.4 V 6000 mAh Lithium Ion battery requires a model that balances computational efficiency, offers real-time performance and adapts to a custom dataset. YOLOv8s was selected for the following reasons:

1) **Anchor-free Detection**: Unlike earlier YOLOv8 versions that relied on predefined anchor boxes, YOLOv8 uses an anchor-free approach. This reduces the complexity of bounding box predictions and improves generalisation, particularly for custom datasets like one tailored for cube pose estimation.
2) **Optimised Accuracy-Speed Tradeoff**: YOLOv8s is engineered to balance accuracy and inference speed, achieving high performance on edge devices. Official benchmarks indicate it can reach 20-30 FPS on Raspberry Pi 5 with the Hailo NPU for object detection, suggesting similar potential for pose estimation.
3) **Support for Pose Estimation**: While YOLOv8 is primarily an object detection model, it supports pose estimation through variants like YOLOv8-pose, trained on datasets like COCO keypoints. For non-human objects like cubes, YOLOv8 can be retrained to detect custom keypoints.
4) **Lightweight Design**: The YOLOv8s model is smaller than its medium or large counterparts, reducing computational demands while maintaining sufficient accuracy for tasks like keypoint detection on a cube.

B. Hardware Compatibility and Performance

The Raspberry Pi 5, paired with the Hailo NPU, provides significant computational power for neural network inference. The Hailo-8 chip in the AI kit offers 26 TOPS (Tera Operations Per Second), accelerating tasks like object detection and pose estimation. Benchmarks demonstrate that YOLOv8s, quantised to uint8 with a 640x640 input size, achieve 20-30 FPS on Raspberry Pi 5 with the AI kit, indicating real-time capability for pose estimation.

The 7.4 V 6000 mAh Lithium-Ion battery supports extended operation, critical for mobile or untethered applications. YOLOv8s's lightweight design minimizes power consumption, aligning with the battery-powered setup. In contrast, larger and more advanced models like YOLOv8m (medium) or YOLOv9 consume more power and run slower, reducing battery life.

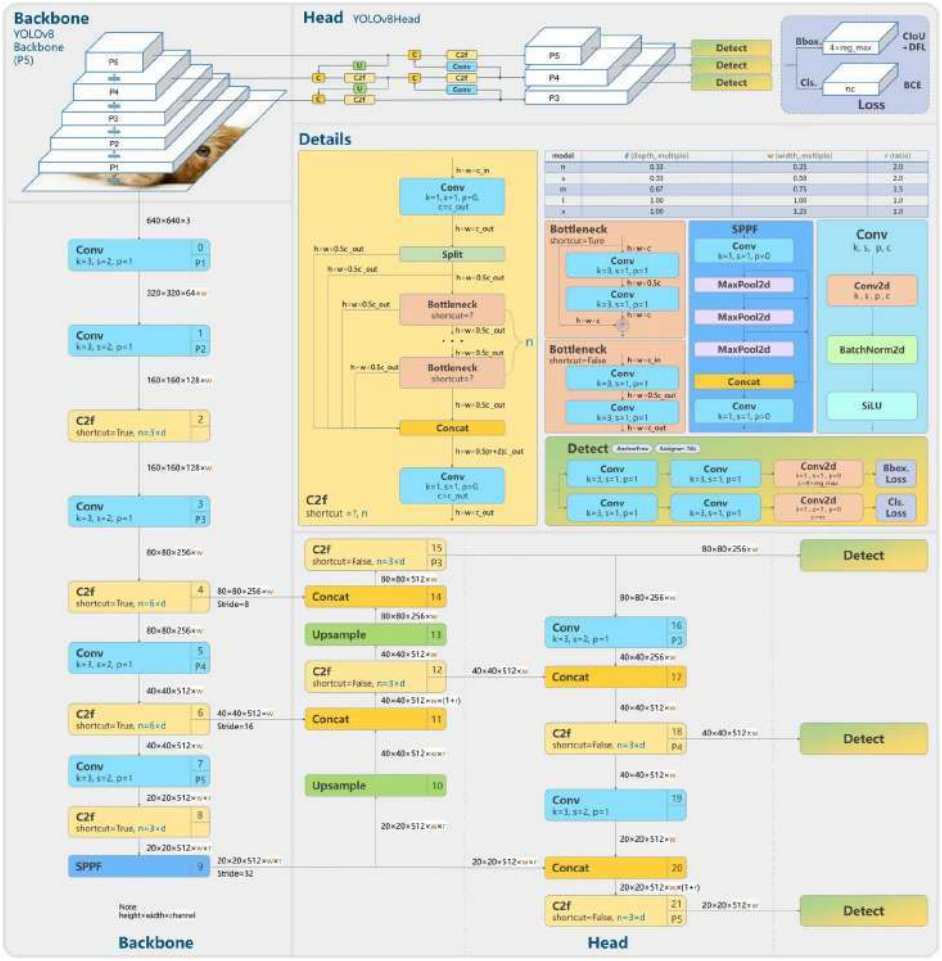


Figure 82 YOLOv8 Model Architecture

YOLOv8 processes images in a single pass, making it fast and ideal for real-time tasks. It has three main components:

1) **Backbone**: It uses CSPDarknet53, a CNN(Convolutional Neural Network) with Cross-Stage Partial (CSP) connections that split and merge feature maps. This captures both fine details and high-level features, and reduces computation.
2) **Neck**: The output from the backbone is aggregated using a Path Aggregation Network (PANet) or an optimised C2f (Cross Stage Partial-2 fusion) module, helping the model detect objects of different sizes more effectively.
3) **Head**: The head outputs the final predictions.YOLOv8 returns bounding boxes, objectness scores, and class probabilities. It also uses dynamic anchor assignment and advanced IoU (Intersection Over Union)-based loss functions for better accuracy.

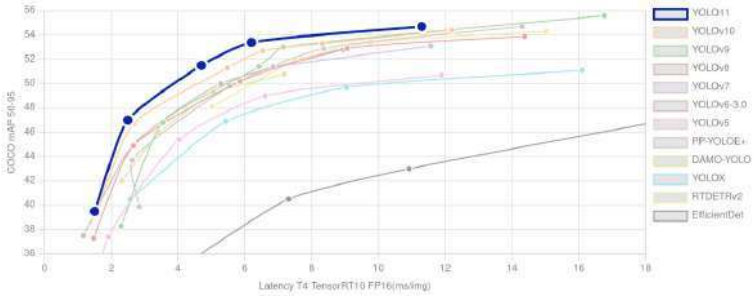


Figure 83 Comparison between YOLO Family Models

YOLOv8s Variant and Pose Estimation Adaptations

YOLOv8 comes in several sizes (n, s, m, l, x) to balance speed and accuracy. YOLOv8s (small) is designed for efficient use on devices with limited resources (like mobile phones or IoT systems). It keeps the same backbone, neck, and head structure but with fewer layers and filters. It has about 11.6 Million parameters and 30.2 Billion FLOPs (Floating Point Operations Per Second), making it much faster (e.g., 233.2 ms on CPU) but slightly less accurate than larger variants.

For pose estimation, YOLOv8s makes specific changes:

1) **Modified Head**: Instead of predicting bounding boxes, the head now predicts the coordinates of keypoints (like vertices on a cube), outputting [x, y] for each point.
2) **Loss Function**: Uses a regression loss function (like Mean Squared Error) focused on accurately predicting keypoint positions, rather than IoU-based losses for bounding boxes.
3) **Training**: Pose models are trained on datasets like the publicly available COCO Keypoints, learning the spatial relationships between keypoints.

Despite these changes, the backbone and neck stay the same, leveraging strong feature extraction and fusion for both object detection and pose estimation tasks.

C. Computational Workflow

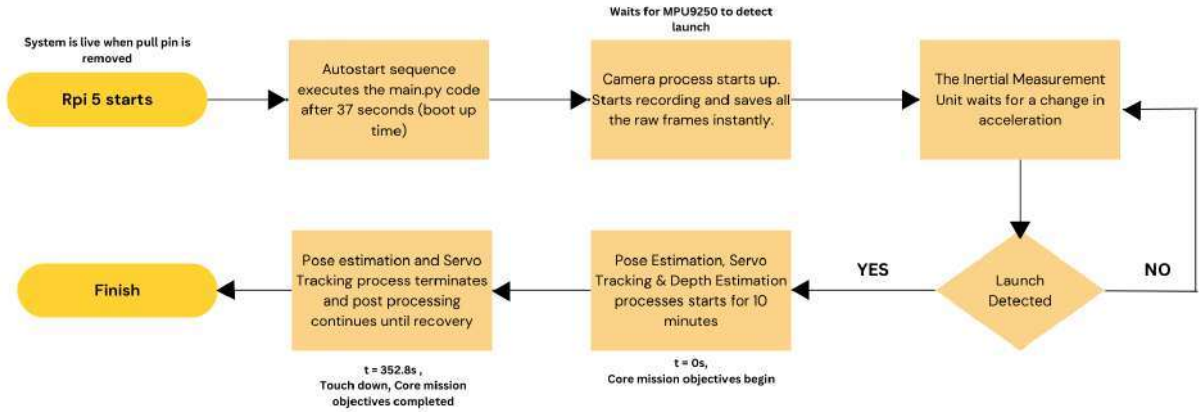


Figure 84 Computational Workflow of Vrishabha

D. Spring Deflection Calculation & Optimisation Code

```
import pandas as pd
import numpy as np
import matplotlib.pyplot as plt

# === Load and prepare data ===
df = pd.read_csv('vayuvega_flight_profile_2.csv')  # Our actual flight profile based on sims
df.columns = [col.strip() for col in df.columns]

# Convert necessary columns to float
df['Time'] = df['Time'].astype(float)
df['Vertical acceleration (m/s  )'] = df['Vertical acceleration (m/s  )'].astype(float)
df['Vertical velocity (m/s)'] = df['Vertical velocity (m/s)'].astype(float)

# === Constants ===
mass = 0.065  # kg (spring load)
g = 9.81  # m/s

# Spring geometry and material
wire_dia = 1.5e-3  # 1.5 mm
r1 = 4.5e-3  # mean radius from 9 mm
r2 = 19.5e-3  # mean radius from 39 mm
n = 3  # active coils
G = 81.37e9  # Pa, shear modulus of stainless steel

# === Load flight data ===
time = df['Time'].values
acc = df['Vertical acceleration (m/s  )'].values

# === Force on spring ===
spring_force = mass * (acc + g)  # N

# === Spring deflection using conical spring equation ===
numerator = 16 * n * (r1 + r2) * (r1**2 + r2**2) * spring_force
denominator = wire_dia**4 * G
deflection = numerator / denominator  # in meters

# === Velocity and Position Estimation ===
dt = np.gradient(time)
velocity = np.cumsum(acc * dt)
position = np.cumsum(velocity * dt)

# === Clip to 30s ===
mask = time <= 30
time_10s = time[mask]
deflection_10s = deflection[mask]
spring_force_10s = spring_force[mask]
acc_10s = acc[mask]
velocity_10s = velocity[mask]
position_10s = position[mask]

# === Plotting Setup ===
fig, axs = plt.subplots(3, 2, figsize=(15, 12))
fig.suptitle('Spring Simulation Summary', fontsize=16)

# === Function to mark only max ===
```

```
    def mark_max(ax, x, y, color):
        max_idx = np.argmax(y)
        max_val = y[max_idx]
        ax.plot(x[max_idx], max_val, 'o', color=color)
        ax.annotate(f'Max: {max_val:.2f}', (x[max_idx], max_val),
                    textcoords="offset points", xytext=(0, 10), ha='center', color=
                        color)

    # === Plots ===

    # 1. Full Deflection
    axs[0, 0].plot(time, deflection * 1000, color='blue', label='Deflection')
    mark_max(axs[0, 0], time, deflection * 1000, 'blue')
    axs[0, 0].set_title('Spring Deflection vs Time')
    axs[0, 0].set_xlabel('Time (s)')
    axs[0, 0].set_ylabel('Deflection (mm)')
    axs[0, 0].grid(True)
    axs[0, 0].legend()

    # 2. Deflection 0  30s
    axs[0, 1].plot(time_10s, deflection_10s * 1000, color='navy', label='Deflection')
    mark_max(axs[0, 1], time_10s, deflection_10s * 1000, 'navy')
    axs[0, 1].set_title('Spring Deflection (0  30s  )')
    axs[0, 1].set_xlabel('Time (s)')
    axs[0, 1].set_ylabel('Deflection (mm)')
    axs[0, 1].grid(True)
    axs[0, 1].legend()

    # 3. Force 0  30s
    axs[1, 0].plot(time_10s, spring_force_10s, color='green', label='Force')
    mark_max(axs[1, 0], time_10s, spring_force_10s, 'green')
    axs[1, 0].set_title('Spring Force vs Time')
    axs[1, 0].set_xlabel('Time (s)')
    axs[1, 0].set_ylabel('Force (N)')
    axs[1, 0].grid(True)
    axs[1, 0].legend()

    # 4. Acceleration 0  30s
    axs[1, 1].plot(time_10s, acc_10s, color='red', label='Acceleration')
    mark_max(axs[1, 1], time_10s, acc_10s, 'red')
    axs[1, 1].set_title('Acceleration vs Time')
    axs[1, 1].set_xlabel('Time (s)')
    axs[1, 1].set_ylabel('Acceleration (m/s  )')
    axs[1, 1].grid(True)
    axs[1, 1].legend()



    # Final layout
    plt.tight_layout(rect=[0, 0, 1, 0.97])
    plt.savefig("spring_simulation_summary_clipped_max_only.png", dpi=300)
    plt.close()

    print("    Max points kept, average lines removed. Saved as '
        spring_simulation_summary.png'")
```



Figure 85 Selected spring based on simulations

Table 45 Springs Tested

S/N	No. of Coils	Wire Diameter (mm)	Smaller Inner Diameter (mm)	Larger Inner Diameter (mm)	Calculated Stiffness (N/mm)	Length of Spring (mm)	Material	Calculated Maximum Deflection (mm)
1	5	2.5	34.7	54.7	1.21	64	Spring Steel	12.17
2	6	2	16.45	45.45	0.95	49	Spring Steel	15.4
3	7	2	12.7	39.7	1.14	53	Spring Steel	12.84
4	8	2	15	29	1.81	64	Spring Steel	8.11
5	9	2	13.3	25.3	2.23	55	Spring Steel	6.58
6	5	1.5	9	39	0.77	42	Stainless Steel 316	19.08
7	6	1.5	17	29	0.83	42	Stainless Steel 316	17.76

L. Appendix: Simulations and Calculations

A. Nosecone

1. Computational Fluid Dynamics

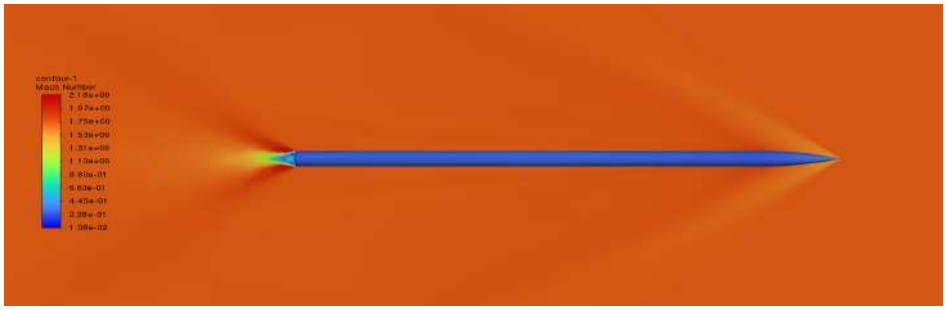


Figure 86 Mach Contour for Fineness Ratio of 4

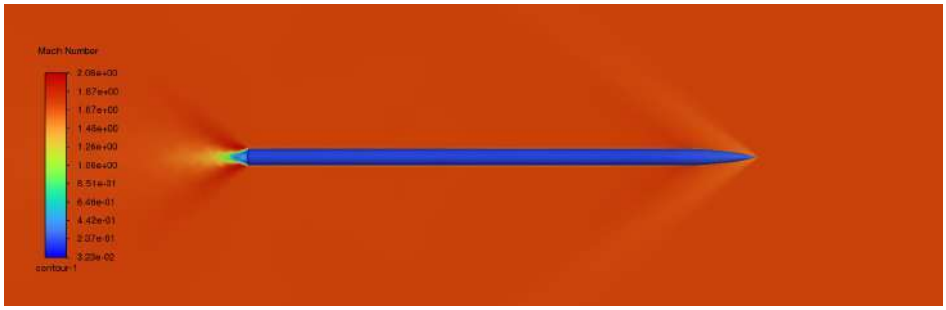


Figure 87 Mach Contour for Fineness Ratio of 4.5

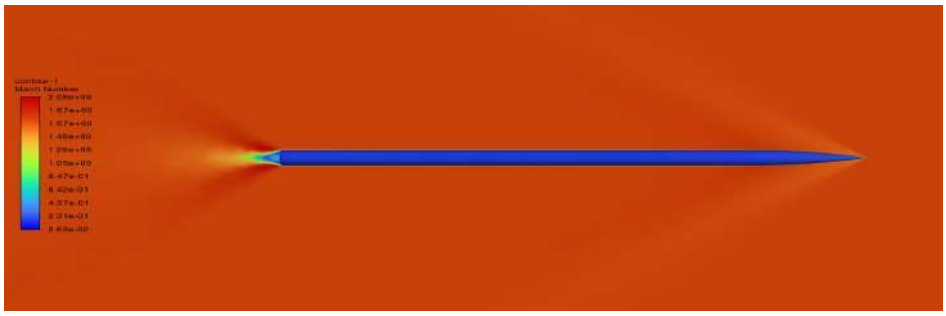


Figure 88 Mach Contour for Fineness Ratio of 5

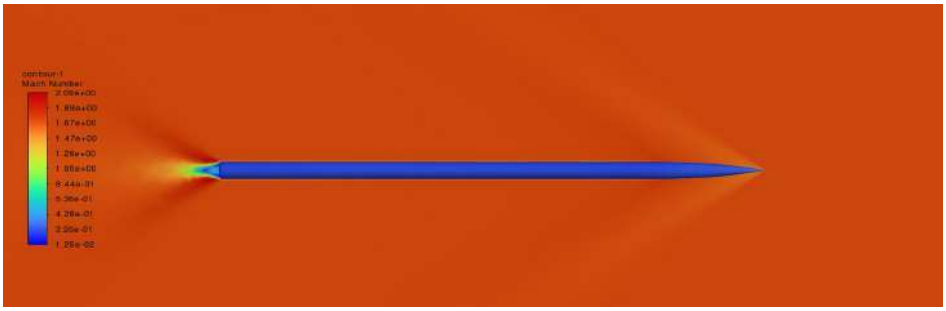


Figure 89 Mach Contour for Fineness Ratio of 5.1

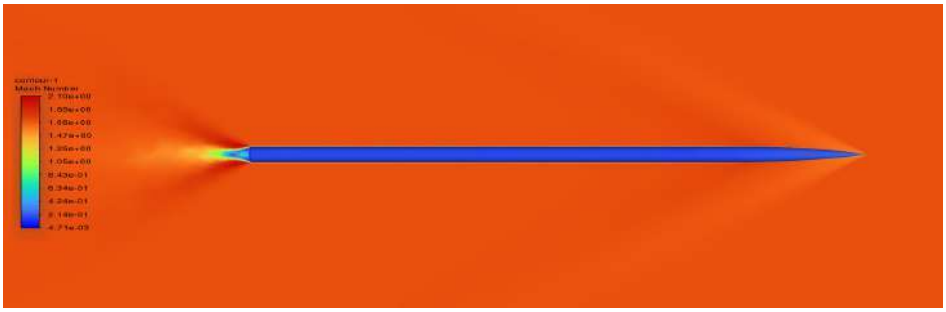


Figure 90 Mach Contour for Fineness Ratio of 5.2

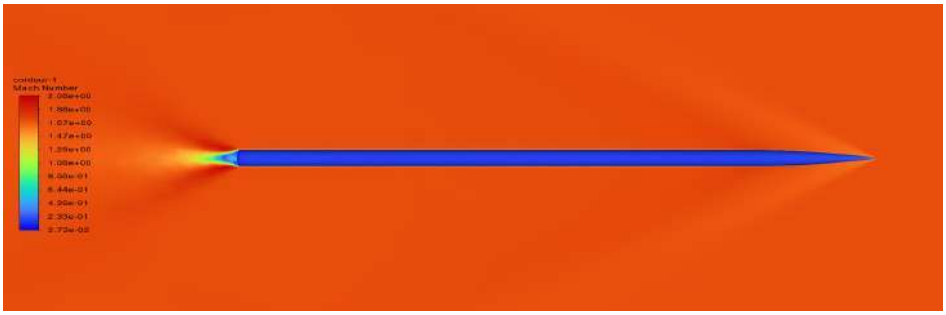


Figure 91 Mach Contour for Fineness Ratio of 5.3

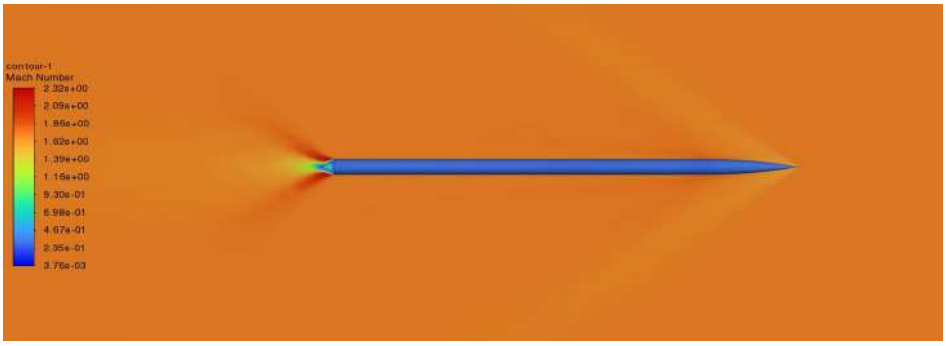


Figure 92 Mach Contour for Fineness Ratio of 5.4

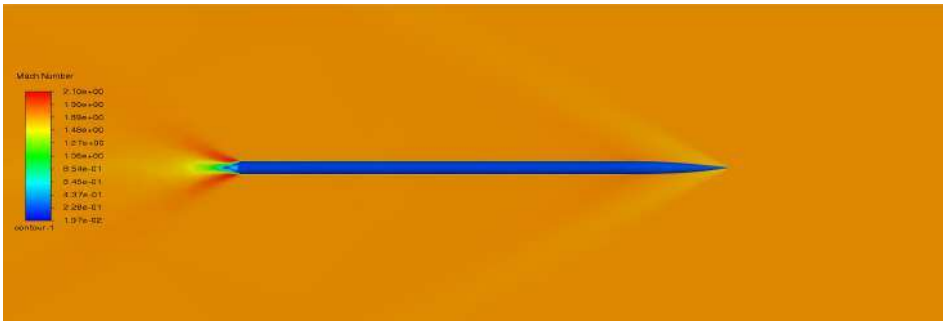


Figure 93 Mach Contour for Fineness Ratio of 5.5

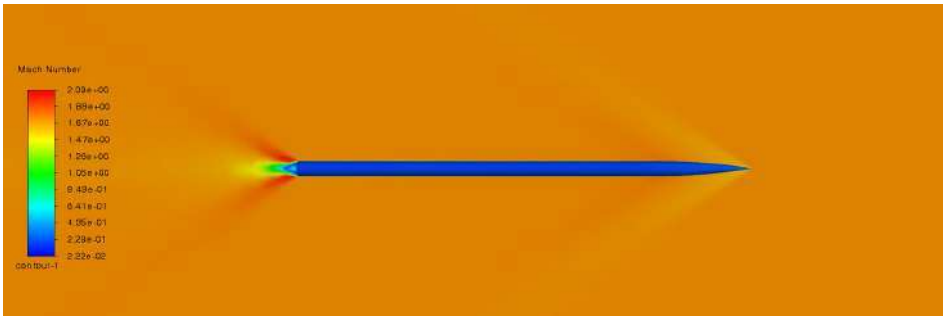


Figure 94 Mach Contour for Fineness Ratio of 5.6

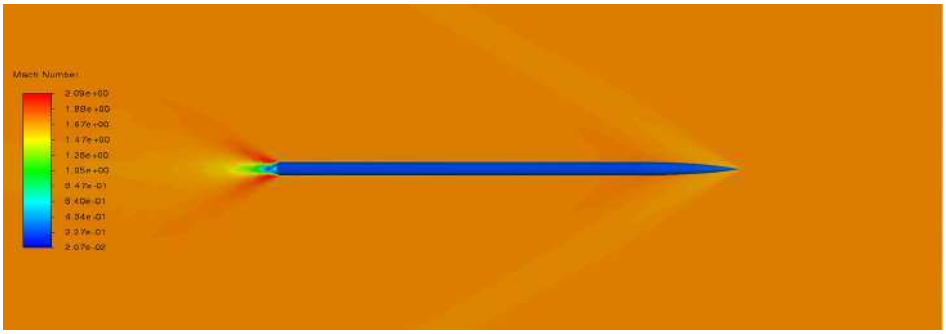


Figure 95 Mach Contour for Fineness Ratio of 5.7

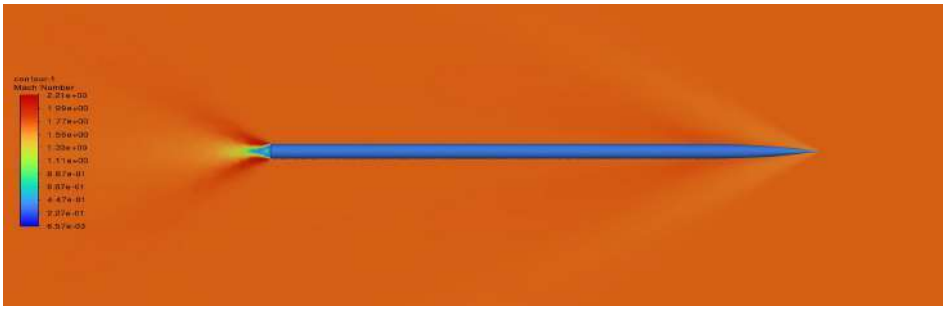


Figure 96 Mach Contour for Fineness Ratio of 5.8

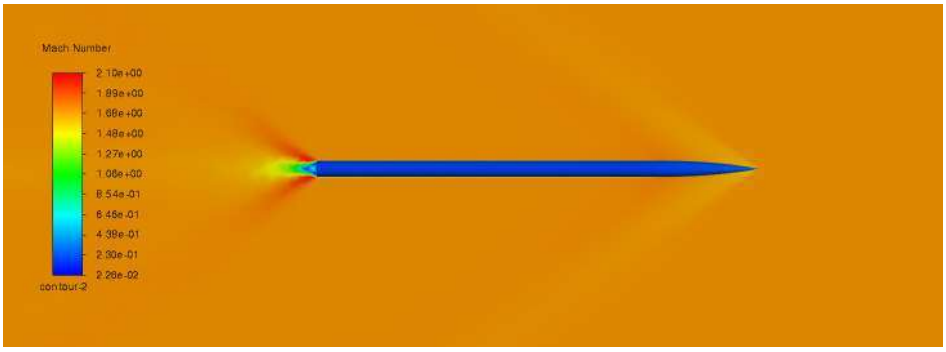


Figure 97 Mach Contour for Fineness Ratio of 5.9

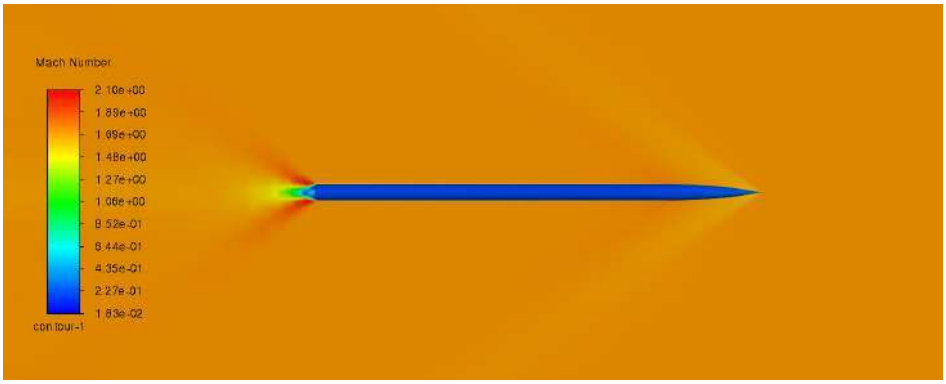


Figure 98 Mach Contour for Fineness Ratio of 6

B. Fins

1. Computational Fluid Dynamics

Hexagonal Cross-Section

a) 5° Half Wedge Angle

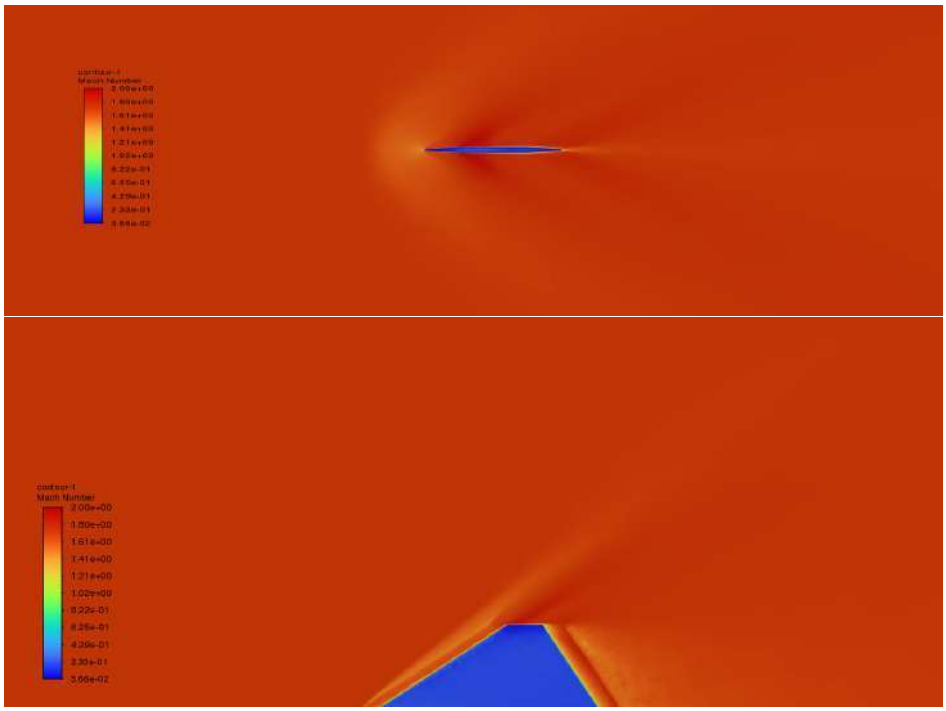


Figure 99 Mach Contour at 0 Angle of Attack

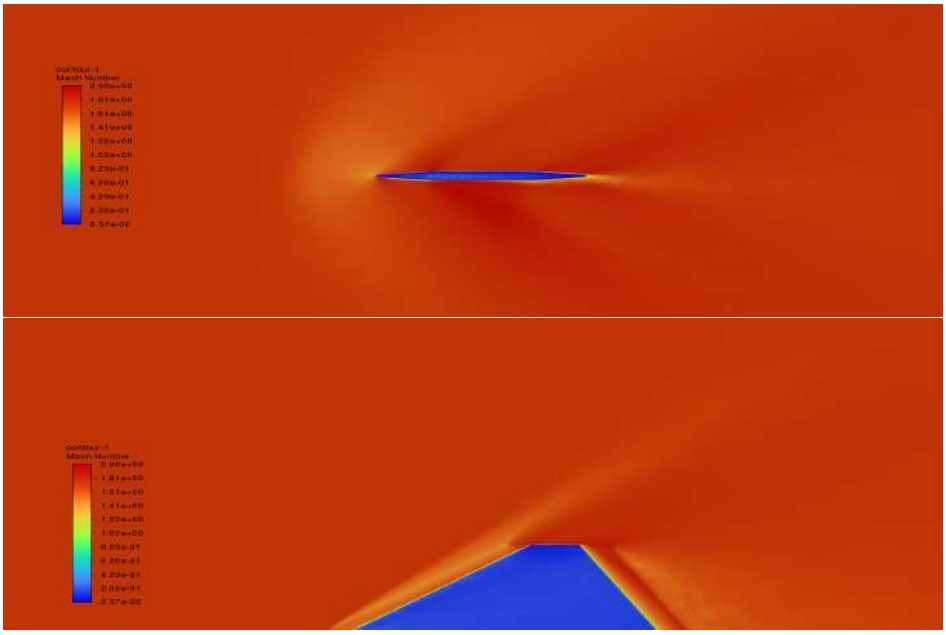


Figure 100 Mach Contour at 3° Angle of Attack

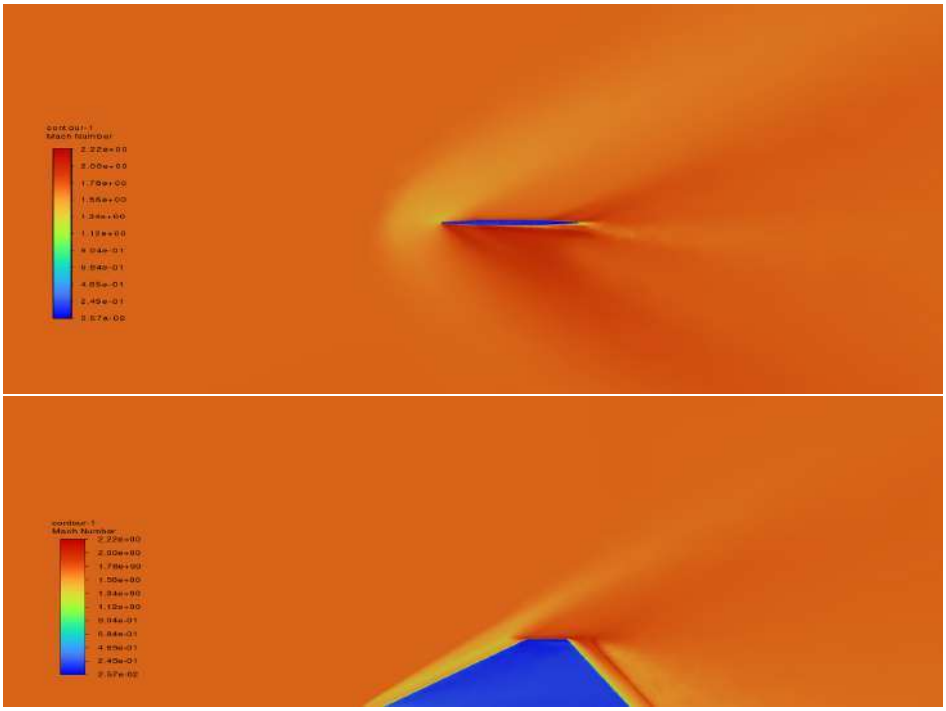


Figure 101 Mach Contour at 6° Angle of Attack

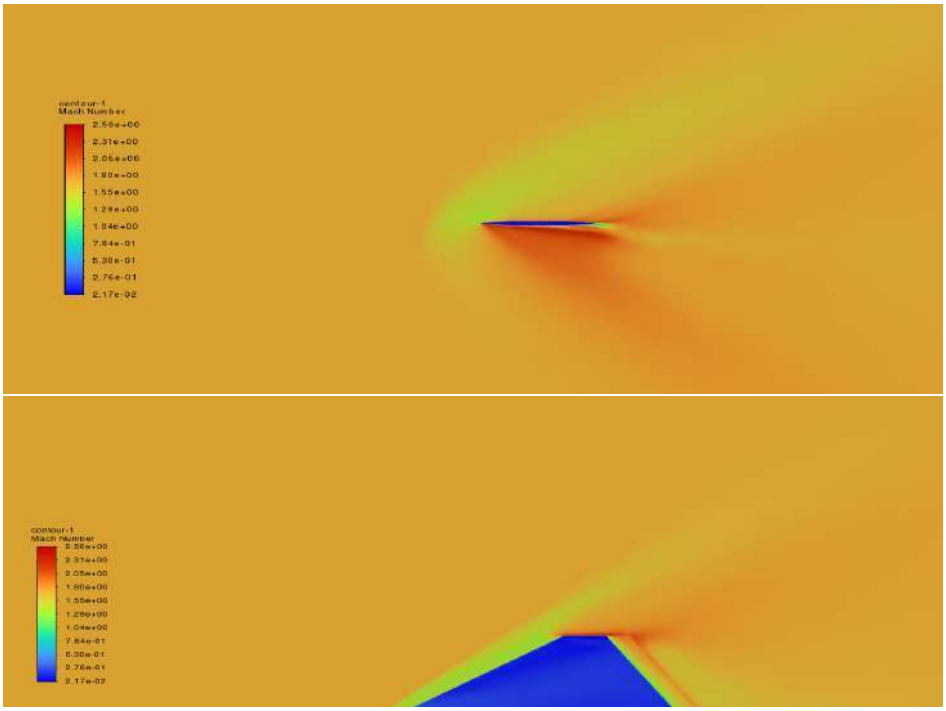


Figure 102 Mach Contour at 9° Angle of Attack

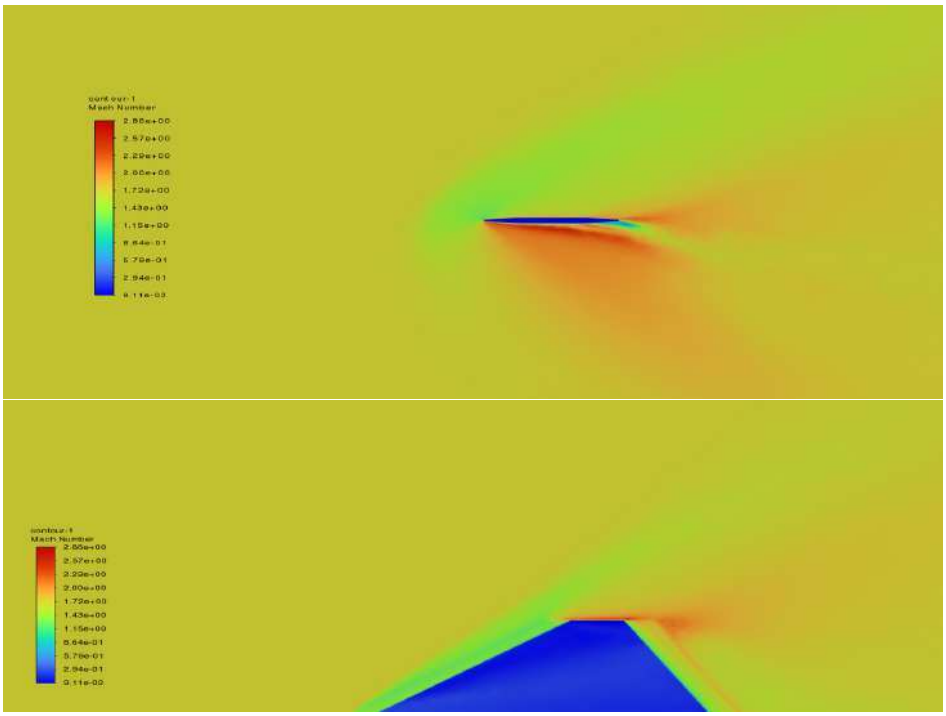


Figure 103 Mach Contour at 12° Angle of Attack

b) 10° Half Wedge Angle

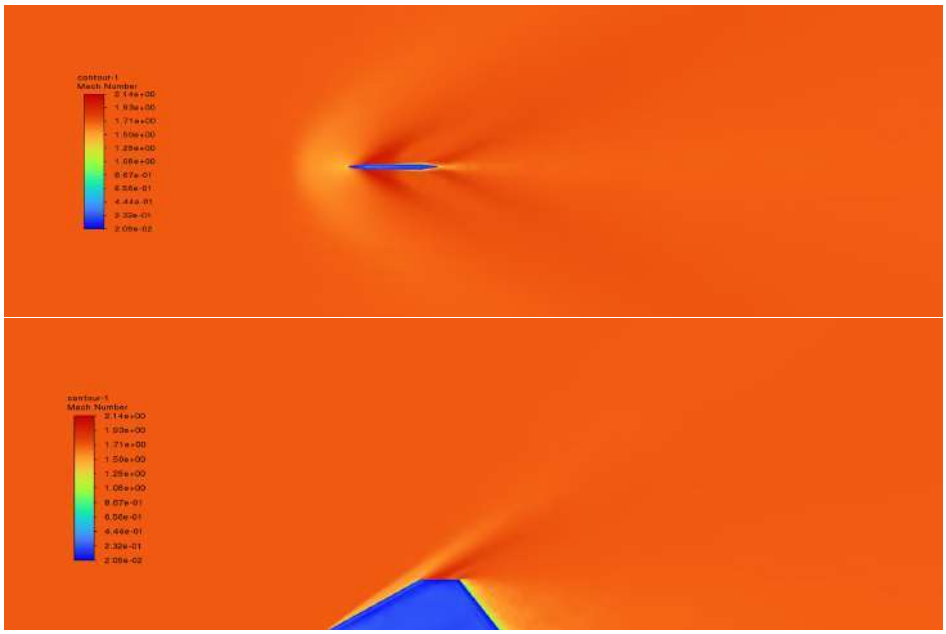


Figure 104 Mach Contour at 0 Angle of Attack

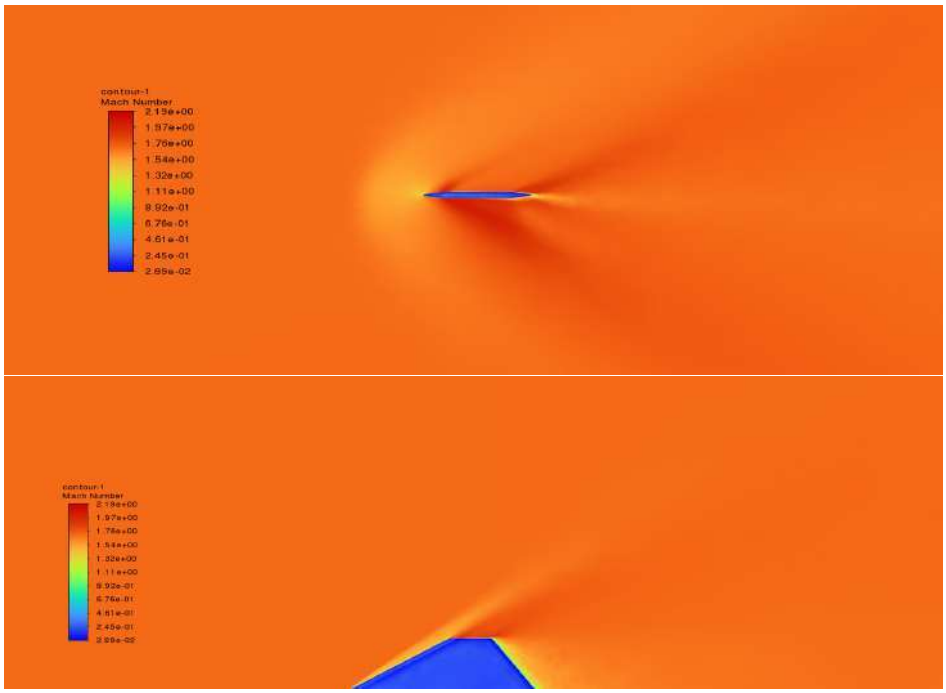


Figure 105 Mach Contour at 3° Angle of Attack

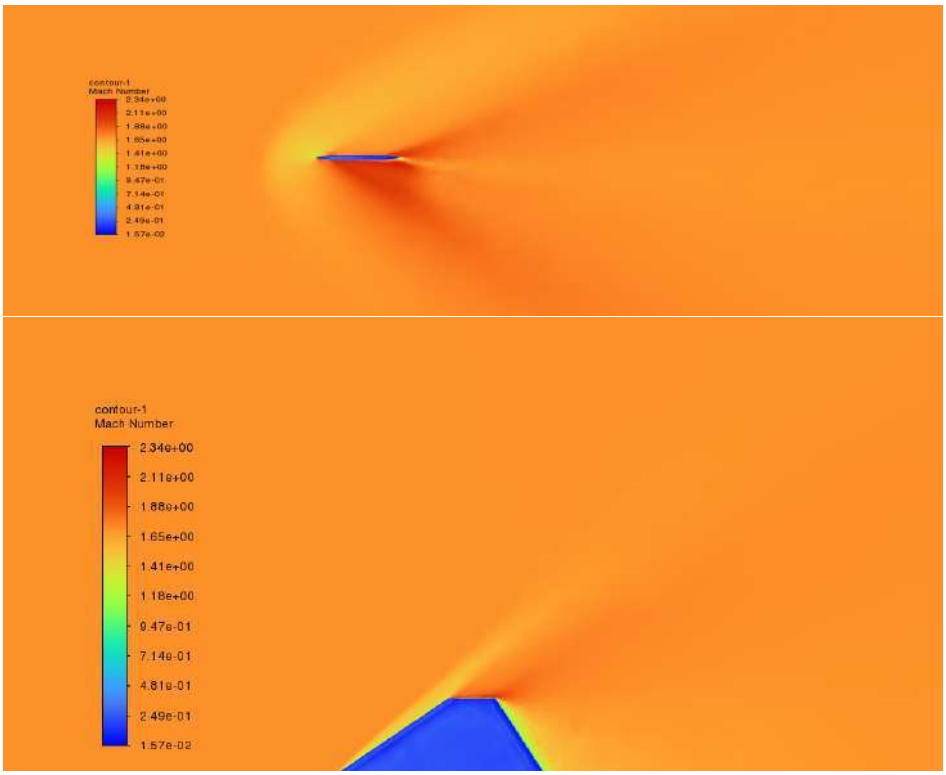


Figure 106 Mach Contour at 6° Angle of Attack

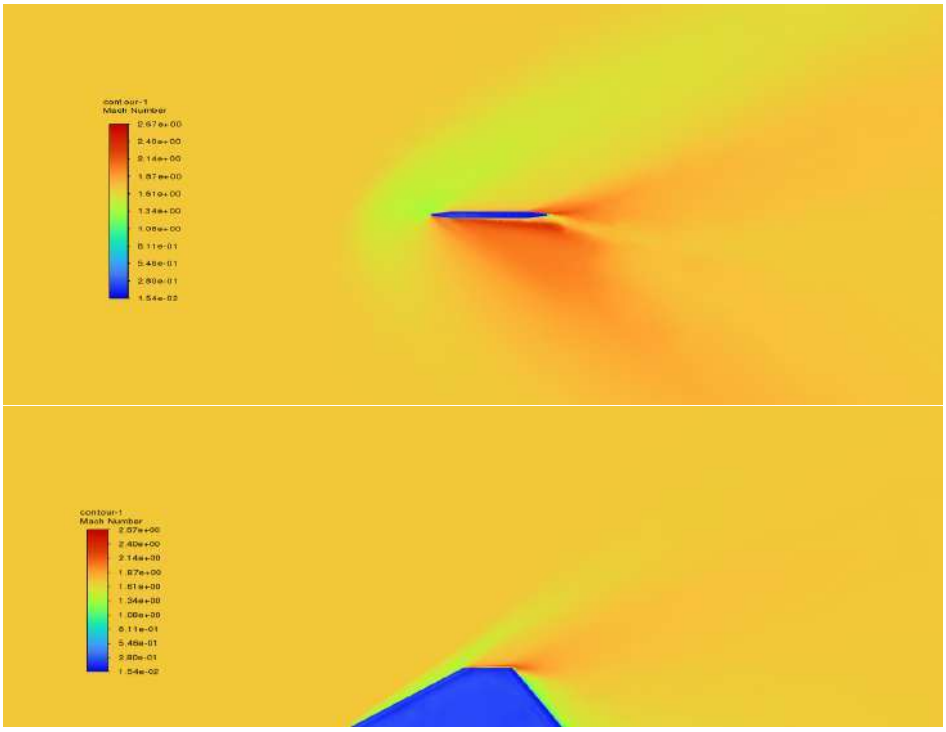


Figure 107 Mach Contour at 9° Angle of Attack

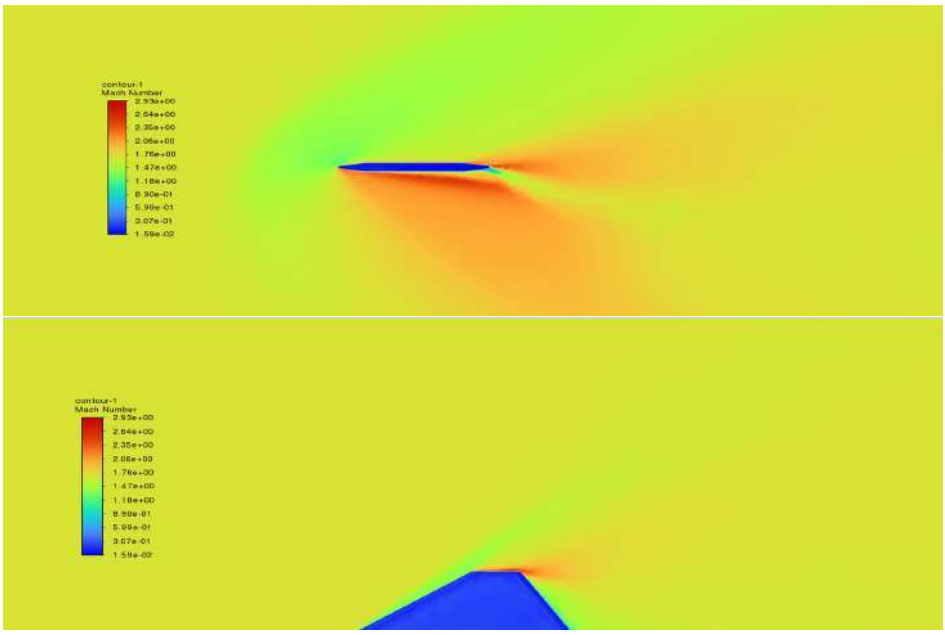


Figure 108 Mach Contour at 12° Angle of Attack

c) 15° Half Wedge Angle

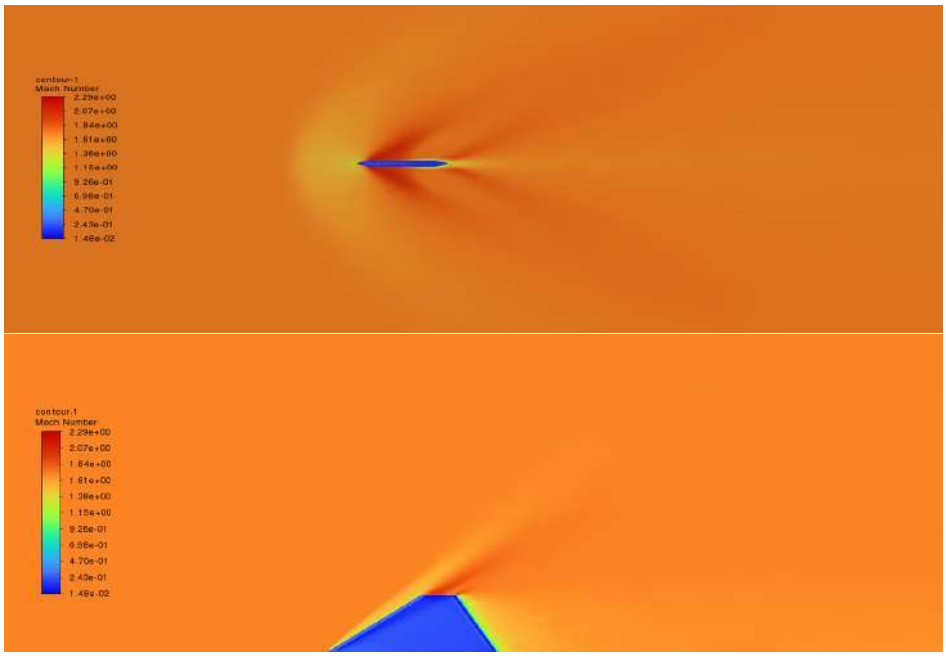


Figure 109 Mach Contour at 0 Angle of Attack

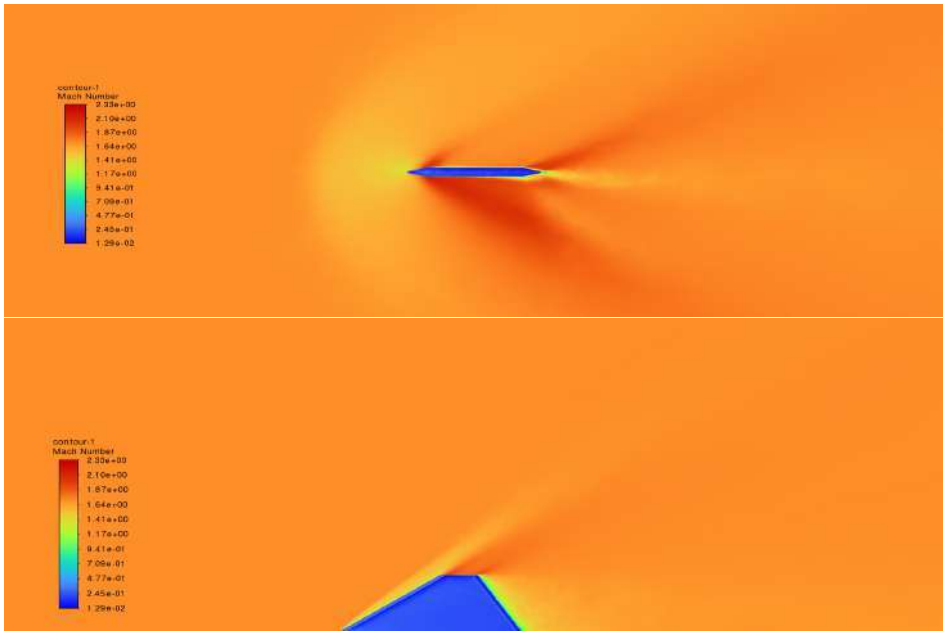


Figure 110 Mach Contour at 3° Angle of Attack

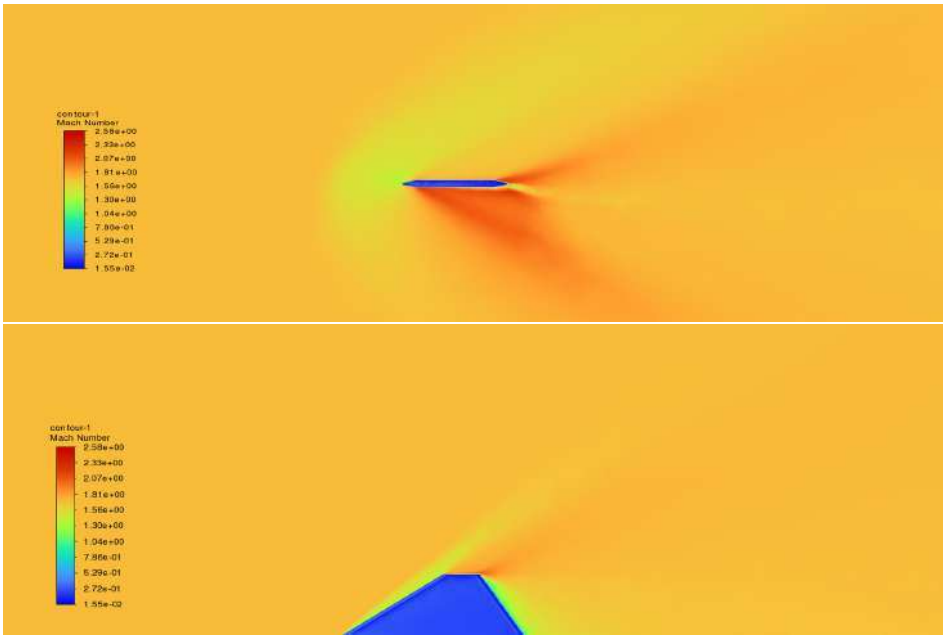


Figure 111 Mach Contour at 6° Angle of Attack

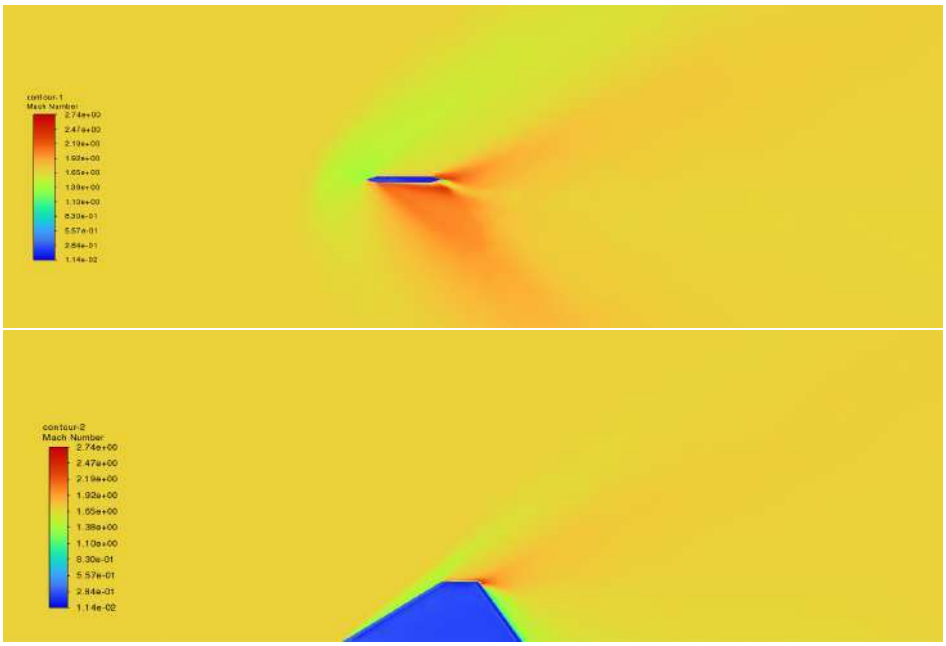


Figure 112 Mach Contour at 9° Angle of Attack

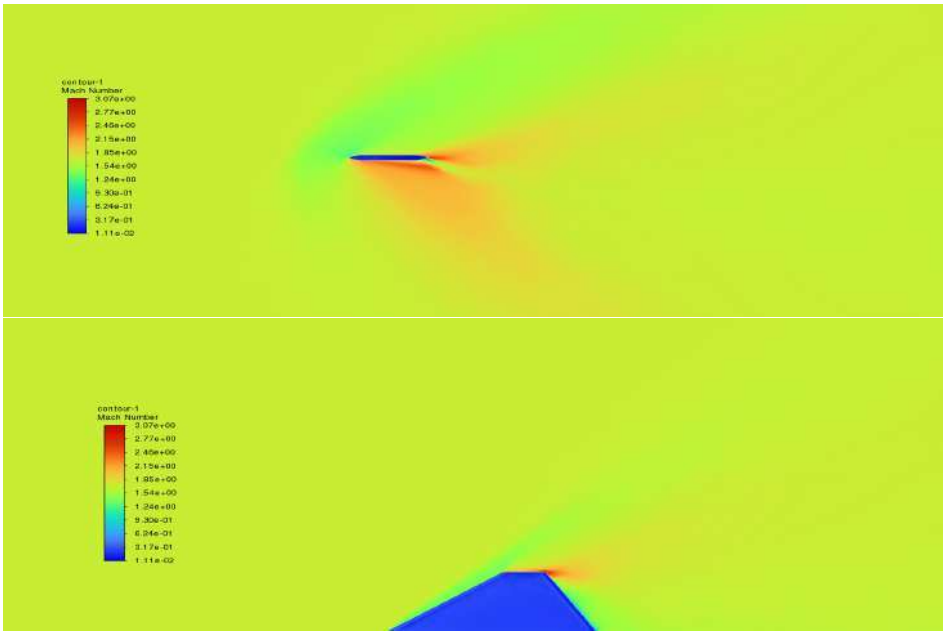


Figure 113 Mach Contour at 12° Angle of Attack

d) 20° Half Wedge Angle

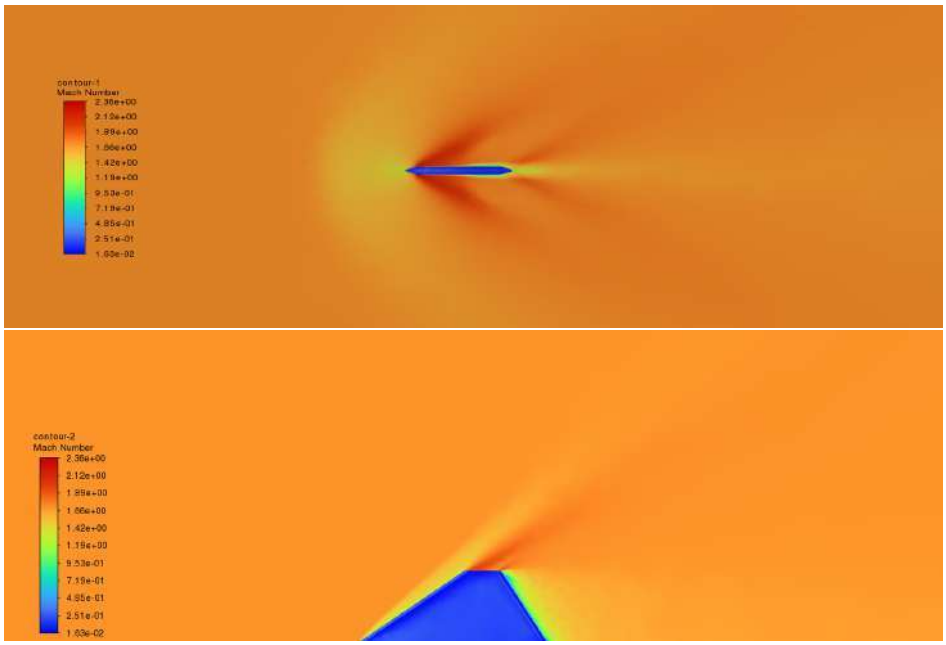


Figure 114 Mach Contour at 0 Angle of Attack

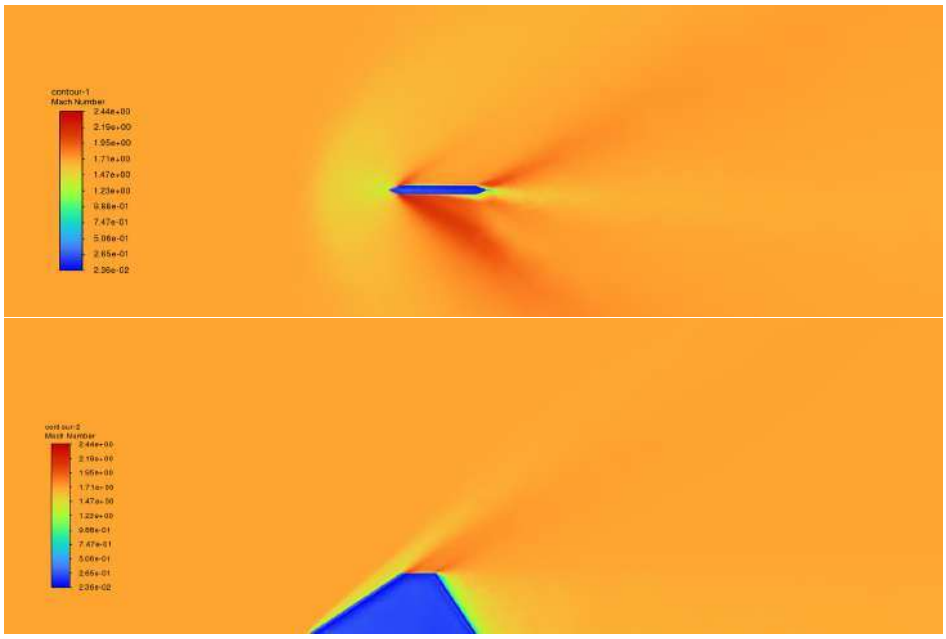


Figure 115 Mach Contour at 3° Angle of Attack

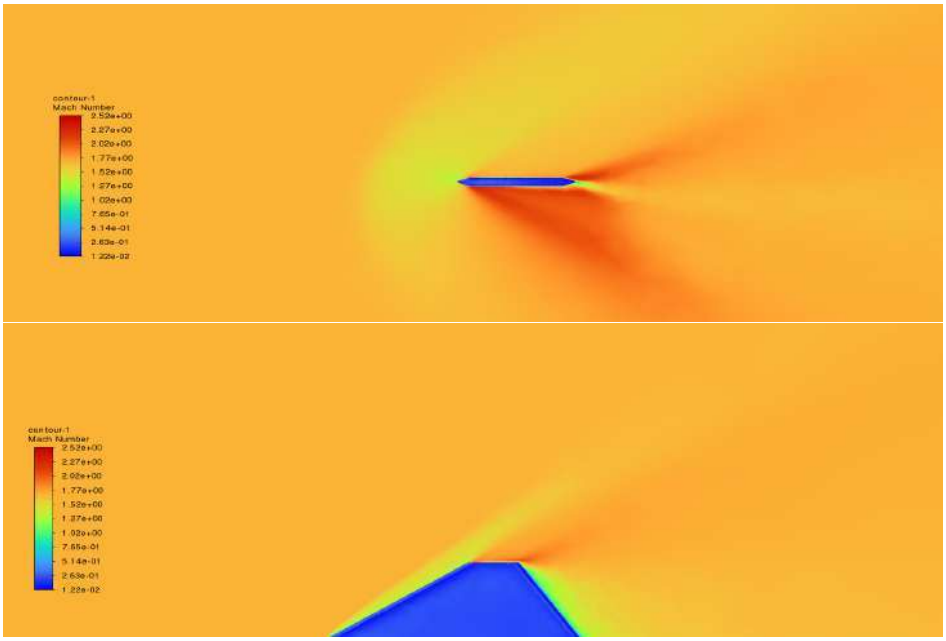


Figure 116 Mach Contour at 6° Angle of Attack

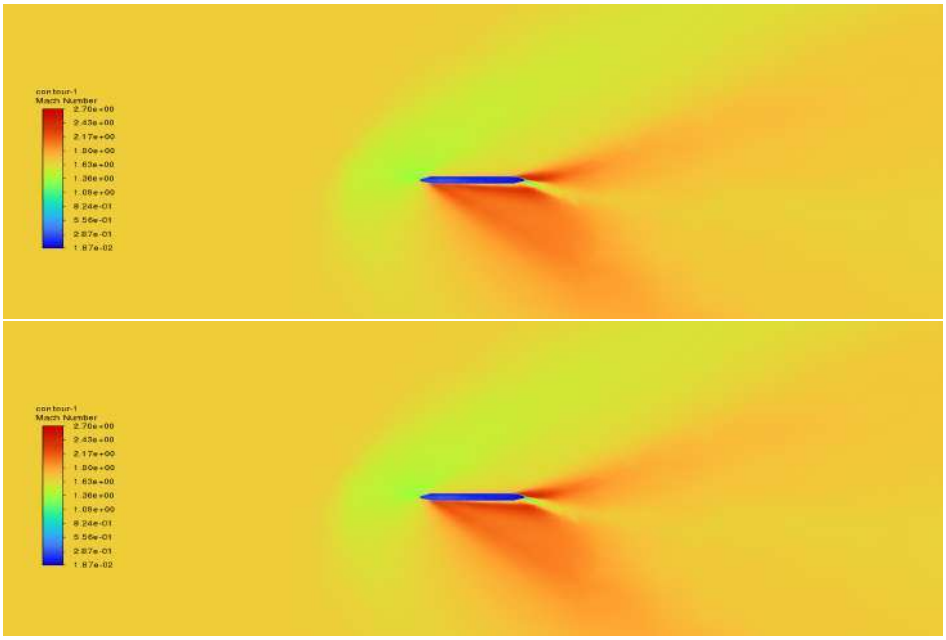


Figure 117 Mach Contour at 9° Angle of Attack

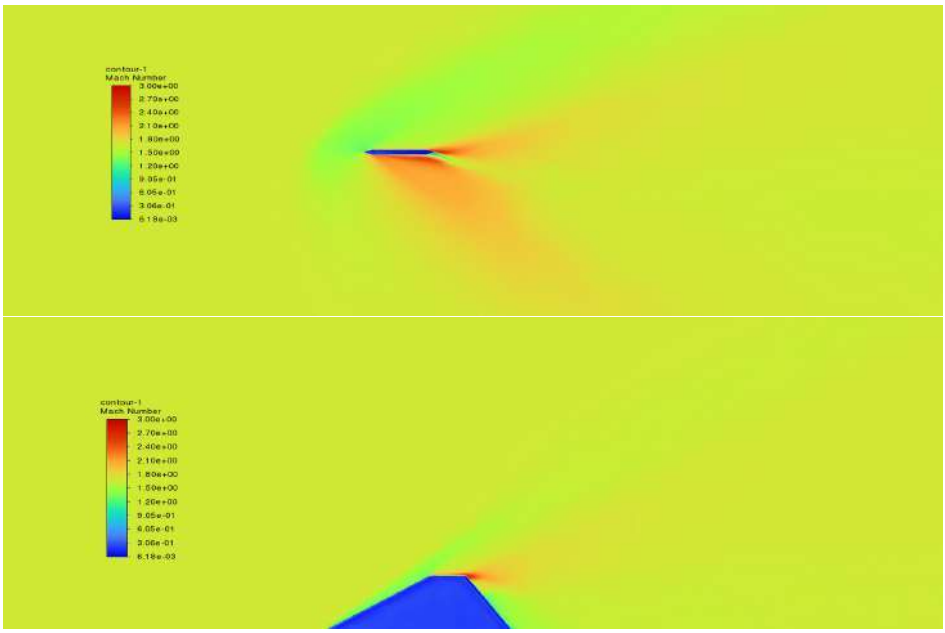


Figure 118 Mach Contour at 12° Angle of Attack

Bi-Convex Cross Section

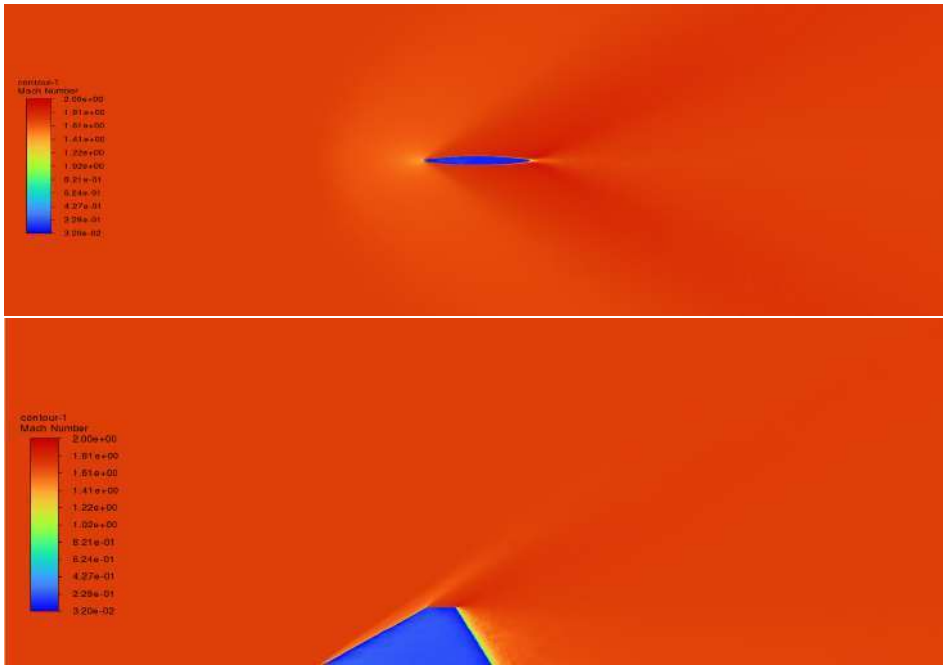


Figure 119 Mach Contour at 0 Angle of Attack

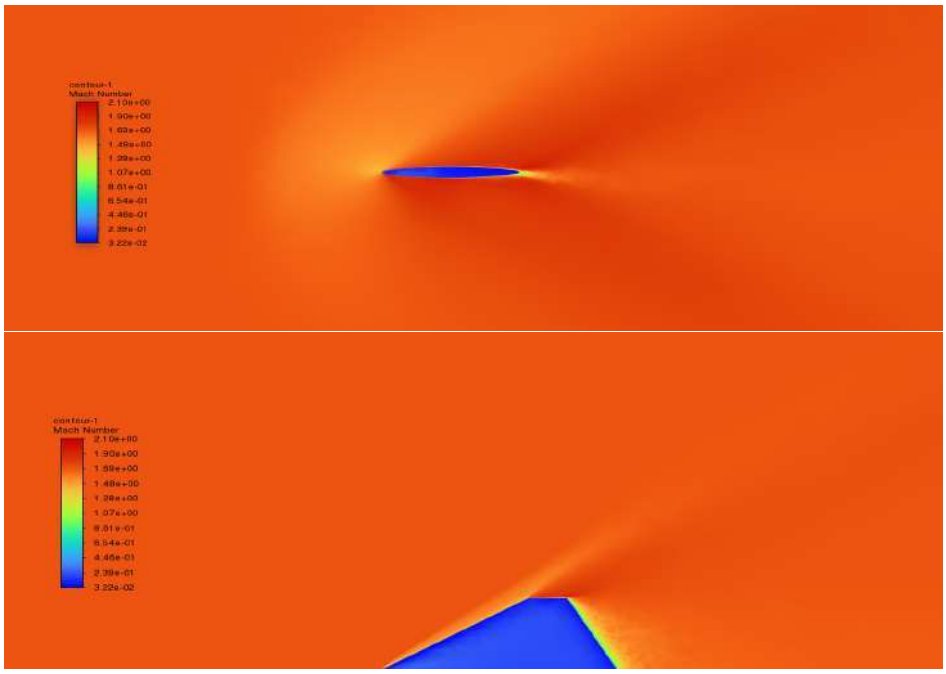


Figure 120 Mach Contour at 3° Angle of Attack

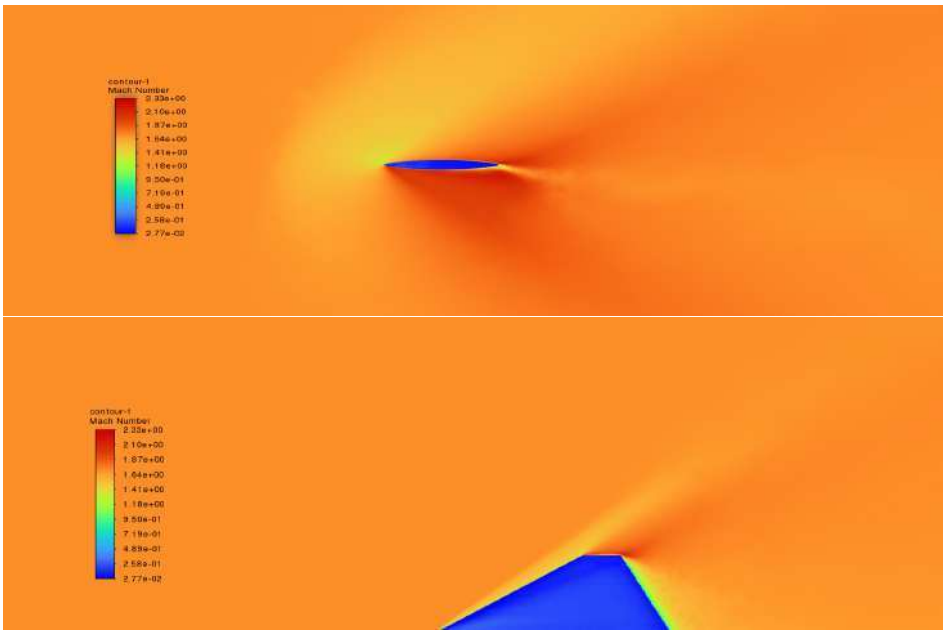


Figure 121 Mach Contour at 6° Angle of Attack

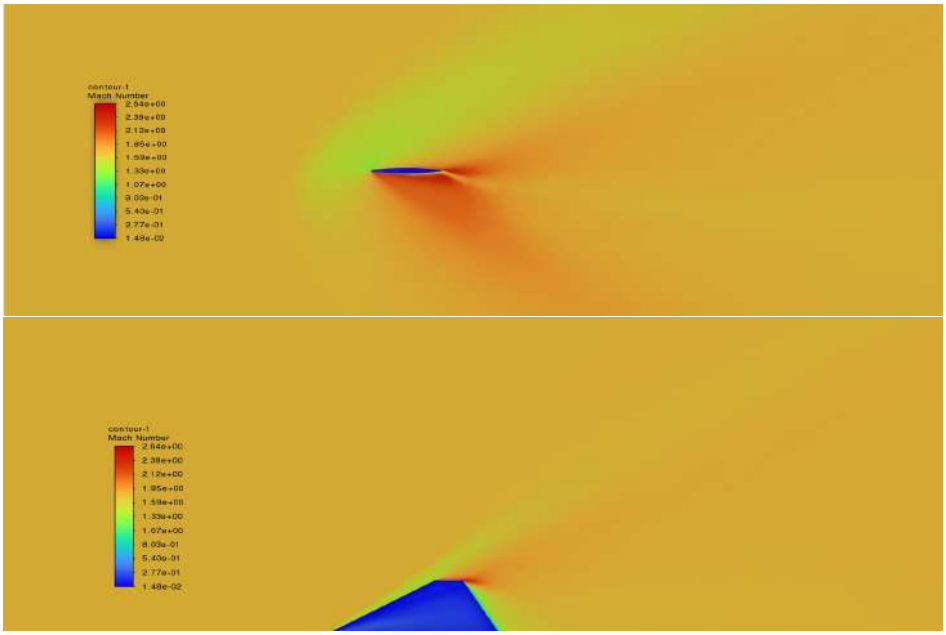


Figure 122 Mach Contour at 9° Angle of Attack

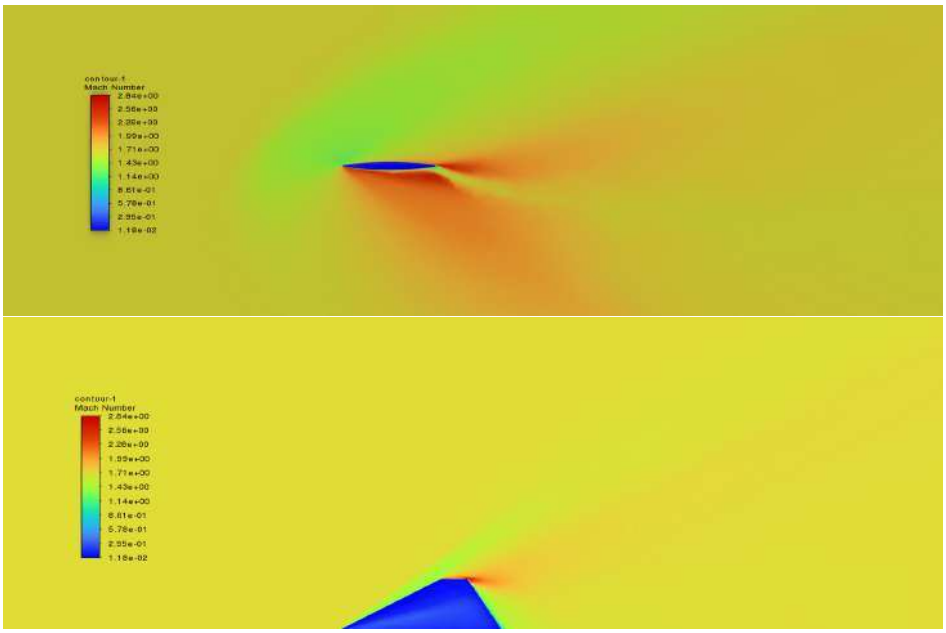


Figure 123 Mach Contour at 12° Angle of Attack

Double Wedge Cross-Section

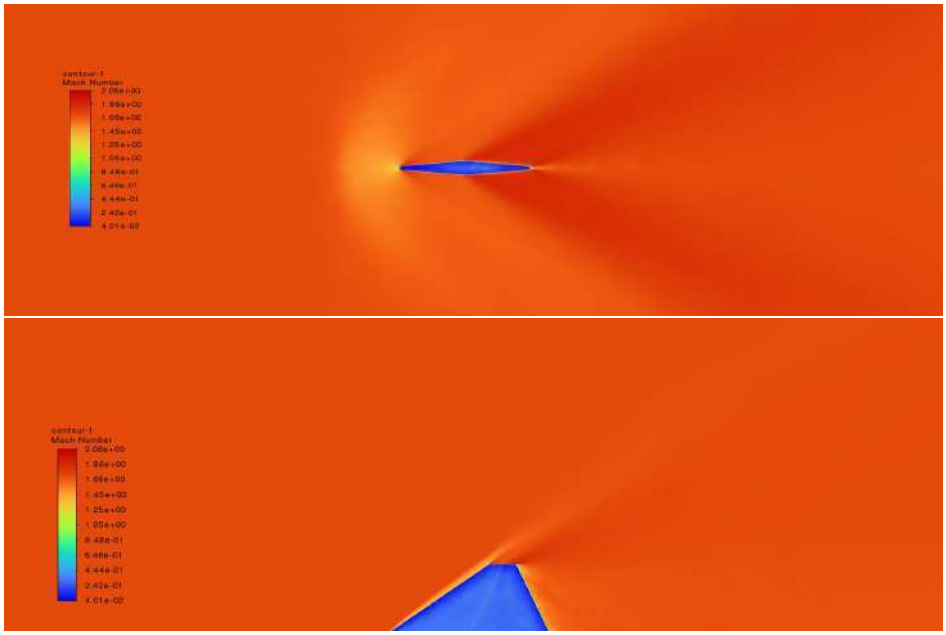


Figure 124 Mach Contour at 0 Angle of Attack

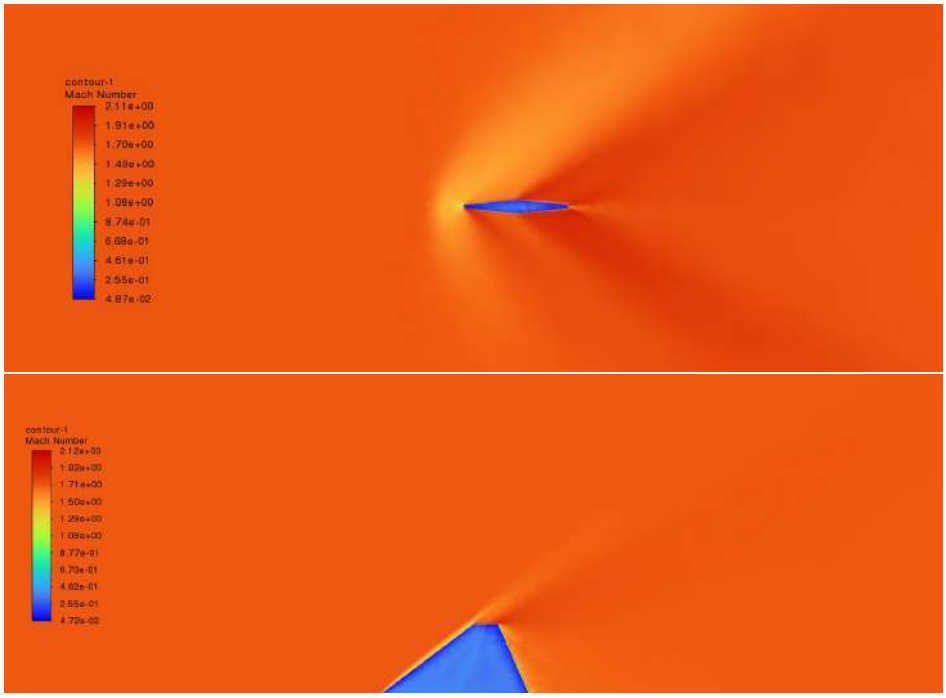


Figure 125 Mach Contour at 3° Angle of Attack

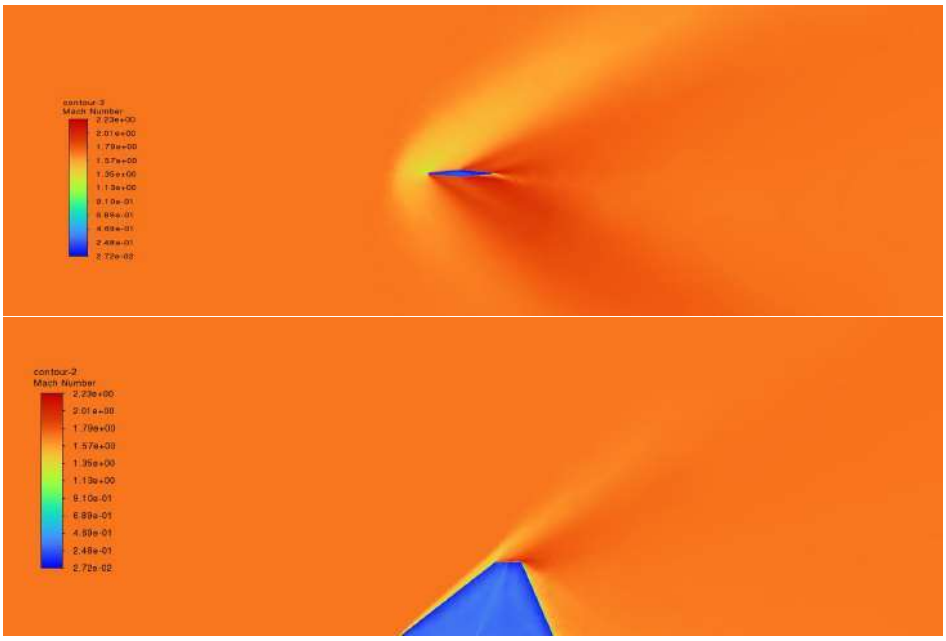


Figure 126 Mach Contour at 6° Angle of Attack

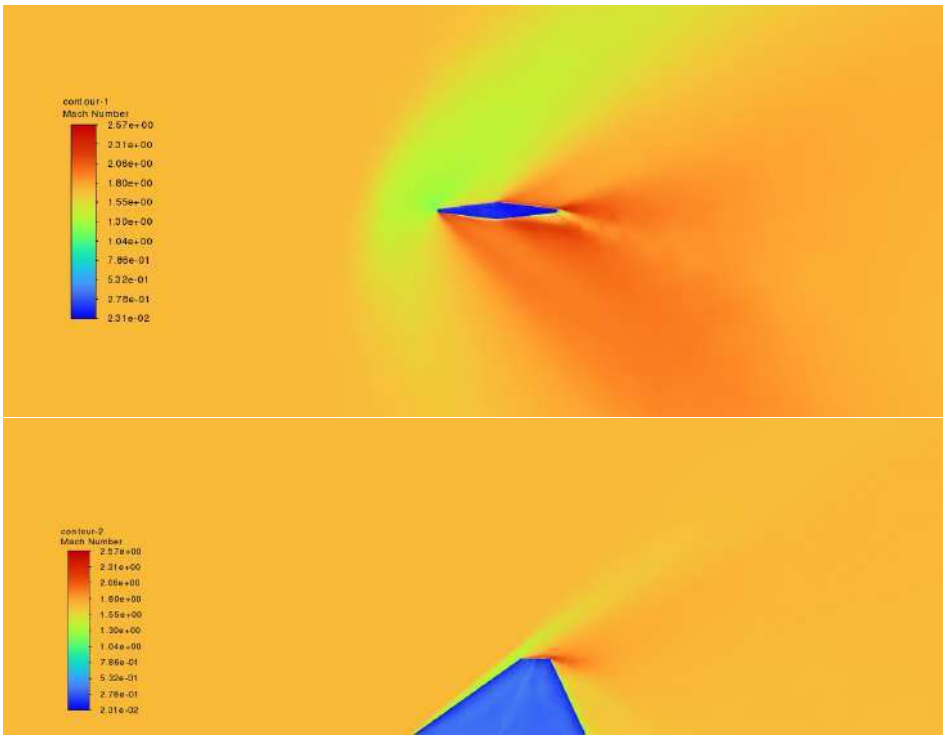


Figure 127 Mach Contour at 9° Angle of Attack

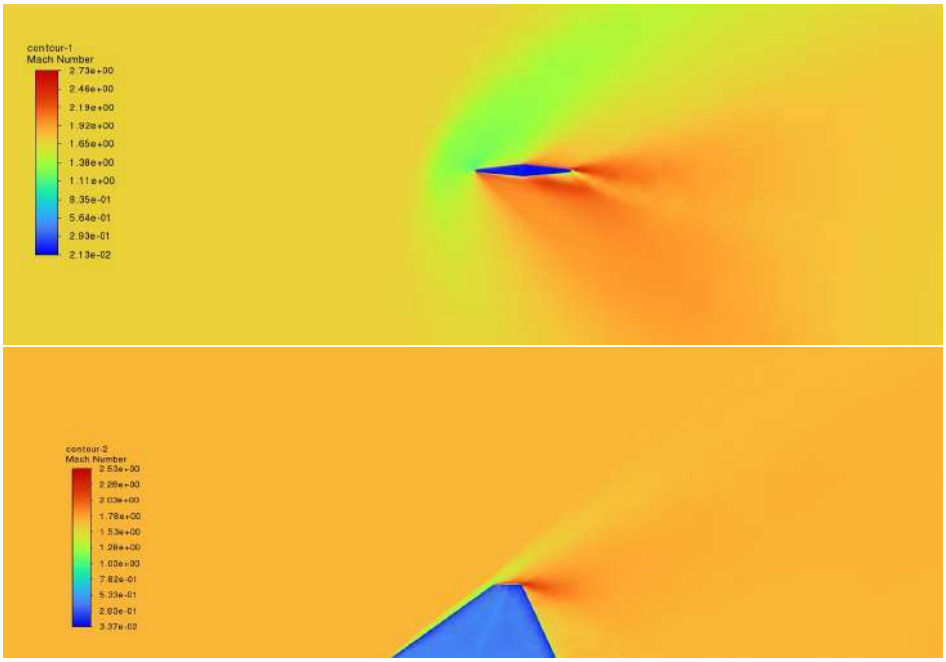


Figure 128 Mach Contour at 12° Angle of Attack

Single Wedge Cross-Section

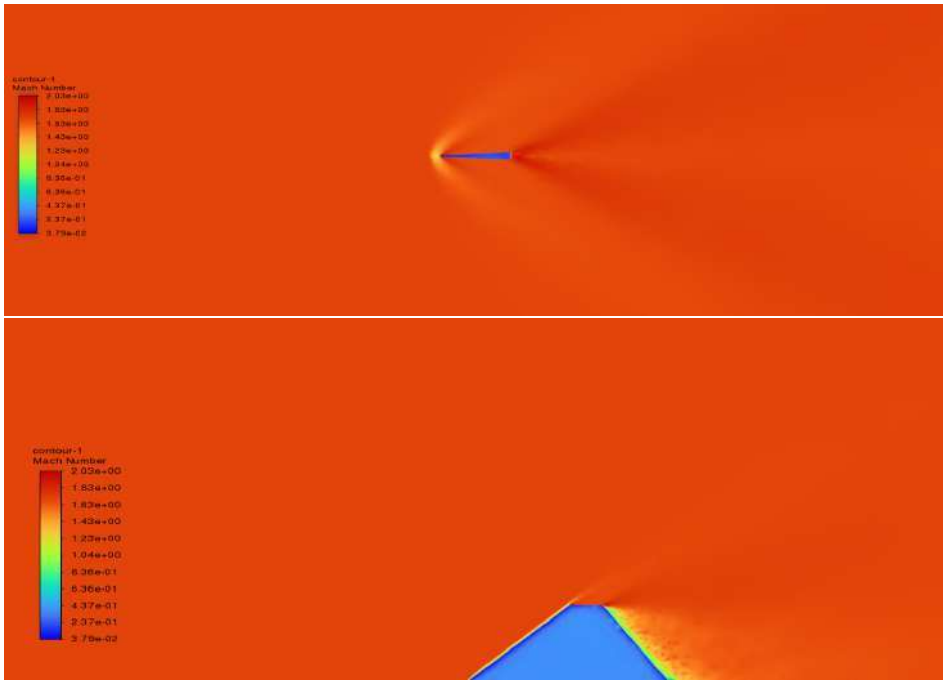


Figure 129 Mach Contour at 0 Angle of Attack

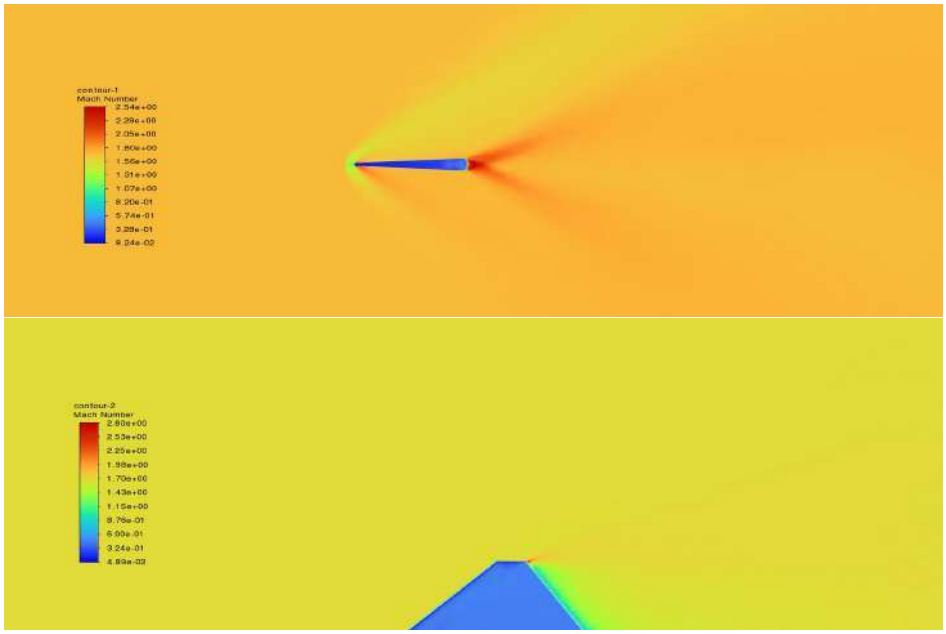


Figure 130 Mach Contour at 3° Angle of Attack

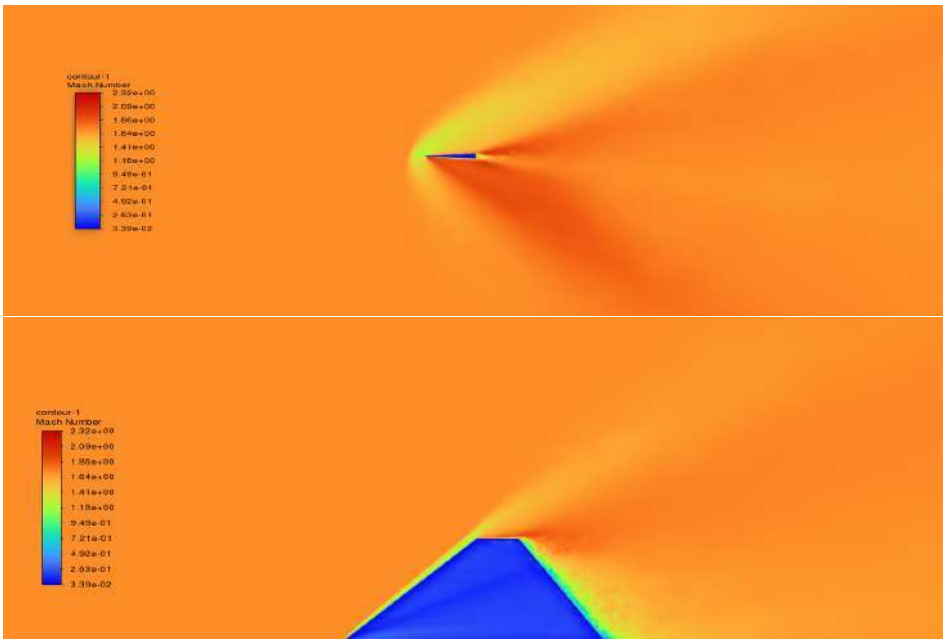


Figure 131 Mach Contour at 6° Angle of Attack

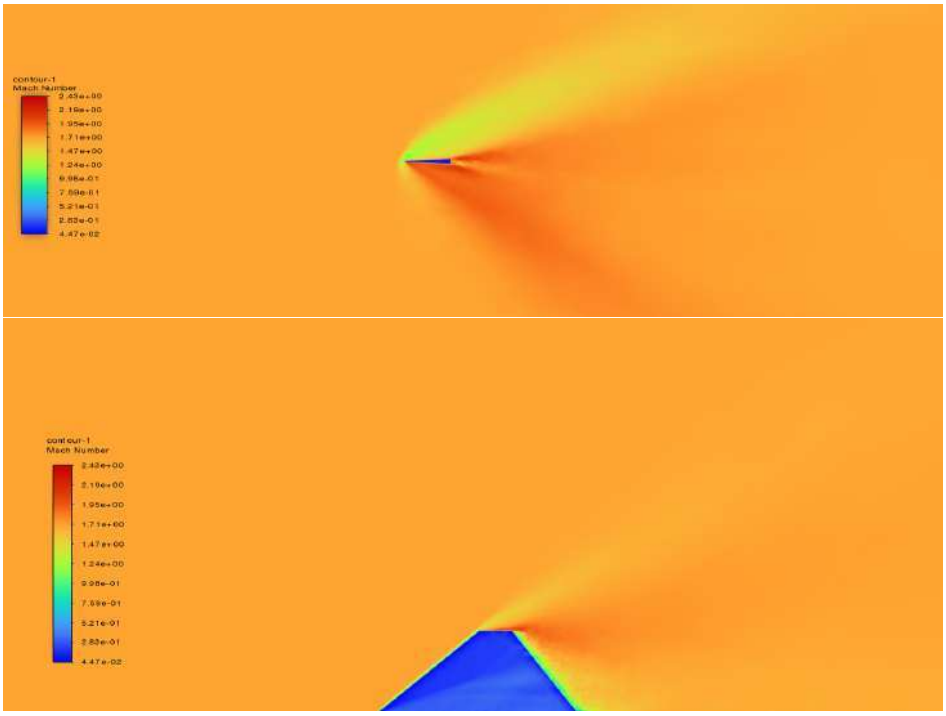


Figure 132 Mach Contour at 9° Angle of Attack

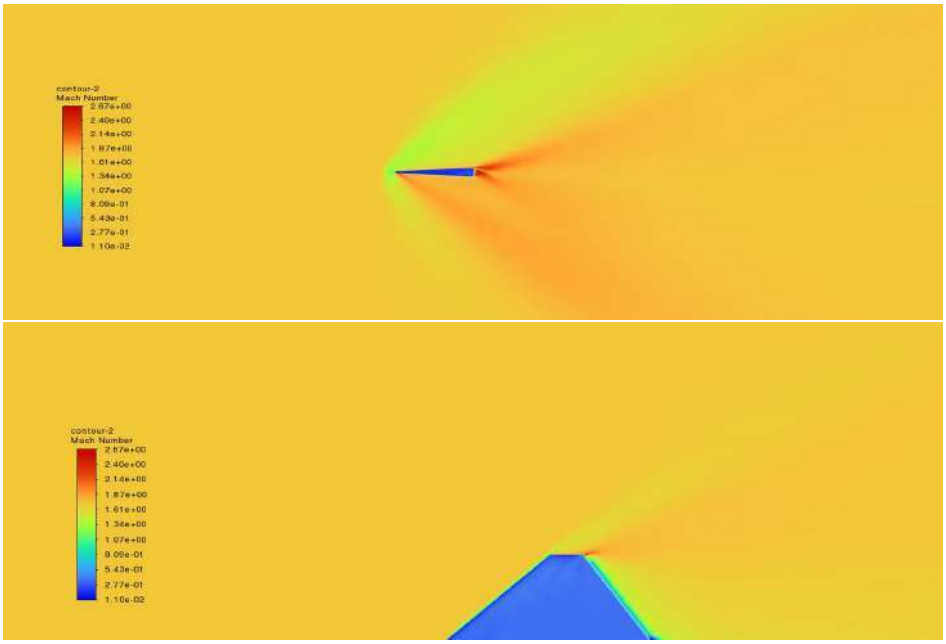


Figure 133 Mach Contour at 12° Angle of Attack

Hexagonal Blunt-Based Cross Section

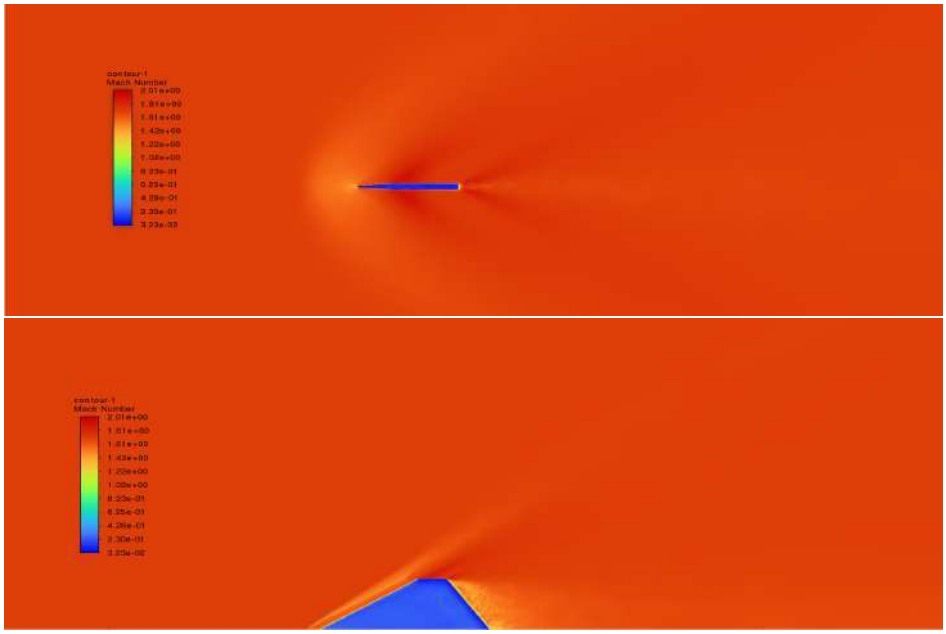


Figure 134 Mach Contour at 0 Angle of Attack

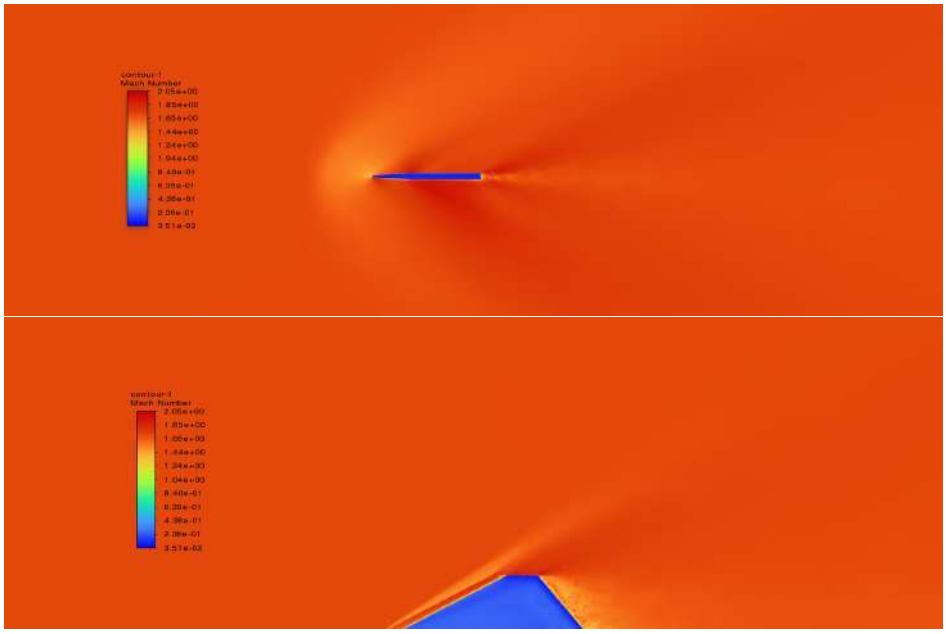


Figure 135 Mach Contour at 3° Angle of Attack

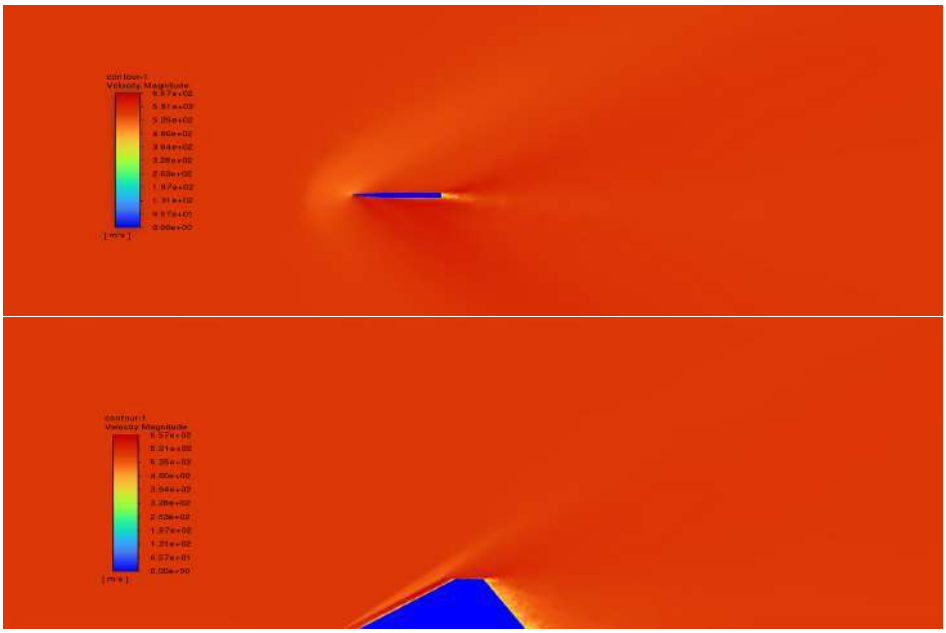


Figure 136 Mach Contour at 6° Angle of Attack

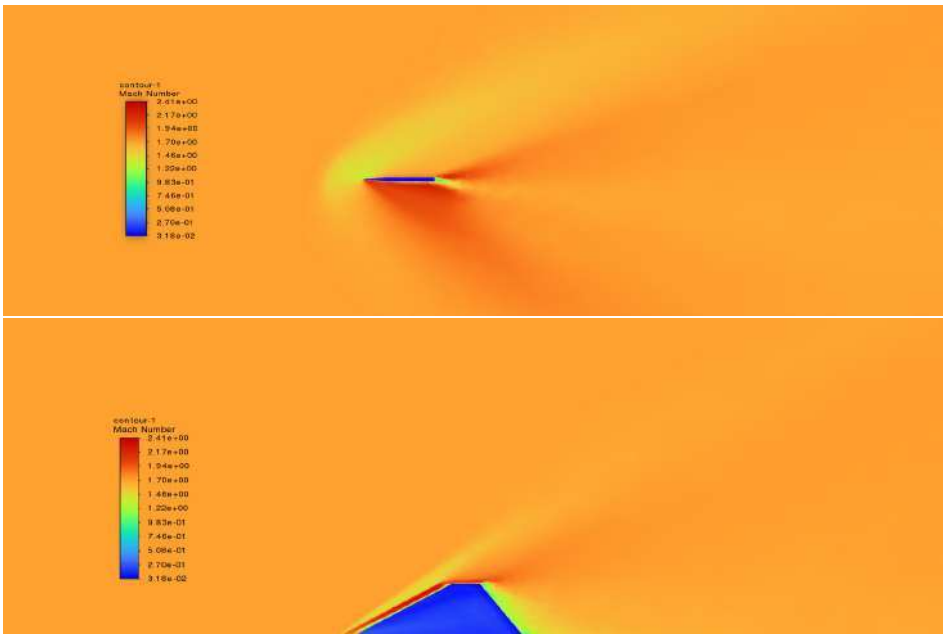


Figure 137 Mach Contour at 9° Angle of Attack

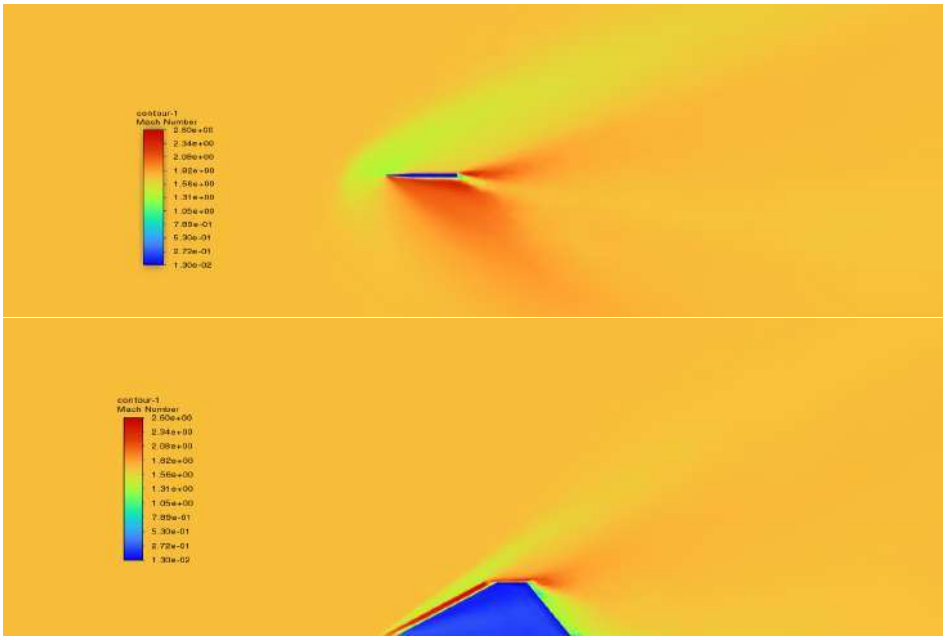


Figure 138 Mach Contour at 12° Angle of Attack

Airfoil Cross Section

a) NACA-0011

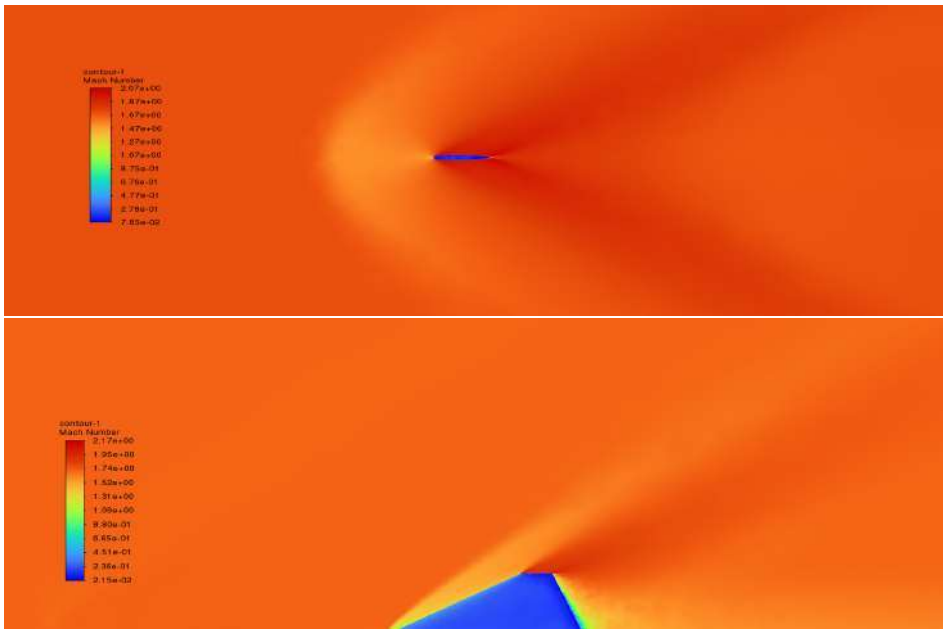


Figure 139 Mach Contour at 0 Angle of Attack

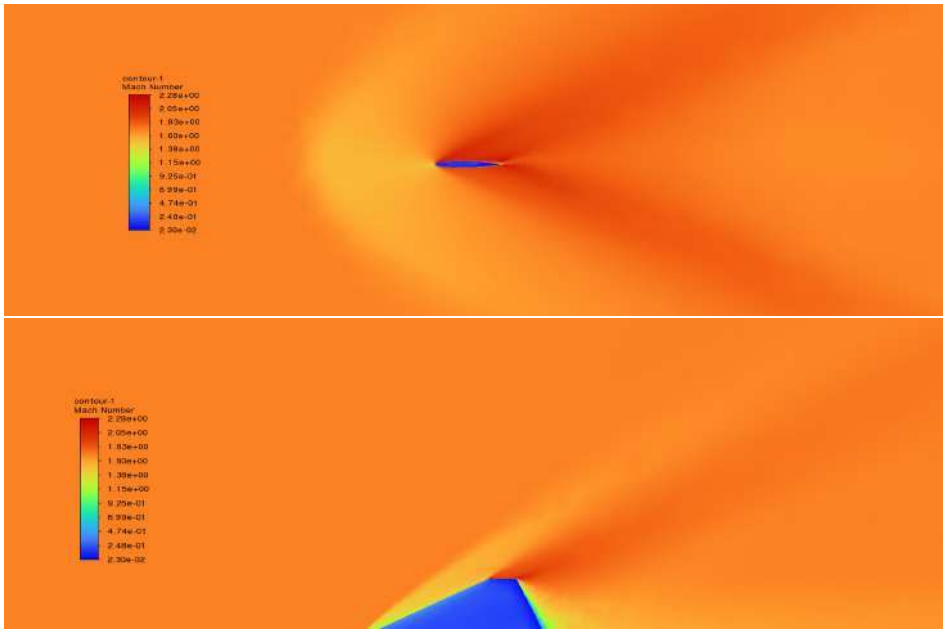


Figure 140 Mach Contour at 3° Angle of Attack

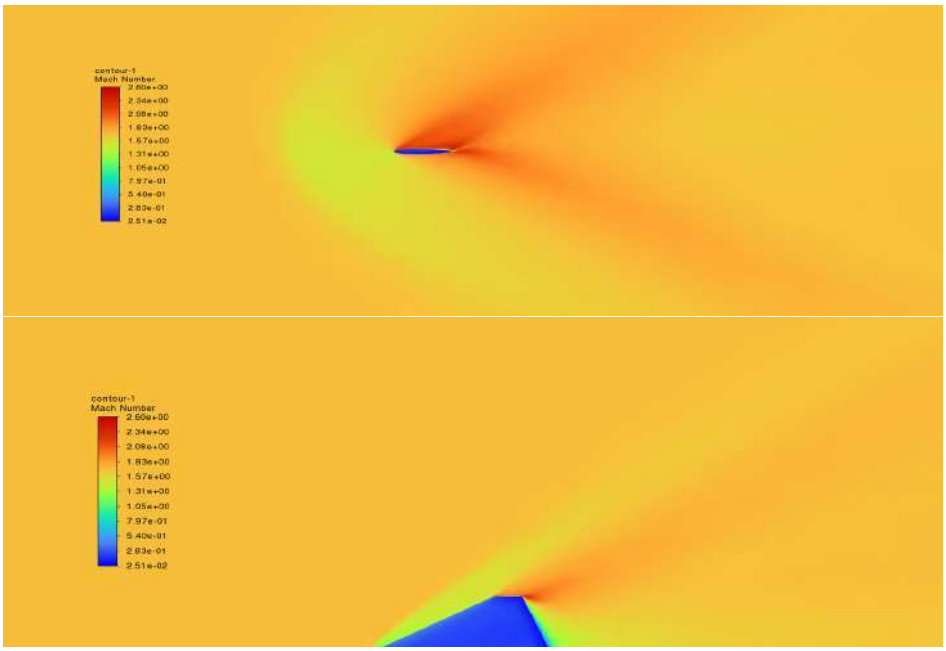


Figure 141 Mach Contour at 6° Angle of Attack

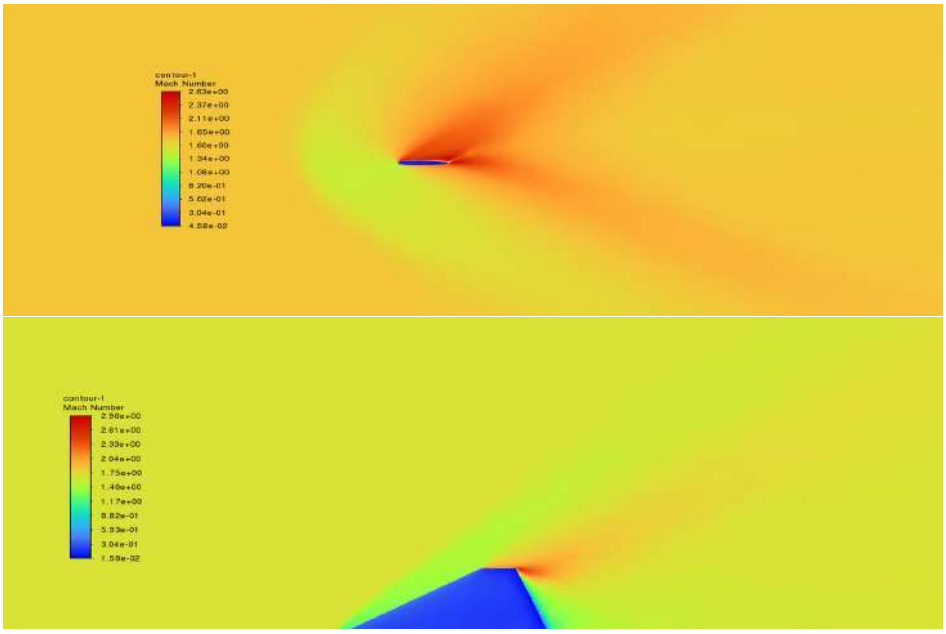


Figure 142 Mach Contour at 9° Angle of Attack

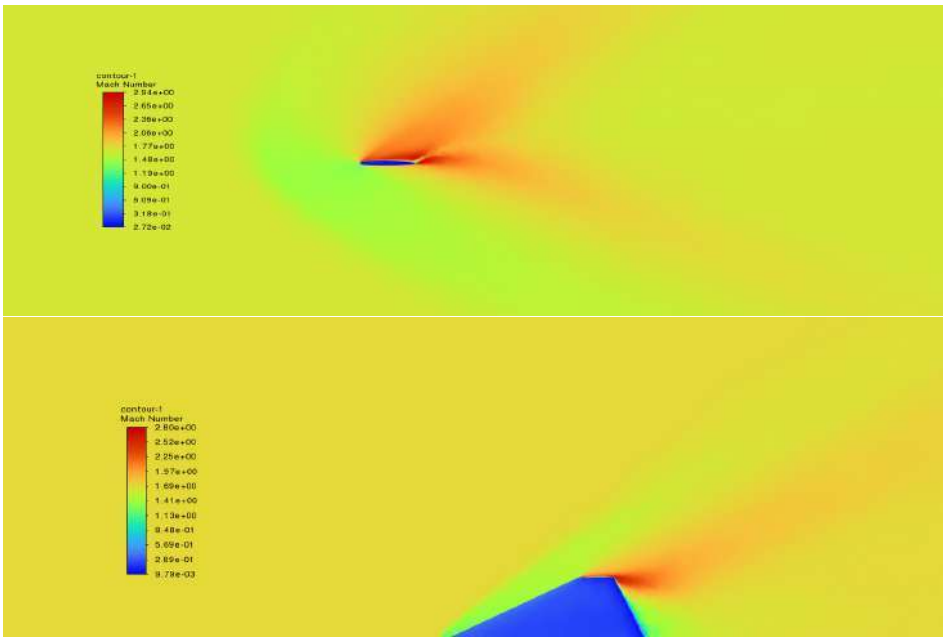


Figure 143 Mach Contour at 12° Angle of Attack

b) NACA-2411

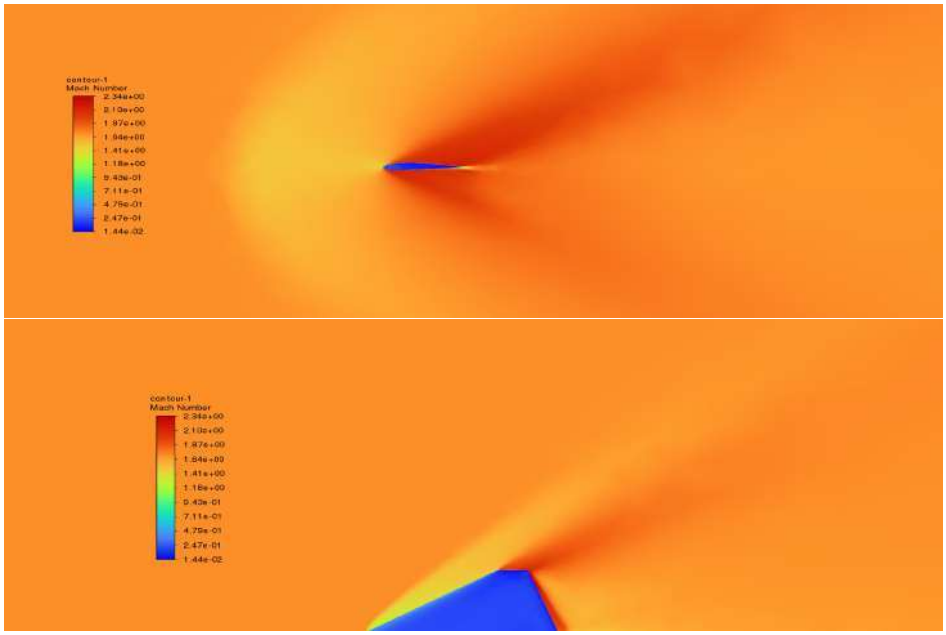


Figure 144 Mach Contour at 0 Angle of Attack

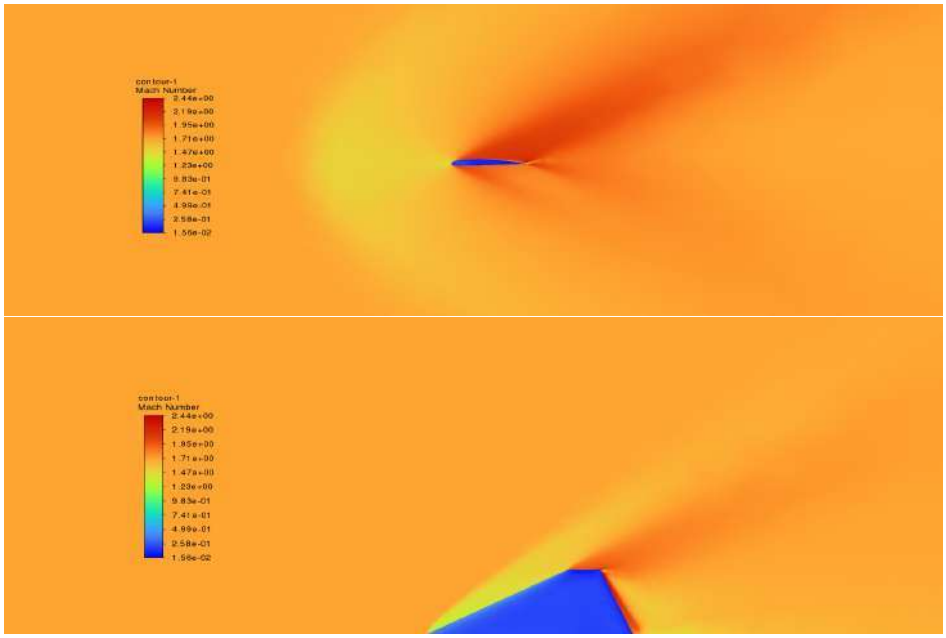


Figure 145 Mach Contour at 3° Angle of Attack

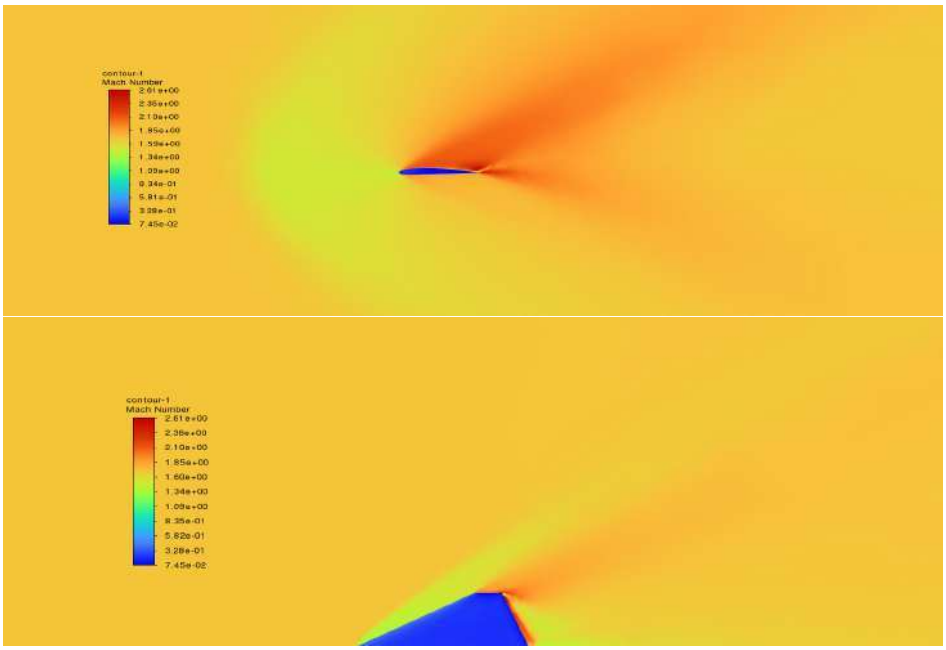


Figure 146 Mach Contour at 6° Angle of Attack

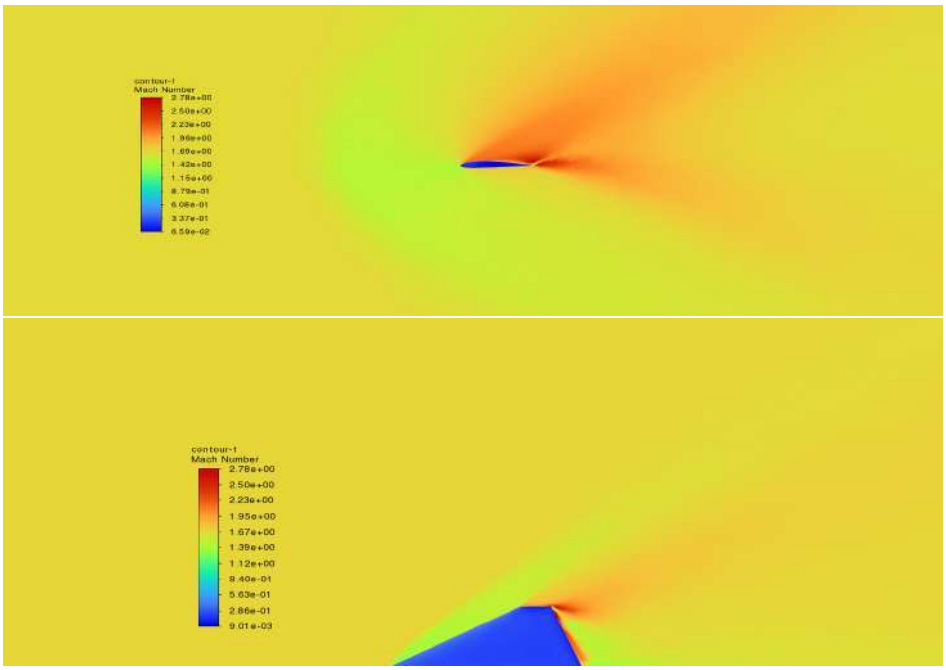


Figure 147 Mach Contour at 9° Angle of Attack

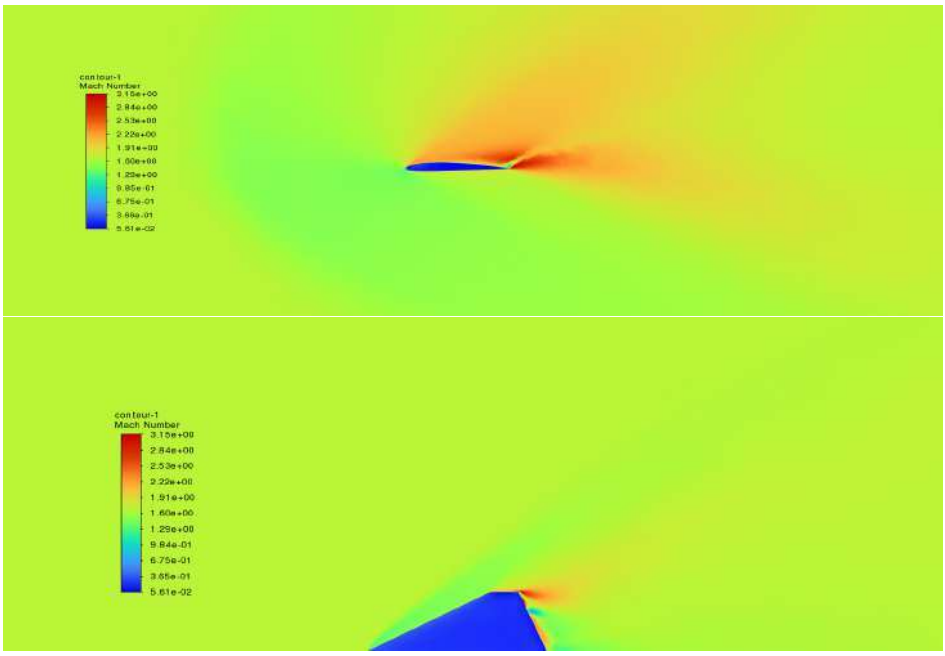


Figure 148 Mach Contour at 12° Angle of Attack

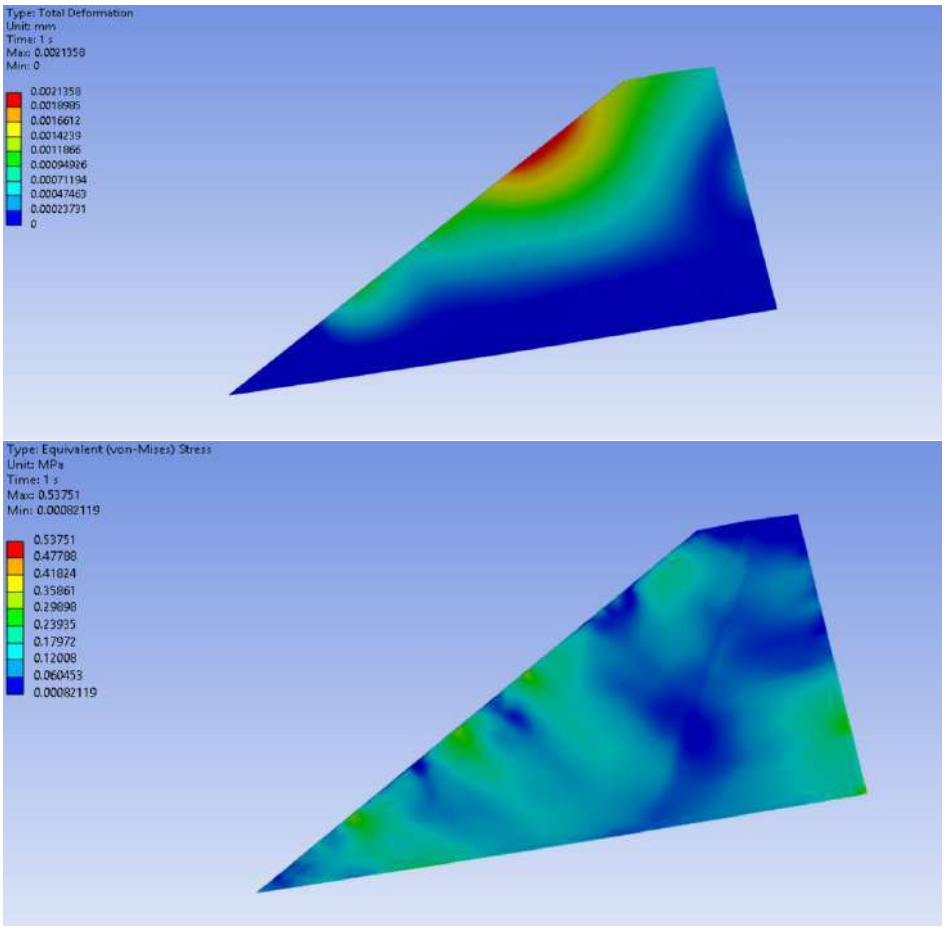


Figure 149 Total Deformation and Stress Contour at 0 Angle of Attack (MaxQ)

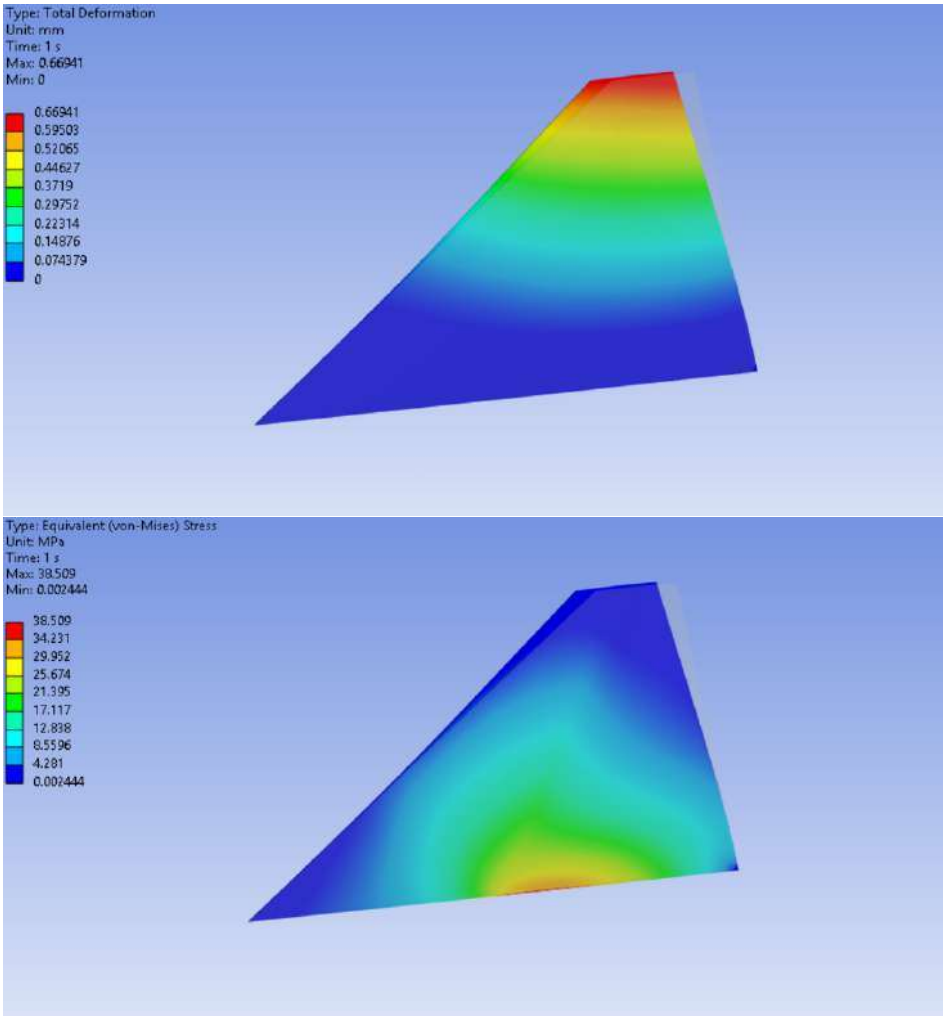


Figure 150 Total Deformation and Stress Contour at 3° Angle of Attack (MaxQ)

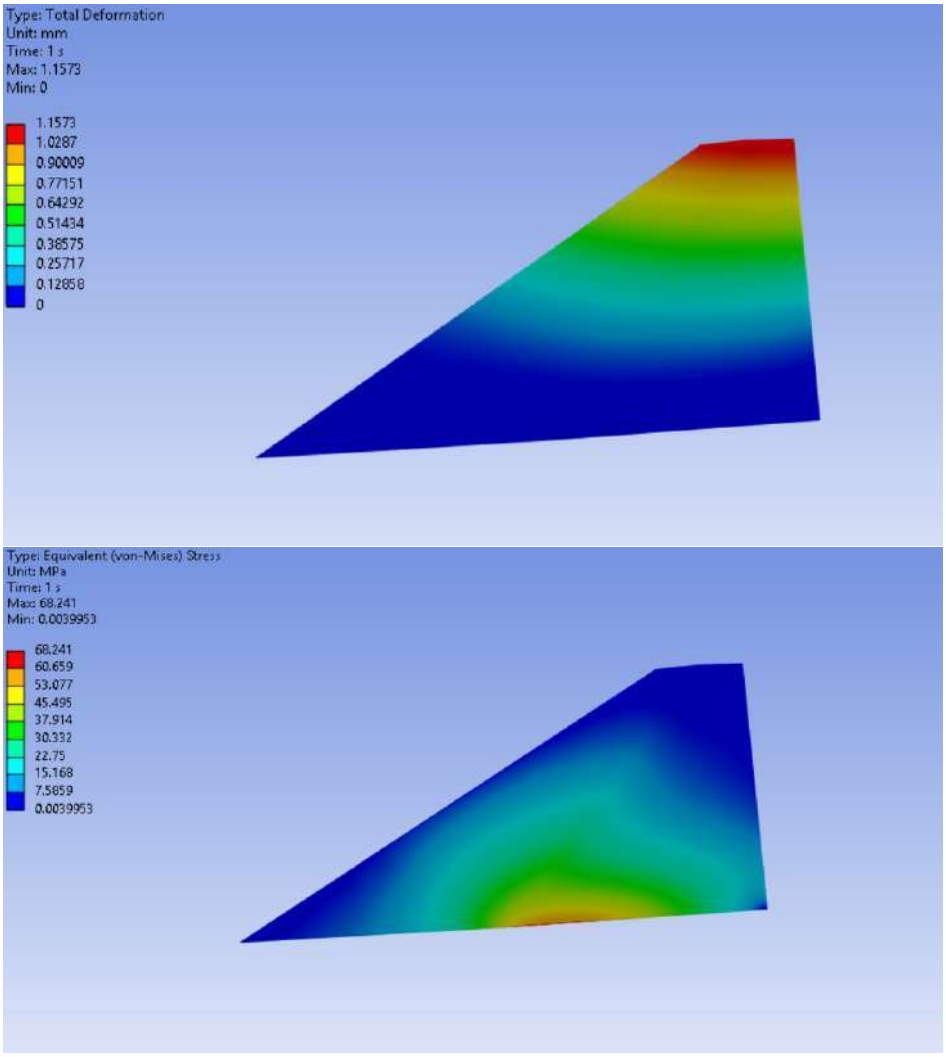


Figure 151 Total Deformation and Stress Contour at 6° Angle of Attack (MaxQ)

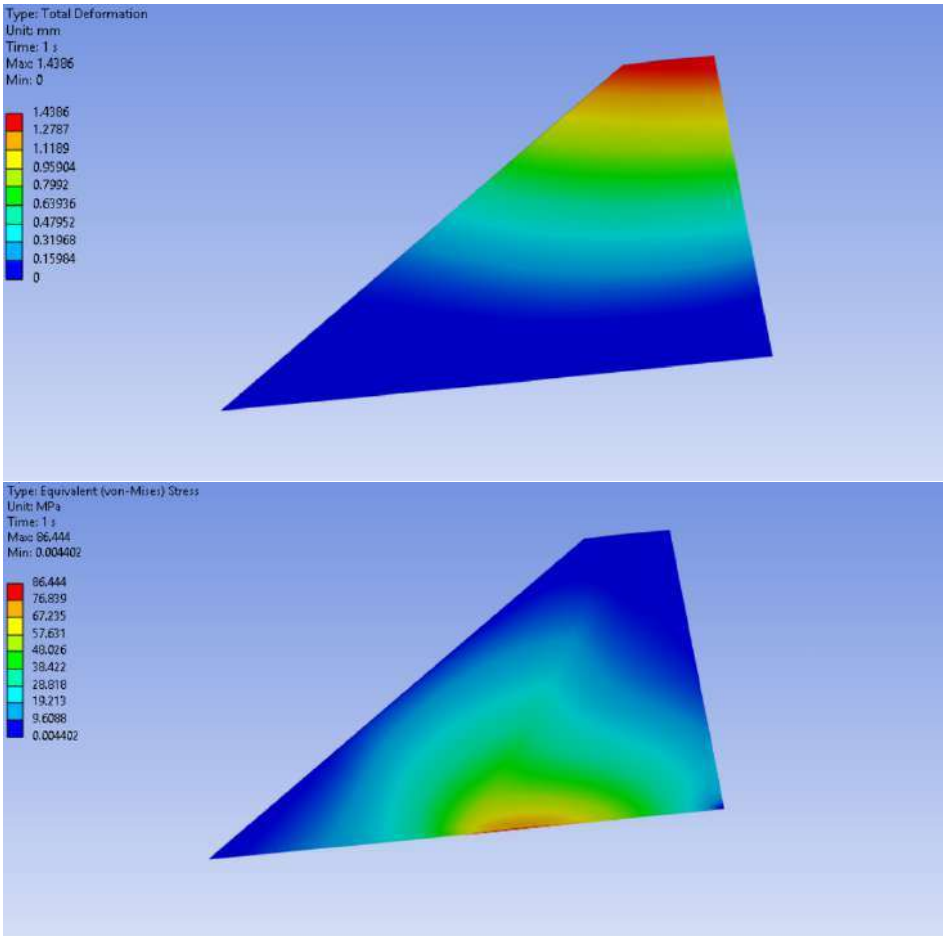


Figure 152 Total Deformation and Stress Contour at 9° Angle of Attack (MaxQ)

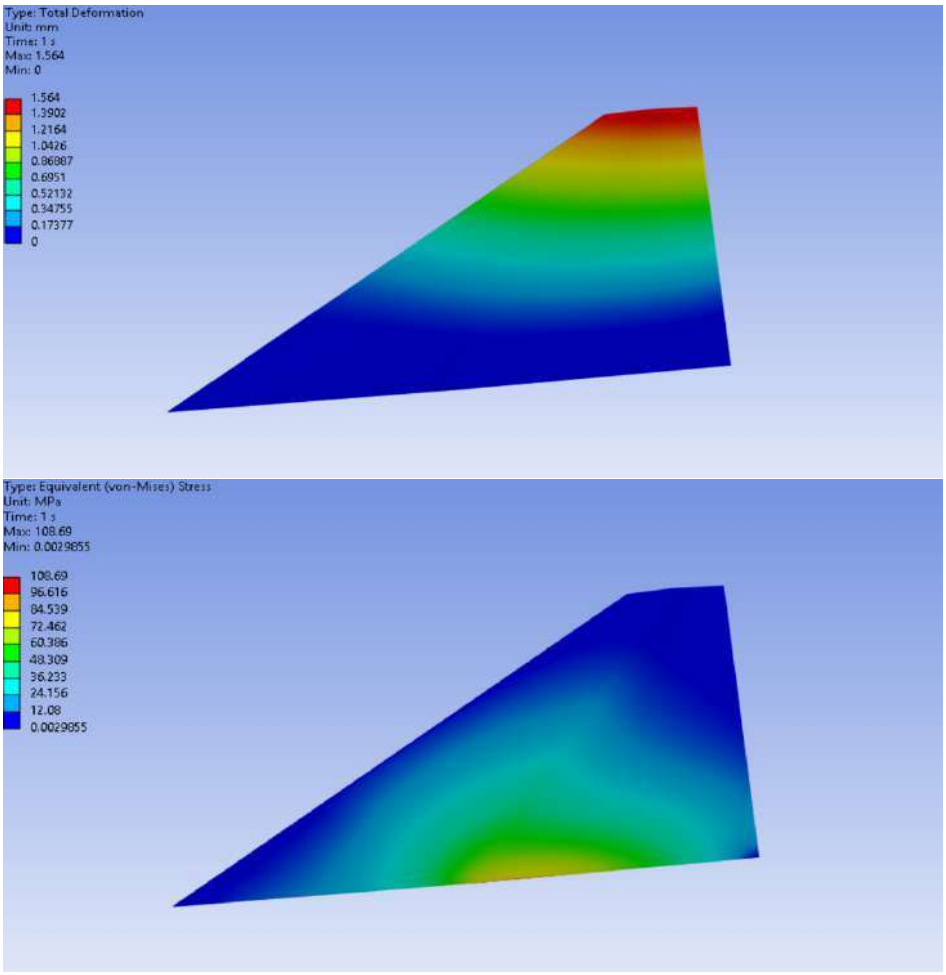


Figure 153 Total Deformation and Stress Contour at 12° Angle of Attack (MaxQ)

Bi-Convex Cross-Section

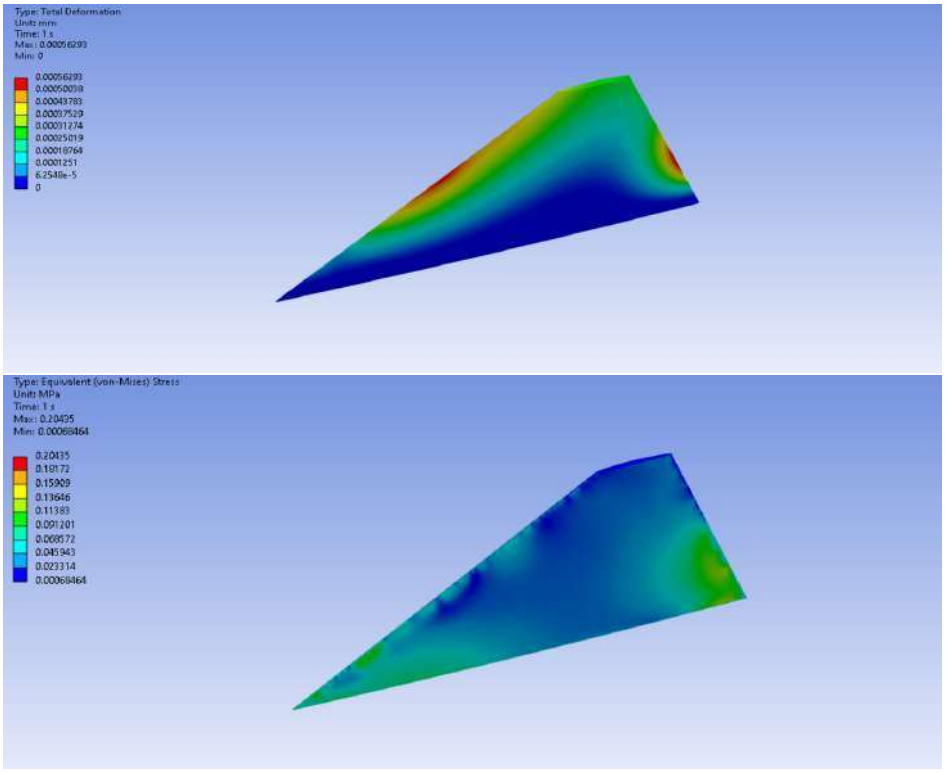


Figure 154 Total Deformation and Stress Contour at 0 Angle of Attack (MaxQ)

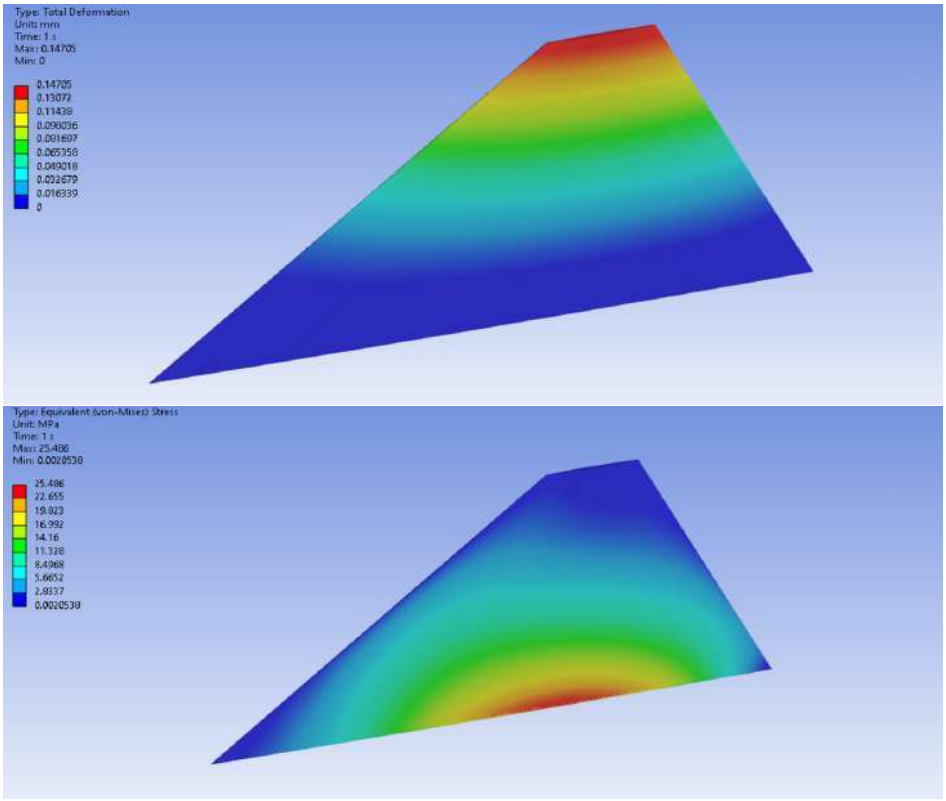


Figure 155 Total Deformation and Stress Contour at 3° Angle of Attack (MaxQ)

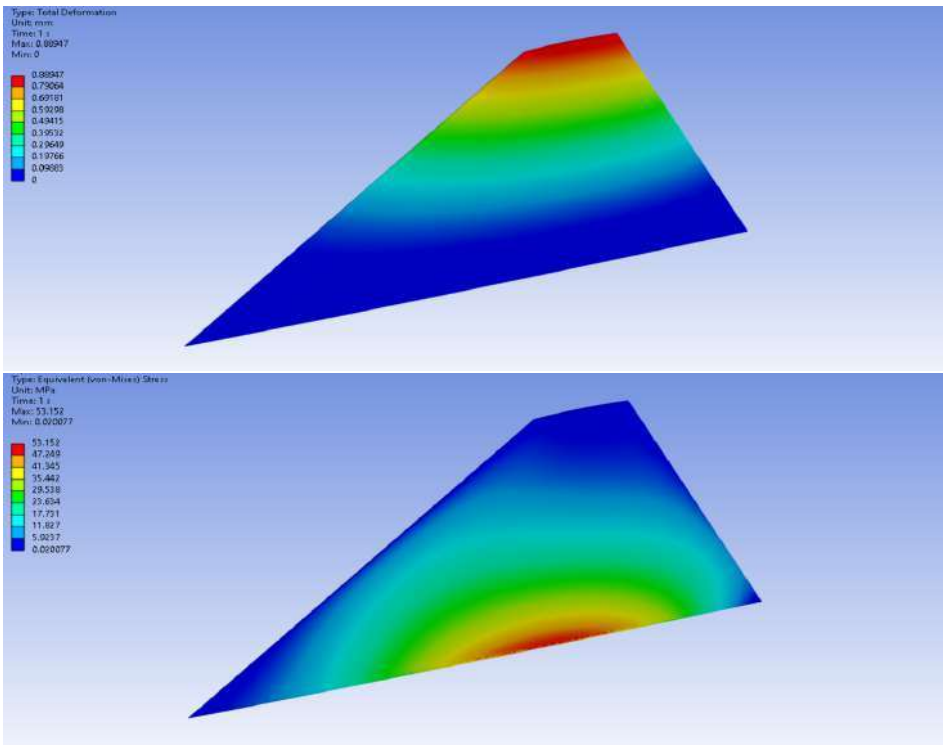


Figure 156 Total Deformation and Stress Contour at 6° Angle of Attack (MaxQ)

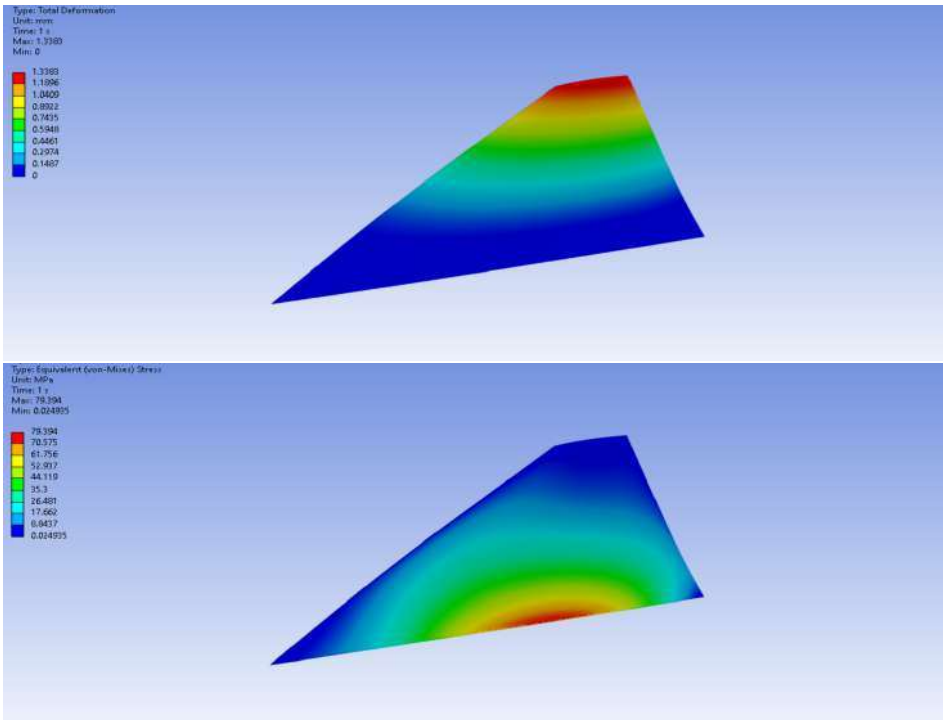


Figure 157 Total Deformation and Stress Contour at 9° Angle of Attack (MaxQ)

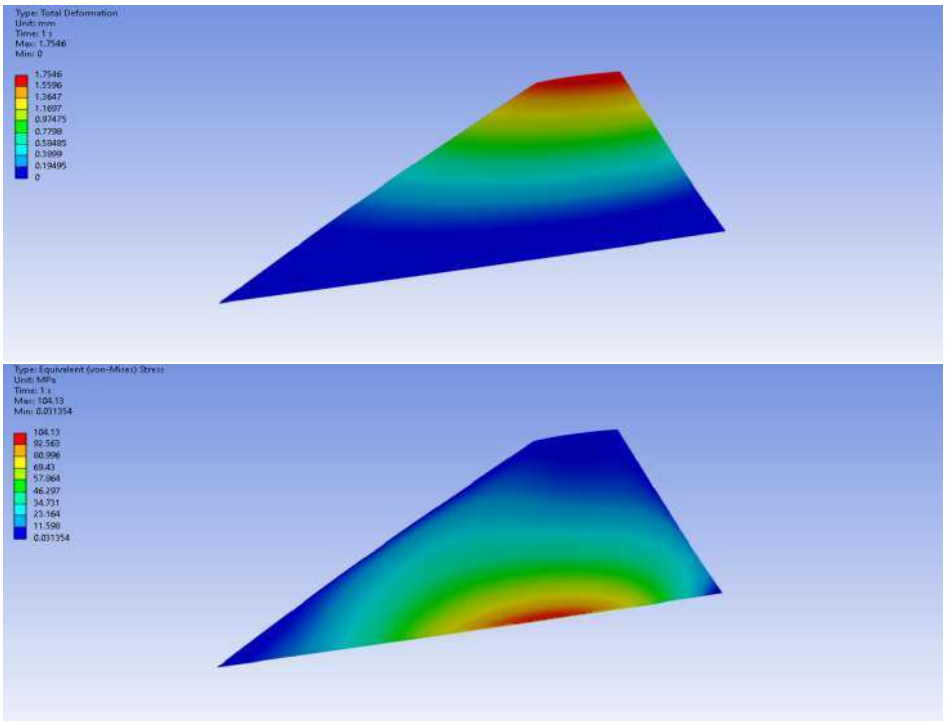


Figure 158 Total Deformation and Stress Contour at 12° Angle of Attack (MaxQ)

Hexagonal Cross-Section with 5° Half Wedge Angle

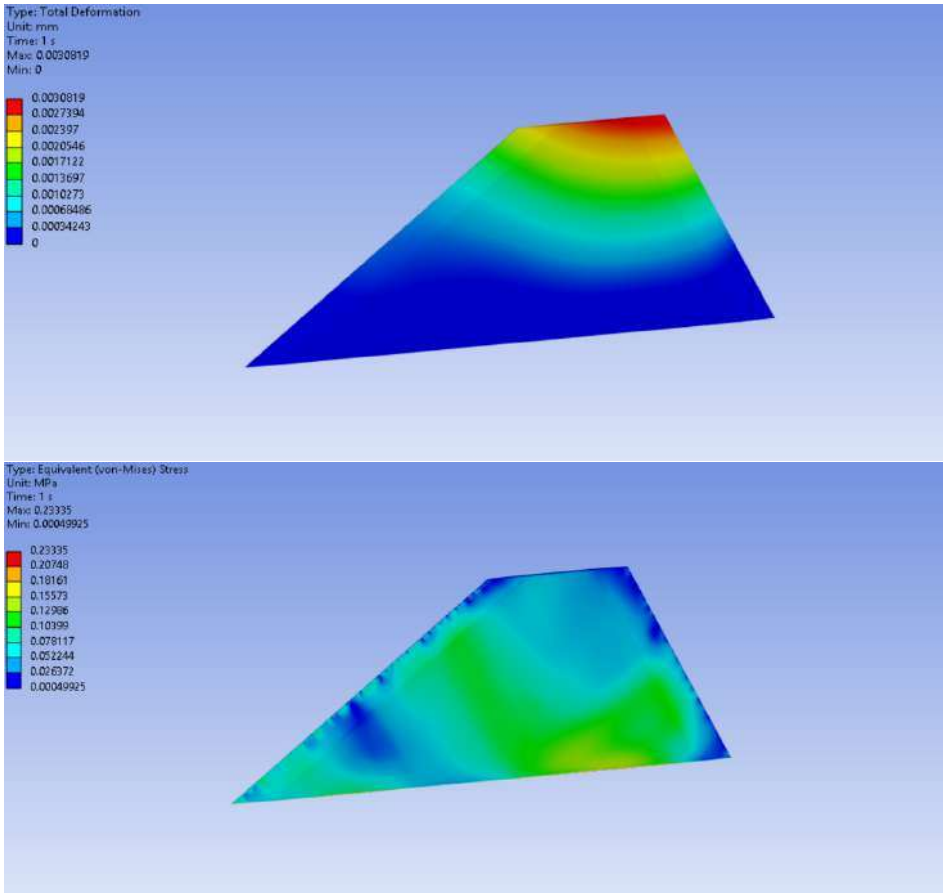


Figure 159 Total Deformation and Stress Contour at 0 Angle of Attack (MaxQ)

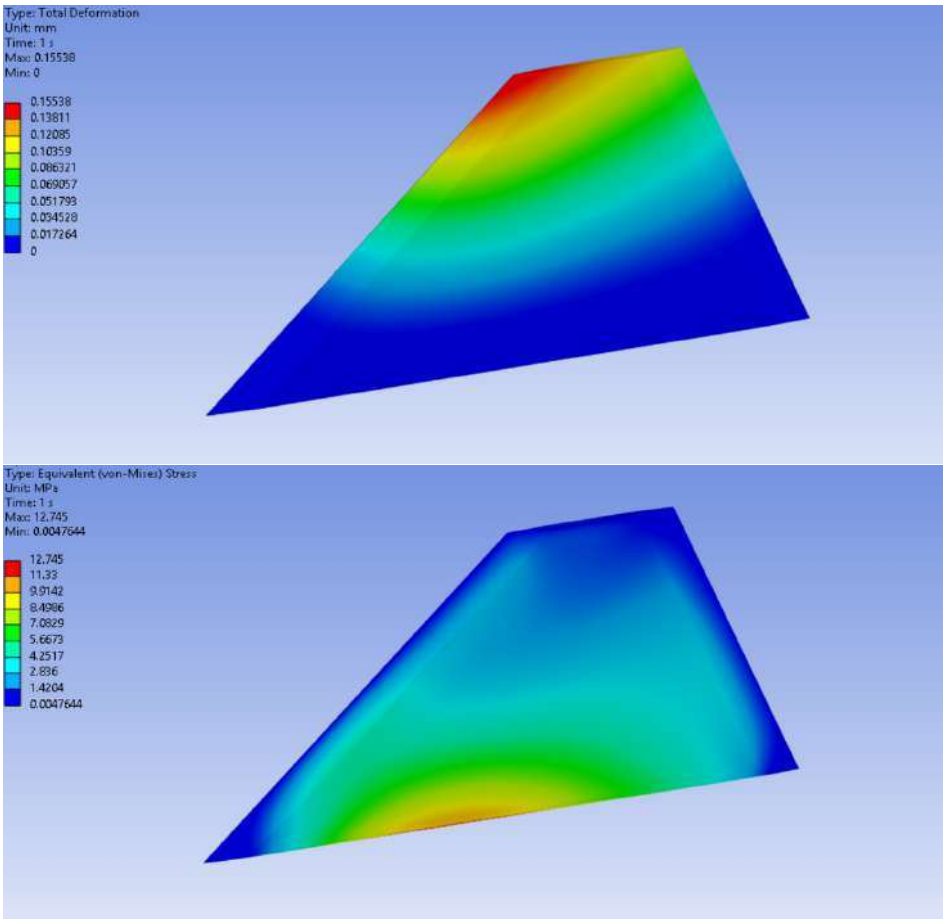


Figure 160 Total Deformation and Stress Contour at 3° Angle of Attack (MaxQ)

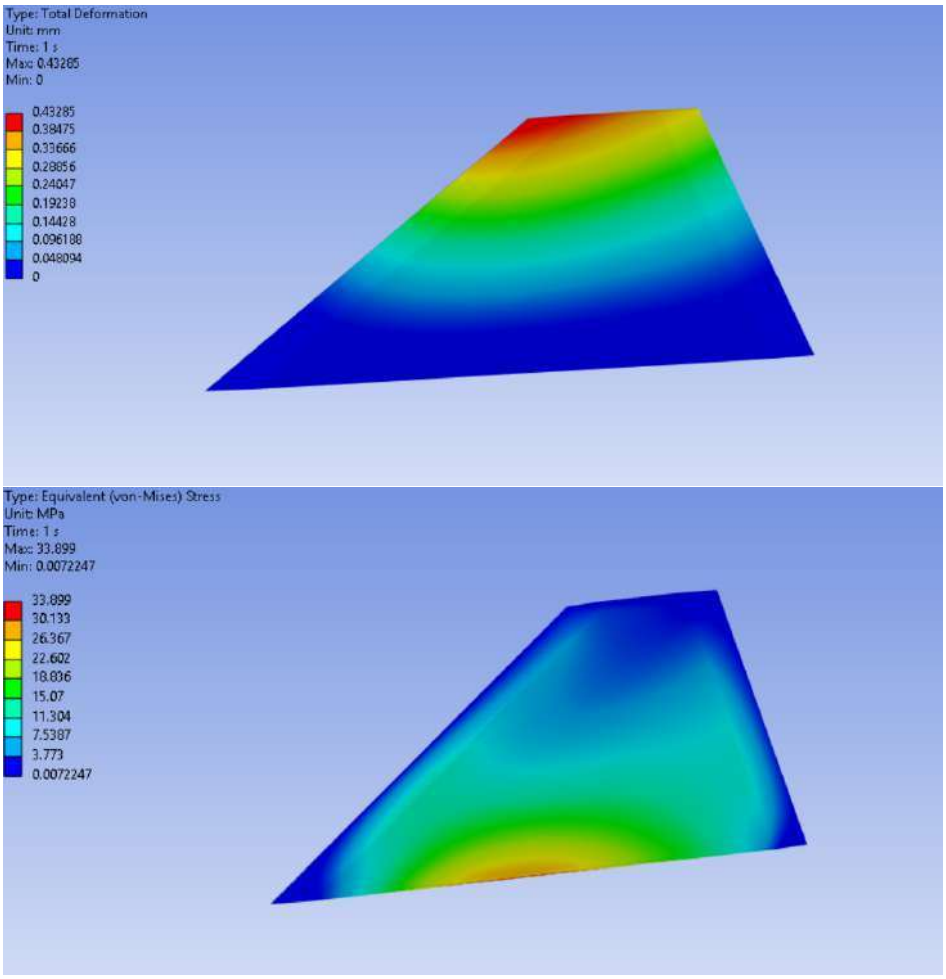


Figure 161 Total Deformation and Stress Contour at 6° Angle of Attack (MaxQ)

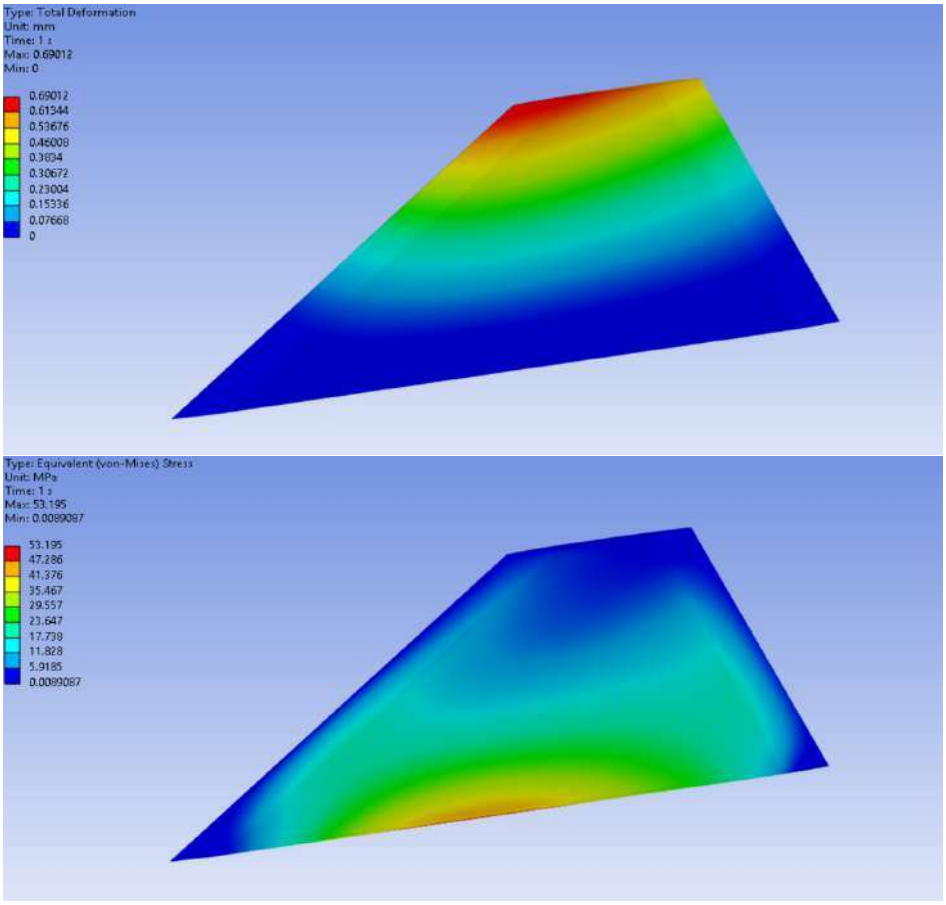


Figure 162 Total Deformation and Stress Contour at 9° Angle of Attack (MaxQ)

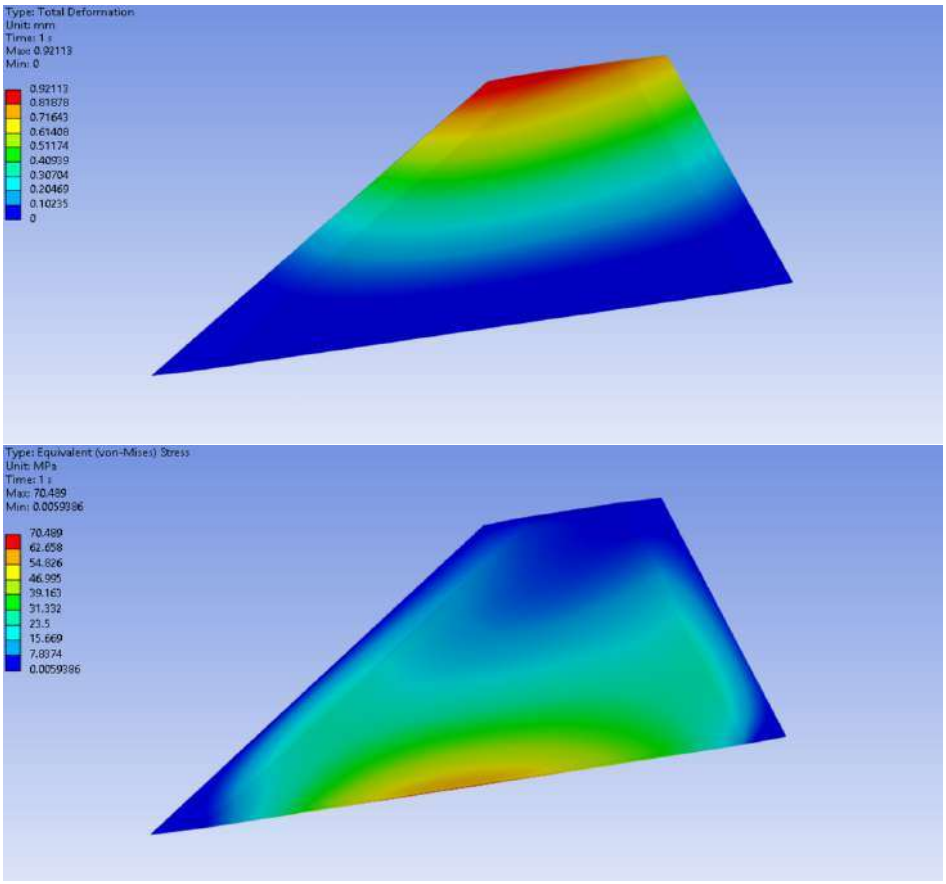


Figure 163 Total Deformation and Stress Contour at 12° Angle of Attack (MaxQ)

3. Modal Analysis
Double Wedge Cross-Section

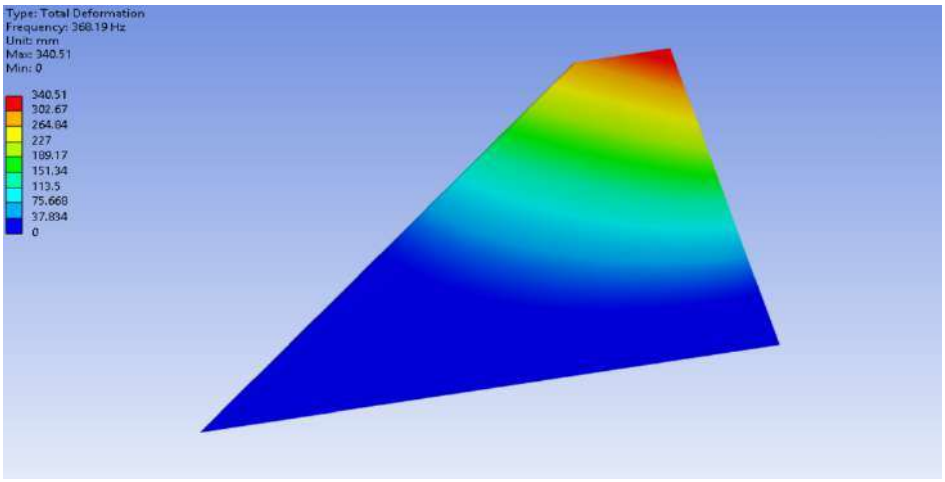


Figure 164 First Bending Mode

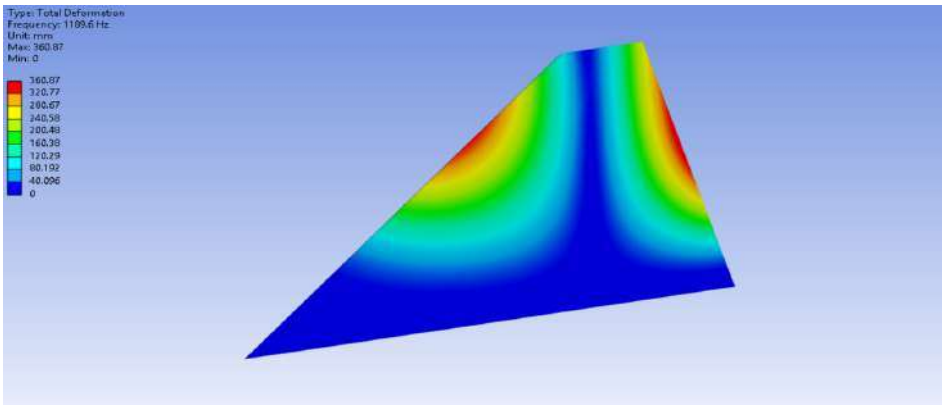


Figure 165 First Torsional Mode

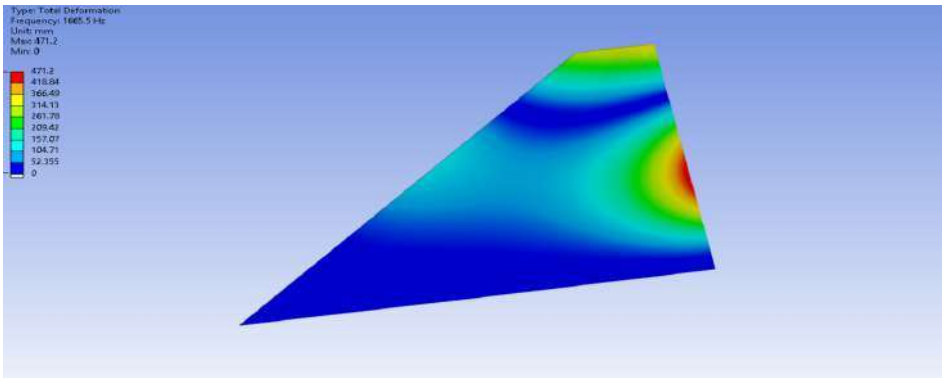


Figure 166 Second Torsional Mode

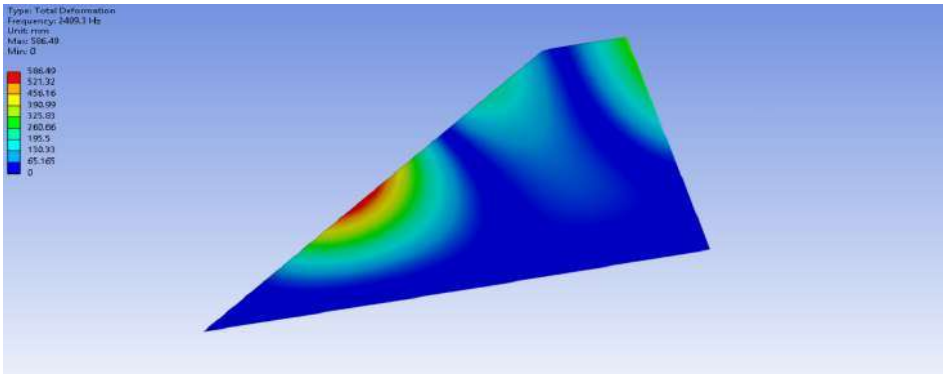


Figure 167 Torsion And Bending Mode

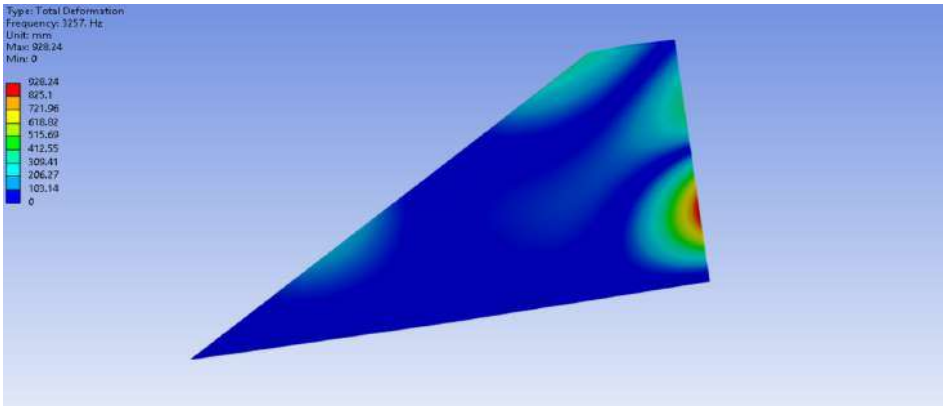


Figure 168 Two Point Bending

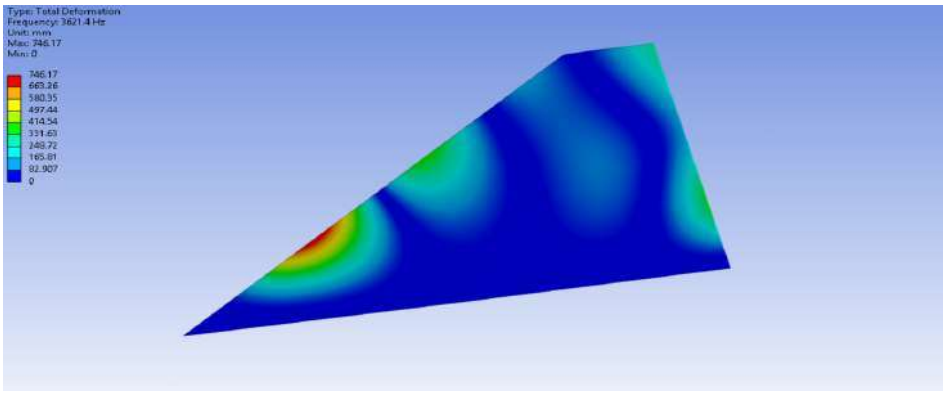


Figure 169 Third Torsional Mode

Bi-Convex Cross-Section

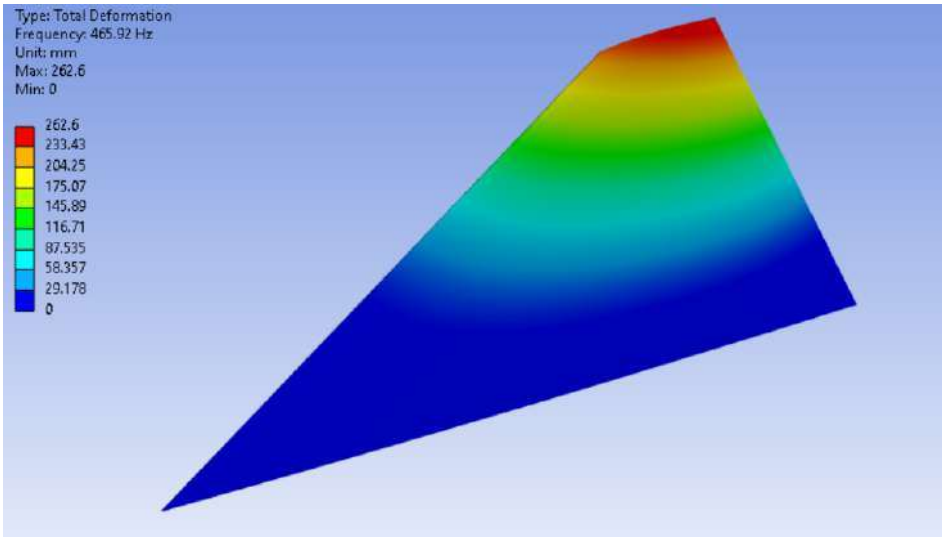


Figure 170 First Bending Mode

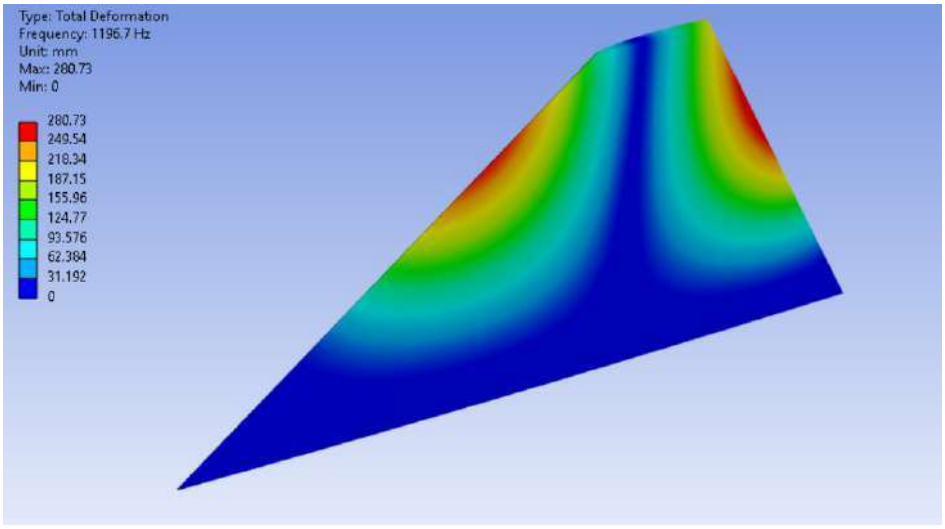


Figure 171 First Torsional Mode

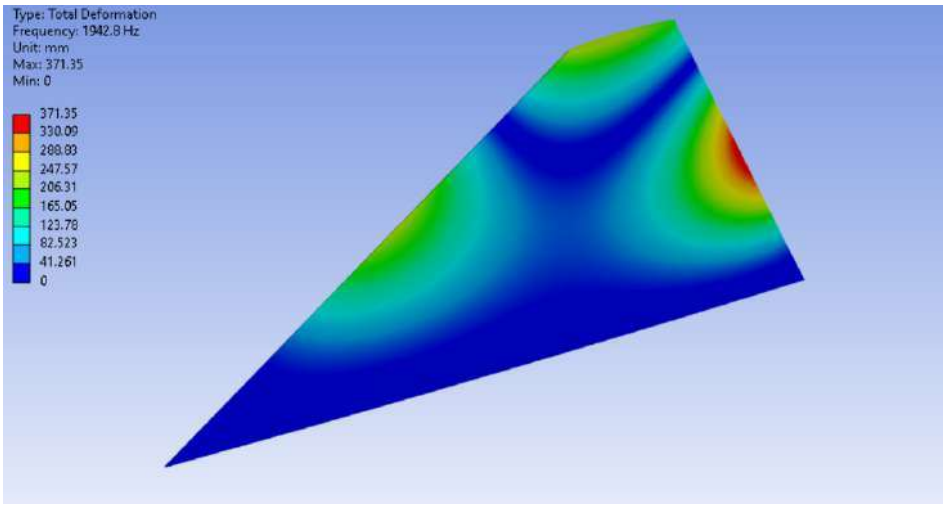


Figure 172 Second Torsional Mode

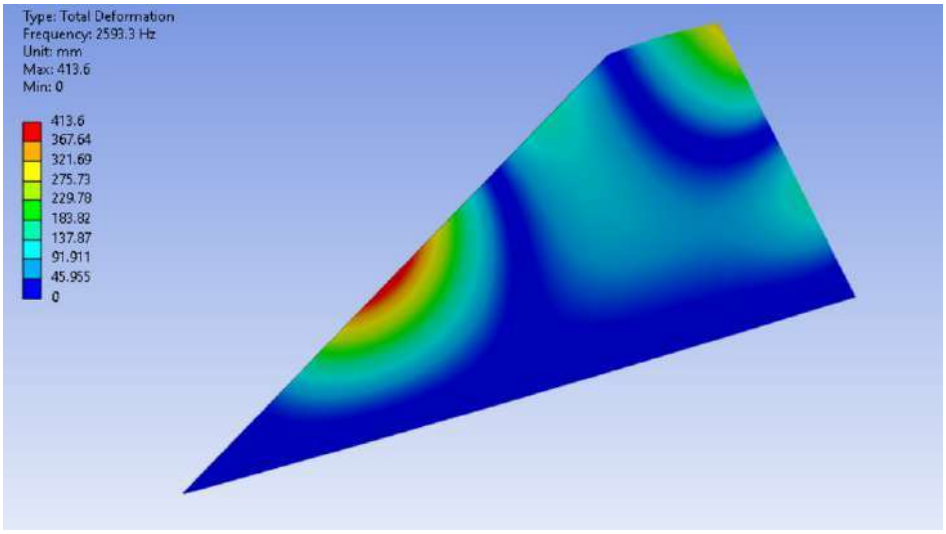


Figure 173 Torsion And Bending Mode

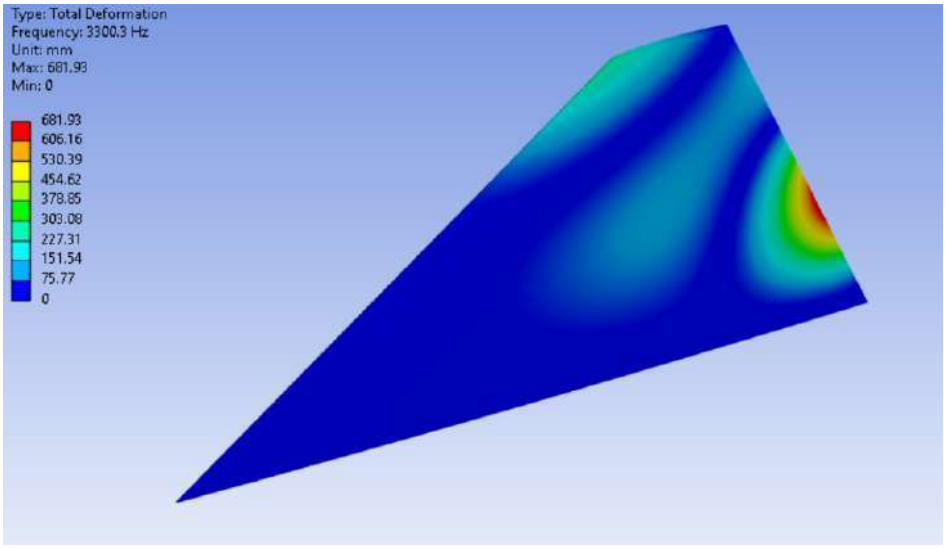


Figure 174 Two Point Bending

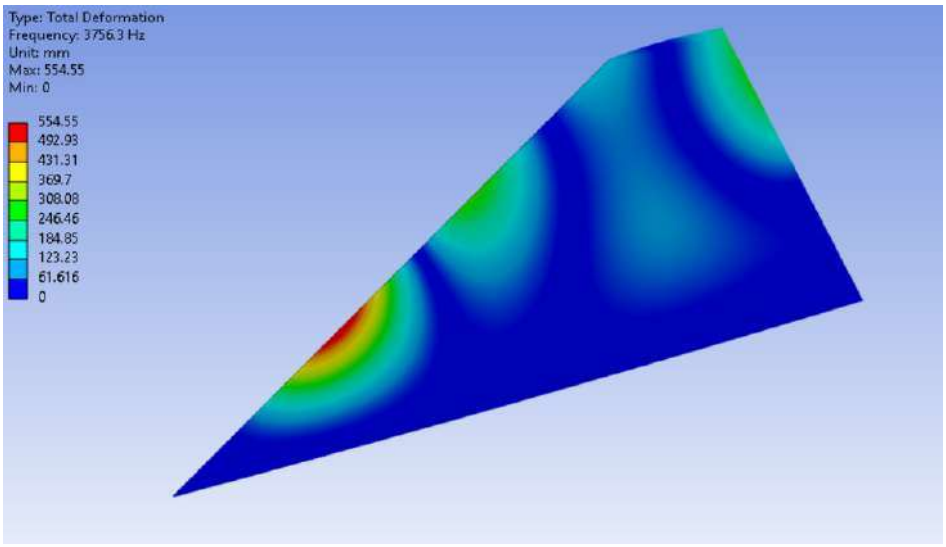


Figure 175 Third Torsional Mode

Hexagonal Cross-Section with 5° Half Wedge Angle

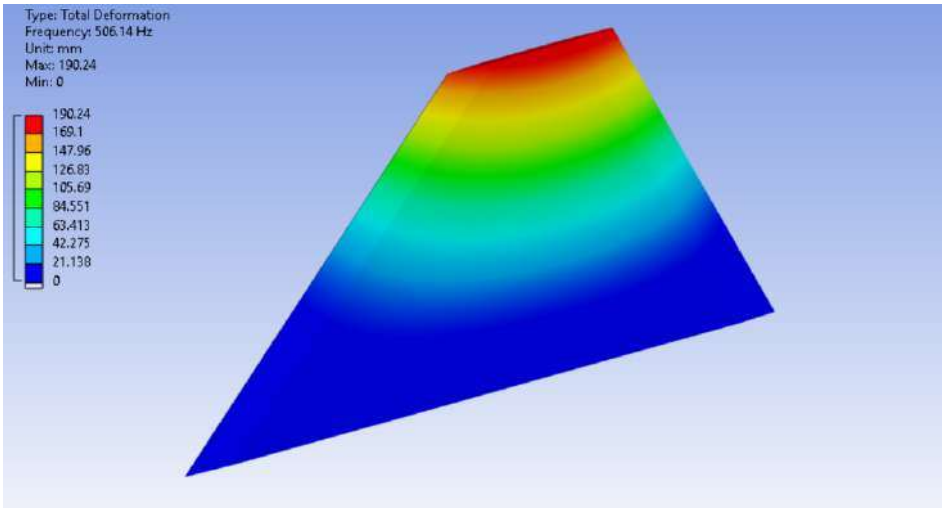


Figure 176 First Bending Mode

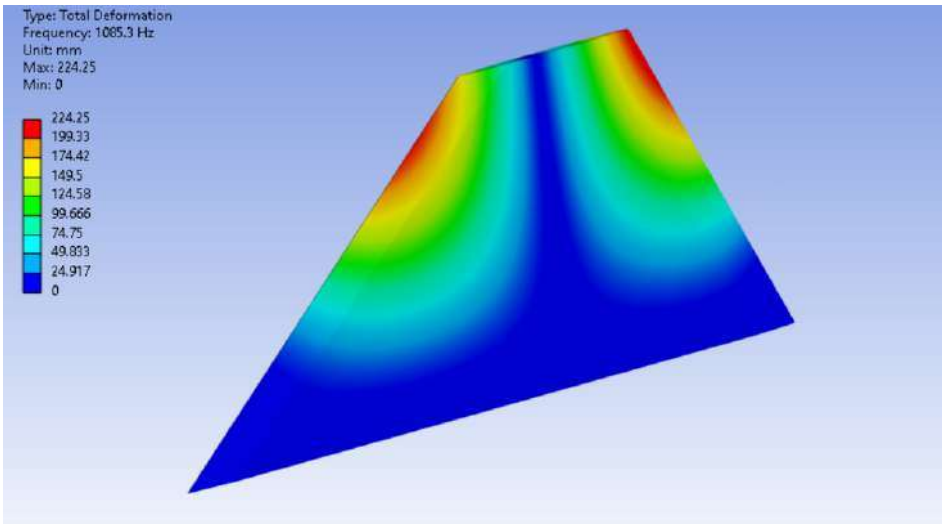


Figure 177 First Torsional Mode

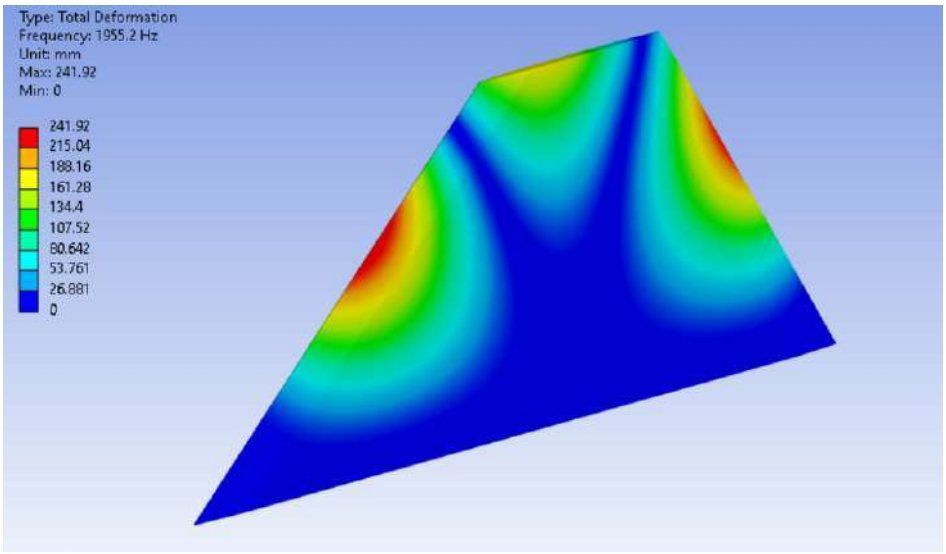


Figure 178 Torsion And Bending Mode

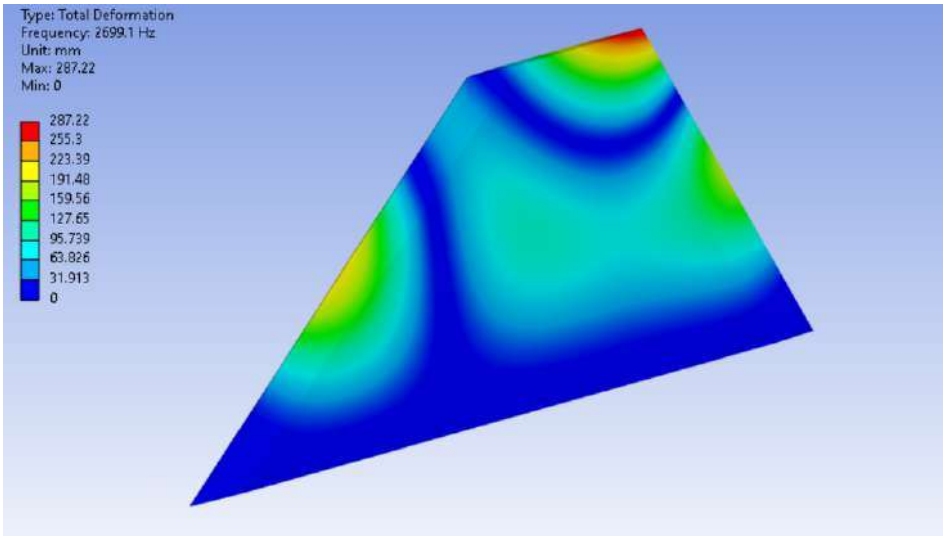


Figure 179 Two Point Bending

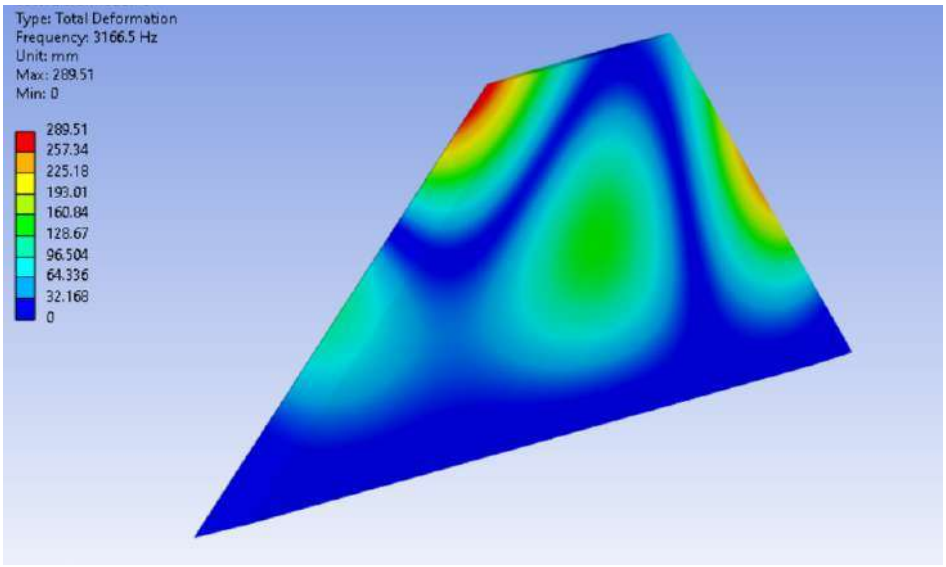


Figure 180 Second Torsional Mode

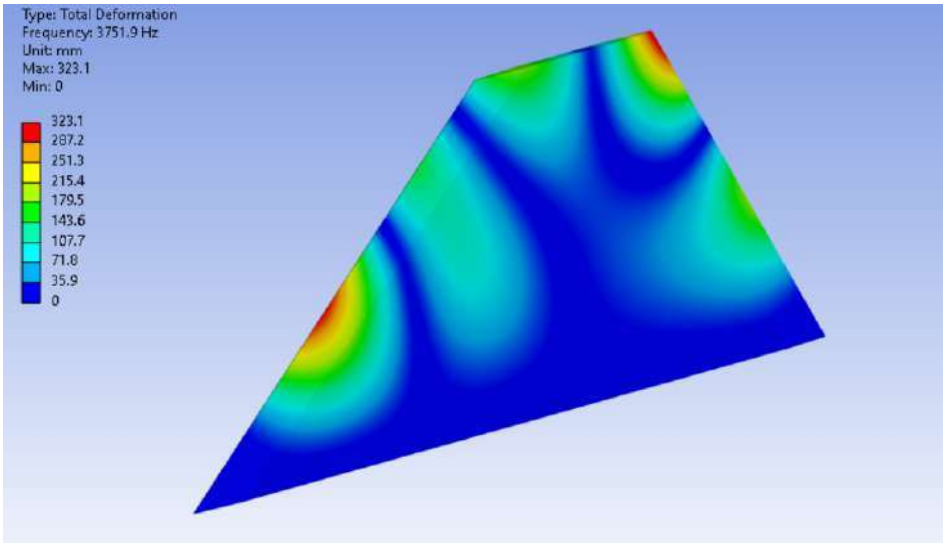


Figure 181 Third Torsional Mode

C. Boattail

1. Computational Fluid Dynamics

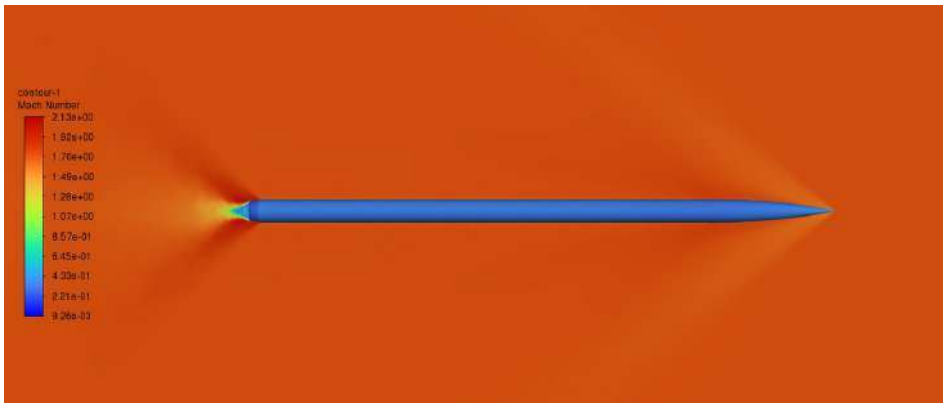


Figure 182 Mach contour for 60mm Boattail

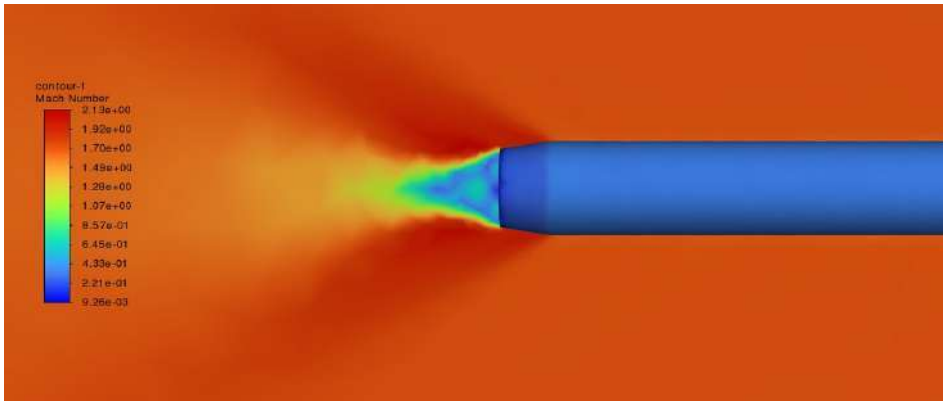


Figure 183 Expansion Fan for 60mm Boattail

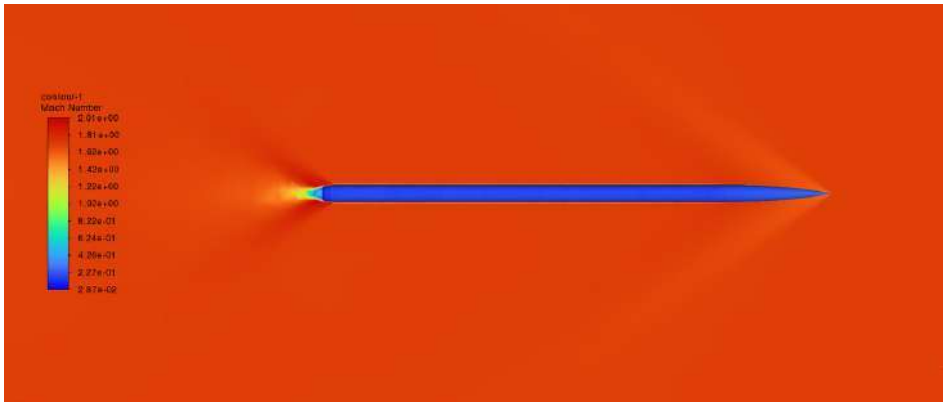


Figure 184 Mach contour for 70mm Boattail

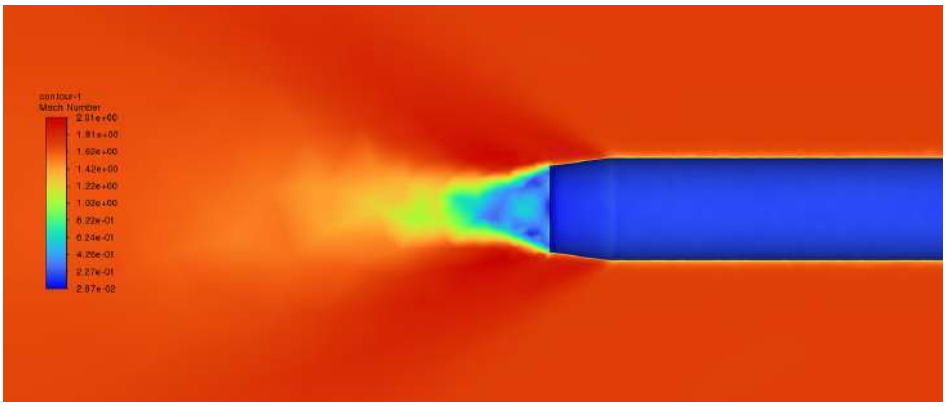


Figure 185 Expansion Fan for 70mm Boattail

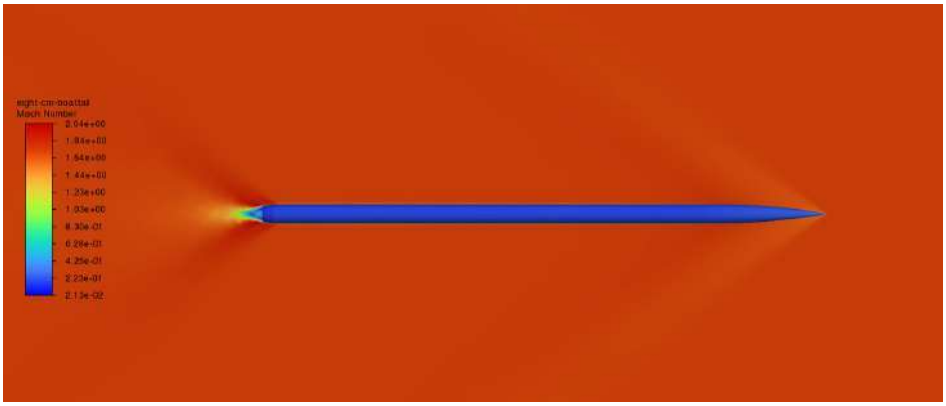


Figure 186 Mach contour for 80mm Boattail

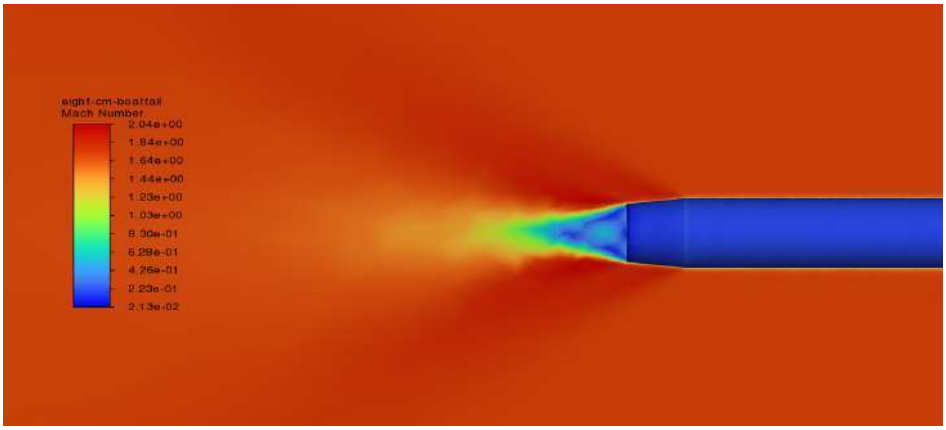


Figure 187 Expansion Fan for 80mm Boattail

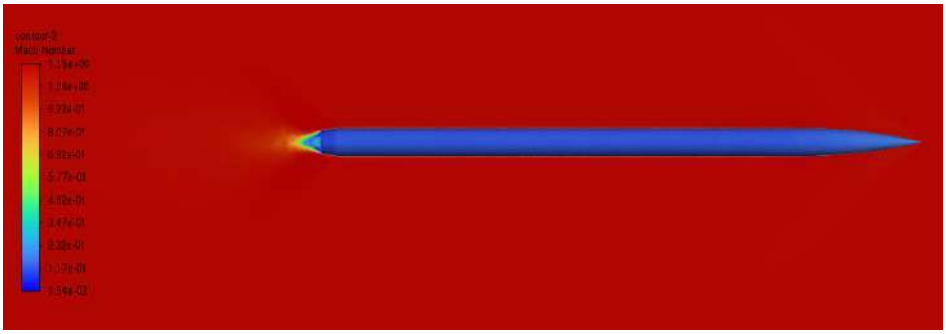


Figure 188 Mach contour for 90mm Boattail

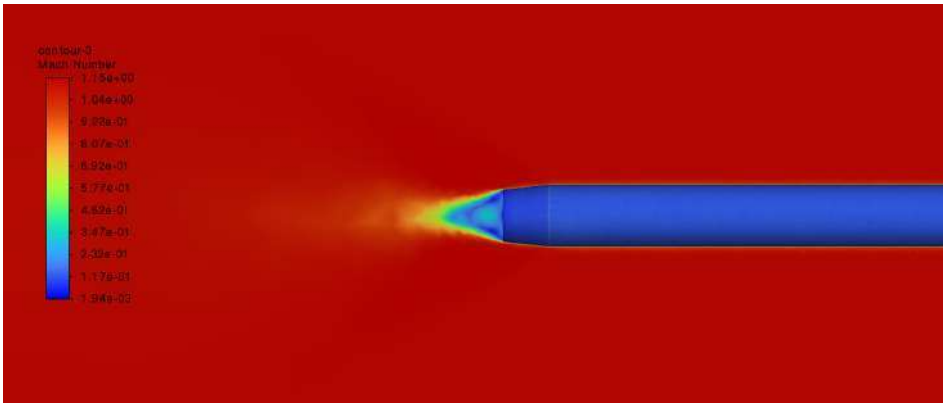


Figure 189 Expansion Fan for 90mm Boattail

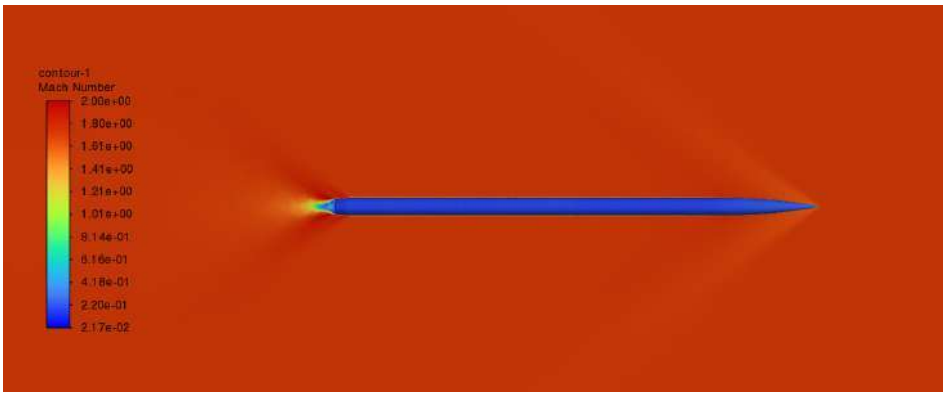


Figure 190 Mach contour for 100mm Boattail

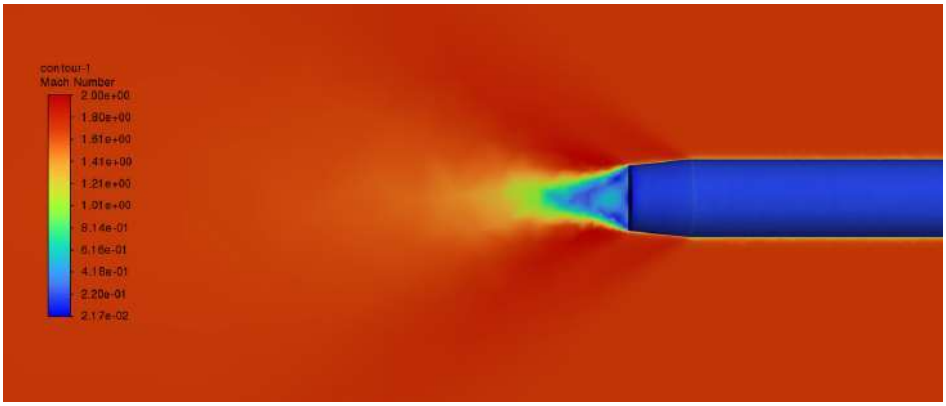


Figure 191 Expansion Fan for 100mm Boattail

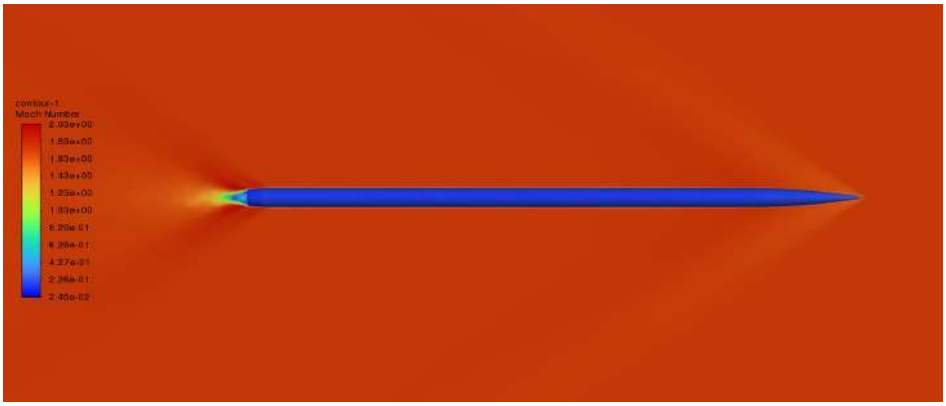


Figure 192 Mach contour for 110mm Boattail

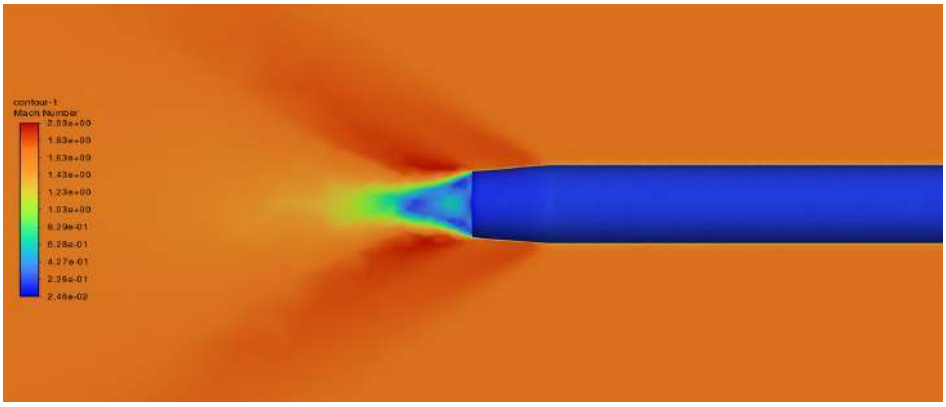


Figure 193 Expansion Fan for 110mm Boattail

D. Payload

1. CanSat Vibrational Analysis

The CanSat was set up and solved for the first three significant modes in which the parts would vibrate in Modal Analysis.

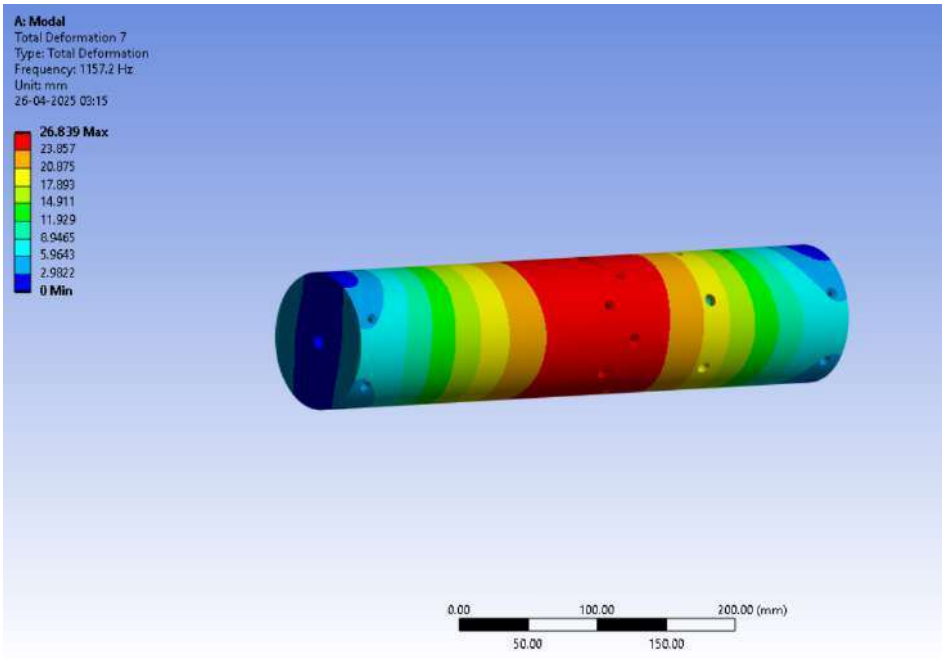


Figure 194 CanSat: First Mode

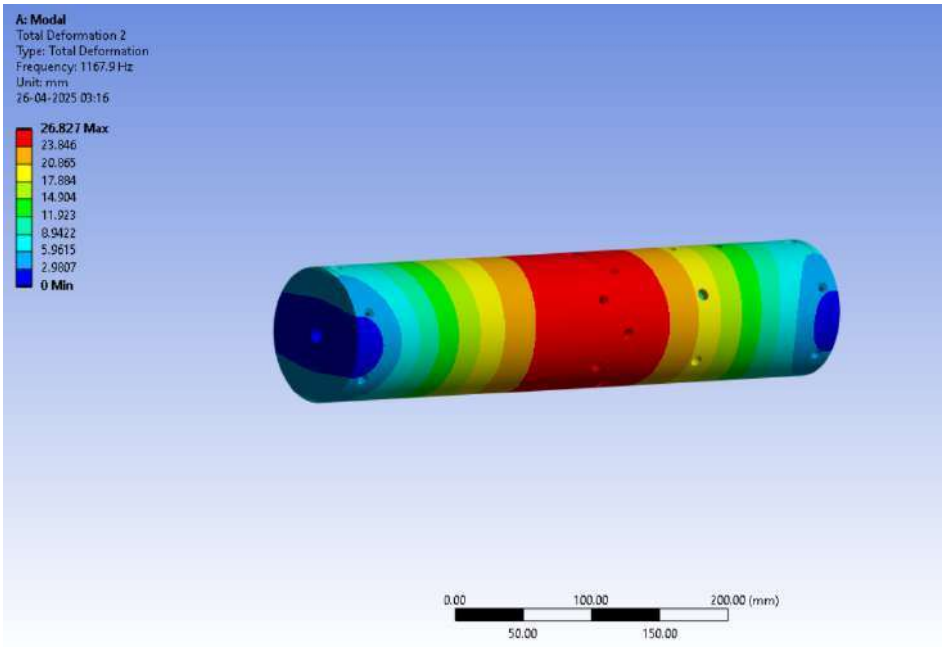


Figure 195 CanSat: Second Mode

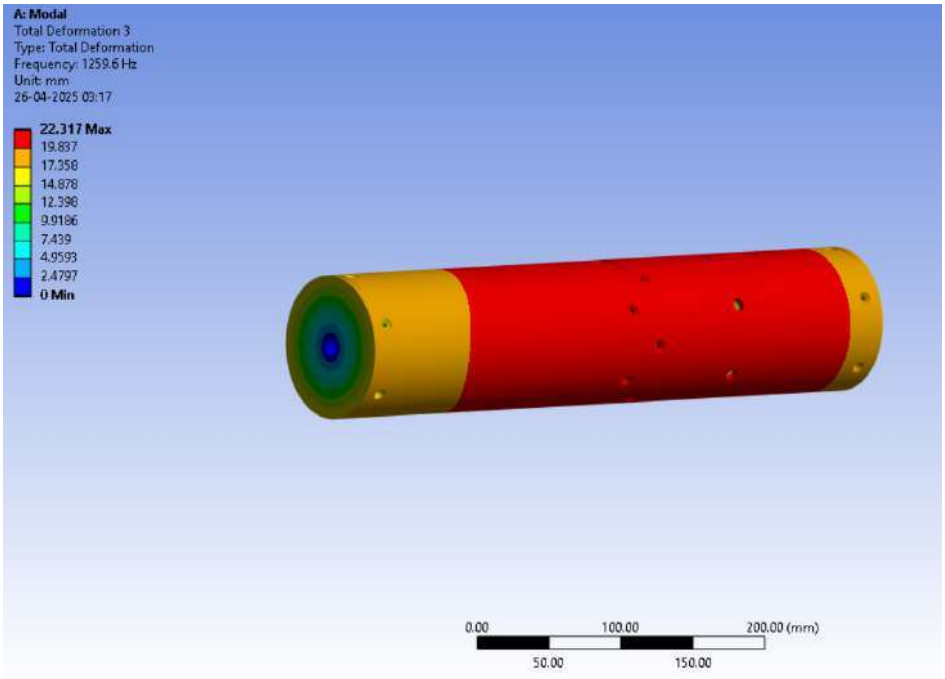


Figure 196 CanSat: Third Mode

The modal frequencies are 1150 Hz, 1250 Hz, and 1434 Hz, showing lateral flex, longitudinal flex, and torsional flex, respectively. These frequencies are in the quiet zone of the spectrum from excitation peaks, explained later.
For a random vibration analysis, a PSD input for acceleration is necessary. The time domain acceleration from the 6-DOF simulator code was taken as a reference, as this is the closest estimation of flight data.

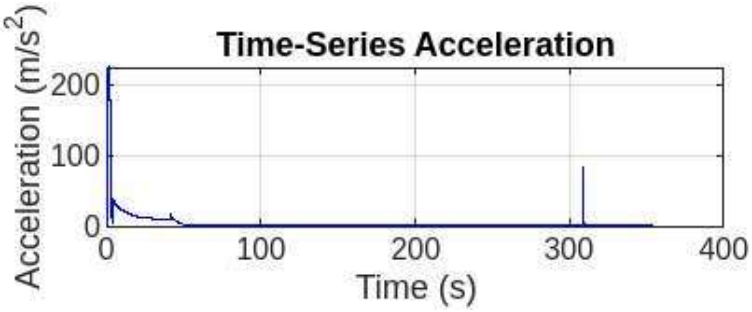


Figure 197 Time Series Acceleration

The time series acceleration cannot be the direct input in random vibrations; these values had to be converted to the PSD acceleration profile. This conversion required the use of Welch's method. The first part of Welch's method is converting the time domain to the frequency domain using the Fast Fourier Transform (FFT). The Welch method divides this signal into segments, performing a Discrete Fourier Transform (DFT) using FFT essentially, and averages out to estimate the PSD. MATLAB was used to create these conversions and obtain the PSD acceleration profile input. The profile shows energy concentrated at lower frequencies, typical of flight-related accelerations.

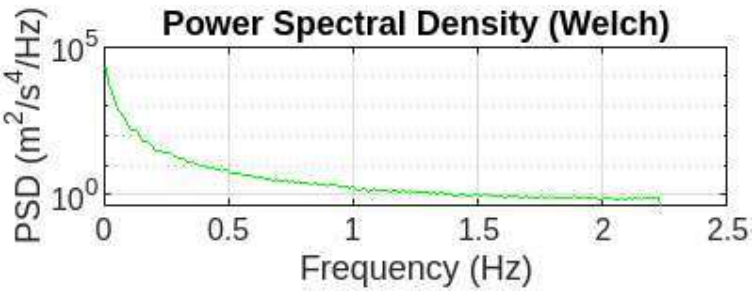


Figure 198 Power Spectral Density Acceleration Profile

A statistical approach must be chosen because random vibrations follow a Gaussian distribution. A 3-sigma scale factor will give a highly conservative value to determine the integrity of the CanSat. The 3-sigma factor is a highly conservative approach, showing the possibility of an event happening at a 0.3% chance.

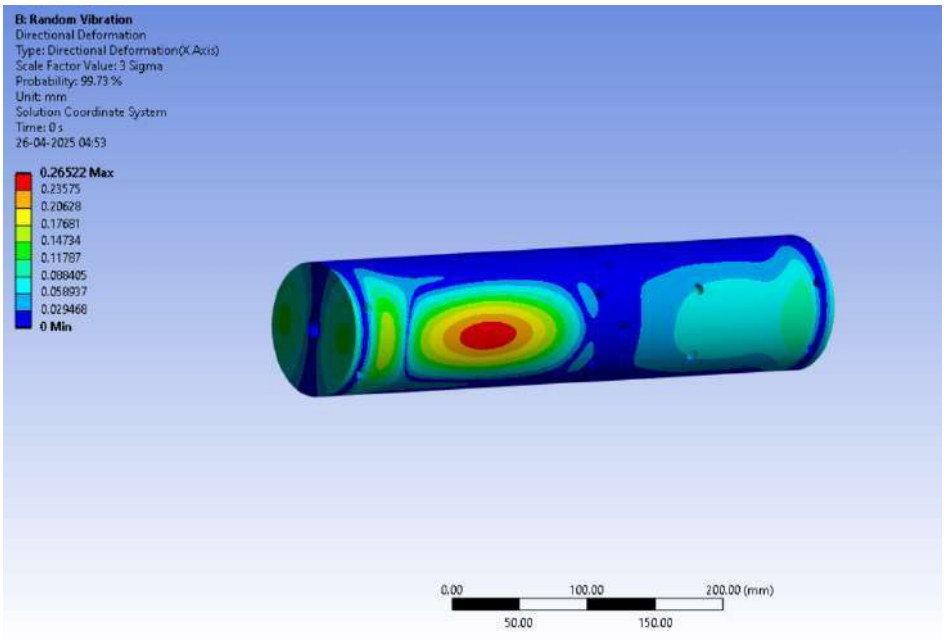


Figure 199 Directional Deformation in X-Axis with Flight Simulated Data

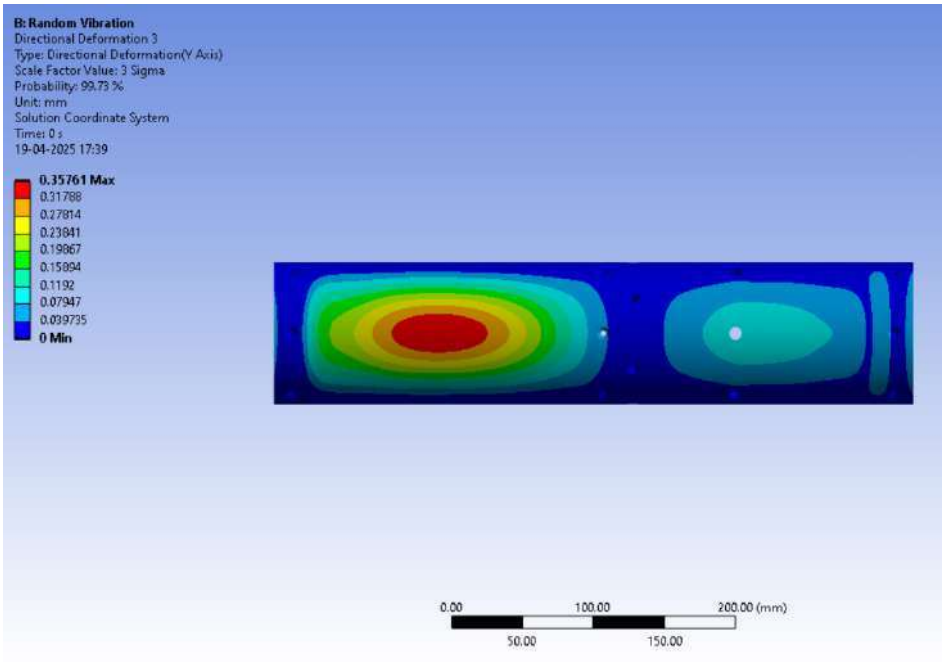


Figure 200 Directional Deformation in Y-Axis with Flight Simulated Data

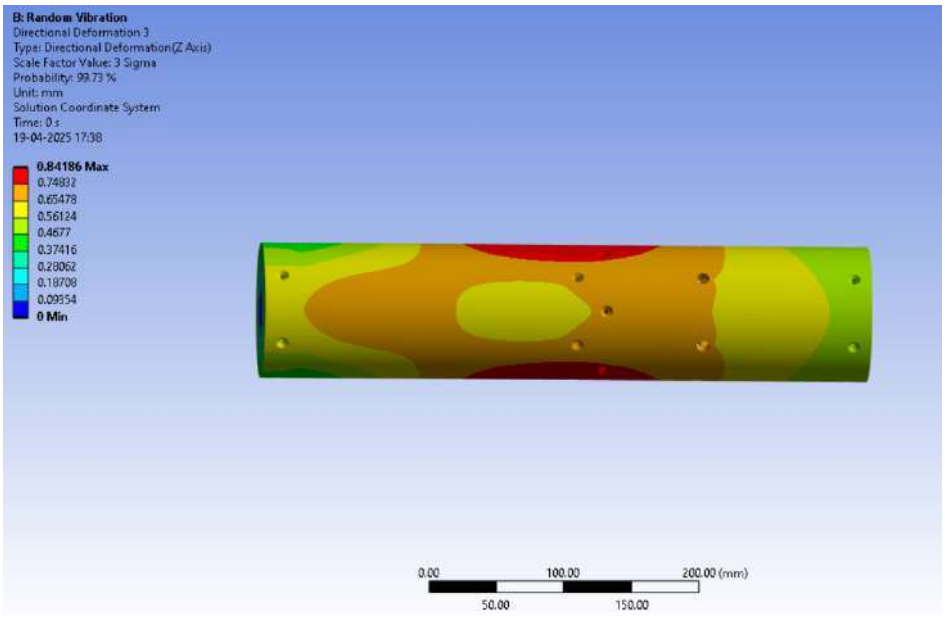


Figure 201 Directional Deformation in Z-Axis with Flight Simulated Data

The findings from this analysis demonstrate that the maximum directional deformations are minimal across all axes. In particular, the peak deformation recorded on the X-axis is 0.265 mm, on the Y-axis is 0.358 mm, and on the Z-axis is 0.841 mm, and has only a 0.3% chance of deforming. Even in this rare event, the clearances in the rocket can accommodate the deformations.

The PSD profile shows no significant energy beyond 500 Hz. The three significant modes clearly are distant from the excitation peaks in the active spectrum. With this, it could be concluded that the modal frequencies will not attain resonance-induced amplifications.

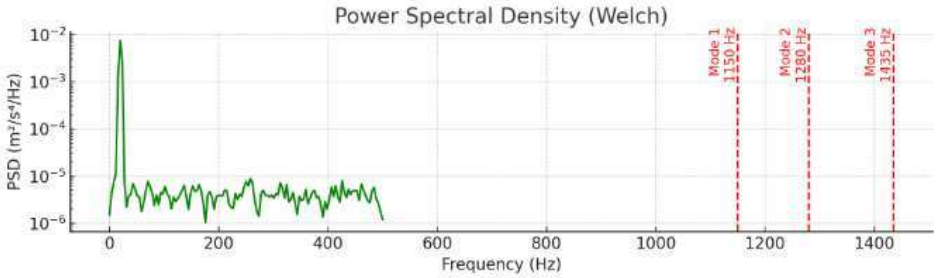


Figure 202 Verification of Non Excitation of the CanSat

Another approach was adopted to test the performance of the CanSat further truly. The NASA General Environmental Verification Standard (GEVS) PSD gravitational acceleration profile was adopted as a baseline input. The GEVS profile, which was created mainly for orbital-class spacecraft, offers a conservative vibration envelope commonly used for hardware verification when mission-specific flight data is unavailable. It provides a strong foundation for testing because its high-energy spectrum captures a broad range of potential dynamic loads. Despite unanticipated high-frequency or high-amplitude launch-induced vibrations, the CanSat will be structurally sound if it passes the qualification criteria. A statistical approach must be chosen because random vibrations follow a Gaussian distribution. A 3-sigma scale factor will give a highly conservative value to determine the integrity of the CanSat. The 3-sigma factor is a highly conservative approach, showing the possibility of an event happening at a 0.3% chance.

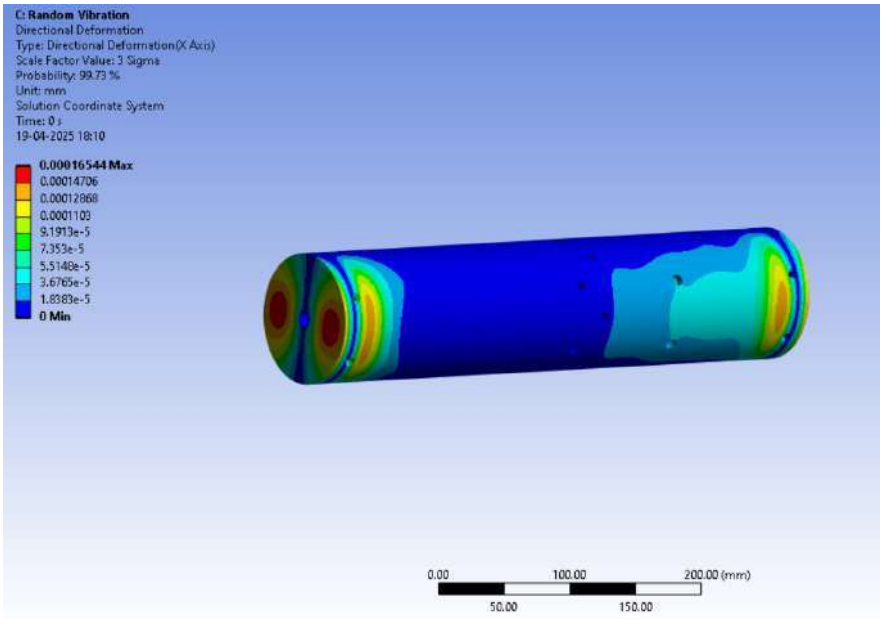


Figure 203 GEVS - Directional Deformation in X-Axis

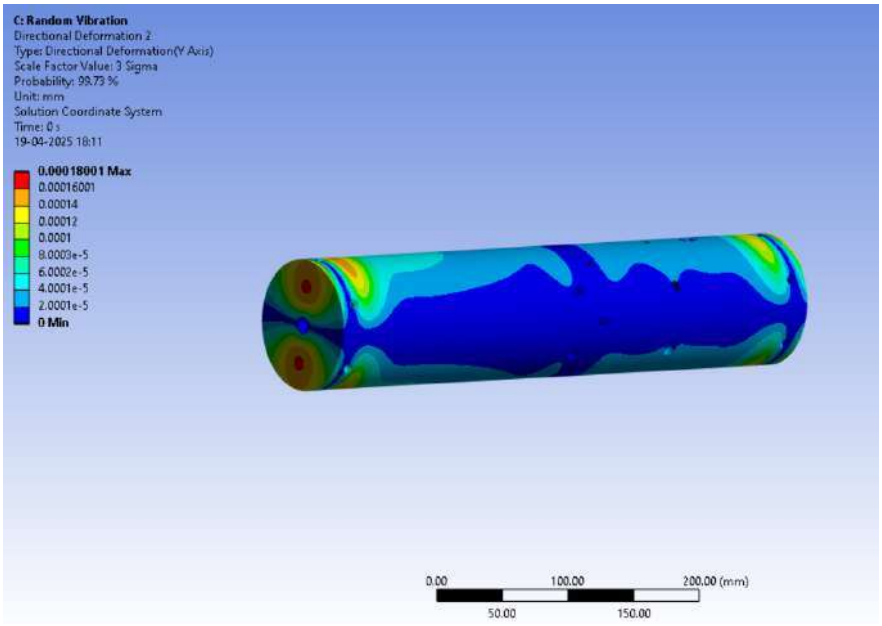


Figure 204 GEVS - Directional Deformation in Y-Axis

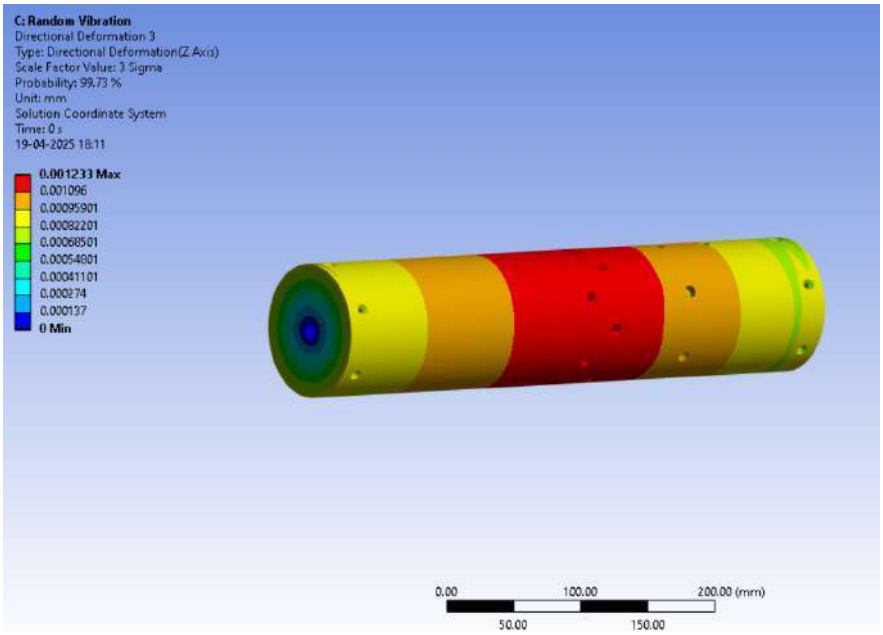


Figure 205 GEVS - Directional Deformation in Z-Axis

The directional deformation along the three principal axes is negligible, indicating that the CanSat's structural stiffness suppresses the amplifications created dynamically. Based on the results obtained using the 3-sigma scale factor, we can conclude that the CanSat can maintain its structural integrity, even under rare loading conditions. The response PSD profile was also verified to be similar to the input profile.

The qualification criteria for hardware in the GEVS testing are the RMS (Root Mean Square) value for the gravitational acceleration in response. The maximum RMS value obtained in all the components is 1.6388 g. This is well under the failure criteria of 8.2 g ensuring the CanSat can fly under highly conservative conditions.

2. *Spring Deflection Calculations*

The following are calculations for spring deflection to determine the optimal spring dimensions.

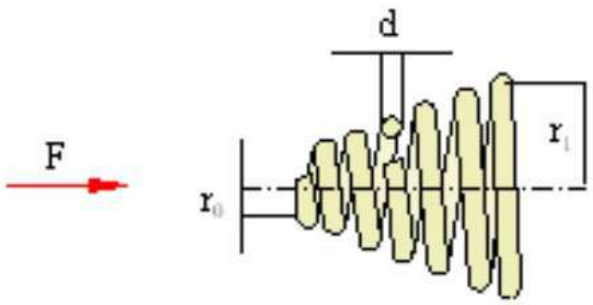


Figure 206 Calculation for Spring Deflection (f and Spring Force (F)

$$F = \frac{\pi}{16}\frac{d^3}{r_1}\tau \tag{7}$$

$$f = \frac{16n(r_1 + r_0)(r_1^2 + r_0^2)F}{d^4 G} \tag{8}$$

Where the values inputted to Eq. (7) are:

- **Diameter of spring wire** (d): $d = 1.510^{-3}$m
- **Mean coil diameter** (2_{r_1}): $2_{r_1} = 40.510^{-3}$m
- **Mean coil diameter** (2_{r_0}): $2_{r_0} = 10.510^{-3}$m
- **Number of active coils** (n): $n = 3$
- **Shear modulus** (G): $G = 81.3710^{9}$Pa
- **Spring force** (F): $F = 14.67$N

The resultant outputs were:

- **Spring length closed** (L_c): $L_c = nd = 4.510^{-3}$m
- **Spring deflection** (f): $f = 19.0810^{-3}$m
- **Spring stiffness** (k): k = $\frac{dF}{df} = F/f = 0.7710^{3}$N/m
- **Spring length free** (L_o): $L_o > L_c + f, L_o = 23.5810^{-3}$m
- **Pitch (lead)** (s): $s = \frac{L_o}{n} = 7.8610^{-3}$m
- **Shear stress** (τ_o): $\tau_o = 448.2810^{6}$Pa

E. Retainer

The team conducted static structural simulation using a motor weight and applied an artificial overload of 1.5 times.

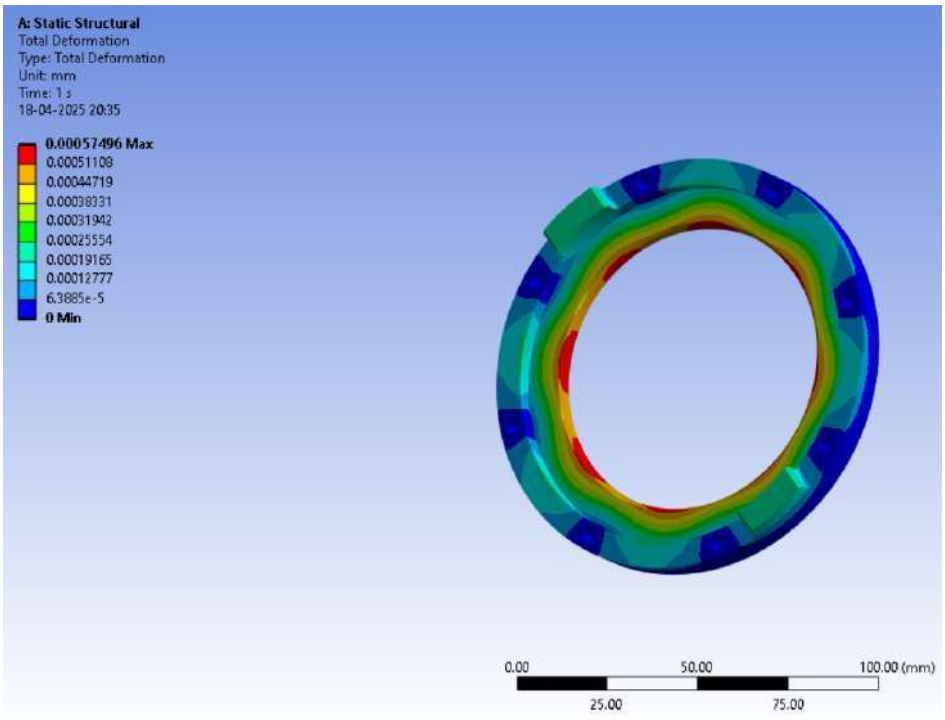


Figure 207 Deformation Contour on Retainer

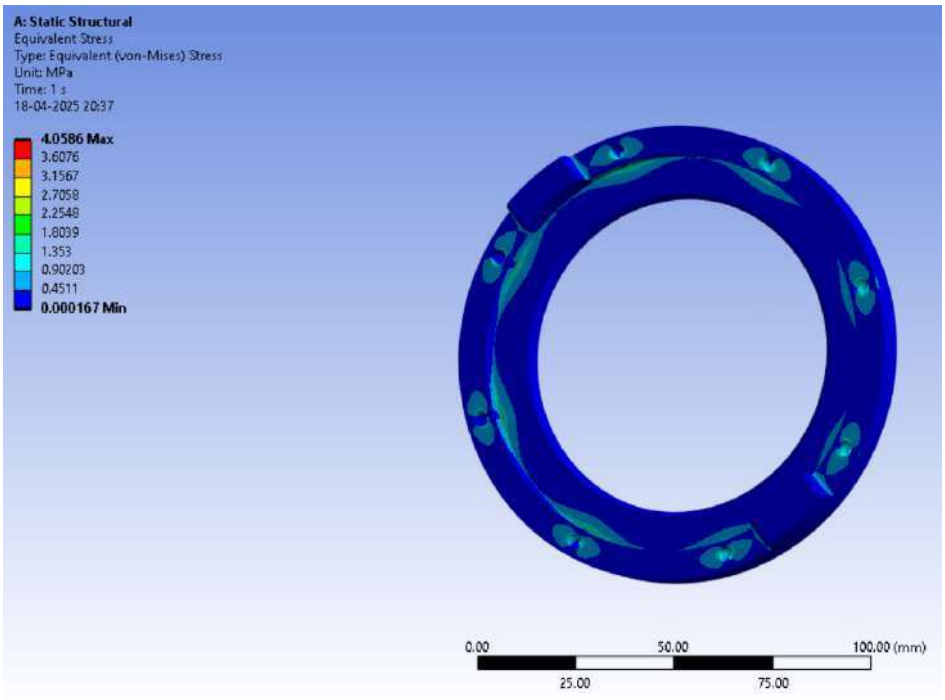


Figure 208 Equivalent Stress on Retainer

The maximum deformation in the simulation is 0.000 574 96 mm, which is inconsequential. The maximum von Mises stress value recorded is 4.06 MPa, which is significantly lower than the yield strength of Aluminium 6061-T6 at 276 MPa. This results in a calculated FOS of nearly 68. The design guarantees that the retainer will not encounter any structural failure in flight.

F. Motor Bay Coupler

The team conducted FEA simulations for structural analysis with the maximum thrust produced by the motor with an artificial overloading of 1.5.

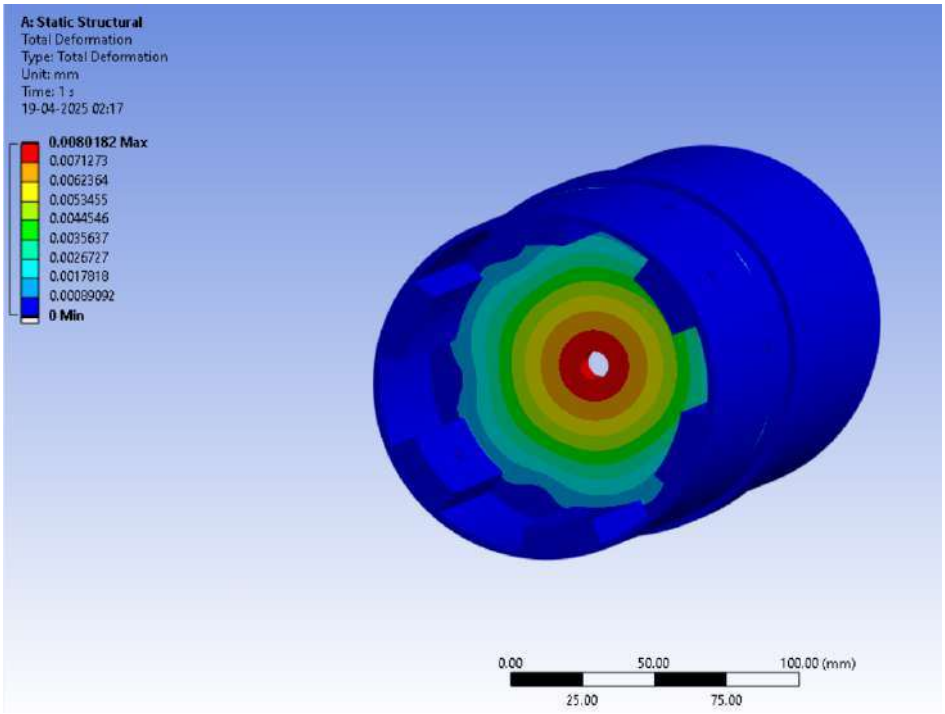


Figure 209 Deformation Contour on Motor Bay Coupler

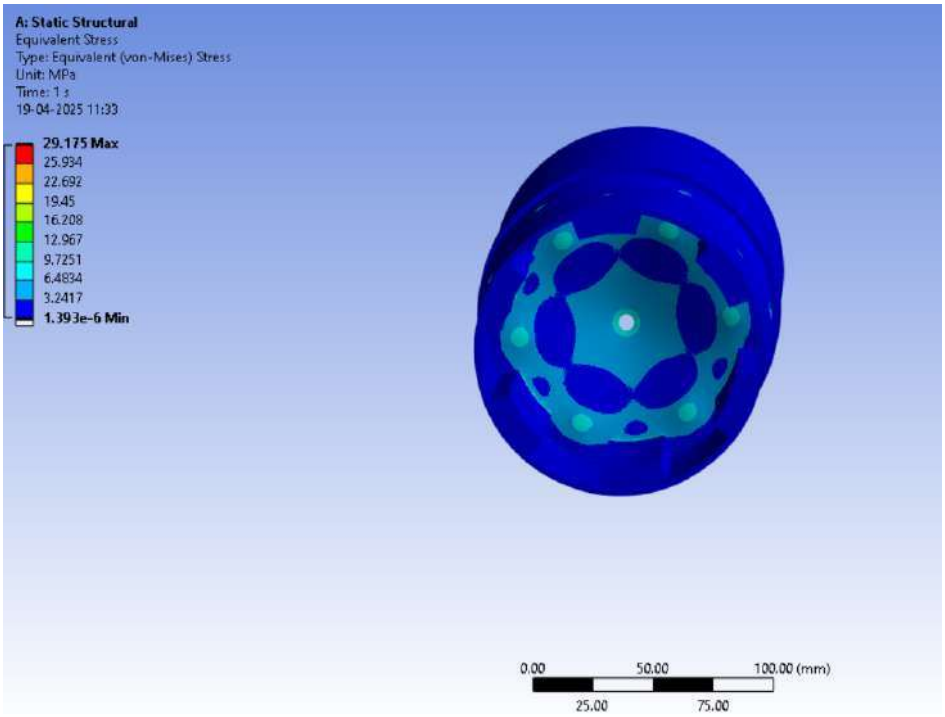


Figure 210 Equivalent Stress on Motor Bay Coupler

It could be observed that the highest value of deformation caused by mechanical straining for the motor bay coupler is 0.008 182 mm, which is comparatively lower to the limit. The maximum von Mises stress achieved is 29.175 MPa, which is much lower than the Aluminium 6061-T6 yield strength of 276 MPa, so the obtained FOS is 9.45.

G. Rocket with Circular Bolts

1. Computational Fluid Dynamics

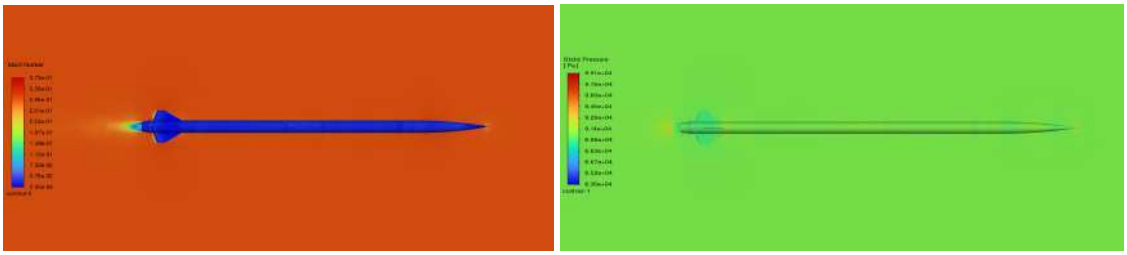


Figure 211 Mach and Static pressure Contour at Mach 0.3

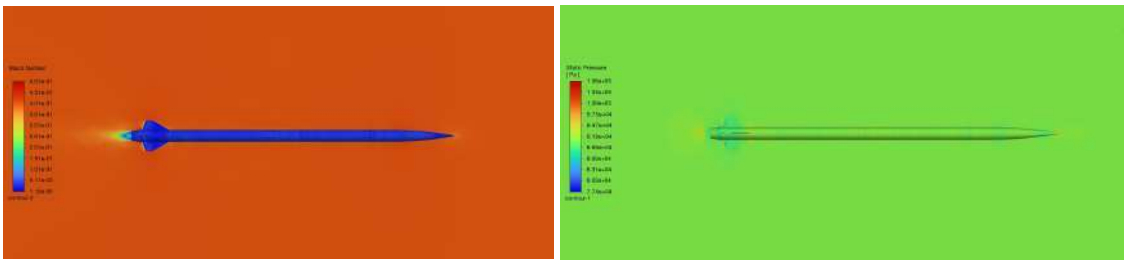


Figure 212 Mach and Static pressure Contour at Mach 0.4

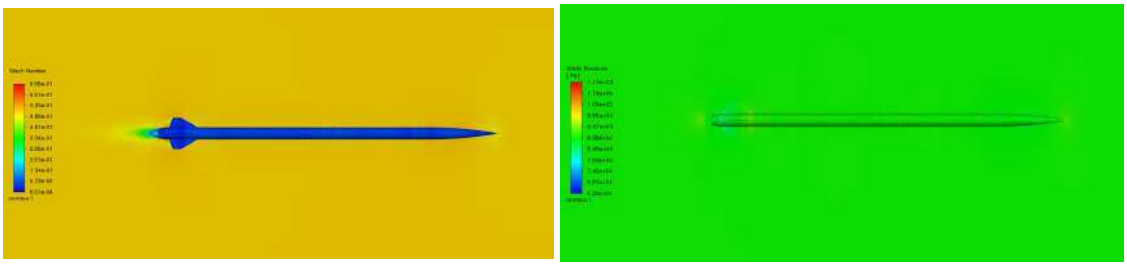


Figure 213 Mach and Static pressure Contour at Mach 0.5

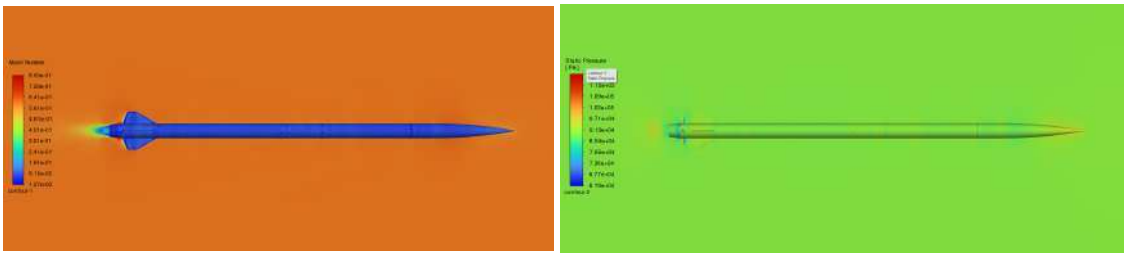


Figure 214 Mach and Static pressure Contour at Mach 0.6

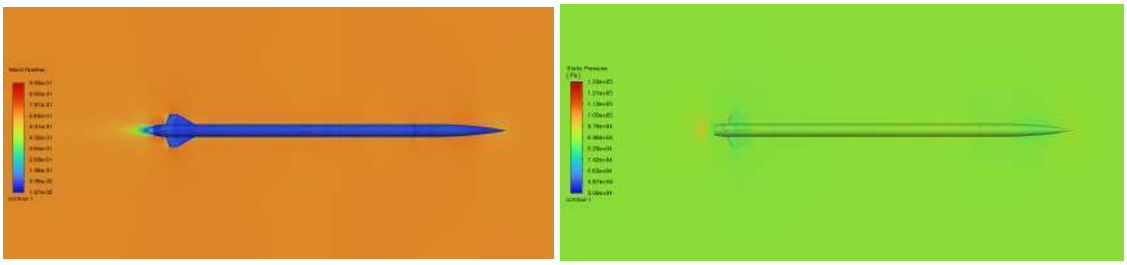


Figure 215 Mach and Static pressure Contour at Mach 0.7

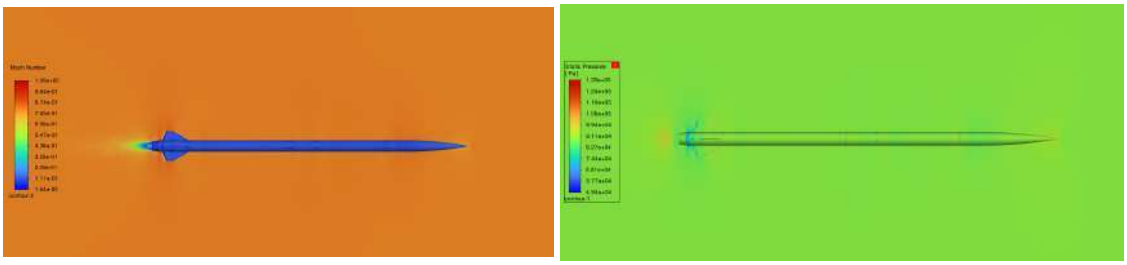


Figure 216 Mach and Static pressure Contour at Mach 0.8

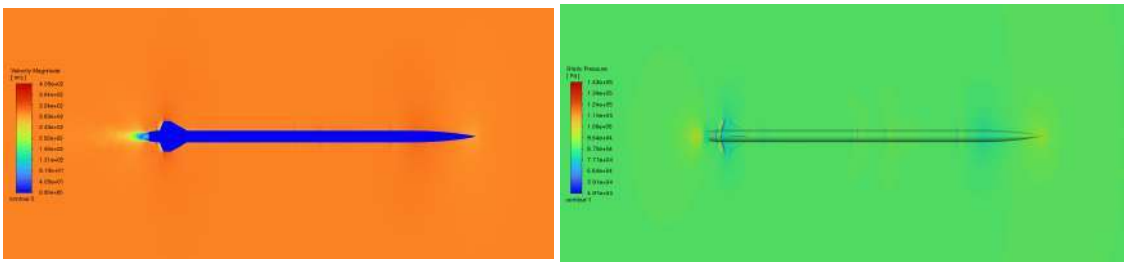


Figure 217 Mach and Static pressure Contour at Mach 0.9

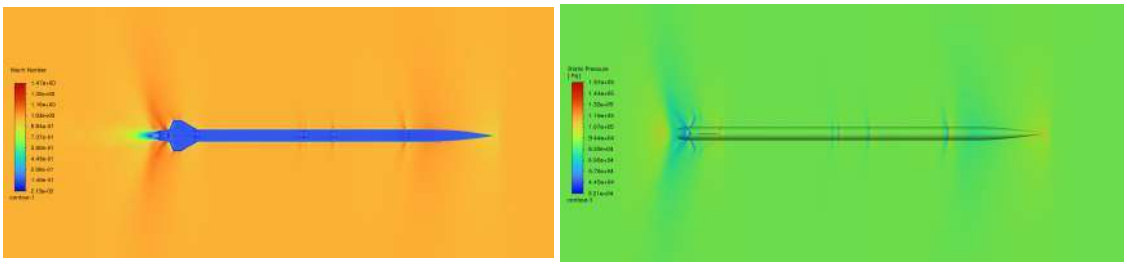


Figure 218 Mach and Static pressure Contour at Mach 1.0

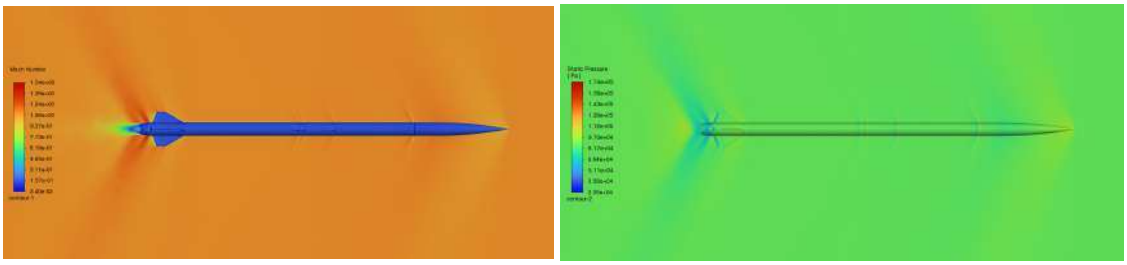


Figure 219 Mach and Static pressure Contour at Mach 1.1

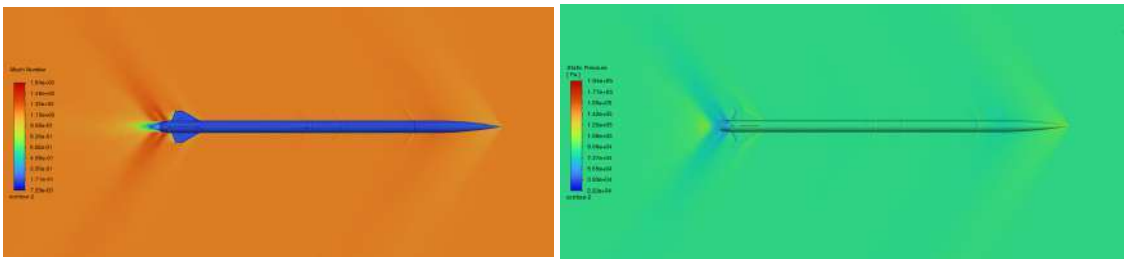


Figure 220 Mach and Static pressure Contour at Mach 1.2

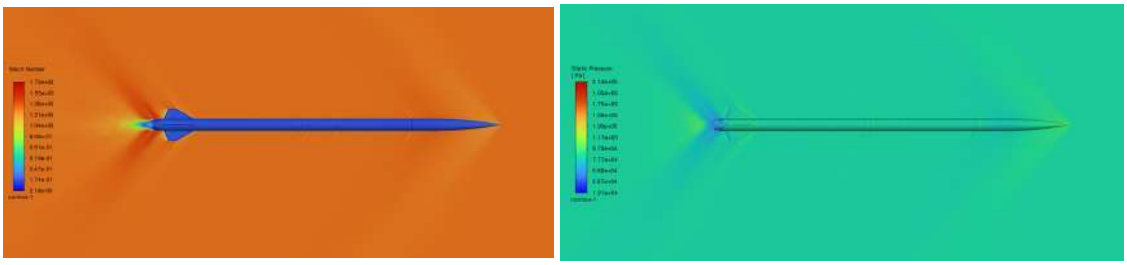


Figure 221 Mach and Static pressure Contour at Mach 1.3

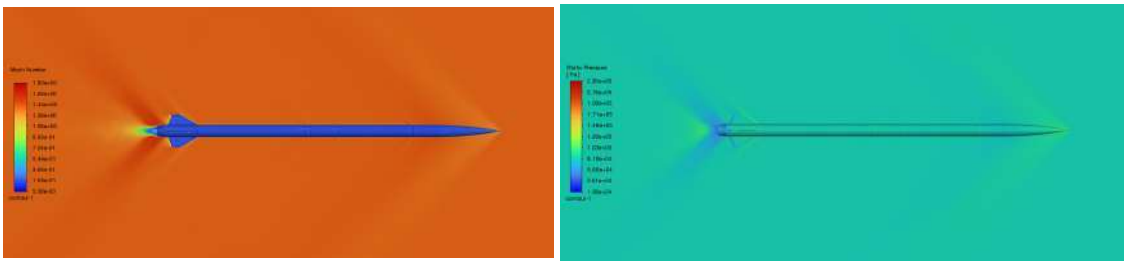


Figure 222 Mach and Static pressure Contour at Mach 1.4

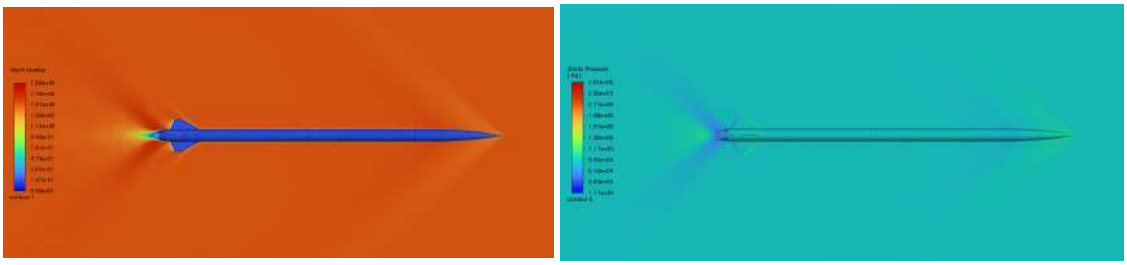


Figure 223 Mach and Static pressure Contour at Mach 1.5

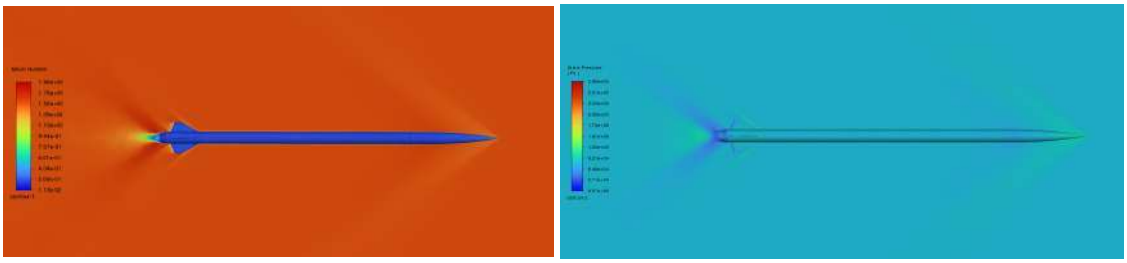


Figure 224 Mach and Static pressure Contour at Mach 1.6

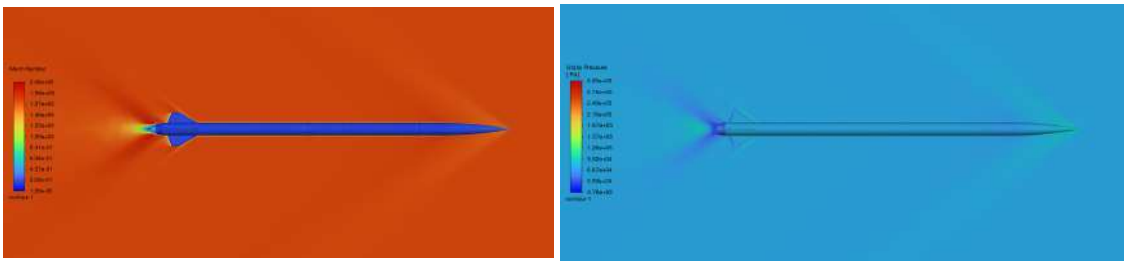


Figure 225 Mach and Static pressure Contour at Mach 1.71 (MaxQ)

H. Rocket with Hex Bolts

1. Computational Fluid Dynamics

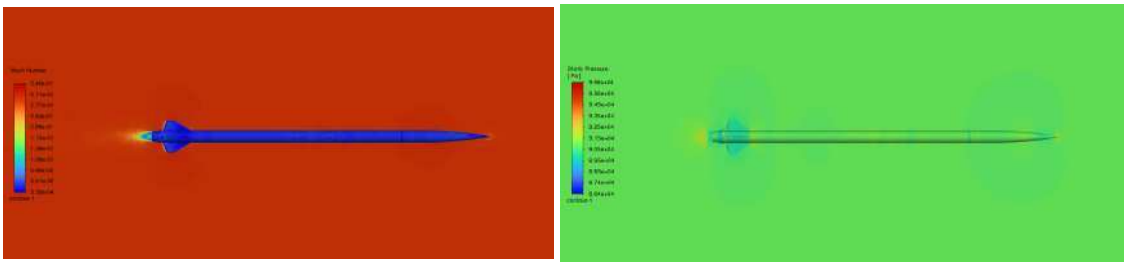


Figure 226 Mach and Static pressure Contour at Mach 0.3

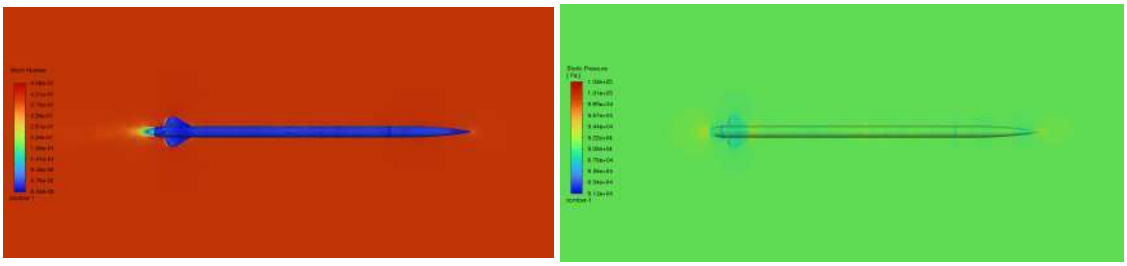


Figure 227 Mach and Static pressure Contour at Mach 0.4

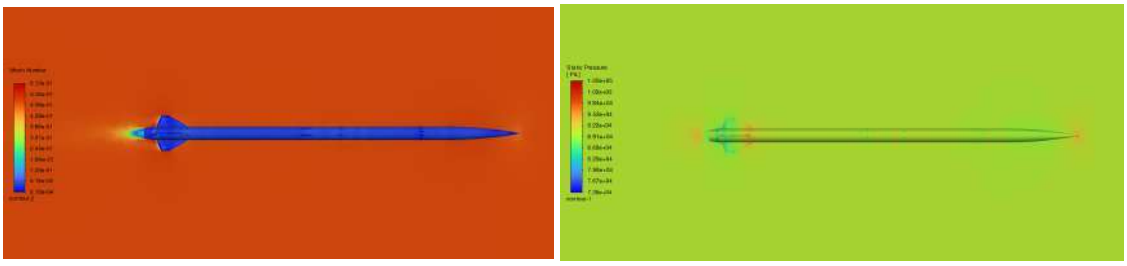


Figure 228 Mach and Static pressure Contour at Mach 0.5

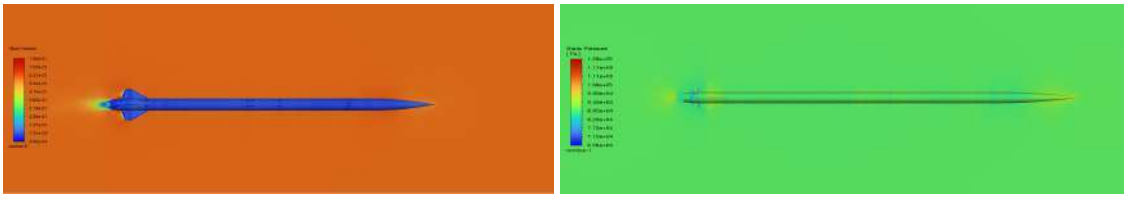


Figure 229 Mach and Static pressure Contour at Mach 0.6

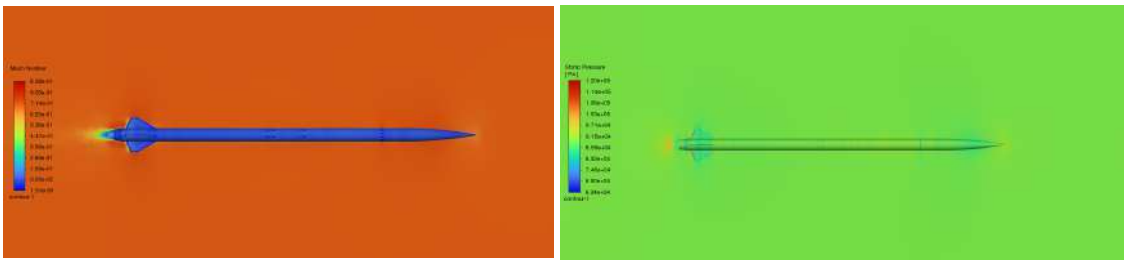


Figure 230 Mach and Static pressure Contour at Mach 0.7

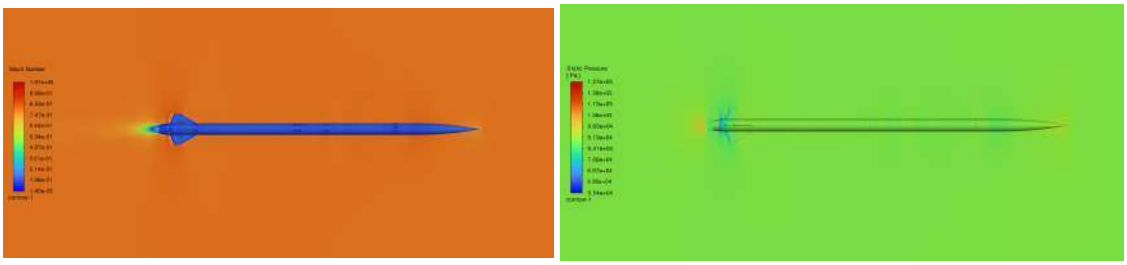


Figure 231 Mach and Static pressure Contour at Mach 0.8

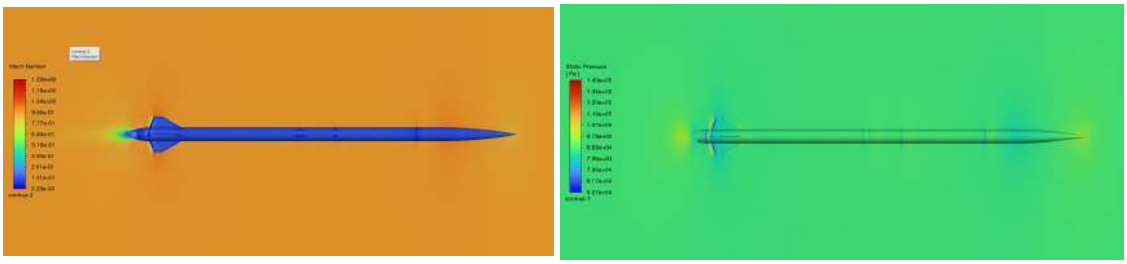


Figure 232 Mach and Static pressure Contour at Mach 0.9

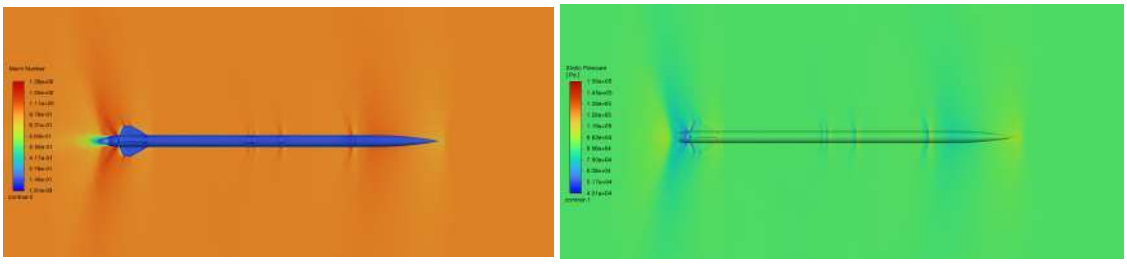


Figure 233 Mach and Static pressure Contour at Mach 1.0

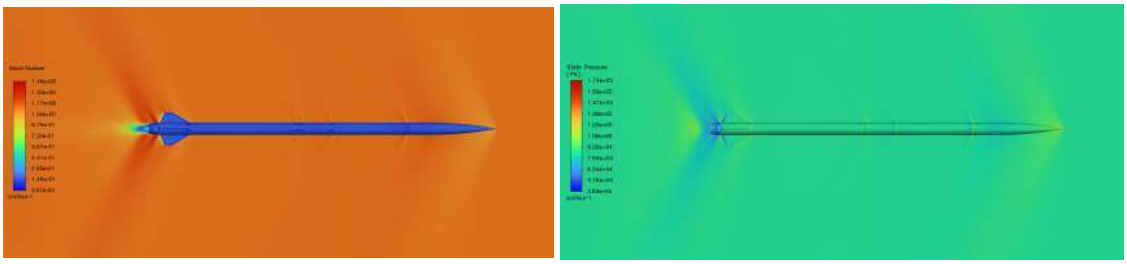


Figure 234 Mach and Static pressure Contour at Mach 1.1

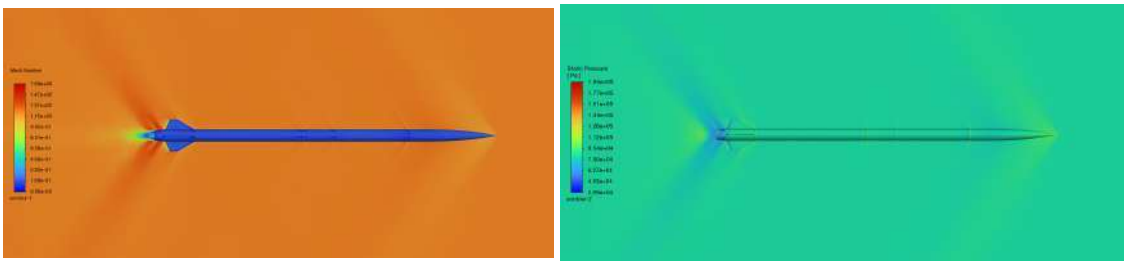


Figure 235 Mach and Static pressure Contour at Mach 1.2

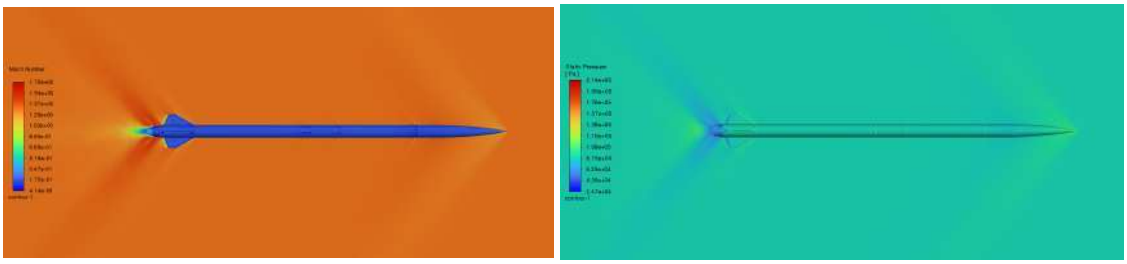


Figure 236 Mach and Static pressure Contour at Mach 1.3

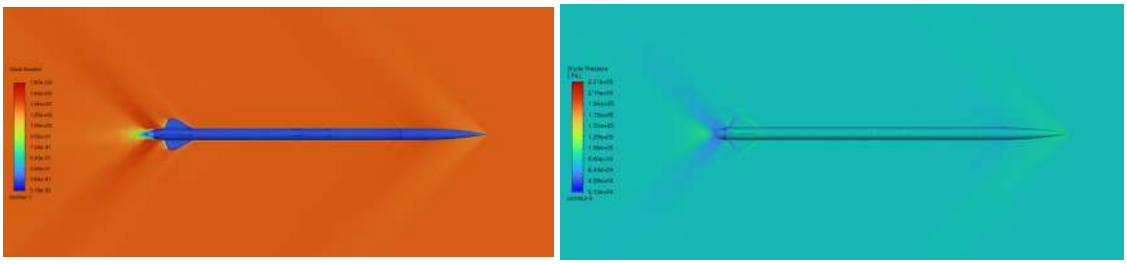


Figure 237 Mach and Static pressure Contour at Mach 1.4

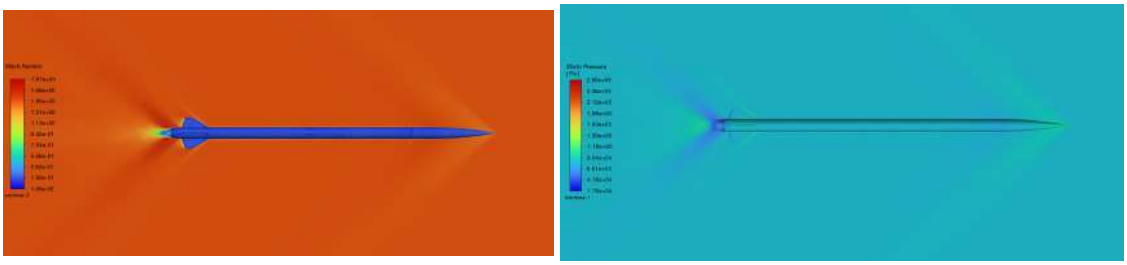


Figure 238 Mach and Static pressure Contour at Mach 1.5

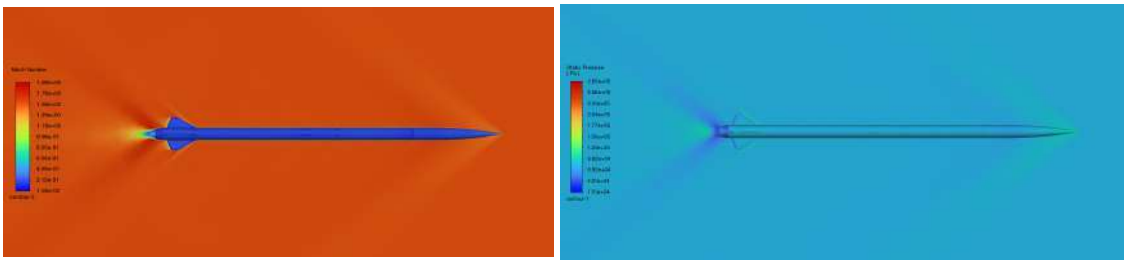


Figure 239 Mach and Static pressure Contour at Mach 1.6

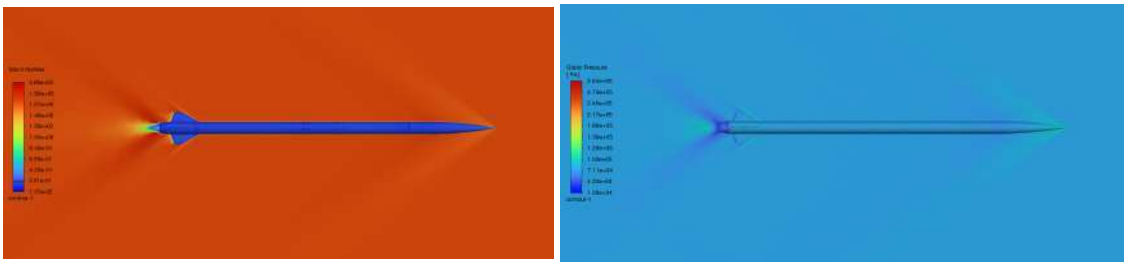


Figure 240 Mach and Static pressure Contour at Mach 1.71 (MaxQ)

I. Deployment Forces and Shock Loading Calculations

Deployment Force, $F_d = \frac{1}{2}\rho V^2 C_d A$

$(F_d)_{Drogue} = \frac{1}{2} \times 0.4128 \times 45.2^2 \times 1.5 \times 0.456$

$(F_d)_{Drogue} = 288.431\ N$

Taking Factor of Safety of 2, $(F_d)_{Drogue} = 576.862\ N$

$(F_d)_{Main} = \frac{1}{2} \times 1.1687 \times 27.9^2 \times 2.2 \times 2.63$

$(F_d)_{Main} = 2631.842\ N$

Taking Factor of Safety of 2, $(F_d)_{Main} = 5263.684\ N$

Now, Shock Loading $= mg\left(\frac{V_o}{V_T}\right)^2 \times F.O.S$

Taking $F.O.S = 2$;

$(\text{Shock Loading})_{Drogue} = 27.029 \times 9.81 \times \left(\frac{45}{27.9}\right)^2 \times 2$

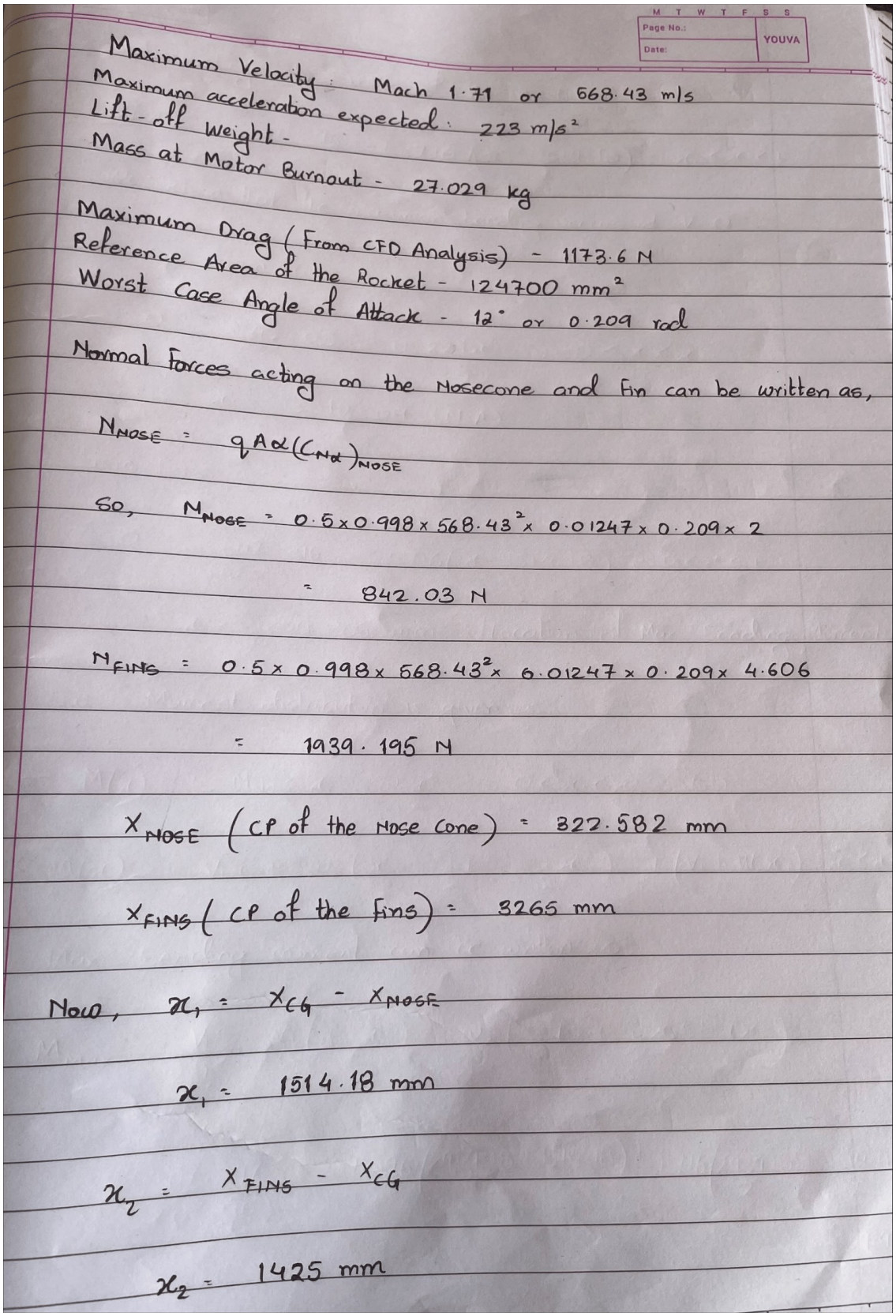
$(\text{Shock load})_{Drogue} = 1379.575\ N$

$(\text{Shock Loading})_{Main} = 27.029 \times 9.81 \times \left(\frac{27.9}{8.93}\right)^2 \times 2$

$(\text{Shock load})_{Main} = 5176.479\ N$

Figure 241 Hand Calculations

J. Load Analysis on Vayuvega



Maximum Velocity : Mach 1.71 or 568.43 m/s
Maximum acceleration expected : 223 m/s²
Lift-off weight -
Mass at Motor Burnout - 27.029 kg

Maximum Drag (From CFD Analysis) - 1173.6 N
Reference Area of the Rocket - 124700 mm²
Worst Case Angle of Attack - 12° or 0.209 rad

Normal Forces acting on the Nosecone and Fin can be written as,

$N_{NOSE} = q A \alpha (C_{N\alpha})_{NOSE}$

So, $N_{NOSE} = 0.5 \times 0.998 \times 568.43^2 \times 0.01247 \times 0.209 \times 2$

$= 842.03$ N

$N_{FINS} = 0.5 \times 0.998 \times 568.43^2 \times 6.01247 \times 0.209 \times 4.606$

$= 1939.195$ N

X_{NOSE} (CP of the Nose Cone) = 322.582 mm

X_{FINS} (CP of the Fins) = 3265 mm

Now, $x_1 = X_{CG} - X_{NOSE}$

$x_1 = 1514.18$ mm

$x_2 = X_{FINS} - X_{CG}$

$x_2 = 1425$ mm

Now, value of distributed inertia loads are calculated.

$$w_1 = \frac{N_{NOSE} + N_{FINS} - W_2 x_2}{x_1}$$

and, $$w_2 = \frac{N_{FINS}(2x_2 + x_1) - N_{NOSE} x_1}{x_2^2 + x_1 x_2}$$

Solving w_2 first,

$$w_2 = \frac{1939.195(2 \times 1425 + 1514.18) + 842.03(1514.18)}{1425^2 + (1514.18 \times 1425)}$$

$$w_2 = 1.716 \text{ N/mm}$$

Now, $$w_1 = \frac{842.03 + 1939.15 - (1.716 \times 1425)}{1514.18}$$

Now, $w_1 = 0.221$ N/mm

lateral Shear loading :

$$V(x) = N_N - w_1 x \quad ; \quad 0 < x \leq x_1 \quad \text{(i)}$$

and, $$V(x) = V_1 - w_2(x - x_1) \quad ; \quad x_1 < x < L \quad \text{(ii)}$$

Here, $L = x_1 + x_2 = 2939.18$ mm

So, $$V(x) = 842.03 - 0.221x \quad ; \quad 0 < x \leq x_1$$

So, $$V(x_1) = 842.03 - (0.221 \times 1514.18)$$

$$V_{x_1} = 507.396 \text{ N}$$

Substituting the value of V_1 in (ii),

$$V(x) = 507.396 - 1.716(x - 1514.18) \; ; \; x_1 < x < L$$

We know that the maximum bending occurs at $V = 0$

Hence, From (i)

$$0 = 842.03 - 0.221x \; ; \; 0 < x < x_1$$

$$\therefore x = 3810.09 \text{ (N.A)}$$

From (ii),

$$0 = 507.396 - 1.716(x - 1514.18) \; ; \; 0 < x < L$$

$$\therefore x = 1809.865 \text{ mm (location of Max. Bending Moment)}$$

Now, Moment distribution is given as,

$$M(x) = N_{NOSE}\, x - w_1 \frac{x^2}{2} \; ; \; 0 < x < x_1 \quad \text{(iii)}$$

$$M(x) = V_1 x + w_2\left(x_1 x + \frac{1}{2}L^2 - \frac{1}{2}x^2\right) - L\left(V_1 + W_2 x_1\right) \; ; \; x_1 < x < L$$

Max. Bending moment can be written as,

$$M_{Max} = \frac{V_1^2}{2w_2} - V_1(L - x_1) + w_2\left(\frac{1}{2}L^2 + \frac{1}{2}x_1^2 - Lx_1\right)$$

$$= \frac{507.396^2}{2(1.176)} - 507.396\left(2939.18 - 1514.18\right) + 1.716\left(\frac{2939.18^2}{2} + \frac{1514.18^2}{2} - 2939.18 \times 1514.18\right)$$

Page No.:
Date:

So, $M_{max} = 1094251.722$ N-mm

Now Section Modulus $= \frac{\pi}{32 d_o}\left(d_o^4 - d_i^4\right)$

So, $Z = \frac{\pi}{32 \times 126}\left(126^4 - 121^4\right)$

$Z = 29365.5503 \text{ mm}^3$

Now Compressive Stress due to drag,

$\sigma_{drag} = \frac{1173.6}{969.966} = 1.206 \text{ N/mm}^2$

Max. Bending Stress, $\sigma_b = \frac{M}{Z}$

So, $\sigma_b = \frac{1094251.722}{29365.5503} = 37.263 \text{ N/mm}^2$

Compressive Stress due to Mass Inertia,

$\sigma_m = \frac{27.029 \times 223}{969.966} = 6.214 \text{ N/mm}^2$

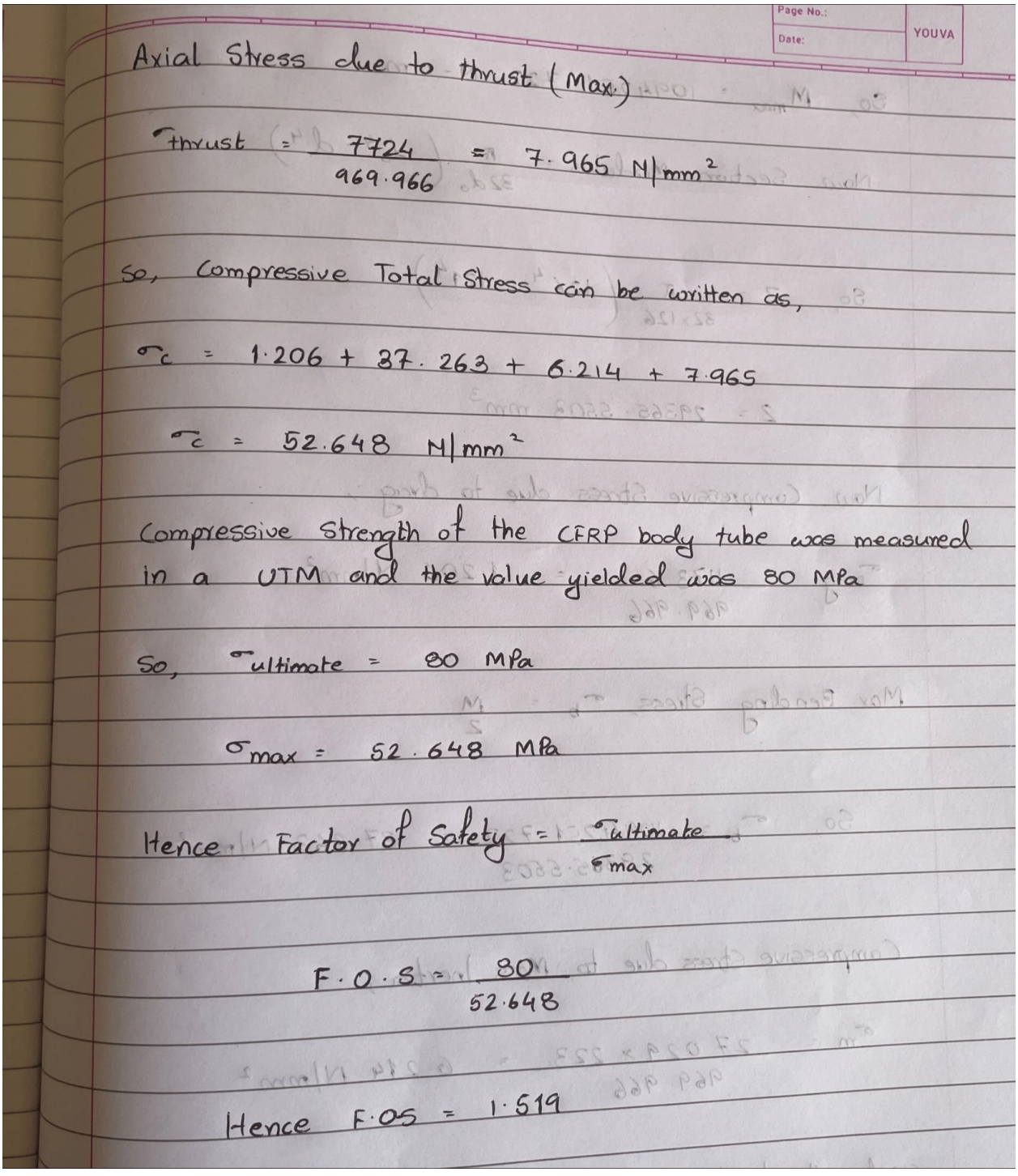


Figure 242 Load Analysis on Vayuvega

M. Appendix: SRAD 6-DoF Simulator Code

THIS PAGE INTENTIONALLY LEFT BLANK.
APPENDIX M BEGINS ON THE FOLLOWING PAGE.

```
acceleration = zeros(800000,1); % Acceleration of the Rocket(in body direction
aligned to roll)
prediction = zeros(800000,1);  %stores predicted apogee at each time step
u = zeros(800000,1); % Body frame axis aligned in direction of thrust & roll axis
v = zeros(800000,1); % Body frame axis aligned to pitch axis
w = zeros(800000,1); % Body frame axis aligned to yaw axis
p = zeros(800000,1); % Yaw Rate
q = zeros(800000,1); % Pitch Rate
r = zeros(800000,1); % Roll Rate
psi = zeros(800000,1); % Yaw Euler Axis Angle
theta = zeros(800000,1); % Pitch Euler Axis Angle
phi = zeros(800000,1);% Roll Euler Axis Angle
Xe = zeros(800000,1); % X Distance in earth frame co ordinates
Ye = zeros(800000,1); % Y Distance in earth frame co ordinates
Ze = zeros(800000,1); % Z Distance in earth frame co ordinates
timer = zeros(800000,1); % Keeps track of time variable
velx = zeros(800000,1); % Keeps track of velocity in X(upwards) direction
dt = 0.001; % Increment in time steps
counter1 = 1; % A counter for flagging and running the loop
temp = 300; % Ground Temperature for density calculations
CP = zeros(800000,1);  %stores centre of pressure position
C_roll = zeros(800000,1);  %stores roll moment coefficient
Cn_yaw=zeros(800000,1);  %stores normal force coefficient for yaw
Cn_pitch=zeros(800000,1);  %stores normal force coefficient for pitch
Cn_alpha = zeros(800000,1); %stores dCn/d alpha
Cd=zeros(800000,1);  %stores drag coefficient
Mass=zeros(800000,1); %stores rocket mass
CG = zeros(800000,1); %Centre of Gravity
Ixx = zeros(800000,1); % Axial Moment of Inertia
Iyy = zeros(800000,1); %Transeverse Moment of Inertia
Stab_Cal=zeros(800000,1); %stability calibers of the rocket
flag = 0; % Flag for signifying state of the air brakes..0 implies airbrakes
retracted, 1 implies airbrakes deployed
phase = 0; % Variable to keep track of flight phase..0 implies ascent phase 1
implies parachute phase
mphase=1;  %flag to keep track of motor burn out... value of 1 means motor is
firing 0 means motor has been burnt out
state = zeros(800000,1);  %flag to keep track of airbrake status...value of 2000
means airbrakes are deployed, 500 means airbrakes are retracted..these values and
this variable is used to plot airbrake state
delay = 1; % Variable to account for delay in opening the air brakes in s
delaytracker = 0; % Variable to keep track of mechanical delay in the loop
turb_gen=zeros(4,4); %helps in turbulence generation
turb_gen(1,1)=1;turb_gen(1,4)=1.5;  %initial values for the pink noise generator
for modelling turbulence in atmosphere
drift=zeros(800000,1); %keeps track of the drifting of rocket from the launch point
vtrajectory=zeros(800000,3); %variable for plotting rocket trajectory during ascent
phase

%% Assembly of rocket part and calculating their mass, cg and mi
```

```
% since for calculating transverse mi we need to have cg position which is
% possible only in main loop due to mass depletion during motor burn
% the transverse mi, mass and distance of cg of each component from the
% nose tip is stored in variable TMI and transverse mi is calculated

%rocket_data=[mass of rocket excluding motor,cg position from tip,axial
mi,transverse mi,maximum od,fuselage total lenght,root chord,tip chord,height,sweep
length,fin position]
     rmas=xlsread('vayuvega_rocketinfo.xlsx','A1:A1'); %rocket mass without motor
     rcg=xlsread('vayuvega_rocketinfo.xlsx','A2:A2'); %rocket cg without motor
     AMI=xlsread('vayuvega_rocketinfo.xlsx','A3:A3'); %rocket axial moment of
inertia without motor
     TMI=xlsread('vayuvega_rocketinfo.xlsx','A4:A4'); %rocket transverse moment of
inertia without motor
     mrad=xlsread('vayuvega_rocketinfo.xlsx','A5:A5'); %rocket's max radius also
used as refrence value for calculating aerodynamic forces and moments
     rlen=xlsread('vayuvega_rocketinfo.xlsx','A6:A6'); %rocket's total length
     fin_details=xlsread('vayuvega_rocketinfo.xlsx','A7:A11'); %5*1matrix for
rocket fin dimension [root chord,tip chord,fin semi span,sweep length,distance of
fin from nose tip]'
     mrad=mrad/2; Aref=pi*mrad^2;mpos=rlen; %refrence area



%% Asking User Input For Initial Pitch and Yaw Angle and atmospheric conditions
psi(1) = 2;
psi(1) = deg2rad(psi(1));
theta(1) = 2;
theta(1) = deg2rad(theta(1));

airbrake = 'n'; %for simulation with or without airbrakes
if airbrake =='y'
    desired = input('Enter Desired Apogee(m): ');
end

%launch site basic atmospheric conditions..... launch site elevation and
tempreature still
%needs to be added
awiny=-2;
awinz=2;
tur_inten=5;

%% Importing aerodynamic and motor data

%importing rocket's aerodynamic data
    data1=xlsread('AA modified.xlsx',1);  %aero data without airbrakes
    data2=xlsread('AA modified.xlsx',2);  %aero data with airbrakes

%the details of motor and its thrust time curve is imported as an excel
%file
```

```
    motor_data=xlsread('Vayuvega_motordata.xlsx');  % imports motor thrust time
data and motor details
    length=motor_data(1,2); %motor length
    odia=motor_data(2,2);  %motor outer diametre
    wetmass=motor_data(3,2);  %motor wet mass
    drymass=motor_data(4,2);  %motor dry mass
    nozmass=motor_data(5,2);  %nozzle mass
    nozlen=motor_data(6,2);  %nozzle length

    thrust=zeros(16,1);time=zeros(16,1);  %motor thrust time curve
    for n=8:1:47
        thrust(n-7,1)=motor_data(n,2);
        time(n-7,1)=motor_data(n,1);
    end
    clear c n;
%% Main Loop
while Xe(counter1) >= 0||timer(counter1)<time(end,1) % Condition given so that loop
will run till rocket hit's the ground

    % Pre Calculating the Trig Values
    sphi = sin(phi(counter1));
    stheta = sin(theta(counter1));
    spsi = sin(psi(counter1));
    cphi = cos(phi(counter1));
    ctheta = cos(theta(counter1));
    cpsi = cos(psi(counter1));

    %other calculations
        %mach no
        [mydensity,mytemp] = density_n_temp(Xe(counter1),temp); %Calculating
density and temperature at current altitude
        v_sound=sqrt(1.4*287*mytemp);  % speed of sound at the current altitude
        mach_no=u(counter1)/v_sound;  % mach number of rocket

     %calculating mass, centre of gravity, axial moment of inertia and
        %transverse moment of inertia for the current time
        [mmass,mcg,mIx,mIy,mythrust] =
thrust_n_other_things(timer(counter1),length,odia,wetmass,drymass,nozmass,nozlen,tim
e,thrust);  %function call to calculate current thrust, instantaneous motor mass,
cg and mi
        %mmas(= motor mass) is in kg, mcg(= position of motor cg wrt motor head) in
cm
        %mIx and mIy are mi of motor in kgcm2
        %mythrust is current hrust in Newtons

            Mass(counter1) = rmas+mmass;  %rocket's total mass
            CG(counter1) = ((rmas*rcg)+(mmass*(mpos-(length+nozlen)+mcg)))/
Mass(counter1); %net centre of gravity
            Ixx(counter1) = (AMI)+(mIx); %net axial moment of inertia
```

```
            Iyy(counter1) = TMI+(rmas*(CG(counter1)-(rcg))^2)+(mIy)+
(mmass*(CG(counter1)-(mpos-length+mcg))^2);  %net transeverse moment of
inertia..rocket is assumed to be symmetric about xy and xz plane mi about y and
z are same

            if timer(counter1) > time(end,1)  %condition for motor burn out
                mphase=0;
            end
            if phase==0  %condition for rocket to be in ascent phase
                %function call to interpolate aerodynamic data(cd,cn,cp etc) based
on motor and airbrakes status(variables phase1 and flag)

[CP(counter1),Cn_pitch(counter1),Cn_yaw(counter1),Cn_alpha(counter1),Cd(counter1)]=a
erodynamic_data(data1,data2,mach_no,psi(counter1),theta(counter1),mphase,flag);
            end


        momentarm = CP(counter1)-CG(counter1);
        Stab_Cal(counter1) = momentarm/(2*mrad);

    %% Air Brakes Prediction Segment
    if timer(counter1) > time(end,1) && phase == 0 && airbrake == 'y' &&
u(counter1)<180  %condition to ensure motor has burnt out, rocket is in ascent
phase and the speed is below the speed allowed by structural limits(needs to be
found from structural sims)

         %prediction function call to predict apogee based on current altitude,
vertical speed
        if flag==0
            prediction(counter1) =
predictor(data1,acceleration(counter1),u(counter1),Xe(counter1),Mass(counter1),Aref,
mytemp);  %data1 has aero data for airbrakes closed
        elseif flag==1
            prediction(counter1) =
predictor(data2,acceleration(counter1),u(counter1),Xe(counter1),Mass(counter1),Aref,
mytemp);  %data2 has aero data for opened airbrakes
        end

        if prediction(counter1) > desired %Desired Apogee
            if timer(counter1) - delaytracker >= delay  %check for mechanical delay
                flag = 1;
                delaytracker = timer(counter1);
            end
        elseif prediction(counter1) < desired %Desired Apogee
            if timer(counter1) - delaytracker >= delay  %check for mechanical delay
                flag = 0;
                delaytracker = timer(counter1);
            end
        end
    else
```

```
        prediction(counter1) = 0;
    end

    if flag == 1
        state(counter1) = 2000; %Registering state of Air Brakes as open
    else
        state(counter1) = 500; %Registering state of Air Brakes as closed
    end
    %% Determining Phase Of Flight
    % Powered Flight & Coasting Phase
    if timer(counter1) < 10 || u(counter1) >=0

        %generation of side wind gusts and turbulence
        [sidey,turb_gen]=turbulence_generator(counter1,turb_gen,awiny,tur_inten,dt);
        [sidez,turb_gen]=turbulence_generator(counter1,turb_gen,awinz,tur_inten,dt);

        %calculation of disturbing side forces and moments

[Fy,Mz]=side_forces1(sidey,CG(counter1),mydensity,mrad,rlen,fin_details);

[Fz,My]=side_forces1(sidez,CG(counter1),mydensity,mrad,rlen,fin_details);

        %My and Mz are disturbing moment about pitch and yaw respectively

        Fy=Fy*sign(sidey)*cos(psi(counter1));Fz=Fz*sign(sidez)*cos(theta(counter1));
        My=My*sign(sidez)*cos(theta(counter1));Mz=-
Mz*sign(sidey)*cos(psi(counter1));

        if Xe(counter1)>5.18  %condition for launch rod clearance

CNY= -(Cn_yaw(counter1)*sign(psi(counter1)))-(Cd(counter1)*sin(psi(counter1)))-
(Cn_alpha(counter1)*atan((q(counter1)*momentarm)/u(counter1))); %net Cn yaw
            CNP=
-(Cn_pitch(counter1)*sign(theta(counter1)))-(Cd(counter1)*sin(theta(counter1)))-
(Cn_alpha(counter1)*atan((p(counter1)*momentarm)/u(counter1))); %net Cn pitch
            C_roll(counter1)= -2*pi*atan((1.5*mrad*r(counter1))/
u(counter1))*sign(r(counter1));  %net roll moment coefficient
        else
            CNY=0;
            CNP=0;
            C_roll(counter1)=0;
            My=0;Mz=0;Fy=0;Fz=0;
        end

        drag = 0.5*Cd(counter1)*u(counter1)*u(counter1)*mydensity*Aref;
%Calculating drag force
        Yaw = (0.5*CNY*mydensity*u(counter1)*u(counter1)*Aref*momentarm)+Mz;
%Calculating net yaw moment
        Pitch = (0.5*CNP*mydensity*u(counter1)*u(counter1)*Aref*momentarm)+My;
%Calculating net pitch moment
```

```
        Roll =
C_roll(counter1)*mydensity*u(counter1)*u(counter1)*(fin_details(3,1)*(fin_details(1,
1)+fin_details(2,1)))*(1.5*mrad); %calculating net rolling moment

        %store x,y,z values for trajectory for ascent
        vtrajectory(counter1,1)=Xe(counter1);
        vtrajectory(counter1,2)=Ye(counter1);
        vtrajectory(counter1,3)=Ze(counter1);


        % Parachute Phase
    else
        pdia=0.95; %parachute diametre in reefed condition
        if Xe(counter1)<460  %condition for dis reef
            pdia=3;  %un-reefed parachute dia
        end
        drag = (0.5*1.2*pi*(pdia)*(pdia)/
4)*mydensity*u(counter1)*u(counter1)*sign(u(counter1)); %1.2 is parachute drag
coefficient found from cfd
        Fy=(0.5*0.1*mydensity*(sidey^2)*(pi*(pdia)*(pdia)/
4)*sign(sidey))-(0.5*0.1*mydensity*(v(counter1)^2)*(pi*(pdia)*(pdia)/
4)*sign(v(counter1))); %0.1 is side force coefficient value from cfd
        Fz=(0.5*0.1*mydensity*(sidez^2)*(pi*(pdia)*(pdia)/
4)*sign(sidez))-(0.5*0.1*mydensity*(w(counter1)^2)*(pi*(pdia)*(pdia)/
4)*sign(w(counter1)));
        Yaw = 0;
        Pitch = 0;
        Roll = 0;
        phi(counter1) = 0;
        psi(counter1) = 0;
        theta(counter1) = 0;
        phase = 1;
        flag = 0;
    end

%% RK4 Method


[udot1,vdot1,wdot1,rdot1,qdot1,pdot1,phidot1,thetadot1,psidot1,xedot1,yedot1,zedot1]
 =
Rk4Derivative(mythrust,drag,Fy,Fz,Mass(counter1),u(counter1),v(counter1),w(counter1)
,p(counter1),q(counter1),r(counter1),cphi,cpsi,ctheta,sphi,spsi,stheta,Yaw,Pitch,Rol
l,Ixx(counter1),Iyy(counter1),Iyy(counter1));

[udot2,vdot2,wdot2,rdot2,qdot2,pdot2,phidot2,thetadot2,psidot2,xedot2,yedot2,zedot2]
 = Rk4Derivative(mythrust,drag,Fy,Fz,Mass(counter1),u(counter1)+udot1*(dt/
2),v(counter1)+vdot1*(dt/2),w(counter1)+wdot1*(dt/2),p(counter1)+pdot1*(dt/
2),q(counter1)+qdot1*(dt/2),r(counter1)+rdot1*(dt/
2),cphi,cpsi,ctheta,sphi,spsi,stheta,Yaw,Pitch,Roll,Ixx(counter1),Iyy(counter1),Iyy(
counter1));
```

```
[udot3,vdot3,wdot3,rdot3,qdot3,pdot3,phidot3,thetadot3,psidot3,xedot3,yedot3,zedot3]
 = Rk4Derivative(mythrust,drag,Fy,Fz,Mass(counter1),u(counter1)+udot2*(dt/
2),v(counter1)+vdot2*(dt/2),w(counter1)+wdot2*(dt/2),p(counter1)+pdot2*(dt/
2),q(counter1)+qdot2*(dt/2),r(counter1)+rdot2*(dt/
2),cphi,cpsi,ctheta,sphi,spsi,stheta,Yaw,Pitch,Roll,Ixx(counter1),Iyy(counter1),Iyy(
counter1));

[udot4,vdot4,wdot4,rdot4,qdot4,pdot4,phidot4,thetadot4,psidot4,xedot4,yedot4,zedot4]
 =
Rk4Derivative(mythrust,drag,Fy,Fz,Mass(counter1),u(counter1)+udot3*(dt),v(counter1)+
vdot3*(dt),w(counter1)+wdot3*(dt),p(counter1)+pdot3*(dt),q(counter1)+qdot3*(dt),r(co
unter1)+rdot3*(dt),cphi,cpsi,ctheta,sphi,spsi,stheta,Yaw,Pitch,Roll,Ixx(counter1),Iy
y(counter1),Iyy(counter1));

    u(counter1+1) = u(counter1) + (1/6)*(udot1 + 2*udot2 + 2*udot3 + udot4)*dt;
    acceleration(counter1+1) =  (1/6)*(udot1 + 2*udot2 + 2*udot3 + udot4);
    v(counter1+1) = v(counter1) + (1/6)*(vdot1 + 2*vdot2 + 2*vdot3 + vdot4)*dt;
    w(counter1+1) = w(counter1) + (1/6)*(wdot1 + 2*wdot2 + 2*wdot3 + wdot4)*dt;
    r(counter1+1) = r(counter1) + (1/6)*(rdot1 + 2*rdot2 + 2*rdot3 + rdot4)*dt;
    q(counter1+1) = q(counter1) + (1/6)*(qdot1 + 2*qdot2 + 2*qdot3 + qdot4)*dt;
    p(counter1+1) = p(counter1) + (1/6)*(pdot1 + 2*pdot2 + 2*pdot3 + pdot4)*dt;
    phi(counter1+1) = phi(counter1) + (1/6)*(phidot1 + 2*phidot2 + 2*phidot3 +
phidot4)*dt;
    theta(counter1+1) = theta(counter1) + (1/6)*(thetadot1 + 2*thetadot2 +
2*thetadot3 + thetadot4)*dt;
    psi(counter1+1) = psi(counter1) + (1/6)*(psidot1 + 2*psidot2 + 2*psidot3 +
psidot4)*dt;
    Xe(counter1+1) = Xe(counter1) + (1/6)*(xedot1 + 2*xedot2 + 2*xedot3 +
xedot4)*dt;
    Ye(counter1+1) = Ye(counter1) + (1/6)*(yedot1 + 2*yedot2 + 2*yedot3 +
yedot4)*dt;
    Ze(counter1+1) = Ze(counter1) + (1/6)*(zedot1 + 2*zedot2 + 2*zedot3 +
zedot4)*dt;
    velx(counter1+1) = (1/6)*(xedot1 + 2*xedot2 + 2*xedot3 + xedot4);
    timer(counter1+1) = timer(counter1) + dt;
    counter1 = counter1 + 1;

    drift(counter1)=sqrt((Ye(counter1)^2)+(Ze(counter1)^2)); %calculating drift
distance

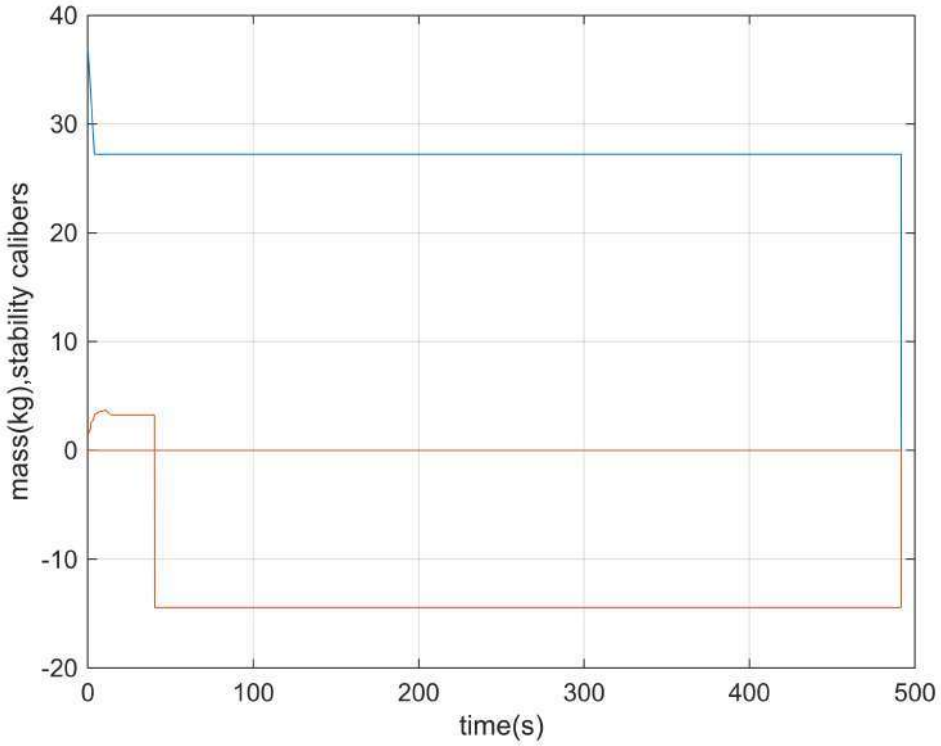
    if phase==0&&Xe(counter1)<0  %condition to take care of motor start
transients.. during start value of thrust might be less than weight
        Xe(counter1)=0;u(counter1)=0;
    end
end
prediction(counter1) = 0; % Compensating the extra count due to the loop
state(counter1) = 500; % Compensating the extra count due to the loop

%% All The Plots & Required Data
```

```
theta = rad2deg(theta);
psi = rad2deg(psi);
phi = rad2deg(phi);

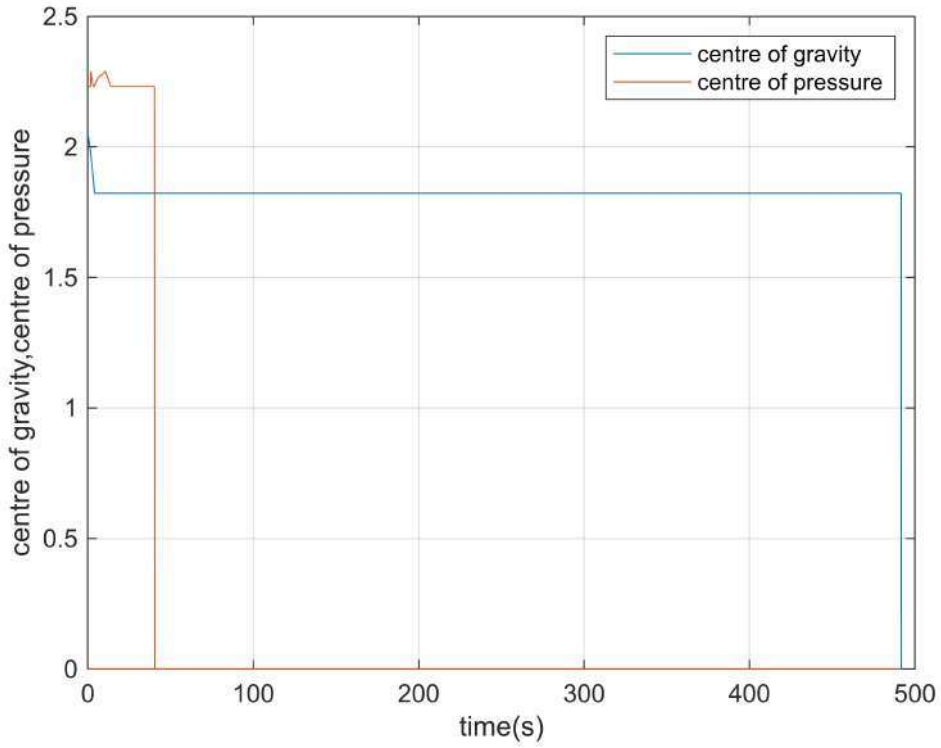
plot(timer,Mass);
hold on
plot(timer,Stab_Cal);
xlabel('time(s)');
ylabel('mass(kg),stability calibers');

grid on;
box on;
```



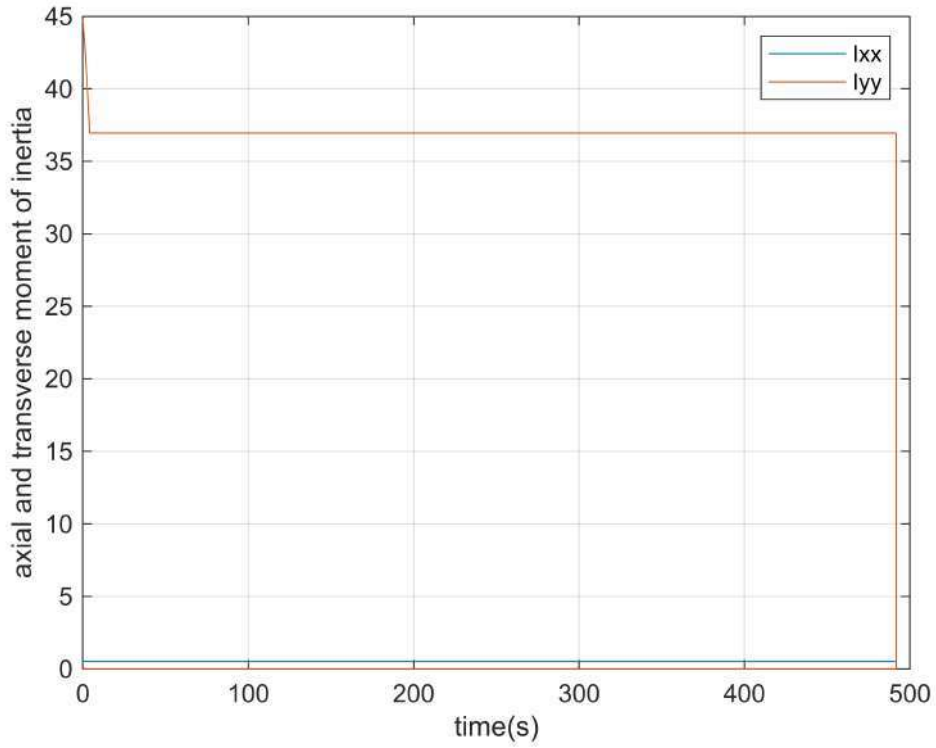

```
figure
plot(timer,CG);
hold on
plot(timer,CP);
xlabel('time(s)');
ylabel('centre of gravity,centre of pressure');
legend('centre of gravity','centre of pressure');

grid on;
box on;
```



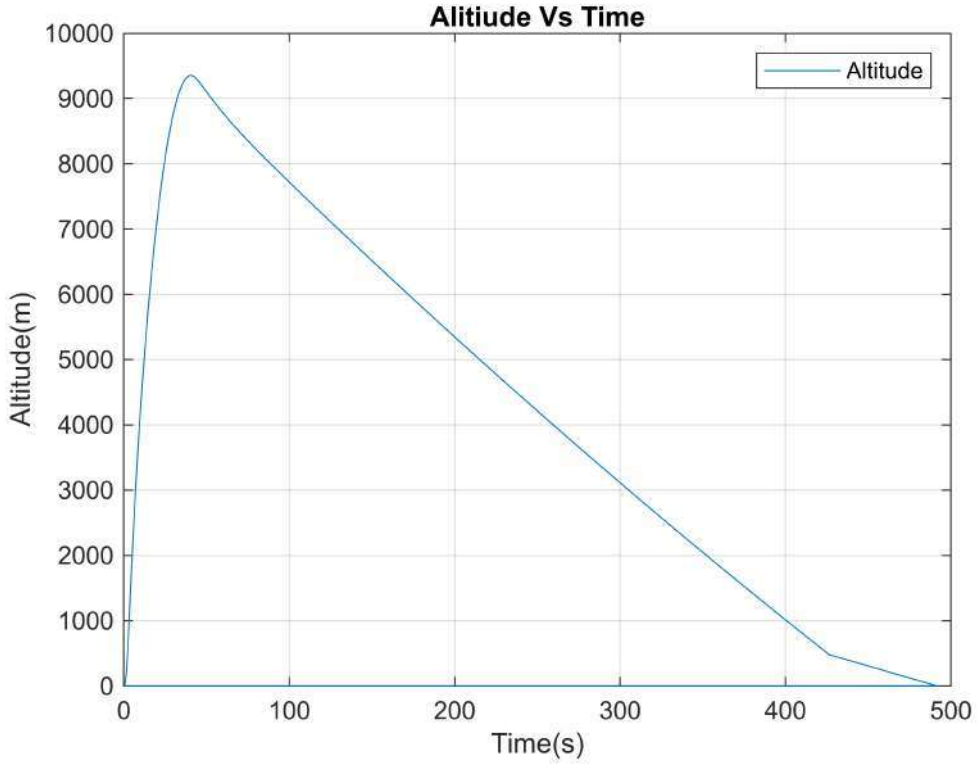

```
figure
plot(timer,Ixx);
hold on
plot(timer,Iyy);
xlabel('time(s)');
ylabel('axial and transverse moment of inertia');
legend('Ixx','Iyy');

grid on;
box on;
```



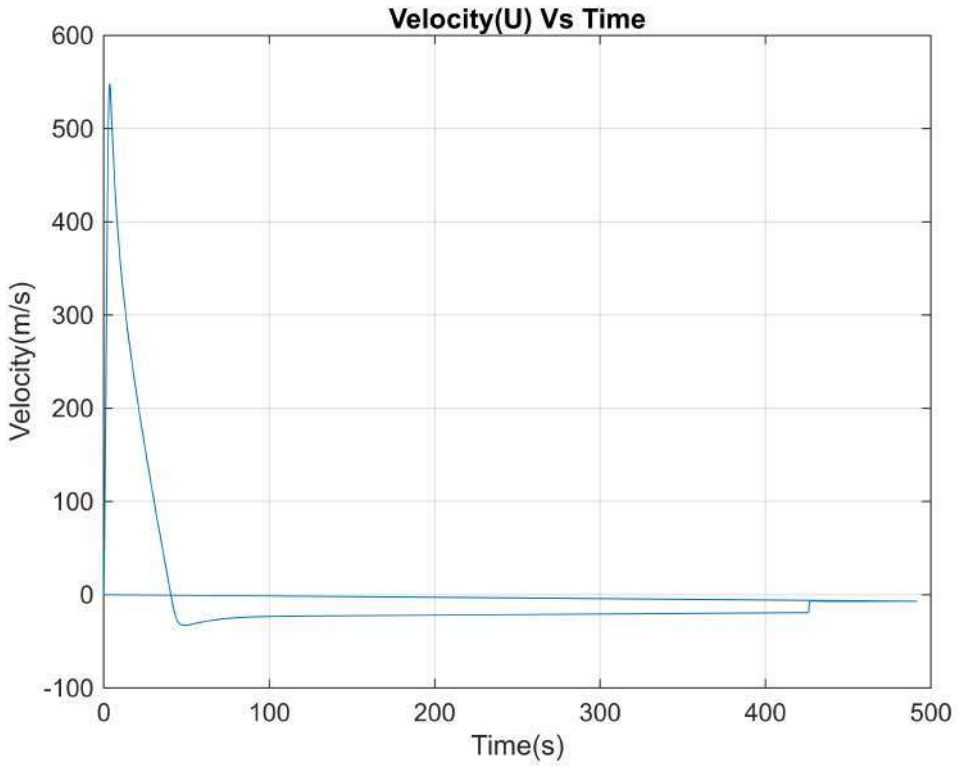

```
figure
plot(timer,Xe);
hold on
title('Alitiude Vs Time');
xlabel('Time(s)');
ylabel('Altitude(m)');
legend('Altitude');

grid on;
box on;
```



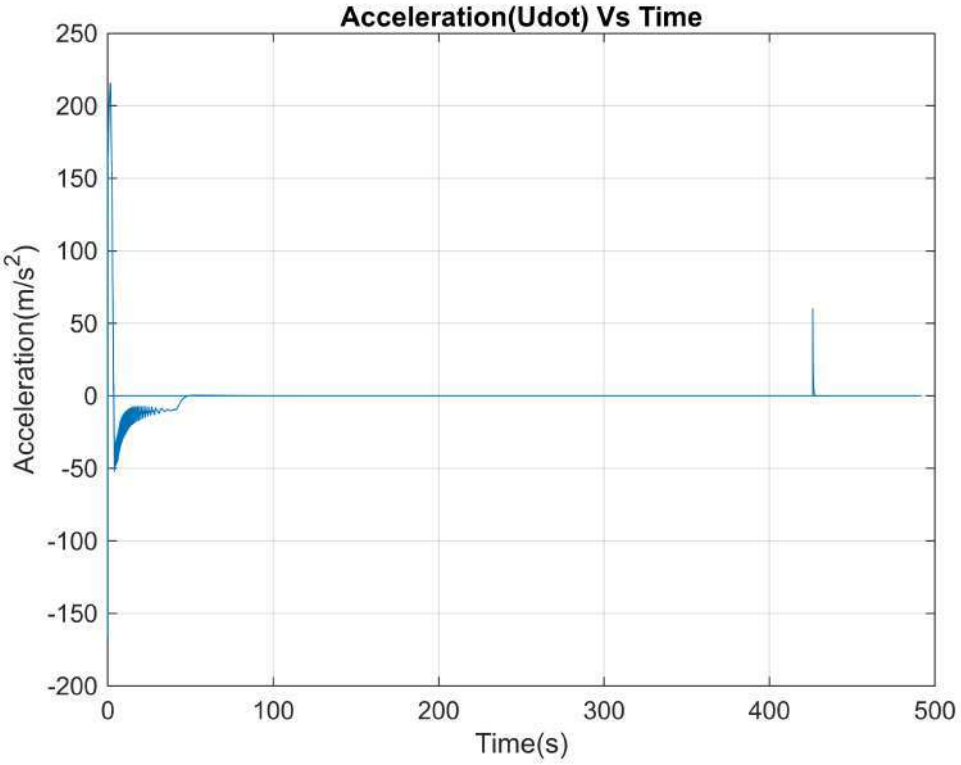

```
figure
plot(timer,u)
title('Velocity(U) Vs Time');
xlabel('Time(s)');
ylabel('Velocity(m/s)');

grid on;
box on;
```




```
figure
plot(timer,acceleration)
title('Acceleration(Udot) Vs Time');
xlabel('Time(s)');
ylabel('Acceleration(m/s^2)');

grid on;
box on;
```




```
figure
plot(timer,theta)

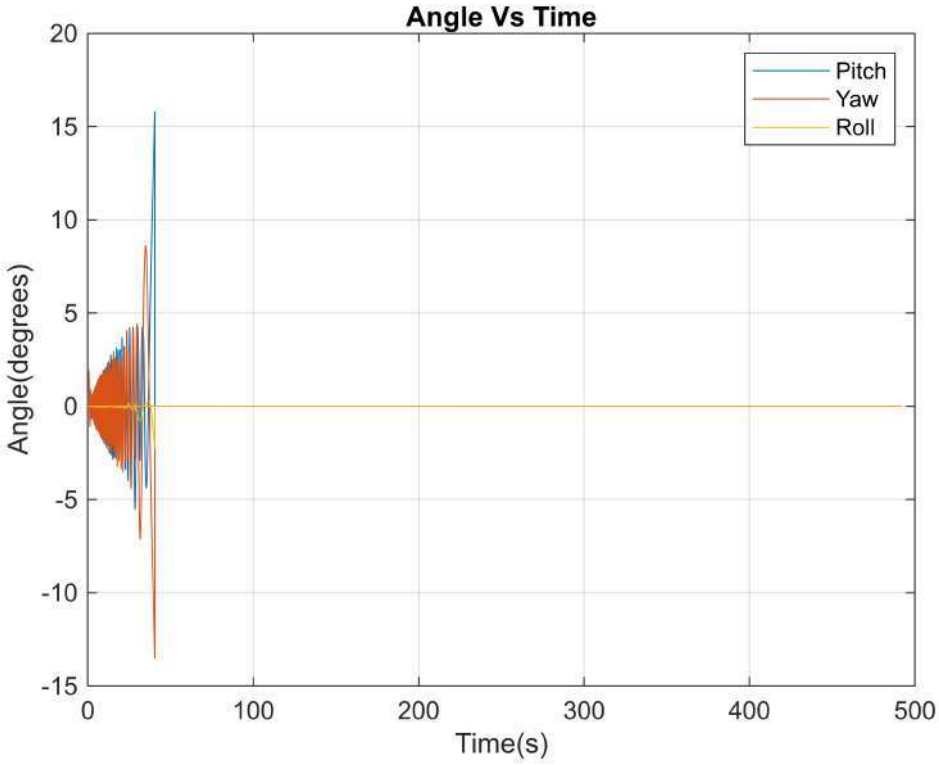

hold on

plot(timer,psi);

hold on

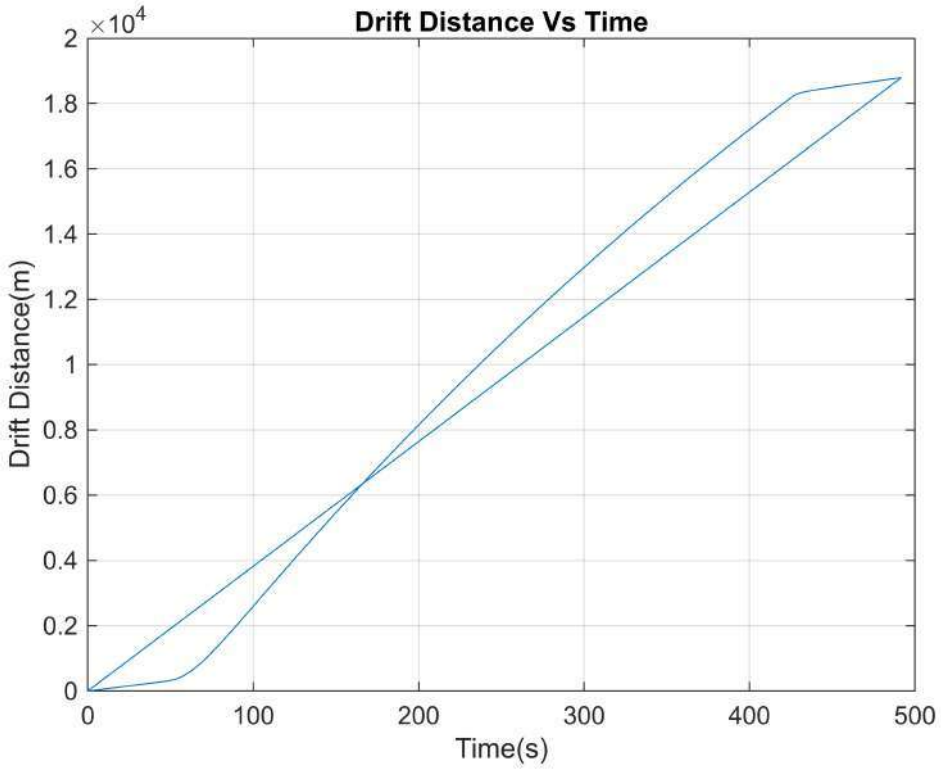
plot(timer,phi);
title('Angle Vs Time');
xlabel('Time(s)');
ylabel('Angle(degrees)');
legend('Pitch','Yaw','Roll');

grid on;
box on;
```



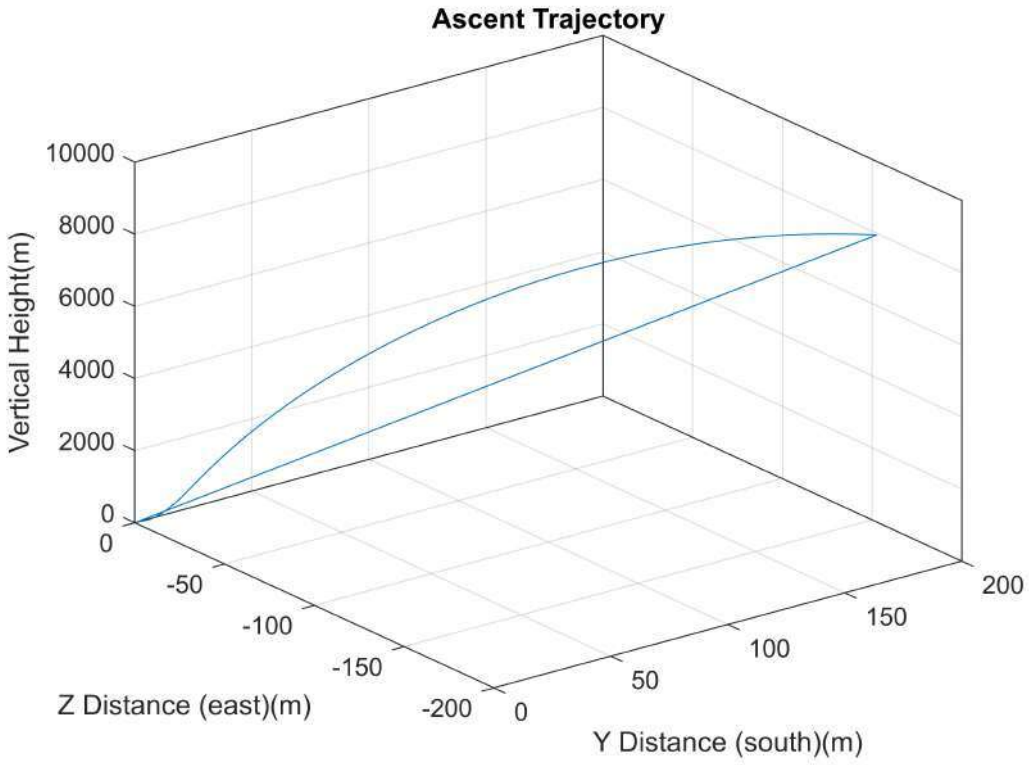

```
figure
plot(timer,drift)
title('Drift Distance Vs Time');
xlabel('Time(s)');
ylabel('Drift Distance(m)');

grid on;
box on;
```



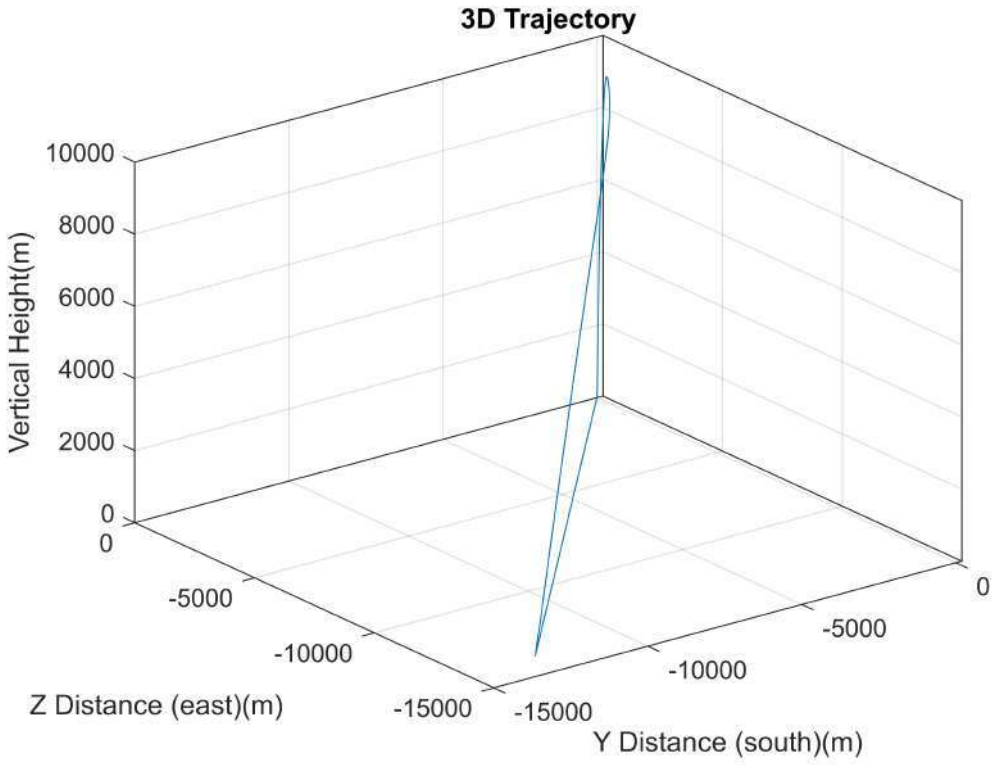

```
figure
plot3(vtrajectory(:,2),vtrajectory(:,3),vtrajectory(:,1))
title('Ascent Trajectory');
xlabel('Y Distance (south)(m)');
ylabel('Z Distance (east)(m)');
zlabel('Vertical Height(m)');

grid on;
box on;
```




```
figure
plot3(Ye,Ze,Xe)
title('3D Trajectory');
xlabel('Y Distance (south)(m)');
ylabel('Z Distance (east)(m)');
zlabel('Vertical Height(m)');

grid on;
box on;
```




```
a = max(acceleration);
b = max(u);
c = max(Xe)*3.281;
fprintf('The max acceleration is: %f m/s^2 \n',a);
```

```
The max acceleration is: 226.797992 m/s^2
```

```
fprintf('The max velocity is: %f m/s \n',b);
```

```
The max velocity is: 570.990679 m/s
```

```
fprintf('The apogee is: %f Feet \n',c);
```

```
The apogee is: 30093.897517 Feet
```

N. Appendix: Apogee Detection

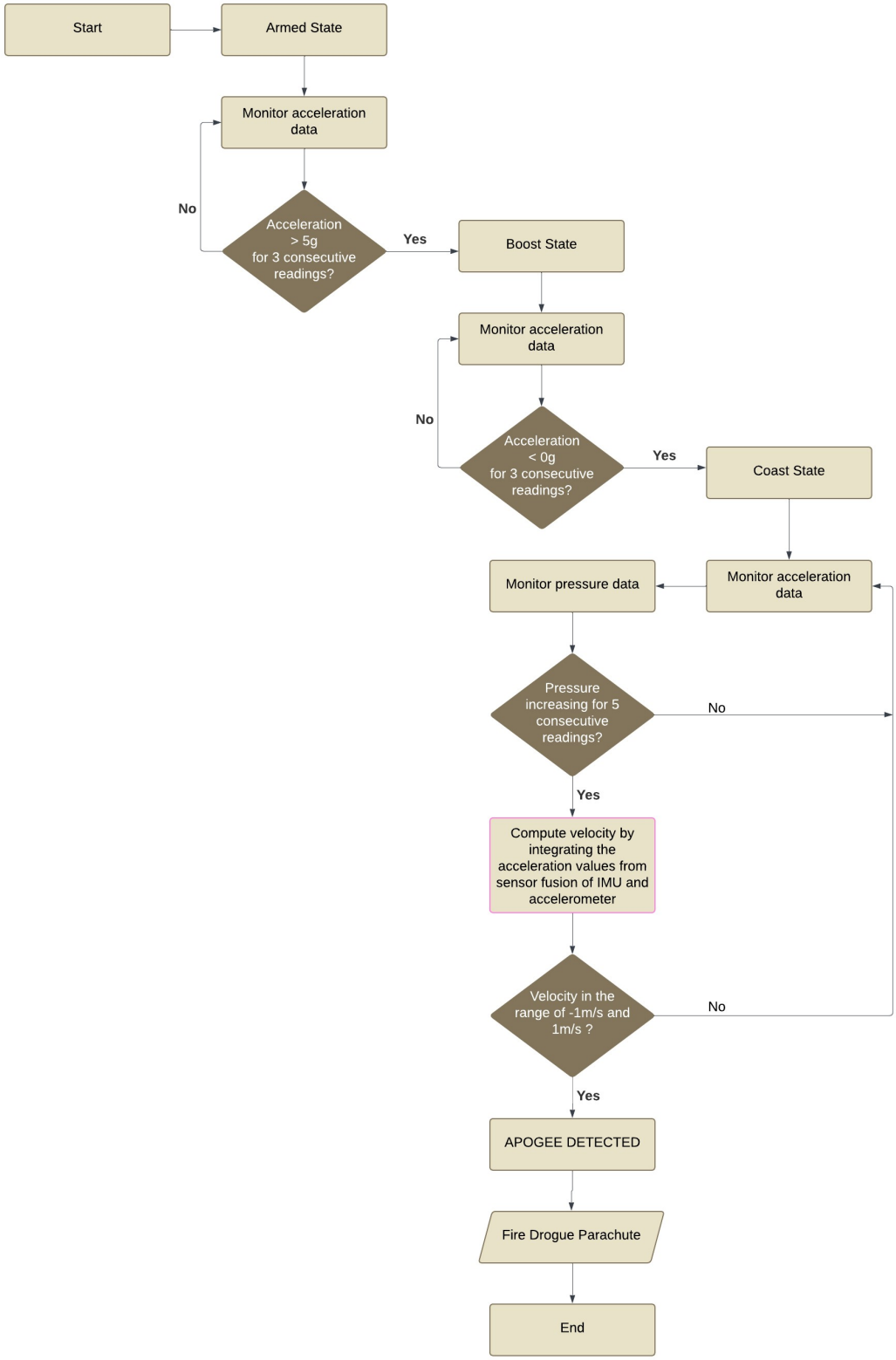


Figure 243 Flowchart for Apogee Detection and Mission Events

O. Previous Progress Reports

THIS PAGE INTENTIONALLY LEFT BLANK.
APPENDIX O BEGINS ON THE FOLLOWING PAGE.



Please note: This is a draft of your entry and is only visible to you. You may return to edit this draft at any time from the main challenge page. Once you have finished and are ready to submit your final entry, click the "Submit entry" button to submit it for judging.

Preview

Edit Submit entry

thrustMIT, Manipal Institute of Technology

Introduction

Title

thrustMIT - 1st Interim Project Report



Eligibility

Choose Your Team
207 Manipal Institute of Technology

University City/Province and Country
Manipal, State of Karnataka, India

Rocket/Project Name
Vayuvega

Category
30k - COTS

Student Lead
Satvik Agrawal / teamleader@thrustmit.in / +91 8920873563

Alternate Student Lead
Geethika Sree Ravu / team.manager@thrustmit.in / +91 9989973265

Faculty Advisor
Dr. Srinivas G / srinivas.g@manipal.edu / +91 8123677706

Alternate Faculty Advisor
N/A

Mailing Address for Awards

Manipal Academy of Higher Education
Manipal Edu Building
Manipal Campus
Manipal - 576104
Udupi, Karnataka
India

Team mentor

Mr. Bob Schoner, TRA #04928, L3, bschoner56@vt.edu, +1 540 231 1457
Mr. Bob Schoner is the Manager of the Aerospace Engineering Design Lab (AEDL) at Virginia Tech University.

Flyer of record

Mr. Bob Schoner, TRA #04928, L3, bschoner56@vt.edu, +1 540 231 1457

Social Media Site(s)

Web page URL - https://www.thrustmit.in/
Facebook - https://www.facebook.com/thrustMIT/
Instagram - https://www.instagram.com/thrustmit/
LinkedIn - https://www.linkedin.com/company/thrustmit
Youtube - https://www.youtube.com/@thrustmit/

Identify the previous IREC competition(s) your team competed in?

2018
2019
2021 (Virtual)
2022
2023
2024

Rocket Information

PLEASE ENTER NUMERIC DATA ONLY! Use periods as decimal separator (e.g., 14.2 not 14,2) Overall rocket parameters

Vehicle Length (meters)

3.45

Airframe Diameter (mm)

126

Number of fins

4

Fin Semi-span (mm)

97

Fin attachment

The rocket incorporates aluminium 6061 hexagonal fins with a half-wedge angle between 25-30 degrees. CFD simulations are currently being done to optimize the fins to decrease the drag. The fins are welded directly to the stringers. The stringers are attached to the thrust plate, 2 Centering rings through bolts. The stringer is 5mm thick (0.196 inches).

The fins possess the following dimensions:
Height: 97mm (3.819 inches)
Root Chord: 250mm (9.843 inches)
Tip Chord: 40mm (1.575 inches)
Sweep Angle: 59 degrees
Thickness: 4.32mm (0.17 inches)
Sweep length: 162 mm (6.364 inches)

The fin tab measures:
Height: 7mm (0.276 inches)
Length: 250mm (9.834 inches)

This method of attachment was successfully employed in our previous rockets, which involved welding the fins directly to the stringers, ensuring both structural strength and ease of assembly.

Fin Flutter Analysis

The fin flutter formula yielded a flutter velocity significantly higher than the rocket's maximum velocity. Additionally, AeroFinSim was used to compute both fin flutter and divergence velocities. The calculated fin flutter velocity is 1121.95 m/s and the divergence velocity is 838.82 m/s, both exceeding our rocket's maximum velocity of 572 m/s by a factor of 1.84.

Various iterations have been performed over the fin dimensions for the best possible combination of the drag, fin flutter velocity and divergence.

Vehicle Weight (kg)

15.332

Empty motor case/structure weight (kg)

7.004

Propellent weight (kg)

9.779

Payload weight (kg)

5.3

Liftoff weight (kg) - should equal all weights

37.415

Static Stability (Calibers)

3.12

Rocket construction narrative/ additional information

The design iterations for this year's rocket began with improving upon the 2024 SA Cup entry, AgniAstra. We identified specific issues and failures that occurred during the assembly and flight to brainstorm solutions that align with ease of assembly and manufacturability.

To improve upon the structural integrity of the 2025 entry, we derived the factor of safety of the body tubes of our previous entry, using an in-house developed calculator for deriving the stress faced during the flight and will be doing the same for this year's entry. To mirror our flight loads, we are adding the drag force faced at each instant along with other fundamental flight loads and we expect this to match our actual flight load profile.

Our solution to improve upon the factor of safety is to increase the thickness of our body tubes to 0.098 inches (2.5mm). This can be validated through compressive tests and three-point bend tests till failure as we progress through manufacturing for both Carbon Fiber Reinforced Polymer (CFRP) and Glass Fiber Reinforced Polymer (GFRP).

The configuration of the rocket involves a nosecone, 3 bays connected with 2 couplers, ending with a boattail. Beginning from the top:

NOSECONE WITH PAYLOAD

To be manufactured from CFRP, this will house the payload along with an Aluminium 6061 bulkhead. Taking the cansat configuration, it will sit

atop the bulkhead and stay integrated. The configuration is designed with assembly and quick dismount in consideration. The nosecone tip will be fastened with a steel threaded rod connected to the top plate of the cansat. The nosecone will be connected to the main bay with the shoulder.

MAIN BAY

To be manufactured from GFRP, it will hold the main parachute and its respective shockcords connected to the steel eyebolts on bulkheads on both ends. The bay will be joined rigidly on one side using bolts fastened to the nosecone bulkhead and the other end with nylon shear pins to the avionics coupler.

AVIONICS COUPLER

To be manufactured from GFRP, bordered with one of both the recovery bulkheads (aluminium 6061) of main and drogue parachutes. The electronic components shall be securely fixed onto a reliable mounting manufactured from PLA or ABS. This mounting shall be supported with four steel threaded rods connected to both bulkheads.

DROGUE BAY

To be manufactured from GFRP; will house the drogue parachute and its respective shock cords similar to the main bay. Shear pins are to be employed to hold the drogue bay in place till recovery.

DROGUE-MOTOR BAY COUPLER

The previous rocket saw a failure at this juncture as the bending moment was concentrated here. The idea is to manufacture this in aluminium 6061 to battle that issue. The assembly-oriented design includes an integrated thrust plate. An option of either integrated centering extrusions or a step in the coupler to perform the same task, is to be decided considering manufacturability. The thrust plate shall also hold one of two rail buttons in place.

MOTOR BAY

To be manufactured from CFRP; will house the thrust plate from the coupler's side, the rocket motor positioned by two centering rings and the retainer. The two centering rings will form the foundation for the fin attachment as explained above with the stringers. One of the centering rings will hold the rail button. The retention mechanism chosen is a

threaded retainer; this will be fastened onto a step integrated onto the centering ring forming a secure joint in the bottom. All motor bay components to be manufactured in aluminium 6061.

BOATTAIL

It is to be manufactured in aluminium 6061. The boattail shall have end slots to allow fins to sit into its attachment mechanism. Bolts securely hold it in place along with the motor bay.

Propulsion System

For 2-stage projects - Use the following fields to describe the booster. Add sustainer information in the Propulsion Narrative field. Cluster Projects - Use the following fields to describe the largest one of the motors and provide the same level of detail in the Propulsion Narrative for additional motors.

Propulsion Type

Solid

COTS or SRAD

COTS

Propulsion Manufacturer

Aerotech

COTS Motor - Manufacturer Designation

AeroTech O5500X-PS

Motor Letter Classification

O

Average Thrust (N)

5514.6

Total Impulse of all Motors (Ns)

21384

Motor Burn Time (s)

4.03

Propulsion Narrative

COTS Solid, 1st Stage, Aerotech, O, 21384 Ns, 5,514.6 N

Our team opted for the Aerotech O5500X-PS motor for our participation in the IREC 2025 rocketry competition. The selection of this specific motor can be attributed to its alignment with the prescribed impulse class suitability for the 30K Commercial Off-The-Shelf (COTS) category. The motor's availability ensures that we can readily procure the required components, minimizing potential logistical challenges in our preparation for the competition.

Switches and Arming Electronics

Wiring diagram (Required)

WIRING_DIAGRAM_VAYUVEGA.pdf

Switches

Arming the device is done by mechanical pull-pin switches. The switches used are the Omron SS-5G. Two of these pull–pin switches will be used, each having two circuit connections. This means one switch can control two circuits.

In this, one switch will control the power for SRAD electronics and COTS GPS. The other switch will control the power for COTS and the arming of the pyro batteries for SRAD and COTS. In summary,

PULL-PIN SWITCH 1 CONTROLS:
SRAD Flight Computer Power for: 3.3V, 5V power line

PULL-PIN SWITCH 2 CONTROLS:
- COTS Altimeter and COTS GPS Power
- Pyro Ejection Circuit

The switches are Normally Open. It is open when the mechanical “pin” is still in. When the pin is pulled, the circuit is made, arming the on-board electronics. Both switches together control the power and arming of avionics in the rocket.

Redundancy

The recovery electronics have COTS and SRAD components for redundancy. The two altimeters employed are as follows:
- COTS EasyMini Altimeter for Pyro Ejection
- SRAD Flight computer consisting of an altimeter (MS5611).

The two GPS Tracking Devices are as follows:
- SRAD Flight computer consisting of MIKROE GNSS MAX CLICK (tracking using telemetry performed by RYLR998 module operating on 900MHz)
- COTS Featherweight GPS (tracking using the app and ground station provided by the manufacturer).

Two charges each are used for main and drogue, one primary and one redundant (for each). The SRAD system will fire the primary charges while the redundant charges are fired by the COTS altimeter.

Firing of main and drogue parachutes is initiated by the following:
- MOSFET-based switches in SRAD Flight computer
- Main and Apogee terminals, EasyMini Altimeter.

The above components with adequate testing ensure redundancy in apogee detection, firing of drogue charge, main charge and recovery using GPS tracking.

Arming Sequence

The arming sequence to be followed is:

1. From a safe distance, remove the first pull-pin switch: This powers the entire SRAD flight system and it can be confirmed using a Telemetry link with the Ground station. It also arms the SRAD pyro ejection circuit (as the SRAD FC is powered, it is now able to fire the drogue and main in flight).

2. Remove the second pull-pin switch: This powers the COTS Altimeter and GPS, this can be verified as follows.
COTS Altimeter: EasyMini beeps on booting up.
COTS GPS: Verified using the phone application.

Switches and Arming Electronics Narrative

The pull-pins will be mounted in the avionics bay (location to be decided). Two circuits will be powered using one pull-pin switch. Two of these pull-pin switches will be used as described in the switches section, hence two holes in total will be made to make the pullpins accessible from the outside.
The arming can easily be performed after completing all safety checks

by sliding out the pull-pin switches and verifying them using the above-written measures.

Predicted Flight Data and Analysis

The following stats should be calculated using rocket trajectory software or by hand. Pro Tip: Reference the Barrowman Equations, know what they are, and know how to use them.

Launch Rail

ESRA Provided Rail

Rail Length (meters)

5.6

Liftoff Thrust-Weight Ratio (X:1)

15.07

Launch Rail Departure Velocity (meters/second)

43.1

Length of Rail (meters) used to calculate the Launch Rail Departure Velocity

5.24

Minimum Static Margin During Boost

1.65

Maximum Acceleration (G)

22.32

Maximum Velocity (meters/second)

572

Target Apogee (feet AGL)

30,000 ft

Predicted Apogee (feet AGL)

31037

Flight Simulation file

ORK_ VAYUVEGA.ork

Flight Profile Graph

FLIGHT_PROFILE_GRAPH_VAYUVEGA.pdf

Predicted Flight Data Narrative

The team's approach involved utilizing OpenRocket for rocket design and both OpenRocket and RASAero II for conducting simulations to predict the rocket's apogee.

In RASAero II, the Rogers-Barrowman equations are integral for predicting the rocket's aerodynamic performance. These equations consider the rocket's geometry, fin design, and other parameters to calculate vital data, such as stability margins, drag coefficients, and apogee altitude predictions. Using these equations, RASAero II provides crucial insights into how the rocket will behave during flight, ensuring more accurate flight simulations.

Integrating the Rogers-Barrowman equations enhances the software's ability to offer precise and reliable aerodynamic analysis for rockets. The apogee is currently at 31,037 feet but is expected to decrease due to changes in dimensions and the actual mass of components differing from the CAD values. The predicted values of apogee from RASAero and OpenRocket are 31,965 feet and 31,037 feet respectively. We have chosen OpenRocket's values (31,037 feet) over RASAero's, given RASAero's idealistic estimations.

RASAero's aerodynamic data is crucial for simulations and fin flutter analysis, ensuring a more accurate understanding of the rocket's performance. The team is conducting Computational Fluid Dynamics (CFD) simulations on the nose cone, fins and boat tail to enhance the overall aerodynamic efficiency.

These simulations gave precise drag values, subsequently integrated into our in-house simulator code. This ensures that the rocket is theoretically flight-ready and can achieve a more realistic trajectory. Furthermore, the team performed aeroelastic simulations on the rocket's fins to prevent fin flutter. They also performed an explicit dynamics analysis on the fin structure to ensure they remained intact upon landing.

Building on the lessons learned from our previous rockets, we have introduced a boat tail design this year to enhance performance. The boat tail, which is a tapered section at the rear of the rocket, effectively

reduces the drag acting on the vehicle by allowing the airflow to transition smoothly from the rocket body. CFD simulations are currently being performed on various boat tail sections to optimize the shape of the boat tail.

Payload Information

NOTE: To compete in the SDL Payload Challenge, you MUST follow the instructions on the IREC Documents and Forms Page. The information provided here is for ESRA purposes only. See http://www.soundingrocket.org/irec-documents--forms.html

Payload - Deployed or Attached

Attached

Deployed Payload - Deployment Mechanism

Not Applicable

Deployed Payload - Deployment Altitude (feet)

N/A

Deployed Payload - Altimeter

Not Applicable

Deployed Payload - Recovery System

Not applicable

Deployed Payload - Main Decent Rate (m/s)

N/A

Deployed Payload - GPS

Not applicable

Payload Narrative

The payload is a functional, non-deployable system housed in the nosecone of the rocket, designed to integrate advanced AI/ML technologies. It features a CANSAT equipped with a spring-mounted object on its top plate. A Raspberry Pi 5 controls a camera mounted on a dual-shaft servo motor, ensuring dynamic tracking of the object throughout the rocket's flight, from ascent to recovery.

The primary objective of this payload is to detect and track the object as it moves due to forces acting on the rocket during its journey. The servo motor, controlled by the Raspberry Pi, dynamically adjusts the camera's

position to maintain continuous focus on the object. This real-time tracking capability is achieved through advanced detection processes, which include four critical functions:

1. OBJECT TRACKING: AI algorithms analyze visual data to consistently identify and track the object throughout the mission.
2. DEPTH DETECTION: Depth maps are generated to measure the spatial position of the object relative to the camera, allowing for an accurate reconstruction of its motion trajectory.
3. EDGE DETECTION: Visual data is processed to isolate the object's contours, improving detection accuracy by minimizing background noise.
4. POSE ESTIMATION: Algorithms estimate the object's orientation and movement patterns, providing insights into how it responds to dynamic forces during the rocket's flight.

The theoretical foundation of this payload includes principles of computer vision, AI-based object recognition, and dynamic kinematics. Algorithms such as YOLO-v11 and META's Segment Anything models are currently under testing for tasks like object detection and instance segmentation, though their final implementation remains unconfirmed. The team is exploring similar algorithms for future optimization, ensuring the payload remains at the cutting edge of technology.

Beyond its immediate role, the payload demonstrates significant potential in various applications. In space exploration, it could support autonomous navigation and precise object tracking in microgravity environments. The real-time tracking capabilities also hold promise for autonomous vehicles, where accurate object detection and tracking are crucial for safe navigation. In industrial robotics, the system could enhance quick automated inspection and monitoring processes, particularly in hazardous or complex environments. A promising feature being looked into by the team is the generation of real-time 3D point clouds, which would enable detailed reconstructions of the object's structure, broadening the payload's functionality and relevance to multiple domains.

The non-deployable design of the payload ensures it remains securely operational within the rocket, safeguarding sensitive equipment while delivering high-quality data for research and development. Its

innovative combination of robust hardware and advanced software provides a reliable testbed for optimizing AI-driven detection and tracking systems.

Recovery

Describe your recovery system; dual-deploy, size and style of chute, number of chutes, length of shock cord. "Chute Release" commercial products no longer approved.

COTS Altimeter

Altus Metrum EasyMini Altimeter

Redundant Altimeter

SRAD

Drogue Primary & Backup Deployment Charges (g)

4F Black Powder, 3.5g, 4g

Drogue Deployment Altitude (feet)

31037

Drogue Decent Rate (meters/second)

28.9

Main Primary & Backup Deployment Charges

4F Black Powder, 5g, 5.5g

Main Deployment Altitude (feet)

1500

Main Decent Rate (meters/second)

9.26

Shock Cords and Mechanical Links

Kevlar, 5/8 in, 6600lb, Drogue - Eyebolt (Lower Avionics Bulkhead) & Quick link (Parachute), Quick link (Parachute) & Eyebolt (Thrust Plate). Main - Eyebolt (Upper Avionics Bulkhead) & Quick link (Parachute), Quick link (Parachute) & Eyebolt (Nosecone Bulkhead).

Flight profile Graphic

CONOPS_VAYUVEGA.pdf

Recovery Narrative

Our recovery strategy employs dual deployment utilizing two parachutes, and we plan to recover the rocket as a whole. The Drogue Bay and Main Bay are connected by the Avionics Coupler, which also functions as the Avionics Bay. The Drogue Bay is positioned aft, while the Main Bay is located at the top. The connection between the bays is secured with shear pins on the main bay and bolted with the drogue bay.

The drogue parachute is situated in the drogue bay. The drogue parachute is an eight-gore elliptical design with a 30-inch diameter deployed at apogee. The shock cord, measuring 7 meters (275.59 inches), is linked to the suspension lines through a quick link and swivel. One end of the shock cord is affixed to the thrust plate using an eye bolt. Additionally, a second shock cord, measuring 4 meters (157.48 inches), is attached to the lower avionics bulkhead via an eye bolt. The drogue aims to achieve a terminal velocity of 25-30 m/s.

The main parachute is housed in the Main Bay. It features a twelve-gore annular design with a 72-inch diameter and is deployed at 1500 feet. The shock cord, measuring 7 meters (275.59 inches), connects to the suspension lines through a quick link and swivel. One end of this shock cord is secured to the upper avionics bulkhead with an eye bolt. Additionally, a second shock cord, measuring 4 meters (157.48 inches), is attached to the nosecone bulkhead via an eye bolt. The main parachute is targeted to achieve a terminal velocity of 9-11 m/s.

Both the drogue and main parachutes will be protected using Nomex Blankets. Ejection will take place using COTS 4F Black Powder. The Upper and Lower Avionics Bulkheads each incorporate two charge wells: one for the primary charge and one for redundancy. The SRAD altimeter will initiate the primary charge while the COTS altimeter (Altus Metrum EasyMini) will initiate the redundant charge.

The SRAD flight computer consists of a barometric pressure sensor (MS5611) used to detect the apogee. As the rocket ascends, pressure decreases. After the rocket reaches its apogee, the pressure recorded by the sensor starts increasing. The drogue is fired when the pressure sensor detects this change in the pressure gradient. The main is fired at a preset altitude of 1500 feet, calculated from the pressure values recorded using lookup tables.

GPS Tracking

Reference: IREC GPS Tracking Requirement and Recommendations

GPS Tracker Manufacturer

Featherweight GPS

Wavelength Band / Frequency Range

33 cm / 902 - 928 MHz

GPS Tracker Narrative

The COTS Featherweight GPS is used as a primary tracking device for the rocket. Featherweight phone application is used to interface with the tracking device along with the ground station.

The secondary/redundant tracking device is the Mikroe GNSS MAX CLICK module which tracks the rocket, and the coordinates obtained by this are sent using the telemetry link (915MHz) to the ground station.

Test Plan

Please include all systems

Planned Tests

[Oct 26, 2024] Ground (Completed) - Performed Surface roughness tests on various test articles using a surface profilometer to obtain data for flight aerodynamics.

[Oct 29, 2024] Ground (Completed) - Test drogue and main ejection mechanisms of EasyMini COTS Altimeter.

[Nov 07, 2024] Ground (Completed) - Test the Ground Station Data Plotter to analyze SRAD GPS and telemetry capabilities.

[Nov 10, 2024] Ground (Completed) - Conduct a Dual Deployment Test to validate proper bay separation and ensure the intended release of the parachutes.

[Nov 14, 2024] Ground (To be done) - Conduct compressive tests on in-

house manufactured composite body tubes to experimentally determine their strength, under axial loading conditions.

[Nov 15, 2024] Ground (Completed) - Initial Dataset Collection using the OpenMV Camera, capturing various augmented and diversified images for model training.

[Nov 21, 2024] Ground (To be done) - Test performance and power consumption of the first iteration of SRAD Flight Computer.

[Nov 28, 2024] Ground (Completed)- Test the power output of Li-ion battery packs to ensure a stable power supply is provided throughout expected uptime.

[Nov 30, 2024] Ground (To be done) - Spring Vibration Testing at the Institute Vibrational Lab to assess spring response and behaviour under simulated vibrational forces.

[Dec 05, 2024] Ground - Test the inflation of the Main Parachute using a pilot and parachute liner. This will be done with the assistance of a vehicle (back of a car).

[Dec 08, 2024] Ground - Test SRAD Flight Computer to gauge the hardware requirements for real-time flight data logging.

[Dec 10, 2024] Ground - Spring G-Force Testing at the Structural Dynamics Lab, examining the spring's behaviour under increasing g-forces for performance validation.

[Dec 15, 2024] Ground - IMU Algorithm Testing at the Dynamics and Control Lab for validating the 9-axis IMU activation sequence required immediately after payload launch.

[Dec 20, 2024] Ground - Test range of SRAD telemetry system paired with antennas to confirm a range of 10 Km. Testing will be done inside an appropriate body tube to recognise any signal attenuation caused.

[Jan 05, 2025] Ground - Servo Latency Testing to evaluate servo response times and optimize latency for effective object tracking.

[Jan 20, 2025] Ground - Point Cloud and Segmentation Algorithm Testing focused on developing point clouds through estimated depth maps, pose estimation, instance segmentation, and object detection.

[Jan 31, 2025] Ground - Li-ion Battery Drain Test to ensure reliable battery performance within specified environmental and operational durations, including necessary buffer periods.

[Feb 01, 2025] Ground - Assemble the entire rocket to ensure proper fitting of all parts.

[Feb 06, 2025] Ground - Assemble Avionics Bay and perform integrated testing of both SRAD and redundant COTS electronics.

[Feb 07, 2025] Ground - Integrated Payload Vibration Testing at the Institute Vibrational Lab, testing the entire payload setup under vibration to assess component integrity and performance.

[Feb 12, 2025] Ground - Perform integrated Dual Deployment test with the entire rocket assembled.

[Feb 28, 2025] Flight - Subscale Launch.

We are actively engaged in securing the necessary permissions to proceed with the launch of a subscale rocket. Efforts are underway to navigate the regulatory requirements, ensuring compliance to facilitate the launch.

Media

Team Video Challenge Participation

Yes

Live Rocket Video Challenge Participation

Yes

Onboard Footage Submission

Yes, recorded 1080p

Additional Comments

Any other pertinent information

Our team's focus has been dedicated to designing a rocket capable of reaching the 30K objective. Extensive efforts have been made to incorporate learnings from previously developed rockets through improvements in aerostructure design and recovery mechanisms.

Our endeavors extend beyond the 30K feet target; we are concurrently engaged in developing an SRAD motor for future missions. Our recent milestone was the successful static fire testing of our SRAD J-class and M-class KNSB-based rocket motors. The success of these tests provided us with insightful data, and experience in conducting static fire tests and developing data acquisition systems.

Additionally, our Application Reviewer had raised some questions regarding our application entry; here are the detailed responses to the same:

1. STRUCTURE:
The design iterations for this year's rocket build on lessons learned from our 2024 SA Cup entry, AgniAstra. Following an in-depth analysis of its assembly and flight performance, we identified specific issues and failure modes, focusing on solutions that enhance ease of assembly, manufacturability, and structural integrity.

To ensure the structural integrity of the 2025 entry, we are conducting compressive tests on in-house manufactured body tubes and will supplement these with three-point bend tests to failure. This testing will be performed on Carbon Fiber Reinforced Polymer (CFRP) and Glass Fiber Reinforced Polymer (GFRP) specimens. By diversifying our testing methods, we aim to capture a comprehensive understanding of our materials' behavior under different load conditions.

We are using an in-house developed calculator to derive the stress experienced by the body tubes during flight. This tool factors in aerodynamic drag, inertial loads, and other fundamental flight forces to simulate a complete flight load profile. To validate that the expected flight loads closely match the competition flight profile, we are incorporating aerodynamic drag forces at each instant of the flight into

our load calculations. This iterative approach ensures that our predictions align with real-world conditions, and deviations will be reconciled through a combination of simulation refinements.

To improve the factor of safety, we are increasing the thickness of our body tubes to 0.098 inches (2.5 mm) this year, balancing structural robustness and weight considerations.

The factor of safety for the design is calculated based on the maximum expected flight loads derived from simulations and validated through physical testing. The aim is to ensure a minimum safety factor of 2, minimizing the risk of structural failure during flight.

2. ELECTRONICS:
Our team plans to flight-test our SRAD electronics through a subscale launch. We have not flight-tested this unit before. Also, we are relying on range tests to confirm the stability of our telemetry link at higher altitudes.

We will be using Lithium-ion 18650 battery cells for powering and recovery (higher C rating). These batteries have a cylindrical form factor with metallic casing and two will be used in series using a commercially purchased battery holder to power our electronics. A total of 4 of these Battery holders will be used in our rocket, which are,
- SRAD power x 2
- COTS recovery + powering
- SRAD recovery

Additionally, we will be using recommended batteries to power the COTS Featherweight GPS.

To summarize, the avionics bay consists of the following components.
- SRAD Flight computer (SRAD PCB and components, 2 antennas described below)
- Altus Metrum EasyMini COTS Altimeter
- Featherweight COTS GPS tracker with antenna + recommended battery
- 2 x Omron SS-5G pull-pin switches (each with two controllable circuit connections)
- 4x battery holders, each with 2 x Li-ion 18650 batteries.

There are two components using antennas in the SRAD electronics. The RYLR998 and the GNSS MAX Click. Only the RYLR helical antenna is used for telemetry, and it operates on 900MHz which does not require an Amateur Radio License. The GNSS uses an omnidirectional antenna operating on the standard GPS frequency of 1575MHz. The COTS GPS tracker also has an antenna installed by the manufacturer.

Edit Submit entry

× Delete this entry

ABOUT HEROX

About Us
Press Kit
Partner With Us
Partners
Careers
Privacy
Terms
Cookie Policy

COMMUNITY

Blog
Organizations Involved
Events & Webinars
Community
General Forums

SUPPORT

Contact Us
How HeroX Works
Knowledge Base
FAQ
Innovation Resources



© Copyright HeroX 2024

Was this page helpful?

○ Yes ○ No



Thanks for submitting your entry for the International Rocket Engineering Competition 2025, we've got it safe and sound.

Good luck!

Submission

Return to editing

thrustMIT, Manipal Institute of Technology

Introduction

Title

Team 207 - 2nd Progress Update Report



Eligibility

Choose Your Team
207 Manipal Institute of Technology

Category
30k - COTS - All Propulsion Types

Category Change
No

Student Lead(Name, Email, Phone number)
Satvik Agrawal / teamleader@thrustmit.in / +91 8920873563

Alternate Student Lead(Name, Email, Phone number)
Geethika Sree Ravu / team.manager@thrustmit.in / +91 9989973265

Faculty Advisor(Name, Email, Phone number)
Dr. Srinivas G / srinivas.g@manipal.edu / +91 8123677706

Alternate Faculty Advisor(Name, Email, Phone number)
N/A

Team mentor (Name, Email, Phone number)
Mr. Bob Schoner, TRA #04928, L3, bschoner56@vt.edu, +1 540 231 1457; Mr. Bob Schoner is the Manager of the Aerospace Engineering Design Lab (AEDL) at Virginia Tech University.

Flyer of record (Name, TRA Number, email, phone)

Mr. Bob Schoner, TRA #04928, L3, bschoner56@vt.edu, +1 540 231 1457

Flyer of Record Status

Will be attending the IREC

Is a current Tripoli L3 certified flyer (Using M, N, or O Motor)

Demographic Data

This is all members working with your project including those not attending the event. This will help ESRA promote the event and get more sponsorships and grants to help the teams improve the event.

Any changes to the team composition since the last report?

Number of Undergraduate Team Members: 36

Number of Team Members who identify as Men: 29 (Previously 30)

Number of Team Members who identify as Women: 7

Visa Status

4 of our attending team members already have US VISAs, and one has US Citizenship. The remaining 7 members have Group VISA Appointments scheduled in the second week of April. We are optimistic about the outcome and hope to get our VISAs soon.

Rocket Information

USE NUMERIC DATA ONLY. DO NOT INCLUDE UNITS WITH YOUR RESPONSE. ALL DATA SHOULD USE THE Metric SYSTEM FOR UNITS. (except where English units are requested)

Airframe Diameter (mm)

126.0

Number of fins

4

Fin Diagram with dimensions

FIN_DIAGRAM_VAYUVEGA.pdf

Fin design discussion

The selection of a trapezoidal fin shape is based on its desirable lift and stability characteristics, as well as its ability to reduce impact damage

during landings. A critical concern is the potential for fin breakage upon landing. To mitigate this risk, a hexagonal fin cross-section with a 0.5 mm tip fillet radius was chosen keeping in mind the manufacturing constraints. Fin dimensions were carefully selected, considering stability, fin flutter and apogee. The thickness ranges from 4 mm to 4.7 mm, and the halfwedge angle varies from 5 to 25 degrees, balancing aerodynamic efficiency with structural integrity. Various fin parameters, including fin height, thickness, root cord, tip cord, and sweep angle, were rigorously simulated using tools such as Finsim, RASAero II and ORK. These simulations provided valuable insights: reducing the root cord decreased stability and increased fin deflection while reducing the tip cord resulted in both higher fin deflection and apogee. Additionally, increasing the fin thickness and half-wedge angle led to increased drag. Following these simulations, Fluid-Structure Interaction (FSI) simulations are being conducted for all fin iterations.

The primary objective is to attain a fin design that effectively minimizes drag while ensuring minimal tip deflection. It is noteworthy that potential adjustments within the ranges of 4.3-4.6 mm for thickness and for the semi-span of the fin in the range of 9.2-10 cm remain feasible for future optimization efforts.

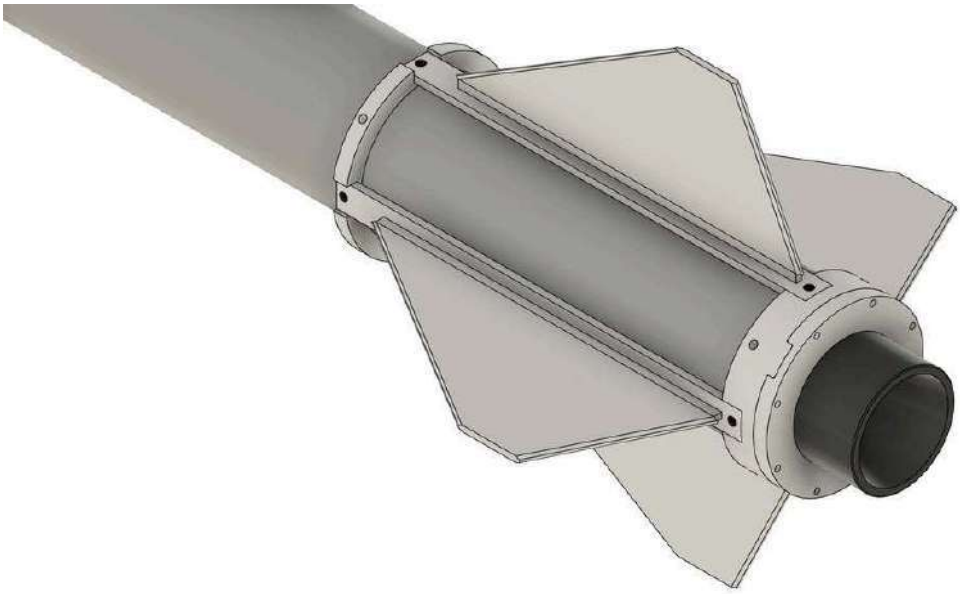
This fin design represents a careful balance of aerodynamic efficiency, structural integrity, and manufacturability, aligned with the overall objective of achieving optimal performance in terms of minimizing drag and tip deflection.

Fin attachment

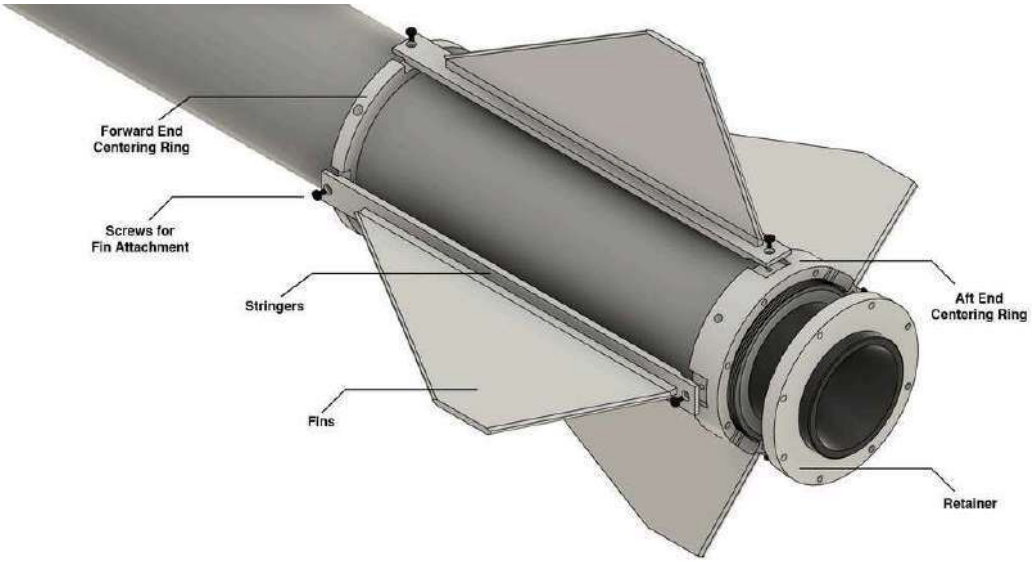
The rocket employs metal fins, manufactured using Aluminium 6061, for this year. The team have decided to opt for the trusted Fin-Stringer attachment, that has withstood previous flights from our team. Four of the fins, each separately, are welded onto four Aluminium 6061 stringers, as the first step of the attachment. These stringers have slots precisely manufactured to hold in the fin tabs, once welded. They run from the forward end centering ring to the aft end centering ring at the end of the motor bay.

These stringers, with the fins, are bolted onto the two centering rings, forming a rigid joint. This iteration gave an issue where the thread engagement of the bolts that are to be used was coming out to be short. To tackle this, the team reduced the thickness of each stringer in the ends of the centering ring, such a way that it sits on the rings with enough engagement.

As it stands now, the stringers have equal thread engagement on each centering ring and are placed in 90 degree intervals to each other.



Fin Attachment



Exploded View of Fin Attachment

This arrangement helps in the ease of the assembly of the motor bay and provides us with the structural strength to hold the fins. This attachment can be slid into the motor bay without any other complications, seamlessly.

Dimensions of the fins:

- Height: 9.85 cm (3.87 inches)

- Root Chord: 25 cm (9.84 inches)
- Tip Chord: 4 cm (1.57 inches)
- Sweep length: 17.1 cm (6.73 inches)
- Height of the tab: 1.09 cm (0.42 inches)
- Length of the tab: 25 cm (9.84 inches)

Fin Flutter Analysis

The analysis of the fin flutter revealed a flutter velocity that significantly surpasses the maximum velocity of the rocket. Both analytical methods, utilizing the fin flutter formula and AeroFinSim software, yielded consistent results. Specifically, the calculated fin flutter velocity stood at 1192.32 m/s, while the divergence velocity reached 890.37 m/s, notably exceeding the rocket's maximum velocity of 576 m/s. Furthermore, the team is conducting extensive Fluid-Structure Interaction (FSI) simulations to comprehensively assess potential fluttering behaviour. These simulations incorporated aerodynamic pressure forces and accounted for thermal effects arising from material temperature variations. The iterative process involved monitoring incremental displacements over time, generating a detailed dataset illustrating gradual displacement phenomena.

Subsequent analysis of this dataset revealed a maximum deformation of 2.66 mm. Notably, the simulation was conducted at 1.5 times the maximum speed, allowing for a thorough evaluation under varied conditions. The findings from these simulations provide critical insights into the structural integrity and performance of the rocket's fins, informing necessary design modifications to mitigate potential fluttering concerns.

Root chord (cm)	Tip chord (cm)	Height (cm)	Sweep Length (cm)	Thickness (mm)	Divergence (m/s)	Flutter velocity (m/s)	FOS divergence	FOS flutter	Deflection FinSim (mm)
24	4	9.85	17.1	0.45	905.82	1191.85	1.573	2.069	2.66
25	4	9.85	17.1	0.45	890.37	1192.32	1.548	2.074	2.65
26	4	9.85	17.1	0.45	875.72	1189.56	1.523	2.069	2.48
24	4	9.75	17.1	0.45	915.78	1203.56	1.573	2.067	2.48
25	4	9.75	17.1	0.45	899.78	1204.38	1.546	2.069	2.66
26	4	9.75	17.1	0.45	884.62	1202.19	1.522	2.069	2.67
24	4	9.55	17.1	0.45	934.25	1229.78	1.633	2.149	2.66
25	4	9.55	17.1	0.45	918.76	1229.71	1.609	2.153	2.66
26	4	9.55	17.1	0.45	903.2	1227.45	1.581	2.149	2.85

Vehicle Length (Meters)

3.46

Empty motor case/structure (kg)

7.004

Propellent weight (kg)

9.779

Payload weight (kg)

4.65

Total Vehicle Weight (kg)

37.051

Center of Gravity (mm)

2050.0

Static Margin

1.64

Couplers & Airframe joints

For an overview, all body tubes are of 12.6 cm (4.96 inches) outer diameter with a thickness of 0.25 cm (0.098 inches), giving an inner diameter of 12.1 cm (4.76 inches). The couplers and the shoulders have an outer diameter of 12.1 cm (4.76 inches) and an inner diameter of 11.6 cm (4.56 inches). The rocket consists of a nosecone, three body tubes, 2 couplers and a boattail.

Beginning from the top, the nosecone is manufactured using carbon fibre, measuring 70 cm (27.55 inches) in length with a base diameter 12.6 cm (4.96 inches). The shoulder is incorporated with an extension of the nosecone after its base diameter, such that the adhesion of the nosecone and shoulder is bolstered. This makes the shoulder stand at 21cm (8.26 inches) in total length. From the separation plane of the nose cone and the main bay, there is 13cm (5.11 inches) extension into the mating component, which is over one body tube caliber as per the IREC Design & Test Evaluation Guide. The shoulders are integrated with the body tube with the help of 12 bolts joint to the bulkhead at the end of the shoulder, forming a robust attachment of the mating components. The bolts are set at 2 layers, offsetting the stress faced on each plane. The number of bolts have been increased to 12, to tackle the shoulder tearout the team faced in the previous year, from a safer perspective.

Onto the coupler joining the main bay and the drogue bay, is the coupler that houses all electronics of our rocket. This coupler is manufactured from fibreglass, at a length of 39 cm (15.35 inches). This coupler from the main bay is securely fastened using shear pins. From the drogue bay end, the coupler is rigidly joined using 6 bolts into the recovery bulkhead.

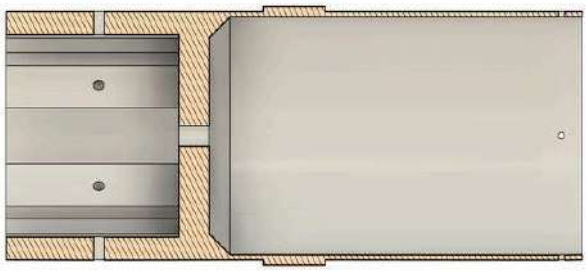
A fibreglass static band, 6cm (2.36 inches) in length, is incorporated onto the middle of the avionics coupler. This attachment slides over the

outer diameter of the coupler. This mirrors the concentric dimensions of the body tube such that its a seamless transition.

Moving on with the configuration, the motor bay coupler joins the drogue bay and the motor bay. Manufacturing this from Aluminium 6061, gives us the room for design iterations for the entire coupler design. This iteration involves the thrust plate manufactured along with the coupler, with extensions from the plate acting as a centering apparatus for the motor. This extension is designed to hold the motor precisely making sure the motor is held in place throughout the flight. The thrust plate in itself has 6 bolts holding the motor bay and the coupler, along with this there is another layer of bolts added onto the extension. This part is engineered to this extent, as the rocket faces the maximum bending moment at this location, and having learnt our lessons from the previous year. The drogue bay is held in place using shear pins onto the coupler.



Motor Bay Coupler



Section View of Motor Bay Coupler

In the bottom, the boattail shoulder, extending 12.6 cm (4.96 inches) into the mating motor bay, is manufactured from Aluminium 6061. The boattail is attached to the motor bay using 4 bolts engaging the aft end centering ring.

Rocket construction narrative/ additional information

Beginning from the top, there is:

Nosecone: This acts as the housing for the payload. The payload is in a Cansat configuration and is affixed upon the nosecone bulkhead in the end of the shoulder. This nosecone bulkhead is designed as stated above, and has a step in the end that matches the shoulder's radial dimensions. As quick dismounts of payload is required, this way the assembly is eased out to a higher extent. The tip of the nosecone is attached to a threaded rod which will be engaged by the top plate of the payload.



Nosecone Assembly

Main Bay: To be manufactured from fiberglass, it will hold the main parachute and its shockcords on each end. The method of fixing this as stated above, would be bolts on the nosecone side and with nylon shear pins on the other side to the avionics coupler.

Avionics Coupler: With recovery bulkheads (Aluminium 6061) on each end, the avionics coupler manufactured from fibreglass, will house the mounting (ABS) for the electronics and the batteries. The mount is designed pragmatically in such a way all electronics and the battery packs can rigidly hold them under vibrations and loads faced throughout the flight. The recovery bulkheads are aligned with a step in the required direction. This design also boasts of a threaded rod arrangement, running through the entire setup strengthening the integrity and the ease of assembly.

Static Band: This fiberglass component will provide the ease in drilling slots that is strategically positioned for the horizon facing camera and for accommodating the pull pin switches. It is held in place on the avionics coupler using epoxy.

Drogue Bay: This bay contains the drogue parachute along with its shockcords. Shear pins hold this bay in place till the ignition of the

charges take place.

Motor Bay Coupler: As mentioned above, this iteration has the thrust plate manufactured along with the coupler. It also includes extensions that provide centering of the motor.

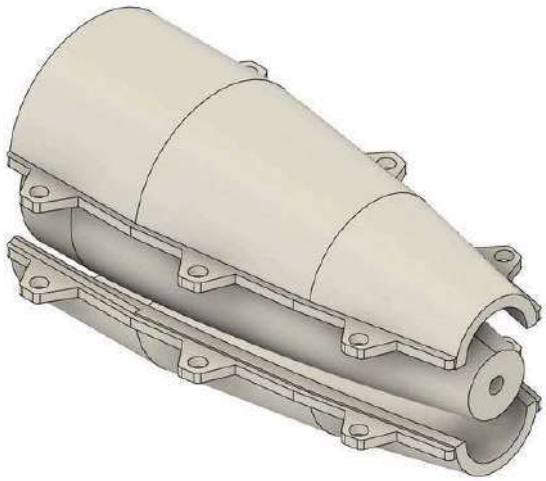
Motor Bay: Manufactured from carbon fiber, this bay houses the motor fixed in place by a bolt running through the thrust plate and the forward closure, acting as the first phase of retention. It also houses the fin assembly explained above. The fin assembly as it ends with the aft end centering ring, the retainer will be robustly attached using 8 bolts. These bolts are to be fixed on axially as radial bolting is an issue in this configuration of our assembly. The forward end centering ring and the thrust plate configuration will hold the rail buttons of the rocket. All these components are manufactured using Aluminium 6061.

Boattail: To be manufactured from Aluminium 6061, this boattail will have slots precisely manufactured such that there would be no interference with the fin tabs running through and allows for the welding beads to sit in smoothly. Further iterations will include topology optimization of the boattail shoulder.

Manufacturing Narrative

The composite body tubes and couplers are to be manufactured in-house with the help of a 3D printed moulds that are connected to fit in the size requirements. The surface is prepared by roughening using lower grit sandpaper. A layer of filler primer is sprayed to fill voids and inconsistencies and eventually even out the surface. A thin layer of even coating of resin is first applied and once cured, the surface is further smoothed using lower grit sandpaper. Release agent is applied for ease of removal and hand layup process is performed over this. The epoxy pair chosen for all composite parts is the Araldite LY5052 and Aradur 5052. The reasoning behind choosing, comes to be reliability, low viscosity, easier impregnation and long pot life and has ample processing time allowing large components to be laid up.

The moulds for nosecone also is to be 3D printed using PETG filament. The surface preparation remains the same as above. It involves 2 female moulds and a male mould for the incorporation of the shoulder. The composites to be used are 200 GSM Bi-directional Plain Woven Carbon Fibre and 450 GSM Bi-directional Plain Woven Glass Fibre with the same epoxy pair.



Nosecone Mould

Propulsion

For COTS - please provide the data supplied by ThrustCurve.org to answer the following questions.

Motor Letter Classification

O

Propulsion Manufacturer

Aerotech

Does the team already have physical possession of the motor?

No

Has the team already purchased the motor?

No

Manufacturers Designation

O5500X-PS

Motor Diameter (mm)

98.0

Initial Thrust (N)

6047

Average Thrust (N)

5514

Maximum Thrust (N)

7551.5

Total Impulse (Ns)

21384

Burn Time (s)

4.03

Propulsion Narrative

Our team has finalized the **Aerotech O5500X-PS** motor for our participation in the IREC 2025 rocketry competition, ensuring compliance with the 30K Commercial Off-The-Shelf (COTS) category requirements. The selection process involved a thorough evaluation of commercially available motors, considering factors such as total impulse and overall compatibility with our vehicle's mission objectives. The O5500X-PS was chosen for its ability to achieve the desired apogee while providing sufficient stability, accounting for the rocket's total mass. Additionally, its availability minimizes potential logistical challenges, ensuring a smooth preparation process for the competition.

Note:

We have already purchased the motor from Offwego Rocketry. Although we do not have physical possession of the motor, Mr Gary has assured us that he will bring the motor to the SA Cup itself, ensuring its availability for our competition launch.

SRAD Solid

This section is only filled out by teams using an SRAD Solid motor.

Maximum Pressure (psi)

0

Initial Kn

0.0

Peak Mass Flux

0.0

Predicted Flight Data and Analysis

The following stats should be calculated using rocket trajectory software or detailed hand calculations. Recommended software: RockSim, OpenRocket, RASAero II

Launch Rail

ESRA Provided 17' Rail

Rail Length (feet)

17.0

Liftoff Thrust-Weight Ratio (X:1)

15.22

Launch Rail Departure Velocity (meters/second)

41.8

Maximum Acceleration (G)

22.55

Maximum Velocity (meters/second)

575

Predicted Apogee - meters above ground level (AGL)

9281

Flight simulation file

ORK_VAYUVEGA.ork

Flight Profile Graph

FLIGHT_PROFILE_GRAPH_VAYUVEGA.pdf

Predicted Flight Data Narrative

The team's approach involved utilizing OpenRocket for rocket design and both OpenRocket and RASAero II for conducting simulations to predict the rocket's apogee. In RASAero II, the Rogers-Barrowman

equations are integral for predicting the rocket's aerodynamic performance. These equations consider the rocket's geometry, fin design, and other parameters to calculate vital data, such as stability margins, drag coefficients, and apogee altitude predictions. Using these equations, RASAero II provides crucial insights into how the rocket will behave during flight, ensuring more accurate flight simulations.

Integrating the Rogers-Barrowman equations enhances the software's ability to offer precise and reliable aerodynamic analysis for rockets. The apogee is currently at 30,451 feet but is expected to decrease due to changes in dimensions and the actual mass of components differing from the CAD values. RASAero and OpenRocket show close values, with RASAero at 30,851 feet and OpenRocket at 30,451 feet. We've chosen OpenRocket's values over RASAero's, given RASAero's idealistic estimations. Our aim is to slightly undershoot RASAero's projections. RASAero's aerodynamic data is crucial for simulations and fin flutter analysis, ensuring a more accurate understanding of the rocket's performance. The team has conducted Computational Fluid Dynamics (CFD) simulations to enhance the predictions' accuracy. These simulations gave precise drag values, subsequently integrated into our in-house simulator code.

By leveraging machine learning algorithms and incorporating a six degrees-of-freedom (6DOF) model, we have further enhanced the accuracy of our simulations. This comprehensive approach ensures that our rocket is not only theoretically flight-ready but also capable of achieving a highly realistic trajectory under various operating conditions. Additionally, continuous validation and refinement of our simulation models contribute to maintaining the highest standards of accuracy and reliability in our predictions.

Building on the lessons learned from our previous rockets, we have introduced a boat tail design this year to enhance performance. The boat tail, which is a tapered section at the rear of the rocket, effectively reduces the drag acting on the vehicle by allowing the airflow to transition smoothly from the rocket body. CFD simulations are currently being performed on various boat tail sections to optimize the shape of the boat tail.

Switches and Arming Electronics

Wiring diagram (Required)

WIRING_DIAGRAM_VAYUVEGA.pdf

Switches

The electronics of COTS and SRAD are armed using a total of 5 mechanical limit switches, the OMRON SS-5GL. These switches are rated to withstand the high G loads that rockets experience. The team will use 5 pull-pin switches out of which 3 will be individual/ single pull-pins and the remaining 2 switches will be paired in a series combination and will be armed with only 1 pin, the exact circuitry concerned with each switch is shown in the wiring diagram and described in detail in the “Switching and Arming Electronics Narrative” section.

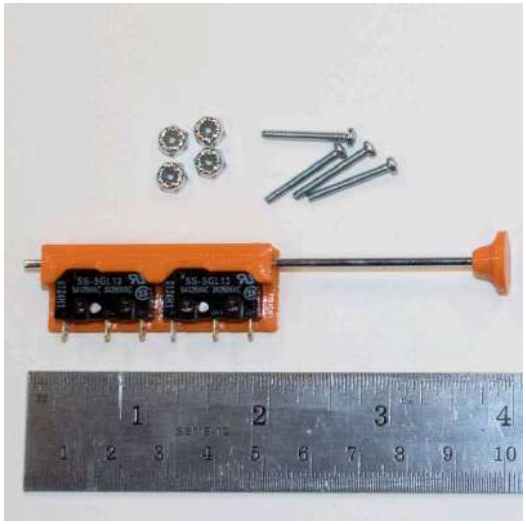
It is ensured that the switches arming the COTS and SRAD recovery systems are completely isolated from each other.

The exact model of the pull-pin switches which will be sourced is given below.

- **Single**: Pull Pin Switch Kit - LRR | Inverted Pursuits Lab



- Double: Double Pull Pin Switch Kit - LRR | Inverted Pursuits Lab



Redundancy

There are 2 recovery systems present in the rocket in terms of electronics, the primary and the redundant:
- Primary Deployment: SRAD Flight Computer named LTS-Iris
- Redundant Deployment: COTS AltusMetrum EasyMini Altimeter
- Primary Tracking: COTS Featherweight GPS
- Redundant Tracking: SRAD Flight Computer consisting of Mikroe GNSS MAX CLICK

The primary recovery electronics is the SRAD Flight Computer. It consists of a pressure sensor (MS5611) used to detect apogee and calculate altitude. The FC then sends a signal to switch the MOSFET which is used to fire the primary charge using the 2 x Lithium-ion 18650 battery for drogue and main deployment. The SRAD flight computer also houses a GNSS module which can track the rocket using GPS signals which are sent to the ground station via a 915MHz Telemetry module. This acts as a redundant method to recover the rocket post-landing.

For redundancy in recovery, a COTS EasyMini altimeter will be used which serves a dual purpose, recovery and official altitude logging. The EasyMini triggers redundant charges for both drogue and main ensuring the deployment of both at apogee and the required 1500ft respectively. The COTS Featherweight GPS is used for tracking the rocket and serves as the primary measure to track the rocket.

Both the systems have independent power supplies (mentioned in batteries) and independent arming switches (mentioned in switches

above) ensuring complete independence and redundancy between the systems.

Arming Sequence

The arming sequence consists of pulling 4 pins from the switches, which will have tags and be numbered as follows. The arming proceeds once all safety inspections and margins are completed.

1. The first pull-pin switch is removed: This powers the COTS Altimeter, the EasyMini, which is identified by beeps.

2. The second pull-pin is removed: This powers the Featherweight GPS, which is confirmed via the mobile iOS application, Featherweight UI, provided by the manufacturer.

3. The third pull-pin is removed: This is the pull-pin connecting two circuits, and it provides power to the SRAD system. The 3.3V and 5V powerlines are activated and the SRAD telemetry link is established, and the activation is confirmed at the ground station.

4. The last pull-pin is removed: This final pull-pin connects the SRAD MOSFET circuitry to the PYRO batteries, which completely arms the system. This is done to ensure that recovery electronics and batteries have independent switches. This is the final step that arms the rocket.

Switches and Arming Electronics Narrative

The switches used are Single-Pole Single-Throw Normally Open switches, which implies that when the pin is pulled, it completes one circuit. The pull-pins are configured as follows:

- **Single pull-pin 1:** Completes the circuit between the positive terminal of the Lithium-ion battery (with two 18650 cells) and the positive terminal of the EasyMini Altimeter.
- **Single pull-pin 2:** Completes the circuit between the positive terminal of the Lithium-Polymer battery (recommended by the manufacturer) and the positive terminal of Featherweight GPS.
- **Double pull-pin 3:** Completes 2 circuits between the positive terminals of two Lithium-ion battery (with 2 x 18650 cells and 2 x 21700 cells, totaling 4 cells) and positive terminals of the SRAD Flight Computer power lines.
- **Single pull-pin 4:** Completes the circuit between the positive terminal of the Lithium-ion battery (with two 18650 cells) and the

positive terminal of the MOSFET switch circuit.

All Pull-pin switches have been strategically mounted near the switch-band for ease of access.

Describe all batteries in your rocket

Avionics (ref: WIRING_DIAGRAM_VAYUVEGA)
"Battery B" - 2 x 5000mAh 3.6V 3C 21700 cylindrical cells with metal casing.
"Battery A" - 2 x 3000mAh 3.7V 5C 18650 cylindrical cells with metal casing.
"Pyro Battery" - 2 x 2800mAh 13C 3.6V 18650 cylindrical cells with metal casing.
"Altimeter Battery" - 2 x 2800mAh 13C 3.6V 18650 cylindrical cells with metal casing.
"GPS Tracker Battery" - 400mAh 3.7V Li-Po (Recommended by Manufacturer).
Payload
NMC 18650 7.4V 6000mAh 3C 2S2P Li-Ion Battery Pack

Using team-provided ground power at the launch pad?

No

Describe the batteries in your launch pad ground support equipment

N/A

Recovery

Describe your recovery system; dual-deploy electronics, size, chute style, number of chutes, colors, decent rates, length of shock cord, and provide any additional detail not recorded in your recovery system as to parachute size(s) and color(s) and size and note shear pins size and quantity if being used." "Chute Release" commercial products are no longer approved.

COTS Altimeter

Altus Metrum EasyMini Altimeter

Deployed Payload - Recovery System

Not applicable

Redundant Altimeter

SRAD Flight Computer with MS5611 Barometric Pressure Sensor.

Altimeter & Battery Drain Testing

The following tests are required to evaluate the performance of the Altimeters and determine the battery drain characteristics:

- Vacuum Jar test (ground-based flight simulation) for EasyMini Altimeter
- Vacuum Jar test (ground-based flight simulation) for SRAD Flight Computer

The above two tests are done to ensure apogee detection and recovery functionality of the flight computers (with altimeter) are fulfilled.

- Battery Drain test of the EasyMini in armed state with the battery specified in Section 9 of this form.
- Battery Drain test of the SRAD Flight computer with data logging and telemetry in the armed state with the specified batteries.
- Drain test for SRAD Pyro batteries that simulates the firing of charges, through ground-based flight simulation (done with pre-existing data, this test is to mainly check the firing of charges and drain rate of the Pyro batteries used).
- Drain test for COTS Pyro batteries, which also powers the EasyMini, to simulate the firing of charges, this is done using the software AltOS UI.

The above tests are for determining the battery drain rate.

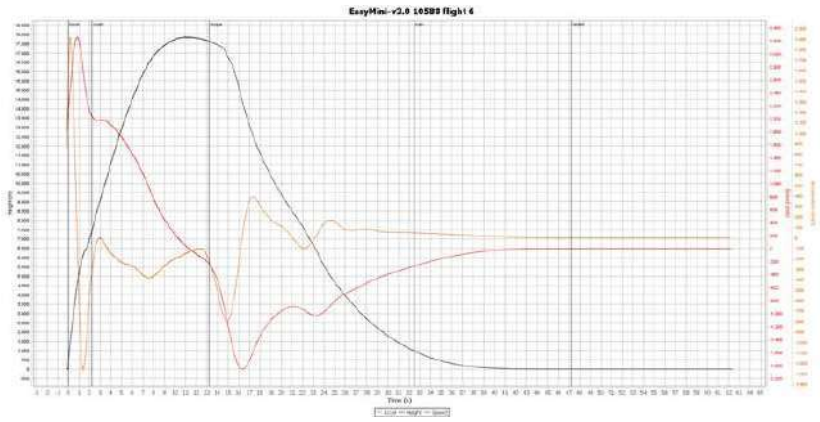
Altus Metrum EasyMini Altimeter Testing:

On November 14th, 2024, we vacuum tested the EasyMini COTS Altimeter. The EasyMini altimeter is a dual deploy altimeter with logging and built-in USB data download. The EasyMini was powered by a regular 9V battery and in place of igniters LEDs were used.

The connections involved connecting the 9V battery to the EasyMini Altimeter's battery +ve and battery -ve terminals. The switch terminals were shorted, and the main and apogee terminals are connected to the LEDs via 1K resistor.

The vacuum chamber setup was made using an airtight glass jar which had a connection for the vacuum pump.

As of November 14^{th,} 2024, the use of 9V is not confirmed as further testing with the ignitors and other batteries is required.



Device	EasyMini-v3.0	Version 1.5.17	serial 10588
Flight	6		
Maximum height	17854.7 m	58585 ft	
Maximum speed	3257.7 m/s	10688 fps	Mach 4.5
Maximum boost acceleration	1919.2 m/s²	6296 ft/s²	195.78 G
Average boost acceleration	-37.1 m/s²	-122 ft/s²	-3.98 G
Ascent time	2.2 s boost	11.0 s coast	
Drogue descent rate	-864.5 m/s	2836 ft/s	
Main descent rate	66.5 m/s	218 ft/s	
Descent time	18.3 s drogue	14.0 s main	
Flight time	47.2 s		

Drogue Deployment Charges - Primary & Backup (g)

4F Black Powder, 3.5g, 4g

Main Deployment Charges - Primary & Backup (g)

4F Black Powder, 5g, 5.5g

Deployment Charge Discussion

Building on our previous experience, we have opted to retain the same deployment charge setup as last year for our IREC 2025 rocket. After carefully evaluating various ejection mechanisms and considering the logistical constraints associated with CO_2-based systems, black powder remains our preferred choice for the ejection system. Its reliability, ease of procurement, and proven effectiveness at high altitudes reinforce our decision to maintain this approach.

Recognizing the challenges posed by high-altitude deployment, extensive research and testing conducted last year confirmed that proper containment of the charge is crucial for ensuring successful recovery. Our deployment setup consists of a charge well filled with black powder, followed by recovery wadding, and sealed with epoxy.

This design is based on principles outlined in Jim Jarvis's article on high-altitude recovery techniques.

To validate black powder ignition under high-altitude conditions, we plan to conduct tests in a low-pressure environment using a vacuum pump to simulate altitudes of approximately 30,000 feet. The test setup includes a bulkhead with the charge well on one side and a WPC bulkhead secured with shear pins on the opposite side. Once the required pressure conditions are achieved, the charge will be ignited to verify that it generates sufficient force to break all shear pins.

The charge well dimensions are 25 mm in diameter and 25 mm in height, with a thickness of 4 mm. These specifications have been carefully selected to provide optimal containment and pressure distribution. As in the previous year, we will use 3.5g and 4g of 4F black powder for the drogue bay and 5g and 5.5g for the main bay, ensuring consistent and effective deployment.

Drogue Deployment Altitude (meters)

9281

Drogue Decent Rate (meters/second)

28.0

Main Deployment Altitude (meters)

457

Main Decent Rate (meters/second)

8.97

Shock Cords and Mechanical Links

Kevlar, 5/8 in, 6600lb, Drogue - Eyebolt (Lower Avionics Bulkhead) & Quick link (Parachute), Quick link (Parachute) & Eyebolt (Thrust Plate). Main - Eyebolt (Upper Avionics Bulkhead) & Quick link (Parachute), Quick link (Parachute) & Eyebolt (Nosecone Bulkhead).

Concept of Operations Graphic

CONOPS_VAYUVEGA.pdf

Recovery System Protection

To guarantee maximum protection for the parachutes against the intense heat and pressure generated by the ejection charges, we are utilizing Nomex blankets for both the drogue and main parachutes. Nomex blanket, a highly heat-resistant material, will shield the

parachutes from potential damage, ensuring their structural integrity and functionality during deployment. The shock cords utilized are made of Kevlar, and are non-flammable, they do not necessitate additional protection.

Recovery Narrative

Our recovery strategy employs dual deployment utilizing two parachutes, and we plan to recover the rocket as a whole. The Drogue Bay and Main Bay are connected by the Avionics Coupler, which also functions as the Avionics Bay. The Drogue Bay is positioned aft, while the Main Bay is located at the top. The connection between the bays is secured with shear pins on the main bay and bolted with the drogue bay.

The drogue parachute is situated in the drogue bay. The drogue parachute is an eight-gore elliptical design with a 30-inch diameter deployed at apogee. The shock cord, measuring 7 meters (275.59 inches), is linked to the suspension lines through a quick link and swivel. One end of the shock cord is affixed to the thrust plate using an eye bolt. Additionally, a second shock cord, measuring 4 meters (157.48 inches), is attached to the lower avionics bulkhead via an eye bolt. The drogue aims to achieve a terminal velocity of 25-30 m/s.

The main parachute is housed in the Main Bay. It features a twelve-gore annular design with a 72-inch diameter and is deployed at 1500 feet. The shock cord, measuring 7 meters (275.59 inches), connects to the suspension lines through a quick link and swivel. One end of this shock cord is secured to the upper avionics bulkhead with an eye bolt. Additionally, a second shock cord, measuring 4 meters (157.48 inches), is attached to the nosecone bulkhead via an eye bolt. The main parachute is targeted to achieve a terminal velocity of 9-11 m/s.

Both the drogue and main parachutes will be protected using Nomex Blankets. Ejection will take place using CO 4F Black Powder. The Upper and Lower Avionics Bulkheads each incorporate two charge wells: one for the primary charge and one for redundancy. The SRAD altimeter will initiate the primary charge while the COTS altimeter (Altus Metrum EasyMini) will initiate the redundant charge.

The SRAD flight computer detects apogee and fires the primary charge, whereas the redundant charge is fired by the COTS altimeter. The SRAD altimeter consists of a barometric pressure sensor MS5611, which detects change in atmospheric pressure. When apogee is reached, the pressure starts increasing and at this point apogee is detected. The SRAD flight computer then switches one of the MOSFETs to fire the primary charge of the drogue parachute. The redundant charge is fired by the COTS Altimeter. Once the rocket starts descending, at 1500ft (altitude calculated from pressure using lookup tables), the second MOSFET in the SRAD flight computer is switched to fire the primary charge of the Main parachute, at the same time the COTS altimeter will be preset to fire the Main at 1500ft, and hence fires the redundant charge.

Radios and GPS Tracking

Reference: IREC GPS Tracking Requirement and Recommendations

GPS Tracker Manufacturer/Model/Location

COTS: Featherweight Altimeter / Featherweight GPS Tracker/ Fiberglass coupler/Avionics Bay
SRAD: Mikroe Electronics/GNSS MAX CLICK/ Fiberglass Coupler/ Avionics Bay

Wavelength Band / Frequency Range

33 cm / 902 - 928 MHz

Licensed Team Member Name, Amateur Radio Call Sign

N/A

What country is the amateur radio licensed team member's amateur radio license from?

N/A

Does that license country have a reciprocal operating agreement with the United States?

Amateur radio license not needed

Does the amateur radio license allow use of the desired frequency, mode, and power in their home country?

Amateur radio license not needed

What callsign will be used during the event?

N/A

GPS Location & Telemetry

COTS GPS: The Featherweight GPS is placed in the avionics bay towards the top. It is ensured that there is no obstruction to the antenna on it, such that clear GPS signals and telemetry link can be obtained through the Fiberglass Avionics Bay.

SRAD Tracking: The Mikroe GNSS MAX CLICK is placed on the bottom side of the SRAD Flight computer Printed Circuit Board. Its antenna is a dipole antenna that extends parallelly beside the board along its length pointing towards the nose of the rocket. The dipole antenna is only used to receive GPS signals on the standard GPS frequency and NOT for telemetry purposes. The MAX CLICK module consists of the U-blox MAX-M10S GNSS chip which has superior performance compared to similar priced modules. It is capable of obtaining a fix in under a minute in outdoor areas. The module is also very accurate, giving a circular error probability of 1.5m as mentioned in the specifications document. The GPS data thus obtained aids in the recovery of the rocket.

The telemetry is conducted using 915MHz communication modules (RYLR998) which has a helical type of antenna. This will be pointed upwards and will be placed at the edge of the board.

GPS Tracker Narrative

The **COTS Featherweight GPS** serves as the primary GPS tracker for the rocket. This tracker communicates with the ground station on the 915MHz band, offering an extended radio range. It will provide us with updates regarding the battery status, rocket altitude and location over the Featherweight UI app.

The **SRAD GPS** module (Mikroe GNSS MAX CLICK) will also capture location data and send it via the common telemetry link facilitated using the RYLR998 module (on 915 MHz band) to the ground station plotter interface. The GPS data thus obtained aids in the recovery of the rocket.

Test Plan

Include all systems electronics, deployment, payload...

Planned Tests

[Oct 26, 2024] Ground (Completed) - Performed Surface roughness tests on various test articles using a surface profilometer to obtain data for flight aerodynamics.

[Oct 29, 2024] Ground (Completed) - Test drogue and main ejection mechanisms of EasyMini COTS Altimeter.

[Nov 07, 2024] Ground (Completed) - Test the Ground Station Data Plotter to analyze SRAD GPS and telemetry capabilities.

[Nov 10, 2024] Ground (Completed) - Conduct a Dual Deployment Test to validate proper bay separation and ensure the intended release of the parachutes.

[Nov 14, 2024] Ground (Completed) - Conduct compressive tests on in-house manufactured composite body tubes to experimentally determine their strength, under axial loading conditions.

[Nov 15, 2024] Ground (Completed) - Initial Dataset Collection using the OpenMV Camera, capturing various augmented and diversified images for model training.

[Nov 28, 2024] Ground (Completed)- Test the power output of Li-ion battery packs to ensure a stable power supply is provided throughout expected uptime.

[Dec 08, 2024] Ground (Completed) - Unit test SRAD Launch Vehicle Electronics to gauge the hardware requirements for real-time flight data logging.

[Dec 20, 2024] Ground (Completed) - Test range of SRAD telemetry system paired with antennas to confirm a range of 10 Km. Testing will be done inside an appropriate body tube to recognise any signal attenuation caused.

[Jan 15, 2025] Ground (Completed) - Servo Latency Testing to evaluate servo response times and optimize latency for effective object tracking.

[Jan 28, 2024] Ground (To be done) - Spring Vibration Testing at the Institute Vibrational Lab to assess spring response and behaviour under simulated vibrational forces.

[Feb 09, 2025] Ground (To be done) - Test the plotter and GPS module to show real-time location on the map using GPS coordinates.

[Feb 10, 2024] Ground (To be done) - Spring G-Force Testing at the Structural Dynamics Lab, examining the spring's behaviour under increasing g-forces for performance validation.

[Feb 25, 2025] Ground (To be Done)- Conduct a Dual Deployment Test under low-pressure environments using a vacuum pump to validate proper bay separation and ensure the intended release of the parachutes.

[Feb 26, 2025] Ground (To be done) - Test the charge and discharge rate of the Li-ion cells to gauge the power required for the given specific task or if held on standby for longer periods.

[Mar 2, 2024] Ground (To be done) - IMU Algorithm Testing at the Dynamics and Control Lab for validating the 9-axis IMU activation sequence required immediately after payload launch.

[Mar 5, 2025] Ground (To be done) - Test performance and power consumption of the first iteration of SRAD Flight Computer.

[Mar 7, 2024] Ground (To be done) - Test the inflation of the Main Parachute using a pilot and parachute liner. This will be done with the assistance of a vehicle (back of a car).

[Mar 8, 2025] Ground (To be done) - Test the battery drain rate of the Li-ion cells when powering the entire Avionics Bay (including separate

redundant power supply to SRAD and COTS systems) to ensure the working of the system even after taking into consideration the standby time at the pad.

[Mar 15, 2025] Ground (To be done) - Assemble the entire avionics bay and perform integrated testing of the whole system.

[Mar 21, 2025] Ground (To be done) - Assemble the entire rocket to ensure proper fitting of all parts.

[Mar 25, 2025] Ground (To be done) - Point Cloud and Segmentation Algorithm Testing focused on developing point clouds through estimated depth maps, pose estimation, instance segmentation, and object detection.

[Mar 28, 2025] Ground (To be done) - Perform integrated Dual Deployment test with the entire rocket assembled.

[Mar 29, 2025] Ground (To be done) - Integrated Payload Vibration Testing at the Institute Vibrational Lab, testing the entire payload setup under vibration to assess component integrity and performance.

[TBD] Flight - Subscale Launch.

Payload Information

NOTE: To compete in the SDL Payload Challenge, you MUST follow the instructions on the IREC Documents and Forms Page. The information provided here is so the ESRA safety reviewer can determine what impact the payload will have on the safety/stability of the rocket. See http://www.soundingrocket.org/irec-documents--forms.html

Payload - Deployed or Attached

Attached

Deployed Payload - Deployment Mechanism

NA

Deployed Payload - Deployment Altitude (meters)

0

Deployed Payload - Decent Rate (meters/second)

0.0

Deployed Payload - Altimeter

NA

Deployed Payload - GPS

NA

Payload Narrative

Our payload is a non-deployable, fully operational system housed within a CANSAT form factor. Its primary mission is to advance cutting-edge computer vision technology for demanding military environments. The prototype enhances object detection and tracking capabilities on compact, power-efficient hardware. By leveraging deep learning, real-time processing, and innovative testing methods, we aim to set new benchmarks in intelligent tracking and visual data processing.

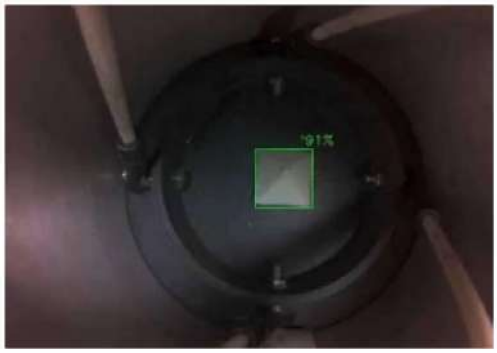




The five key areas of our research and development include:

- **Real-Time Active Tracking:** Building on last year's payload, we integrated a high-torque dual-shaft metal gear servo (35 kg-cm) to precisely maneuver the camera module. Our goal is to refine an advanced active tracking system that dynamically locks onto a target with exceptional accuracy. To achieve this, we developed a sophisticated tracking algorithm paired with an optimized feedback loop, ensuring seamless servo control in real time—even in complex, fast-changing scenarios.
  Initial Testing done to test Servo response while Tracking:
  https://youtu.be/PRIJv4OSzQM

- **Deep Learning-Based Vision Tasks:** A core objective is to maintain precise object pose estimation despite intense vibrations and high G-forces. We leverage state-of-the-art deep learning models such as YOLOV11 and convolutional neural networks (CNNs) to enhance pose prediction robustness. Our framework executes both object detection and image segmentation, providing a rich contextual understanding of the target. The model was trained from scratch on a custom in-house dataset of over 3000 self-annotated images —thoroughly tested and augmented for our specific conditions. This meticulous data preparation allows our system to achieve an unprecedented 150+ FPS inference rate on a 60 FPS raw input stream, demonstrating exceptional computational efficiency.

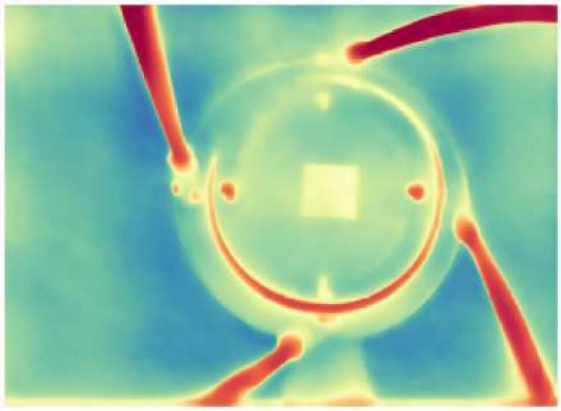


Object Tracking Algorithm running on a test setup

- **Hardware Innovation:** Historically, computationally intensive vision tasks relied on high-end GPUs, which are impractical for sounding rockets due to high power consumption, cost, and size. This year, we adopted a novel approach by integrating a Hailo-8L Neural Processing Unit (NPU) alongside a Raspberry Pi 5 (8 GB), significantly boosting our inference capabilities. Our current system delivers 150 FPS on a 60 FPS input, while the NPU reduces power consumption by up to 90% compared to conventional GPUs—making it ideal for aerospace and defense applications. Additionally, we updated the mechanical structure of our CANSAT with a split design attached centrally using countersunk screws. This redesign streamlines the assembly process and facilitates a systematic division of power and technical systems, thereby enhancing modularity and accessibility during integration and testing.

- **Depth Estimation and 3D Reconstruction:** By leveraging advanced deep learning techniques, we implemented a depth estimation algorithm trained on over 1000 images with ground truth depth data. Utilizing models such as the Depth Anything V2, we achieve high-accuracy depth inference that enables precise measurement of object distances in 3D space—a capability critical for target acquisition, reconnaissance, and autonomous navigation in military operations. Furthermore, by integrating Gaussian Splatting techniques, we developed a robust 3D reconstruction framework capable of creating a detailed spatial representation of our payload environment. Although still in its initial testing stages, this technology promises significant improvements in battlefield

situational awareness by enabling real-time tracking and analysis of dynamic targets under challenging conditions.



Depth Estimation algorithm running on a test setup

- **Realistic Testing Environment:** To validate our algorithms under mission-relevant conditions, we have designed and integrated a custom-engineered conical spring mechanism that accurately simulates real-world rocket vibrations and G-forces. This setup directly transmits the dynamic forces to the payload-attached object, enabling high-fidelity testing. By replicating these extreme conditions, we ensure our technology remains reliable and effective for potential military-grade applications, reinforcing our system's ability to handle complex operational environments.



Conical Springs

Conclusion: To validate our algorithms under mission-relevant conditions, we engineered a custom conical spring mechanism that accurately simulates the vibrations and G-forces encountered during rocket flight. This setup transmits dynamic forces directly to the payload, enabling high-fidelity testing that replicates extreme

operational conditions. Such rigorous validation ensures our technology remains reliable and effective for potential military-grade applications, reinforcing its capacity to operate within complex environments.

Payload RF Narrative

N/A

Video Challenges

Are you participating in the Video Challenge?

Yes

Are you participating in the Live Video Challenge?

No

Live Video Challenge Narrative

N/A

Additional Comments

Any other pertinent information

Our team's dedication remains unwavering as we strive to actualize our 30K COTS mission. Extensive efforts have been devoted to refining our recovery mechanisms and manufacturing processes.

Additionally, our team is actively working towards obtaining permissions for a rocket test flight. Engaging with our university and government authorities, we are navigating the process to secure the necessary approvals for this endeavour, further propelling us towards our goals in rocketry and engineering.

Return to editing

ABOUT HEROX

About Us
Press Kit
Partner With Us
Partners
Careers
Privacy
Terms
Cookie Policy

COMMUNITY

Blog
Organizations Involved
Events & Webinars
Community
General Forums

SUPPORT

Contact Us
How HeroX Works
Knowledge Base
FAQ
Innovation Resources



© Copyright HeroX 2025

Was this page helpful?

○ Yes ○ No



Please note: This is a draft of your entry and is only visible to you. You may return to edit this draft at any time from the main challenge page. Once you have finished and are ready to submit your final entry, click the "Submit entry" button to submit it for judging.

Preview

Edit Submit entry



thrustMIT, Manipal Institute of Technology

Introduction

Title

Team 207_MIT_Progress Report 3



IMPORTANT - Title of Submission entered above should follow this naming convention: TeamID_Formal University Name_Purpose . Example: Team 100_ESRA University_Progress Report 3. Any other naming convention will not be accepted and will lose points.

Title of Submission entered above should follow this naming convention: TeamID_Formal University Name_Purpose . Example: Team 100_ESRA University_Progress Report 3. Any other naming convention will not be accepted and will lose points.

Choose Your Team

207 Manipal Institute of Technology

Category

30k - COTS - All Propulsion Types

Category Change

No

If yes, please provide a detailed explanation and if you have received permission from ESRA to do this.

N/A

Student Lead

Satvik Agrawal / teamleader@thrustmit.in / +91 8920873563

Alternate Student Lead

Geethika Sree Ravu / team.manager@thrustmit.in / +91 9989973265

Faculty Advisor

Dr. Srinivas G / srinivas.g@manipal.edu / +91 8123677706

Alternate Faculty Advisor

N/A

Flyer of Record (FoR)

Mr. Bob Schoner, TRA #04928, L3, bschoner56@vt.edu, +1 540 231 1457

Lead Team Mentor(s)

Mr. Bob Schoner, TRA #04928, L3, bschoner56@vt.edu, +1 540 231 1457; Mr. Bob Schoner is the Manager of the Aerospace Engineering Design Lab (AEDL) at Virginia Tech University.

Estimated number of Team Members attending the Competition

10

Safety and Testing Updates

Safety Remediation - Describe resolutions to any remaining safety issues

After the 1st Progress Update, our safety reviewer had raised concerns regarding shorter fin spans, for which we had provided our detailed rationale for the design choice. Additionally, upon review of our wiring diagram, our safety reviewer had recommended isolated battery sources for COTS GPS and COTS Flight Computer systems. We have integrated this recommendation as part of our recovery electronics.

Following our incorporation of the above feedback, we documented our rocket construction narrative in the second progress update report. Our safety reviewer has commended the completeness and detail of the report, and the inclusion of supporting graphics and diagrams.

However, the reviewer had reiterated that the only potential concern regarding our flight was the fin size, for which she had requested our RasAero II simulation file for further rationale. We had provided the requested document and are still awaiting a response regarding the same.

Therefore, apart from the aforementioned concern regarding fin size, our team has successfully remediated all safety issues raised by our safety reviewer.

Test Flight

No

SRAD Static Test

N/A

Testing Discussion

Avionics:

- COTS - EasyMini Battery Drain Test: https://youtu.be/qbuZVcxmK_s
- COTS - EasyMini Vacuum Test: https://youtu.be/5XN-ov6Brq4
- SRAD PCB - GPS Test: https://youtu.be/bAvBCfTWCD0
- SRAD PCB - Vacuum Test: https://youtu.be/NMMK9rdM40c

Payload:

- IREC 2025 - Payload Presentation: https://youtu.be/yE9L-qSnc2Y
- Battery Drain Test of Payload: https://youtu.be/9PKvHUd9CD8
- Pipeline Test of Payload: https://youtu.be/iLAd32p_UVQ
- Testing of Algorithm on Custom-Trained Dataset: https://youtu.be/DhsaWG3oNs8

Testing of Ejection Charges:

- Ground Testing: https://drive.google.com/drive/folders/1NebetLLM8tOkquxyTZ86PsKKguxSwCcd?usp=sharing

Event Economic Information

Event Economic Information

Has your team secured all required travel tickets, vehicles, and visas to attend?

Yes

Which city or cities will your team be staying in?

Midland

What accommodations will your team have in Texas?

Hotel

Have you reviewed how to get to the launch site from your accommodations?

Yes

Media and Livestream Information

Media and Livestream Information

Will you fly a media UAS/drone at the launch site?

No

If flying a media UAS/drone, do you have an acceptable insurance policy?

Not flying a media UAS/drone

Will you participate in the Team Video Challenge?

Yes

Will you participate in the Live Rocket Video Challenge?

No

What is your team's name (exactly as it should appear in Livestream graphics)?

thrustMIT

What is your university name (exactly as it should appear in Livestream graphics)?

Manipal Institute of Technology

What is your university location (exactly as it should appear in the Livestream graphics)?

Manipal, Karnataka, India

What is your rocket name (exactly as it should appear in the Livestream graphics)?

Vayuvega

What is your country flag emoji (exactly as it should appear in the livestream graphics)?

IN

Do you want to be interviewed on the event Livestream?

Yes

If you are participating in the Live Video Challenge, what video interface and format will you use?

Not Participating

If you want to assist the announcers with pronouncing your team name, university name, place name, or rocket name, you may upload a video here



Please provide a brief description/comment on your team and rocket for the Launch Control Officer to announce right before your flight.

Brace yourselves! From Manipal Institute of Technology, it's thrustMIT with Vayuvega! Derived from Sanskrit, the name "Vayuvega" captures the unstoppable force of wind and speed — a name that mirrors our rocket's agility, power, and precision. With this, we charge into the skies, forging new paths and pushing the boundaries of sounding rocketry.

Will your team be bringing any media personnel who are not student team members?

No

If you answered yes to the above question, please describe

N/A

Other

Does your team intend to bring their own rocket launchpad?

No

Please describe how you are getting your rocket to the competition.

The transportation logistics for our rocket to the competition are being facilitated by our trusted shipping partner, Babaji Shivram, with whom we have had a successful collaboration since 2018. Our rocket will be transported via air freight. This mode of transportation ensures timely delivery and careful handling of the crate. In terms of schedule, our team members are planning to be in Midland by June 4th, allowing ample time for preparations ahead of the competition. We anticipate that the rocket will reach the US by June 3rd or 4th, ensuring that we have sufficient time for final inspections and any necessary adjustments before the competition commences.

Edit

Submit entry

× Delete this entry



© Copyright HeroX 2025

Was this page helpful?

○ Yes ○ No